UCRL-18981

cy. 2

RADIOACTIVATION BY ^{3}He BOMBARDMENT: A PRACTICAL ANALYTICAL SYSTEM

James Francis Lamb
(Ph.D. Thesis)

September 1969

AEC Contract No. W-7405-eng-48

LAWRENCE RADIATION LABORATORY
UNIVERSITY of CALIFORNIA BERKELEY

UCRL-18981

cy. 2

DISCLAIMER

RADIOACTIVATION BY ^{3}He BOMBARDMENT: A PRACTICAL ANALYTICAL SYSTEM

Contents

RADIOACTIVATION BY ^{3}He BOMBARDMENT: A PRACTICAL ANALYTICAL SYSTEM

James F. Lamb

Lawrence Radiation Laboratory
University of California
Berkeley, California 94720

ABSTRACT

Charged-particle activation analysis using 1-30-MeV ^{3}He ions as the nuclear reaction inducing particle is discussed from a practical point of view with emphasis upon the light elements, especially oxygen.

Definitions and expressions fundamental to charged particle activation analysis are given with brief discussions. Also included are convenient ^{3}He activation analysis reference curves for estimating Coulomb barriers and the effects of Rutherford scattering upon the incident beam. Range-energy tables for ^{3}He ions in nongaseous targets of the stable isotopes of all elements and an extensive Q-value table for the more important ^{3}He-induced reactions appear as appendices.

A summary of excitation functions and reaction data for ^{3}He induced reactions in Be, B, C, N, O, F, Na, Mg, Al, Si, Ca, Ti, Fe, Ni, Cu, Ge, Ta, and Au is given which contains our experimental measurements as well as those from the literature. All the excitation functions have been re-drawn to the same scale to permit convenient comparison. A brief discussion of the recognizable trends in the excitation functions for the more important ^{3}He-induced reactions follows the experimental data.

The results of several analyses illustrating special methods and applications of ^{3}He activation analysis are given. These include simultaneous isotopic analysis of ^{16}O and ^{18}O and the preparation of thick Ta_2O_5 oxygen standards, surface depth profile analysis of oxygen in silicon, use of matrix activation as an internal normalization standard in the analysis of oxygen in iron and nickel, and the use of Au, Pt, and Ta as target supports and cover foils.

The report is concluded with a discussion of the applicability, interference, sensitivity, and unique features of ^{3}He activation analysis.

I. INTRODUCTION

The importance of good analytical data to the scientist is adequately stressed by the short time which elapses between major research advances and their application to chemical analysis. The development of nuclear analytical techniques provides a striking example.

The rapid growth of nuclear physics[1] dates from the development of the particle accelerators by Lawrence and Cockroft and Walton in 1930 and van de Graaf in 1931. Before this time the only available projectiles suitable for use as nuclear probes were natural alpha particles, and these were not available with sufficient energy and intensity to provide data for any great understanding of the nucleus itself. By 1934, however, a number of remarkable developments had occurred. The existence of the neutron was recognized by Chadwick, Cockroft and Walton had accomplished transmutations of elements using artificially accelerated particles, artificial radioactivity was discovered by Curie and Joliot, and the first neutron-induced activity had been produced by Fermi. Within two years a neutron activation analysis had been reported by Hevesy and Levi,[2] and in 1938 Seaborg and Livingood[3] had published the results of an activation analysis using charged particles.

The research following the discovery of fission by Hahn and Strassmann in 1939 provided for such a rapid development of high-flux neutron sources that since 1943 radioactivation analysis has become an everyday procedure at the Oak Ridge National Laboratory.[4]

Developments in electronics, radiation detection, and counting equipment such as pulse height analyzers, scintillation detectors,[5] and more recently, semiconductor detectors,[6,7,8,9] have been applied to activation analysis almost immediately.

Charged-particle activation analysis has received much less attention than has neutron activation because of the limited access to accelerators capable of producing ion beams of high enough beam-intensity and energy. In 1962, however, Markowitz and Mahony[10] showed that activation analysis based upon ^{3}He induced nuclear reactions was, potentially, a powerful analytical system. Sufficient interest was aroused that the first small, relatively inexpensive, practical-application cyclotron[11] was designed and built, primarily for ^{3}He activation analysis at the Lawrence Radiation Laboratory in Berkeley. The use of ^{3}He, in particular, as the activating particle was suggested by Markowitz and Mahony because the low binding energy of the ^{3}He nucleus enables nuclear reactions to proceed with minimum energy bombardment, because the two-proton, one-neutron configuration of ^{3}He leads to a wealth of possible reaction products, and because most of the reactions induced give rise to neutron-deficient products whose decay characteristics are favorable.

From the outset, the main interest in charged-particle activation analysis has been the determination of light elements. Of the elements in the first three periods, few are amenable to thermal neutron activation analysis because of low capture cross sections and low relative abundances of suitable stable isotopes and because of unfavorable decay charactistics of product activities. There is little doubt that the

most exciting aspect of the ^{3}He activation analysis system is the ability to detect oxygen with such fantastic sensitivity[12]--an element for which there exist no other analytical methods of general applicability at this sensitivity. Much of this report is concerned, therefore, with reactions involving those light elements which cannot be easily determined by thermal neutron activation, and the systematic features of ^{3}He activation analysis are illustrated using oxygen analysis as an example. The system is by no means limited to light elements, however, A few reactions involving very heavy targets have also been studied.

Methods of charged particle analysis not covered in this report include "in beam" detection of emitted particles,[13] detection of prompt reaction γ-rays,[14] use of Rutherford scattered incident particles,[15] and use of ^{3}He reactions as a source of neutrons.[16] These techniques are potentially powerful, although not as generally applicable as direct activation.

II. FUNDAMENTAL DEFINITIONS AND EXPRESSIONS

Many of the concepts and mathematical relationships encountered in ^{3}He activation analysis will be listed, for convenience, in this section. For detailed discussions and derivations, the reader is referred to various texts[17,18,19] and review articles.[20,21,22,23]

A. Production of Activity by Charged-Particle Bombardment

The disintegration rate of a particular induced activity present at time t in a target following a charged-particle bombardment of duration τ is given by

$$D = \frac{A}{ODC} = N\sigma I(1-e^{-\lambda\tau})\, e^{-\lambda t} \qquad (1)$$

where

D = disintegration rate, in disintegrations per min

A = count rate of activity present in counts per min

ODC = overall detection coefficient incorporating detector efficiency, detector geometry, and decay scheme corrections

N = target thickness in nuclei of target isotope per cm^2

σ = reaction cross section in cm^2

I = beam intensity in $^3He^{++}$ ions per min

λ = decay constant of induced activity, $0.693/T_{1/2}$.

The quantity $(1-e^{-\lambda t})$ is usually referred to as the saturation factor and represents the fraction of the equilibrium activity realized by a bombardment of duration τ. The quantity $e^{-\lambda t}$ represents the fraction of the induced activity which remains at the time of radio assay. The end of bombardment disintegration rate D_o, is then given by

$$D_o = \frac{D}{e^{-\lambda t}} \; . \qquad (2)$$

Time, t, the true decay time, is measured from the end of bombardment to the time of count, corrected for decay during the counting interval.

The true decay time is given by [24]

$$t = t_s + t_{1/2}\,\Delta t \tag{3}$$

where t_s is the time from the end of bombardment to the start of the counting interval, $t_{1/2}$ is the half life of the radionuclide, and Δt is the time correction factor given by

$$\Delta t = \frac{-t_{1/2}\ln\left[\frac{(1-e^{-R\ln 2})}{R\ln 2}\right]}{\ln 2} \quad . \tag{4}$$

The quantity R is the number of half lives counted,

$$R = \frac{\text{counting interval}}{\text{half life}} \quad . \tag{5}$$

Figure 1 shows this correction factor plotted as a function of half lives counted.

The beam intensity, I, which enters Eq. (1) as $^3He^{++}$ ions per unit time, may be measured in a variety of units by electrometers and integrating electrometers. The most common unit of beam current is the microamp, which, for $^3He^{++}$ ions, is

$$I = 1\mu A = (1.873 \times 10^{14})\ {}^3He^{++}/\text{min.} \tag{6}$$

Usually the total charge deposited by the ion beam impinging upon the target is collected in a Faraday cup. This integrated beam is then averaged over the bombardment time so that

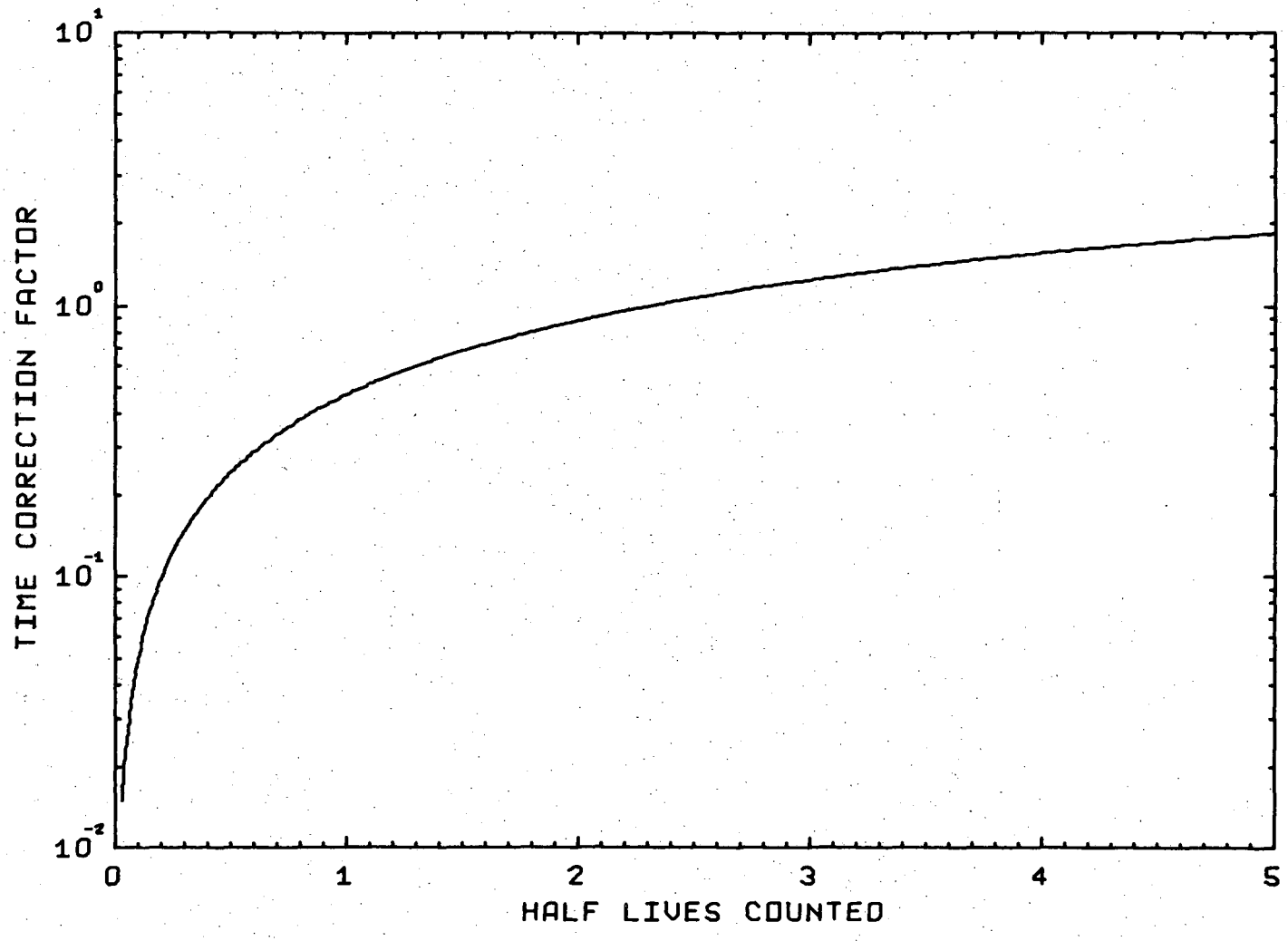

Fig. 1. Time correction for the finite length of counting interval.[24]

$$I = \frac{(\text{microamphours})(1.873 \times 10^{14})}{\tau} \ {}^3He^{++}/\text{min} \qquad (7)$$

where τ is the bombardment time in hours, or

$$I = \frac{\text{microcoulombs}}{(3.2 \times 10^{-13})\tau} \ {}^3He^{++}/\text{min} \qquad (8)$$

with τ in minutes.

B. Beam Energy

Experimental measurements of the energy loss by charged particles as they traverse target materials are very few. A number of theoretical range-energy tables have been prepared, however, which reproduce existing experimental data fairly well.[25,26,27,28] A method has recently been developed by Steward[29] for calculating ranges of any charged particle in non-gaseous media. An extensive table of ^3He ion ranges in pure elements and a few compounds, calculated using Steward's computer program, is included as Appendix A of this report. The table may be used to approximate ^3He ion ranges in other compounds by Bragg's formula

$$\frac{1}{R_c} = \sum_i \frac{W_i}{R_i} \qquad (9)$$

where R_c is the range of the ion in the compound, W_i is the weight percent of element, i, and R_i is the ion range in pure element, i. The agreement between ranges of elements which may be found in both Appendix A of this report and the widely used tabulations of Williamson, et al,[25] is satisfactory.

The residual energy, E_r, of the ^3He ion beam after it has traversed a target or degrader of thickness t mg/cm^2, may be found from Appendix 1 by calculating the residual range from

$$R_r = R_I - t \qquad (10)$$

where R_r is the range of the emerging ^3He beam and R_I is the range of the incident beam whose energy is E_I. The residual energy, E_r, is the energy which corresponds to residual range, R_r, in the table. The amount of absorber necessary to degrade an incident beam from its initial energy, E_I, to a final energy, E_r, may be calculated similarly.

C. Reaction Q-values

The Q-value of a nuclear reaction, which is a measure of the energy released or absorbed during the process, is determined from the mass difference between reaction products and reactants. An extensive tabulation of reaction Q-values has been prepared by Maples, Goth, and Cerny[30] which includes some of the reactions of interest in ^3He activation analysis. Not included in that work are reactions in which more than two neutrons, more than one proton, or unbound (pn) and (p2n) are emitted from the compound system. The tables may be extended to these and other reactions, however, using their mass excess data and the equation

$$Q = \sum \Delta reac - \sum \Delta prod \qquad (11)$$

where Δreac and Δprod are the mass excesses of reactants and products, respectively. Appendix B contains reaction Q-values for the following ^{3}He induced nuclear reactions with stable targets, calculated using the mass data of Maples, Goth, and Cerny:[30]

(1) (^{3}He,n)
(2) ^{3}He,2n)
(3) (^{3}He,3n)
(4) (^{3}He,p)
(5) (^{3}He,2p)
(6) (^{3}He,^{4}He)
(7) (^{3}He,pn)
(8) (^{3}He,p2n)
(9) (^{3}He,^{4}He+n)

D. Reaction Threshold

An energy threshold may be defined for an endoergic reaction representing the minimum kinetic energy which must be supplied to the incident particle for the reaction to be energetically possible;

$$T_m = -Q\left(\frac{M_1 + M_2}{M_2}\right) \qquad (12)$$

where T_m is the reaction threshold, M_1 and M_2 are the masses of the ^{3}He ion and target nucleus, respectively, and the negative sign arises because the reaction Q-value is negative for an endoergic reaction.

E. Coulomb Barrier

In order for an incident charged particle to penetrate a target nucleus, the potential-energy, "Coulomb" barrier must be surmounted. This barrier may not be thought of as an energy threshold for the nuclear

reactions because of the quantum-mechanical effect of barrier tunneling and because the barrier is, at best, an approximation. Reactions are often observed to commence at incident particle energies somewhat below the Coulomb barrier where energetically possible. The height of the Coulomb barrier is given by

$$E_b = \frac{Z_1 Z_2}{R} \tag{13}$$

where E_b is the barrier height in ergs if Z_1 and Z_2 are the charges of the ^{3}He ion and target nucleus, respectively, in esu and R is the interaction radius, approximated by

$$R \approx 1.5 \times 10^{-13}(A_1^{1/3} + A_2^{1/3})\text{cm} \tag{14}$$

with A_1 and A_2 the mass numbers of ^{3}He ion and target nucleus. Fig. 2 shows the approximate Coulomb barrier in MeV to penetration of target nuclei by a $^3He^{++}$ ion as a function of target atomic number. The values of A_2 were chosen to lie roughly along the line of stability to β-decay.

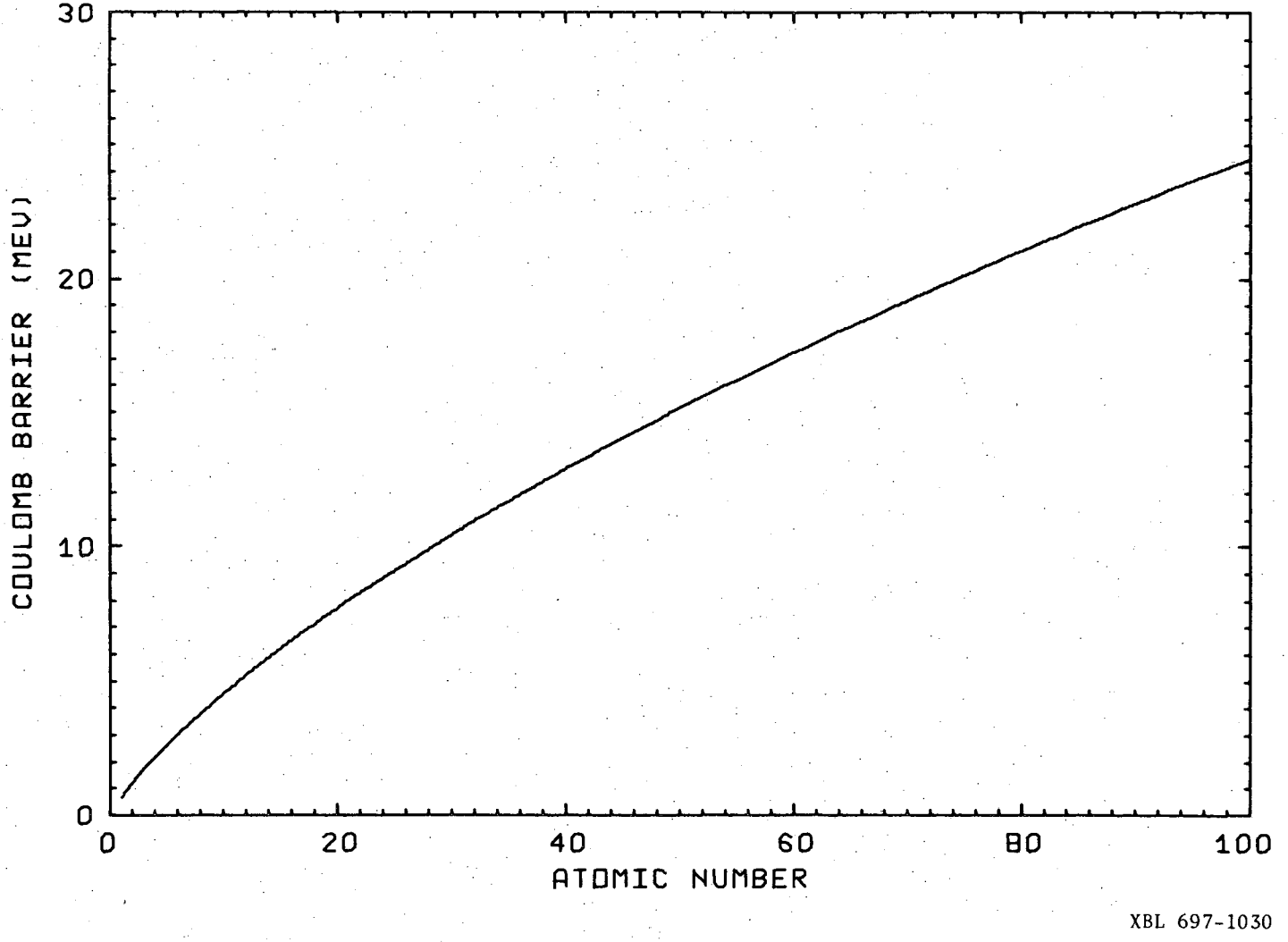

Fig. 2. Coulomb barrier to penetration of target nuclei by incident ^{3}He ions. Target masses lie along line of β-stability.

F. Excitation Energy

A $^{3}He^{++}$ ion which has surmounted (or tunneled through) the Coulomb barrier of a target may form a compound nucleus composed of all the nucleons of both $^{3}He^{++}$ ion and target nucleus. The compound nucleus will have an excitation energy given by

$$E_{cn} = Q + \left(\frac{M_2}{M_1 + M_2}\right) E_{^3He} . \qquad (15)$$

Since the reaction Q is usually positive or only slightly negative for ^{3}He induced reactions of interest, the excitation energies encountered are large. At these energies there is little competition from de-excitation by gamma-ray emission so that particle emission predominates until the excitation energies of product nuclei formed are below the binding energies of nuclear particles.

Direct reaction mechanisms lead to formation of product nuclei in states of excitation below particle binding energies. Most of the kinetic energy of the incident ^{3}He ion remains with directly ejected particles and nucleons whose angular distribution about the beam line is predominately in the forward direction.

G. Reaction Cross Sections

The cross section, σ, of a nuclear reaction is a measure of its probability of occurrence during a bombardment and is a function of the kinetic energy of the incident particles. The variation of reaction cross section with incident particle energy is called the "excitation

function" for the reaction. Several types of cross section data may be found in the literature for ^{3}He induced reactions. For activation analysis, the excitation functions for total production of individual product nuclei are most useful. Other types of cross section data encountered involve σ as a function of the scattering angle, and often, they involve observation of reactions leading to only a limited number of specific energy states of the product nuclei. These "differential cross sections" make up the bulk of the nuclear reaction literature because of the wealth of theoretical information which may be contained within them. In this report the term "excitation function" will refer to total σ for individual reactions as a function of incident ^{3}He ion energy in the laboratory system.

Of the ^{3}He reaction excitation functions which have been measured at this writing, only a few have shown details which might be attributable to structural or resonance effects.[34,35,36] Small structural details tend to be "washed out" in most experimental data because of the uncertainty in the energy distribution in the incident ion beam. Furthermore, at the high excitation energies encountered in most ^{3}He reactions the high level densities cause serious overlap of individual energy levels so that resonance structure is not observed. While this lack of structure in the cross section data tends to limit the usefulness of excitation functions in nuclear structure and reaction theory studies, it enhances their value for activation analysis by reducing complications resulting from sudden, large, energy dependent fluctuations in sample activation.

The new cross section data presented in Sec. IV of this report, together with the compilation of literature excitation functions also included there, indicate definite trends which may be useful in predicting interferences from reactions whose excitation functions have not been measured. Further discussion of reaction cross sections is given in Sec. IV.S.

H. Absolute Analysis

If the excitation function for a nuclear reaction has been accurately determined, an absolute activation analysis can be performed using Eq. (1). As the ion beam traverses the sample the average beam energy is degraded, and this degradation may be reflected in cross section variation. Thus, a restriction on sample thickness is imposed such that the variation in cross section as the sample is traversed must fall within accuracy limits. A target which meets this requirement is called a thin target with respect to that particular bombarding energy.

Absolute analyses may also be performed using targets of intermediate thickness, in which cross section variations are large, and thick targets which completely stop the incident beam. In either case an average reaction cross section replaces σ in Eq. (1). Ricci and Hahn[16,37] have proposed an alternate form for the reaction cross section for analysis of homogeneous thick targets called the "thick target average cross section, $\bar{\sigma}$," defined by

$$\bar{\sigma} = \frac{1}{R} \int_0^R \sigma_t \, dt \qquad (16)$$

where R is the total range of the incident ^{3}He ion in the target material and σ_t is the cross section as a function of target thickness. $\bar{\sigma}$ is intended to be a parameter independent of the target matrix and a function of the particular nuclear reaction alone. For example, the thick target average cross section for production of ^{18}F activity from oxygen in a target of tantalum oxide is the same as that for ^{18}F production from an oxygen impurity in a target matrix of silicon. The thick target average cross sections may be experimentally measured much more easily than excitation functions and, since extensive range data is available, the analysis of thick targets is almost reduced to the simplicity of neutron activation analysis. Ricci and Hahn have shown valid by rigorous mathematical treatment the approximation that $\bar{\sigma}$ is independent of target matrix and have supported the calculations with experimental evidence.

I. Comparison Standards

Excitation functions presently available may be considered accurate to no more than about 10 to 20 percent, and some systematic variations have led to larger discrepancies among literature values. Comparison standard techniques remove much of the dependence upon system calibration and provide the most accurate analytical data.

For He activation analysis, the general form is

$$\frac{A_x}{A_s} = \frac{N_x \, _x I_x (1 - e^{-\lambda \tau_x}) e^{-\lambda t_x}}{N_s \, _s I_s (1 - e^{-\lambda \tau_s}) e^{-\lambda t_s}} \qquad (17)$$

where x signifies "unknown" and s stands for a comparison standard whose composition is known. The terms are as defined in Eq. (1). For homogeneous thick targets, the average cross sections are approximately equal, but the number of nuclei in the sample and standard which are irradiated depend upon the ranges of the beam in the target matrix. Then

$$\frac{A_x}{A_s} = \frac{N_x R_x I_x (1 - e^{-\lambda\tau_x}) e^{-\lambda t_x}}{N_s R_s I_s (1 - e^{-\lambda\tau_s}) e^{-\lambda t_s}} \qquad (18)$$

where R_x and R_s are the ^3He ion ranges in unknown and standard matrices.

For the important class of intermediate thickness targets which may be encountered (due either to lack of sufficient sample material to produce a thick target or difficulty in preparing a uniform "thin" target), a comparison standard must be used which accurately matches the degrading power of the sample. If such a standard cannot be obtained, then a semi-absolute analysis may be performed using a standard whose degrading power is as near as possible to that of the unknown sample. A correction factor obtained from the excitation function for the reaction is then applied to account for the difference in the average cross sections. This technique is more accurate than the strictly absolute analysis because the shape of the excitation function suffers less from systematic errors than does its magnitude.

J. Rutherford Scattering

Ions incident upon a target may be deflected from the beam line by collisions with target nuclei. The number of particles scattered from the beam, their geometrical distribution, and their energy change must be calculated both for proper placement of particle detectors for beam energy measurement and for determining convenient geometrical arrangement of degrader foils and targets. Figure 3 shows the percent change in the incident energy of Rutherford scattered ^{3}He ions as a function of the laboratory angle through which the beam is deflected by a single collision in gold and aluminum scattering foils. The angular dependence of the number of particles scattered by those materials which would pass through a detector whose surface area is 1 cm^2 placed 20 cm from a 1 mg/cm^2 scattering foil is shown in Fig. 4 for several incident energies. An incident ion beam intensity of 1μA (1.87×10^{14} ^{3}He/min) is assumed.

At low bombarding energies the number of particles deflected through small angles may exceed the count-rate capacity of solid-state particle detectors, while large angle scattering produces significant energy change. Reduction in intensity of these scattered particles may be accomplished by use of thinner scattering foils, collimators in front of the detector, and increased distance between the detector and the foil.

The number of ^{3}He ions in the incident beam which might be lost by scattering from beam degraders placed more than a few cm upstream from the target or Faraday cup may also be estimated from Fig. 4. The total number of particles scattered through 6 degrees from the beam line, integrated for all angles about the beam line, is about ten times the value shown in Fig. 4. For higher energy beam (>15 MeV), the scattering

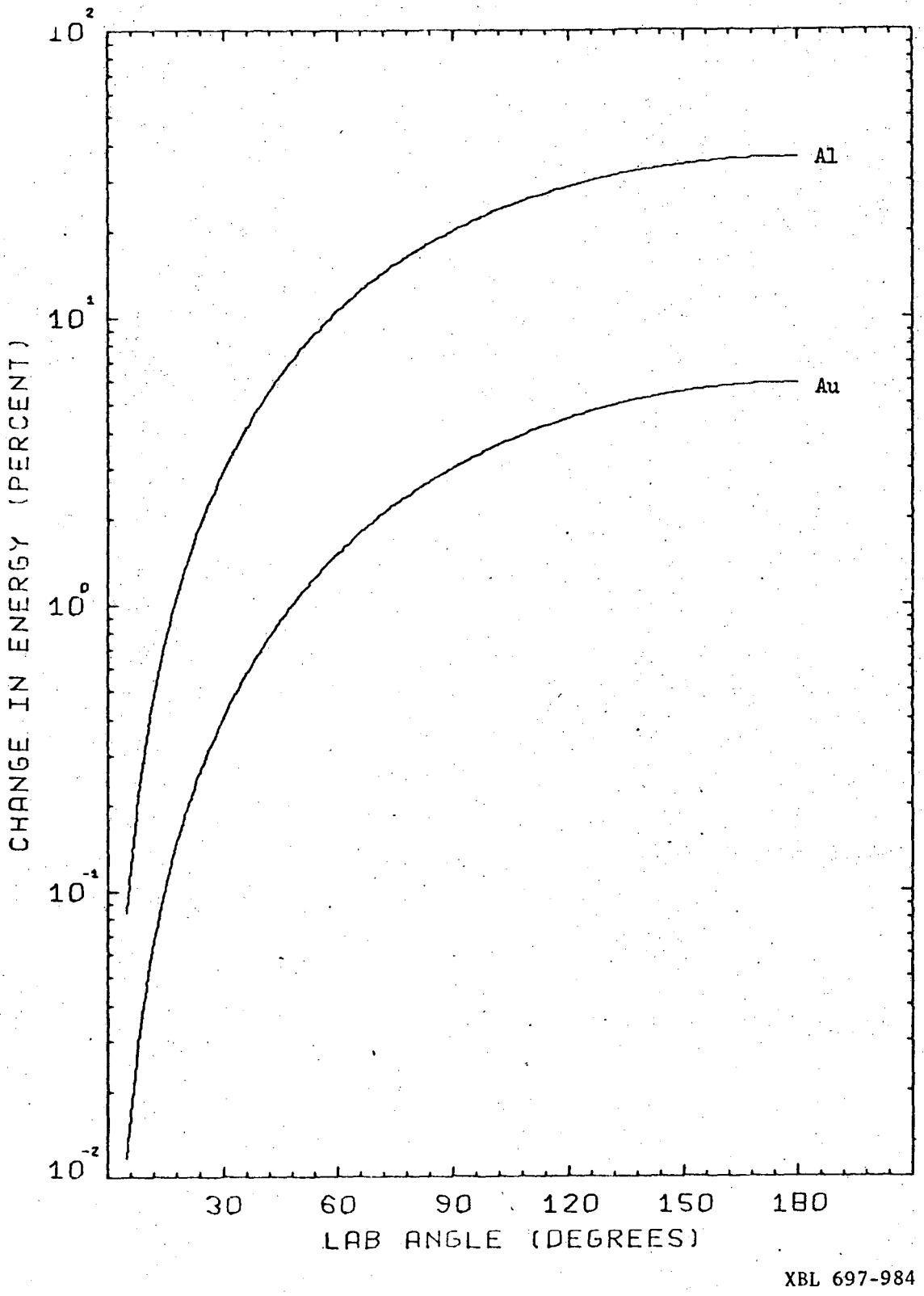

Fig. 3. Energy loss of accelerated $^3He^{++}$ ions by Rutherford scattering from Au and Al foils.

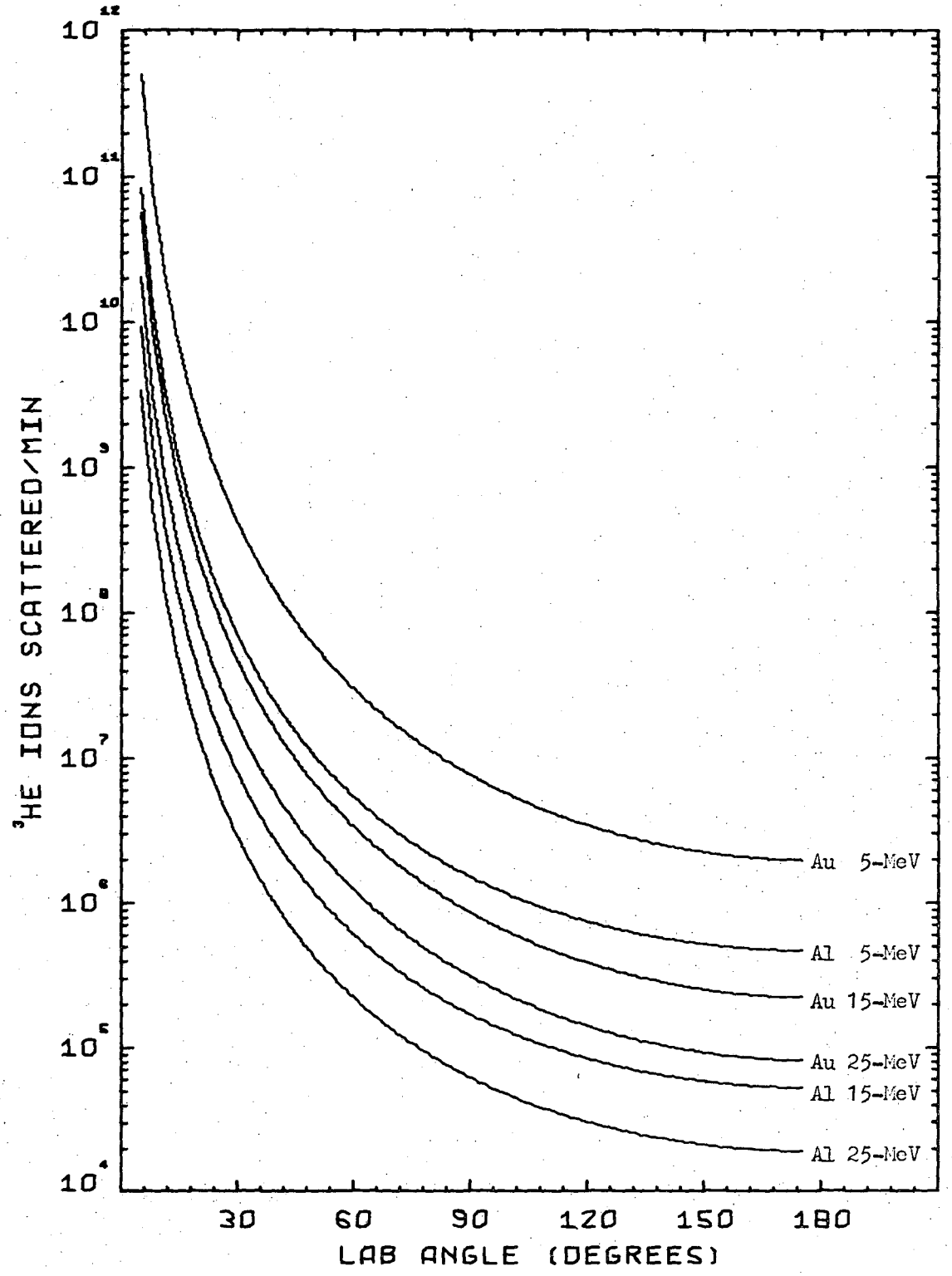

Fig. 4. Angular dependence of the number of $^3He^{++}$ ions Rutherford scattered from Au and Al at various incident energies. I = 1μA.

loss is negligible; but for a low energy bombardment, with degraders placed about 10 cm upstream, for example, from a 1 inch diameter target, a loss in intensity of the 3/8-in collimated beam of 10-15% is incurred. Targets are usually arranged to minimize distances between degraders, targets, and charge collectors.

III. EXPERIMENTAL EQUIPMENT

A. Accelerators

Nuclear analytical techniques employing the activation principle; that is, techniques in which a sample is bombarded with particles and the reaction products detected after the beam is switched off, may be performed using almost any type of particle accelerator that can supply (preferably external) ion beams of sufficient energy and intensity. Other techniques which may involve direct detection of reaction products, emitted particles, or prompt radiation, often have limitations imposed by the design characteristics of the accelerator. The large accelerators such as the Berkeley Heavy Ion Linear Accelerator (Hilac) and the 88-inch Variable Energy Cyclotron supply external $^{3}He^{++}$ ion beams whose energies are above about 30 MeV. At this energy even the heavy elements usually used for beam collimation undergo nuclear reactions with appreciable cross sections. These reactions include $(^{3}He,xn)$ reactions where x may be as high as 3 or 4 (see Sec. IV). Thus the higher energy accelerators impose a condition of high neutron background surrounding the bombardment apparatus. This neutron background severely

damages radiation detectors placed too near the target so that routine "in beam" analyses are unattractive. The new 27-inch ^{3}He cyclotron should not suffer from such limitations since its full energy beam of less than 18 MeV is below the Coulomb barrier to penetration of the tantalum nucleus. Because the small cyclotron is, at this writing, not available for more than very limited experimental use, this work is exclusively confined to activation techniques. All three of the Berkeley accelerators mentioned above have been used during these experiments.

The design characteristics of these accelerators have been previously described.[38,39,11] The Hilac, which was used throughout most of this work, supplies a pulsed beam of $^{3}He^{++}$ ions of 2 msec duration at the rate of about 15 pulses per sec. The beam energy is fixed at 31.2 ± 0.6 MeV. The 88-inch cyclotron supplies an external beam whose lowest available energy is about 30 MeV with energy resolution of about 0.14%. The 27-inch ^{3}He cyclotron produces an external beam of $^{3}He^{++}$ ions whose energy is about 18 MeV. A beam current of up to 10 μA should be obtainable.

B. Bombardment Appparatus

The bombardment apparatus used throughout most of this work, shown in Fig. 5, consists of a welded aluminum vacuum chamber with lucite viewports, at the upstream end of which is the 3/8-inch bore tantalum front collimator. An initial 3/8-inch diameter tantalum beam collimator, not shown, is mounted within the beam pipe about 10 cm upstream from the bombardment chamber. At the downstream end of the front collimator assembly is the monitor foil which is insulated from

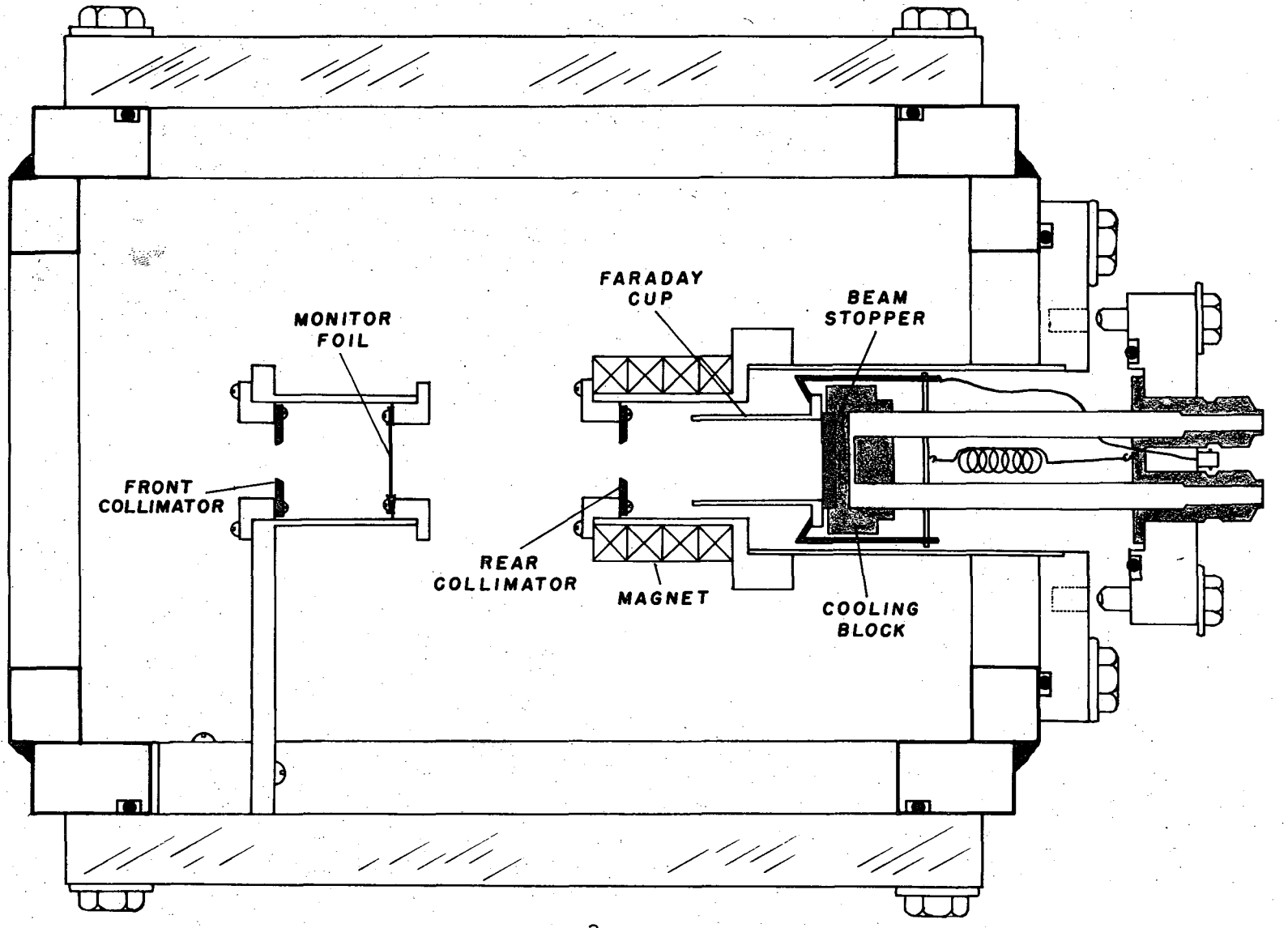

Fig. 5. Bombardment chamber for ^{3}He activation analysis. The combination Faraday Cup-target holder is shown partially withdrawn. The target (not shown) is held in position between the Faraday Cup and the beam stopper by spring tension. XBL 697-1038

its surroundings and connected to an integrating electrometer. In the space between the monitor foil and the 3/8-in-bore tantalum rear collimator may be placed an optional sample holder such as the assembly shown in Fig. 6. The combination sample holder-Faraday cup, pictured partially withdrawn from the chamber in Fig. 5, is connected to a second integrating electrometer. The electrometers used were designed by D. A. Landis[40] and built at this Laboratory. The charge collection efficiency of the Faraday cup was calibrated by attaching a 1.0186 V Weston standard cell directly to the Faraday cup body. Precision resistors were used to vary the currect for electrometer readings on the various scales.

The target holder-Faraday cup was designed to incorporate fairly rapid sample retrieval with the precision and accuracy afforded by in-cup bombardment. Removal of an irradiated sample from the chamber, initially at accelerator vacuum,may be accomplished within 10-15 sec. Surrounding the cup body, when the assembly is locked into place within the chamber, is a magnet whose field serves to deflect away from the cup any electrons produced upstream as the beam strikes foils, residual gas, and collimators and to retain any electrons which might be ejected from the target. The magnet field strength necessary was prescribed by the distance from the rear collimator to the cup body (1 cm) and calculated for maximum ejected electron energy, E_e, given by[1]

$$E_e \approx 4\left(\frac{m}{M}\right) E_{^3He} \qquad (19)$$

where m and M are the masses of the electron and ^3He ion, respectively,

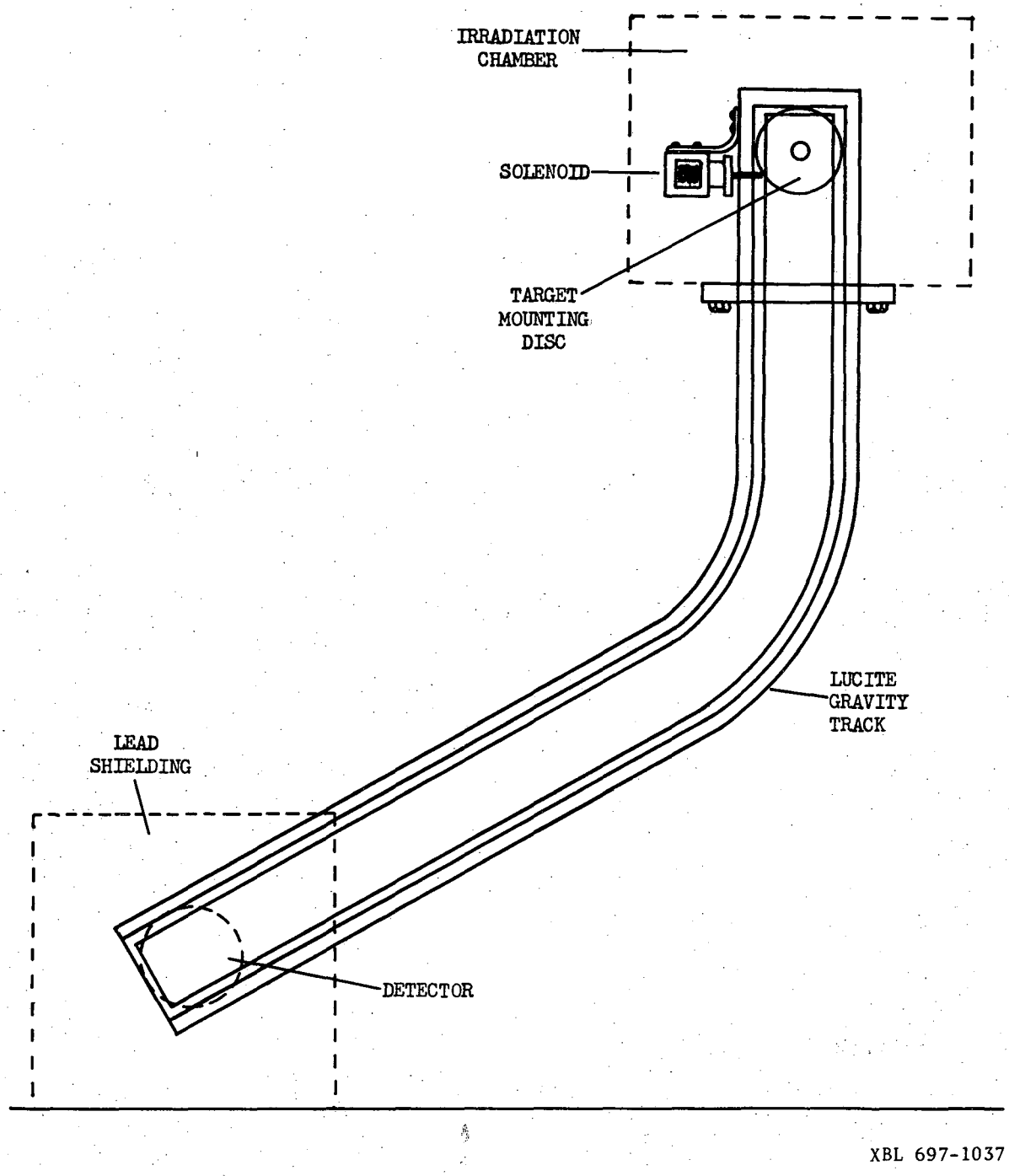

Fig. 6. Optional gravity-track sample holder used for rapid retrieval of an activated target.

and $E_{^3He}$ is the bombarding energy. For a 30 MeV $^3He^{++}$ beam, E_e is about 22 keV. The field strength necessary to deflect an electron of this energy into a curved path of radius 1 cm is about 500 gauss.

The sample, with any necessary cover foils and beam energy degraders, is held in place between the stainless-steel cup body and the tantalum beam-stopper by spring tension. The beam-stopper, targets, and cup body are conduction cooled by water flow through the copper cooling block. The amount of cooling necessary is determined by the power deposited by the beam, which is 1 watt per microamp per MeV of energy lost in traversing the target. A thick target which is a poor heat conductor will heat at the rate of about 0.24 cal per sec per microamp for each MeV of degradation so that such a target, which completely stops an incident 20-30 MeV beam, could undergo a localized temperature increase of several hundred degrees per minute. In practice, 1/4 to 1/2 mil plastic foils have been bombarded for 30 minutes in this apparatus without charring at beam currents up to several tenths of a microamp at energies of 10-20 MeV.

For irradiations in which the half-life of the activity to be detected was less than about 30 sec the optional sample holder shown in Fig. 6 was used. In this case a 1 mil aluminum vacuum foil separates the accelerator from the atmosphere within the chamber, which is natural helium gas flowing at a low leak-rate. The helium atmosphere allows fast sample removal without breaking the accelerator vacuum, with negligible scattering or degrading of the $^3He^{++}$ ion beam. The target is mounted over the 0.75-in diameter centerhole of an aluminum disc held in place, during bombardment, by a pin attached to the solenoid. At the termination

of the bombardment the solenoid is activated, releasing the pin, and the disc to which the target is affixed rolls down the plastic gravity track to the shielded detector. This apparatus allows counting to begin within a few seconds after bombardment.

The beam current may not be measured directly during irradiations performed using the gravity track sample holder because the beam is partially stopped or scattered away from the Faraday cup by the target. The beam current is measured, in this case, by the monitor foil. As the ion beam passes through the 0.25 mil aluminum monitor foil, many of the electrons knocked out by primary and secondary collisions escape to the surroundings, leaving the foil positively charged. The rate of electron loss is proportional to the incident beam intensity so that an integrating electrometer connected to the monitor foil will provide a relative measurement of beam current. The monitor is calibrated by allowing the beam to pass through an empty sample-holder into the Faraday cup, which is connected to a second integrating electrometer. The monitor foil must be placed upstream from any degrader foils to prevent erroneous electron pickup. Therefore, the ratio of the integrator readings, monitor foil: Faraday cup, will increase as the thickness of degrader foils increases due to Rutherford scattering losses at decreased beam energy. Experimentally, the foil : cup ratios vary smoothly from about 1.4 : 1 at 30 MeV to about 2 : 1 at 5 MeV.

C. Detection Equipment

The parallel development of high-resolution lithium-drifted germanium gamma-ray detectors, associated electronics equipment, pulse-height analyzers, and computerized data-reduction systems has made possible the non-destructive measurement of all cross section and analytical data presented in this report. The radiation counting equipment will be described in this section and data treatment in the next section.

1. Gamma-ray detectors.

a. Ge(Li). There is extensive literature available concerning the fabrication and operating characteristics of the Ge(Li) semiconductor γ-ray detectors[41] and their application to nuclear spectroscopy[42,43] and activation analysis.[6,7,8,9] In the experiments described in this report planar detectors having active volumes of 16 cm^3 and 6 cm^3 were used. The resolutions of these detectors were about 2.5 keV and 6 keV (full width at half maximum), respectively, for the 1332-keV γ-ray line from ^{60}Co. The detector systems were designed and built at this Laboratory.

b. NaI(Tl). Sodium iodide scintillation detectors were used to obtain high-energy γ-ray spectra, to measure clearly resolved γ-ray photopeaks at lower energy, and in conjunction with γ-γ coincidence measurements. The detectors used were 3-in × 3-in diameter Harshaw integrally-mounted units having energy resolutions of about 50-keV(FWHM) for the 662-keV γ-ray line from ^{137}Cs.

2. Associated electronics and analyzers.

Linear amplifier-biased amplifier systems designed by Goulding and Landis[44] and built at this Laboratory were used with both Ge(Li) and

NaI(Tl) detectors. The amplifier signals were routed to either a 400-channel R.I.D.L.[45] or a 1024-channel Northern Scientific[46] pulse-height analyzer for singles spectra.

Activities whose half-lives were less than about 30 sec were detected using the circuitry shown in the block diagram of Fig. 7. The amplified signals from two detectors, mixed to increase detection efficiency, were routed to a single-channel analyzer adjusted to cover only the spectral region of the photopeak. The single-channel signals were stored in the pulse-height analyzer operated in time mode as a multichannel scaler. Scaling pulses were generated by the switch-programmed Time Base Oscillator (TIBO) designed by K. B. Russell[47] and built at this Laboratory. The TIBO may be programmed to allow storage of detector signals during intervals from 10 μsec to 16.5 min with scaling intervals adjustable over the same time range. The complete range of each interval selector is divided into 7 decades with 99 positions per decade. Signal storage may be inhibited during the scaling interval or data accumulation may proceed for a maximum counting interval of 33 min between scaling pulses. A decay curve of the activated target was automatically obtained with this apparatus.

Because most of the products of ^{3}He induced nuclear reactions with light elements are neutron deficient and therefore decay predominately by positron emission, a simple coincidence circuit such as that shown in the block diagram in Fig. 8 may be used. The annihilation of positrons emitted by the activated target results in simultaneous emission of two 511-keV photons directed 180° with respect to each other. The

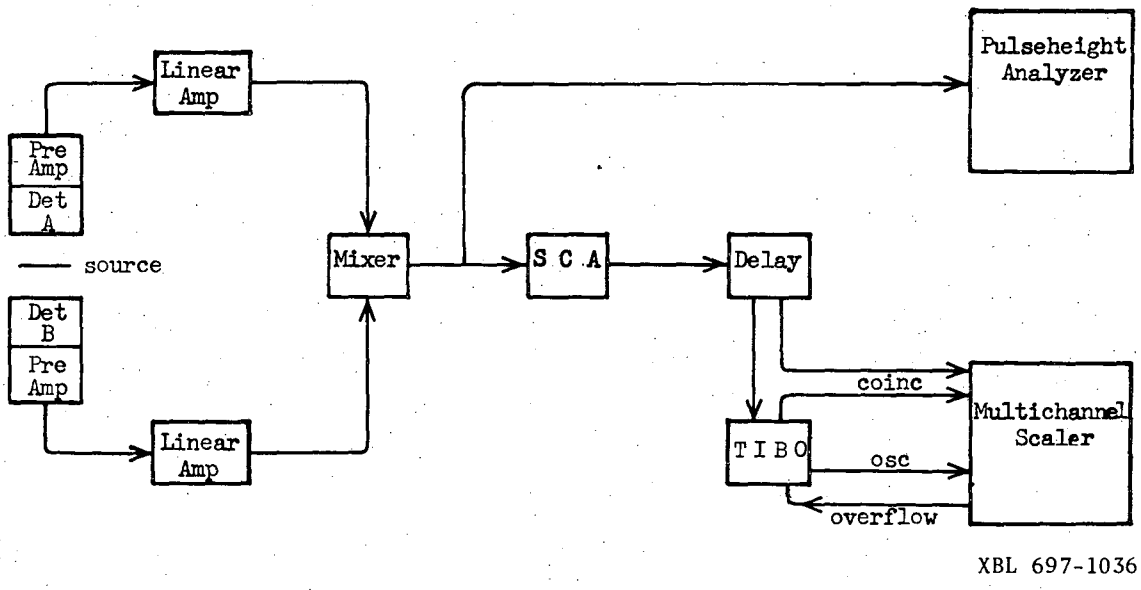

Fig. 7. Block diagram of time-mode multiscaler system.

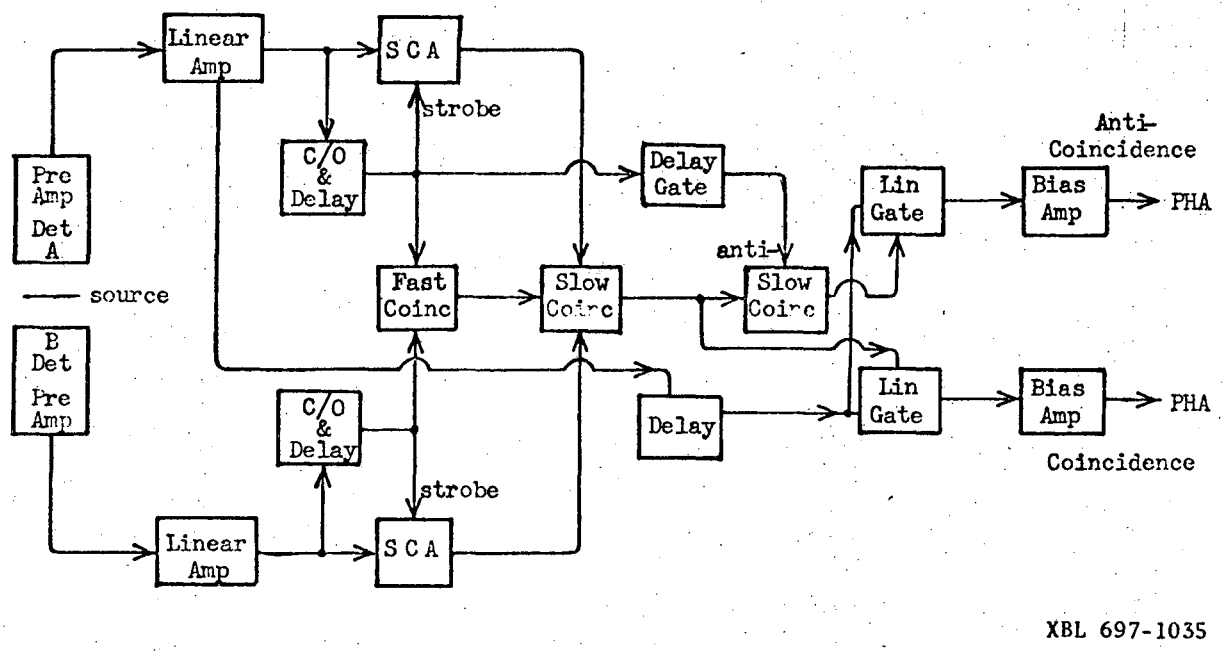

Fig. 8. Block diagram of coincidence-anticoincidence counting system.

true coincidence rate of the 511-keV photons striking identical detectors placed in mirror geometry about a fully annihilated positron source is very nearly 100% of the maximum obtainable with the particular detector geometry. The single-channel analyzer associated with detector B may be adjusted to transmit signals corresponding to γ-ray energies of 511-keV or less while the single-channel analyzer associated with detector A covers only the region of the 511-keV photopeak. In this way a coincidence rate of 70-80% of the detector A singles rate may be obtained which results in efficient measurement of the annihilation radiation almost background free.

The anticoincidence portion of the circuit of Fig. 8 is designed to increase the sensitivity of non-destructive measurement of γ-ray lines whose energies are less than 511-keV and not in coincidence with emitted positrons by removing much of the detected partial energy radiation resulting from Compton interactions. This Compton distribution, which is very high because of the preponderance of β^+ emitters in the activated sample, often obscures lower energy photopeaks in the spectra. A Ge(Li) detector is used as detector A and a more efficient NaI(Tl) detector as detector B. The signal from the NaI(Tl) detector serves to block transmission of any Ge(Li) signal arising during the 110-nsec coincidence resolving time. The efficiency of detection of the Ge(Li) detector for < 511 keV photons is virtually unaffected, while the height of the Compton distribution has been reduced by a factor of about 4. The effect on analytical sensitivity of this lessening of the background beneath a photopeak is discussed in a later section.

3. Detector calibration.

In all experiments the photopeak efficiencies of the γ-ray spectrometers were calibrated using a set of eight absolute γ-ray standards, obtained from the IAEA Laboratories,[48] whose activities were accurate within ±1%. The γ-ray energies of the standards cover the energy range 60-1836-keV. Gamma-ray energy and relative intensity data for the standard sources were obtained from Haverfield,[49] while other γ-ray energy and relative intensity data were taken from the Table of Isotopes.[50] The ranges of photopeak efficiency for the detectors with the sources placed 1 cm from the face of the detector were:

$$\begin{aligned} 16\ \text{cm}^3\ \text{Ge(Li)} - 1.25 \times 10^{-3} &\text{ at 1332-keV } (^{60}\text{Co}) \text{ to} \\ 4.5 \times 10^{-2} &\text{ at 122-keV } (^{57}\text{Co}) \\ 6\ \text{cm}^3\ \text{Ge(Li)} - 6.1 \times 10^{-4} &\text{ at 1332-keV } (^{60}\text{Co}) \text{ to} \\ 3.0 \times 10^{-2} &\text{ at 122-keV } (^{57}\text{Co}) \\ 3"\ 3"\ \text{NaI(Tl)} - 2.3 \times 10^{-2} &\text{ at 1836-keV } (^{88}\text{Y}) \text{ to} \\ 7.3 \times 10^{-2} &\text{ at 511-keV } (^{22}\text{Na}). \end{aligned}$$

The photopeak efficiency for 511-keV annihilation radiation detected using the coincidence apparatus (Fig. 8) with two NaI(Tl) detectors 2.5 cm from the source was 2.1×10^{-2}. This efficiency was determined with both single channel analyzers adjusted to transmit signals arising from the spectral region of the 511-keV photopeak only and represents approximately 43% of the photopeak efficiency for the singles spectrum.

D. Data Treatment

All excitation functions and analyses presented in this report were calculated from nondestructive measurements of the γ-ray spectra of activated targets. The data reduction procedures consisted of spectrum analysis, decay curve resolution, and mathematical treatment of the resulting activity data by the methods outlined in Sec. II.

1. Spectrum analysis.

Because high-resolution Ge(Li) γ-ray detectors were available for measurement of all complicated spectra, hand photopeak-area calculation by the method discussed by Haverfield[49] was extensively used. In this method the background counts beneath the photopeak are defined by averaging the number of counts in the channel corresponding to the maximum radius of curvature (linear plot) on the photopeak's low energy tail and the number of counts in the channel corresponding to its high energy base, and then multiplying this average by the number of channels falling between these limits. The resulting photopeak above this background base is a gaussian shape with an exponential tail. Haverfield has found the method to be consistent to within 1-1.5%.

For some later experiments, automatic data recording equipment was available so that spectrum analysis could be conveniently performed by a computer code. The FORTRAN IV code SAMPO, developed by Routti and Prussin[51] for the CDC 6600 computer, has been used. A detailed discussion of the experimental use of this code is given by Bernthal.[78]

2. Decay curve resolution.

Exponential decay curves of product activities were resolved by a

least squares computer code. Two codes have been used, RAD[52] and CLSQ,[53] modified for use with the CDC 6600 computer system. The RAD code requires parameter estimates for both the half-lives of the components and their A_o values while CLSQ requires estimates of half-lives only. Both codes successfully treat decay curves of up to 10 components whose half-lives differ by at least a factor of two and yield iterative solutions for half-lives, A_o values, and standard deviations in the fitted parameters.

3. Errors.

There are many sources of systematic error in nuclear reaction measurements, most of which can be made quite small. Among the errors which are, or can be held to, less than about 1%, are weighing, time measurement, integrating electrometer calibration, half-life data, and decay scheme correction. Decay scheme errors may be somewhat larger, especially in older data obtained before high-resolution γ-ray spectrometers became available. Calibration of spectrometers may be accomplished to within about 2-2.5% using absolutely calibrated 1% γ-ray standards. The variation in uniformity of the target with respect to the collimated incident beam may be about 1% for most targets; but with some plastics and targets prepared by sedimentation it may be as high as about 5%.

Statistical counting errors and decay curve analysis errors probably are the chief contributors to the total error in cross section. For nondestructive measurement the statistical counting error is determined from the standard deviation given by

$$\text{std dev} = \sqrt{\sigma_t^2 + \sigma_b^2} \qquad (20)$$

where σ_t is the standard deviation in measurement of the total number of counts between the defining limits of the photopeak, and σ_b is the standard deviation in measurement of the spectrum background beneath the photopeak. Since the standard deviations σ_t and σ_b are given by

$$\sigma_t = \sqrt{N_t} \qquad \text{and} \qquad \sigma_b = \sqrt{N_b} \tag{21}$$

where N_t and N_b are the numbers of counts in total photopeak and background beneath the photopeak, respectively, the standard deviation can be written[8]

$$\text{std dev} = \sqrt{N_p + 2N_b} \quad . \tag{22}$$

Here, N_t has been replaced by $N_p + N_b$, where N_p is the number of counts in the photopeak after the background has been subtracted.

The decay curve analysis errors are very small for single component exponential decays, but may be quite large for minor constituents of multicomponent systems. The standard deviations obtained as output from the least squares programs have been used to estimate these errors.

The total propagated error can then be estimated by

$$\text{error} \approx \sqrt{\sigma_S^2 + \sigma_P^2 + \sigma_D^2} \tag{23}$$

where the subscripts S, P, D, signify the sum of squares of small errors (weighing, time measurement, electrometer calibration, etc.) photopeak

counting statistical error, and decay curve analysis error, respectively. The total error for a measurement to within 10% accuracy for both photopeak and decay curve resolution would be about ±15%.

IV. ^{3}He INDUCED REACTIONS

A convenient compilation of excitation functions and reaction data is presented in this section for the ^{3}He induced nuclear reactions studied in this work and for those in the literature, followed by a discussion of the trends in the activation data in relation to activation analysis.

The data are arranged in order of target atomic number with a tabular summary of possible reactions, radiations emitted, and interferences preceding the experimental excitation functions. Unambiguous reactions; that is, reactions which involve the formation of a particular product nuclide through a single reaction of a specific target nuclide, are listed with the mass number of the target (e.g., ^{9}Be(^{3}He,n)^{11}C), while the formation of a product nuclide via the sum of reactions which may involve several different target isotopes are listed as total production excitation functions or by reaction equations such as ^{3}He + Si → ^{30}P. The target isotopic abundances and the product half life, decay mode, γ-ray energy, and percent γ-ray per decay were taken from the Table of Isotopes.[50] The interferences listed are energetically possible ^{3}He induced reactions with stable isotopes of other elements which may

result in the same product as the target at bombarding energies below about 30-MeV. These interferences may be minimized by proper choice of incident energy and length of bombardment by referring to reaction data for the interfering nuclides themselves, if such data are available, or by estimating the behavior of their excitation functions on the basis of reaction type (see Sec. IV.S), energy threshold, and Coulomb barrier. The excitation functions from the literature have been redrawn without experimental points and error estimates. Data smoothing follows, as closely as possible, each author's interpretation. Discussion of individual reactions is limited to any unusual features in the data and to error estimates. Numbers labeling individual excitation functions in the figures correspond to reference numbers in the discussion.

Our own experimental data are treated similarly, with the exceptions that experimental points are shown in the excitation functions and that a detailed discussion of the experimental procedures is included.

All excitation functions have been drawn to the same scale to permit convenient comparison. It must be kept in mind, when comparing data among different authors, that some apparent disagreement may arise from variations in beam inhomogeniety and from use of different range-energy data.

A. BERYLLIUM

Figure 9

$^{9}Be(^{3}He,n)^{11}C$

1. Hahn and Ricci[54]
2. Hahn and Ricci[55]
3. Markowitz and Hall[56]
4. Brill'57

The estimated errors in σ are 10% for Hahn and Ricci(1), 15% for Hahn and Ricci(2), and 25% for Brill'(4). Markowitz and Hall(3) indicated a large uncertainty in their energy scale below about 10 MeV because of the inadequacy of available range-energy data.

The excitation function of Brill'(4) is approximately an order of magnitude lower than that of Markowitz and Hall(3) but of quite similar shape. In view of the fair agreement between the other workers at energies below about 15 MeV, it seems reasonable to suspect a power of ten error in the data of Brill'. It must be noted that this reaction has the highest cross-section of the (^{3}He,n) reactions studied.

Hahn and Ricci(2) calculated the excitation function by numerical differentiation of thick target yield curves. At increasing energies above that of maximum cross section, the differentiation data is more subject to error because the increments in bombarding energy produce smaller increments in total activity.

It will become apparent as the data in this section are compared that curves 3 and 4 have shapes quite typical of this type of reaction.

Table I. Reactions induced in Be by ^{3}He ion bombardment. Isotopic abundance: ^{9}Be(100%)

Product	Reactions	Q(MeV)[a]	$T_{1/2}$[b]	Decay[b]	Associated γ-rays[b] keV(% per decay)	Interferences[c]
^{11}C	$^{9}Be(^{3}He,n)$	7.56	20.3m	$\beta^{+}EC$	511(200)	$^{10}B(^{3}He,pn)^{11}C$
						$^{11}B(^{3}He,p2n)^{11}C$
						$^{12}C(^{3}He,\alpha)^{11}C$
						$^{16}O(^{3}He,2\alpha)^{11}C$
^{10}C	$^{9}Be(^{3}He,2n)$	-5.52	19.4s	β^{+}	511(200), 717(100), 1023(1.7)	$^{10}B(^{3}He,p2n)^{10}C$
						$^{12}C(^{3}He,\alpha n)^{10}C$
^{7}Be	$^{9}Be(^{3}He,\alpha n)$	0.01	53 d	EC	477(10.3)	$^{6}Li(^{3}He,pn)^{7}Be$
						$^{7}Li(^{3}He,p2n)^{7}Be$
						$^{12}C(^{3}He,2\alpha)^{7}Be$

[a] Appendix B

[b] Reference 50

[c] Interferences are ^{3}He induced reactions with other elements which may lead to the same product at bombarding energies below about 30 MeV.

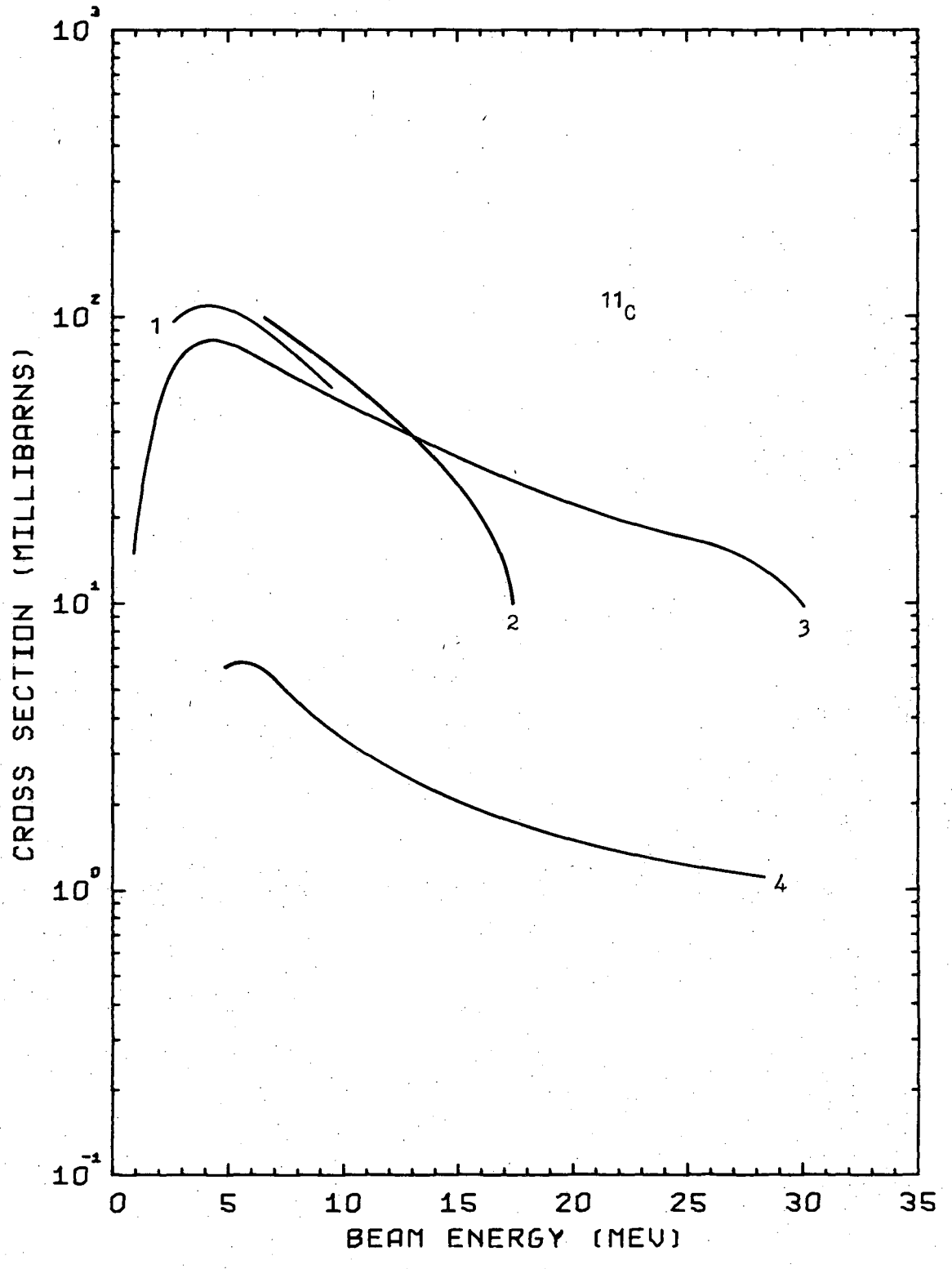

Fig. 9. Excitation function for $^{9}Be(^{3}He,n)^{11}C$. The numbers refer to references given in the text.

B. BORON Figure 10

$^{10}B(^{3}He,pn)^{11}C$	1. Patterson[58]
	2. Hahn and Ricci[55]
	3. Brill',[57]
Total B + $^{3}He \rightarrow {}^{11}C$	4. Hahn and Ricci[55]
$^{11}B(^{3}He,p2n)^{11}C$	5. Brill',[57]
$^{11}B(^{3}He,n)^{13}N$	Hahn and Ricci[55]

Estimated errors in σ are 30% for curve 1, 25% for curves 3 and 5, 15% for curves 2 and 4, and 45% for ^{13}N. The functions of Hahn and Ricci are calculated by numerical differentiation of thick target yields and show a sharper decrease with increasing energy than does the curve of Brill', just as in the Be functions previously discussed. Here, there is no reason to prefer either set of data. Curve 4 represents the total production of ^{11}C from ^{3}He + B. Weighted averaging of curves 3 and 5 of Brill' produce a total-production ^{11}C excitation function which agrees very well with curve 4 at about 9 MeV but remains substantially higher at higher energies.

Din and Weil[59] have obtained excitation function data at energies below about 5 MeV (not shown) by integration of the angular distributions of $^{11}B(^{3}He,n_{o})^{13}N$. Their data passes through a maximum of about 40 mb at about 4.5 MeV with an estimated error of less than 30%.

Table II. Reactions induced in B by ^{3}He ion bombardment. Isotopic abundance: $^{10}B(19.7\%)$, $^{11}B(80.3\%)$

Product	Reactions	Q(MeV)[a]	$T_{1/2}$[b]	Decay[b]	Associated γ-rays[b] keV(% per decay)	Interferences[c]
^{11}C	$^{10}B(^{3}He,pn)$	0.97	20.3m	β^{+},EC	511(200)	$^{9}Be(^{3}He,n)^{11}C$
	$^{11}B(^{3}He,p2n)$	-10.48				$^{12}C(^{3}He,\alpha)^{11}C$
						$^{16}O(^{3}He,2\alpha)^{11}C$
^{10}C	$10^{b}(^{3}He,p2n)$	-12.11	19.4s	β^{+}	511(200), 717(100), 1023(1.7)	$^{9}Be(^{3}He,2n)^{10}C$
						$^{12}C(^{3}He,\alpha n)^{10}C$
^{13}N	$^{11}B(^{3}He,n)$	10.18	10m	β^{+}	511(200)	$^{12}C(^{3}He,pn)^{13}N$
						$^{13}C(^{3}He,p2n)^{13}N$
						$^{14}N(^{3}He,\alpha)^{13}N$
						$^{15}N(^{3}He,\alpha n)^{13}N$

[a] Appendix B

[b] Reference 50

[c] Interferences are ^{3}He induced reactions with other elements which may lead to the same product at bombarding energies below about 30 MeV.

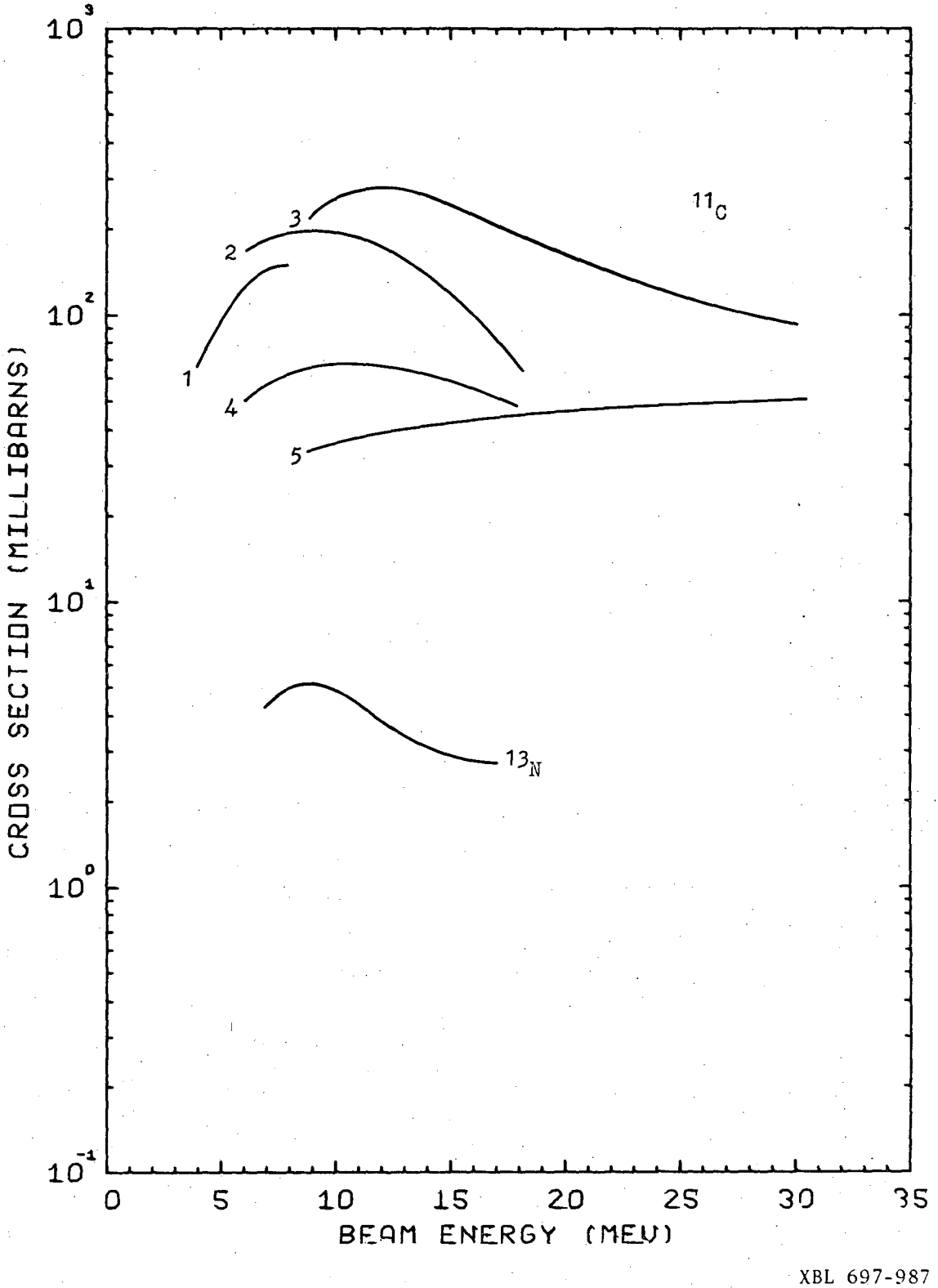

Fig. 10. Excitation functions for $^{10}B(^{3}He,pn)^{11}C$ (1,2,3), total $B + {}^{3}He \rightarrow {}^{11}C$ (4), $^{11}B(^{3}He,p2n)^{11}C$ (5), and $^{11}B(^{3}He,n)^{13}N$. The numbers refer to references given in the text.

C. CARBON

Figure 11
Figure 12

$^{12}C(^{3}He,\alpha)^{11}C$

$^{12}C(^{3}He,d)^{13}N$

1. Markowitz and Hall[56]
2. Markowitz and Mahony[10]
3. Brill'[57]
4. Cochran and Knight[60]
5. Hahn and Ricci[54]

Cirilov[35] and Gorodetzky, et al[68] (not shown)

Estimated errors in σ are given as ±5% in curve 2, ±8% in curve 4, ±10% in curve 5, and ±25% in curve 3. The agreement among the various functions is fairly good above about 10 MeV for both ^{11}C and ^{13}N. The energy scale of Markowitz and Hall is in error below this energy. The data of Cochran and Knight show the presence of maxima and minima in the excitation functions of both ^{11}C and ^{13}N. Presumably, poor beam-energy resolution precluded observation of any resonance structure by other workers.

The production of ^{13}N has been attributed to a $(^{3}He,d)$ reaction because the threshold for this reaction is only 4.4 MeV while that for a $(^{3}He,pn)$ reaction is 7.2 MeV.

C. CARBON (Cont) Figure 13

$^{12}C(^{3}He,n)^{14}O$	1. Hahn and Ricci[54] Osgood[34] and Cirilov[35] (not shown)
$^{12}C(^{3}He,2\alpha)^{7}Be$	2. Cochran and Knight[60]

Error estimates are 10-13% for the ^{14}O data and ≈15% for ^{7}Be. The structure of the ^{14}O function of Hahn and Ricci agrees well with that of Osgood (not shown) but is lower by a factor of 2.4. The difference is assumed to be attributable to systematic errors.

Table III. Reactions induced in C by ^{3}He ion bombardment. Isotopic abundance: ^{12}C(98.89%), ^{13}C(1.11%)

Product	Reactions	Q(MeV)[a]	$T_{1/2}$[b]	Decay[b]	Associated γ-rays[b] keV(% per decay)	Interferences[c]
^{14}O	$^{12}C(^{3}He,n)$	-1.15	71s	β^+	511(200), 2312(99)	$^{14}N(^{3}He,p2n)^{14}O$
	$^{13}C(^{3}He,2n)$	-6.09				$^{16}O(^{3}He,\alpha n)^{14}O$
^{13}N	$^{12}C(^{3}He,d)$	-3.55	10m	β^+	511(200)	$^{14}N(^{3}He,\alpha)^{13}N$
	$^{13}C(^{3}He,p2n)$	-10.72				$^{15}N(^{3}He,\alpha n)^{13}N$
						$^{11}B(^{3}He,n)^{13}N$
^{10}C	$^{12}C(^{3}He,\alpha n)$	-11.23	19.4s	β^+	511(200), 717(100), 1023(1.7)	$^{9}Be(^{3}He,2n)^{10}C$
						$^{10}B(^{3}He,p2n)^{10}C$
^{11}C	$^{12}C(^{3}He,\alpha)$	1.85	20.3m	β^+,EC	511(200)	$^{9}Be(^{3}He,n)^{11}C$
	$^{13}C(^{3}He,\alpha n)$	-3.09				$^{10}B(^{3}He,pn)^{11}C$
						$^{11}B(^{3}He,p2n)^{11}C$
						$^{16}O(^{3}He,2\alpha)^{11}C$
^{7}Be	$^{12}C(^{3}He,2\alpha)$	-5.69	53d	EC	477(10.3)	$^{9}Be(^{3}He,\alpha n)^{7}Be$
						$^{6}Li(^{3}He,pn)^{7}Be$
						$^{7}Li(^{3}He,p2n)^{7}Be$

[a] Appendix B

[b] Reference 50

[c] Interferences are ^{3}He induced reactions with other elements which may lead to the same product at bombarding energies below about 30 MeV.

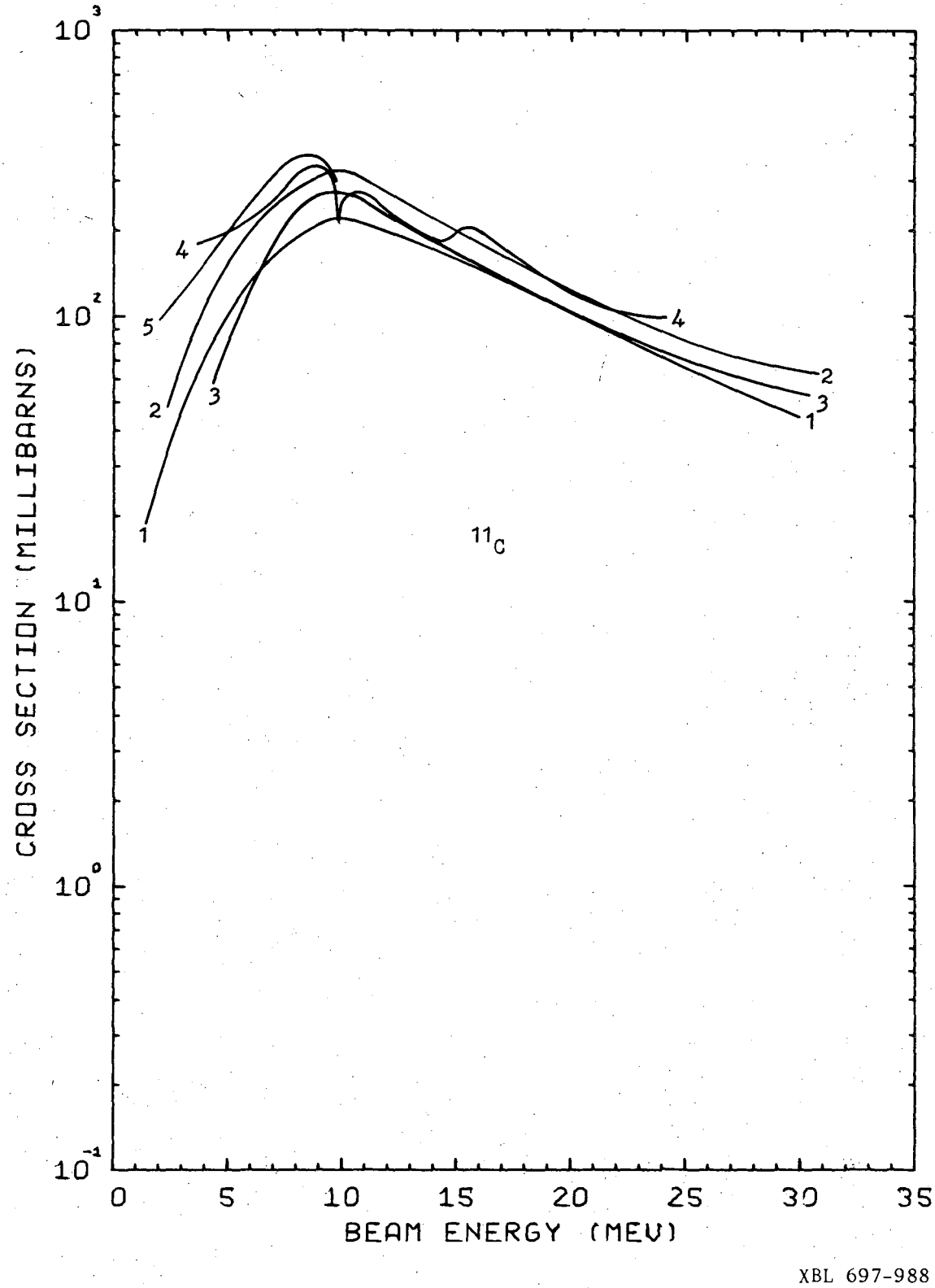

Fig. 11. Excitation function for $^{12}C(^{3}He,\alpha)^{11}C$. The numbers refer to references given in the text.

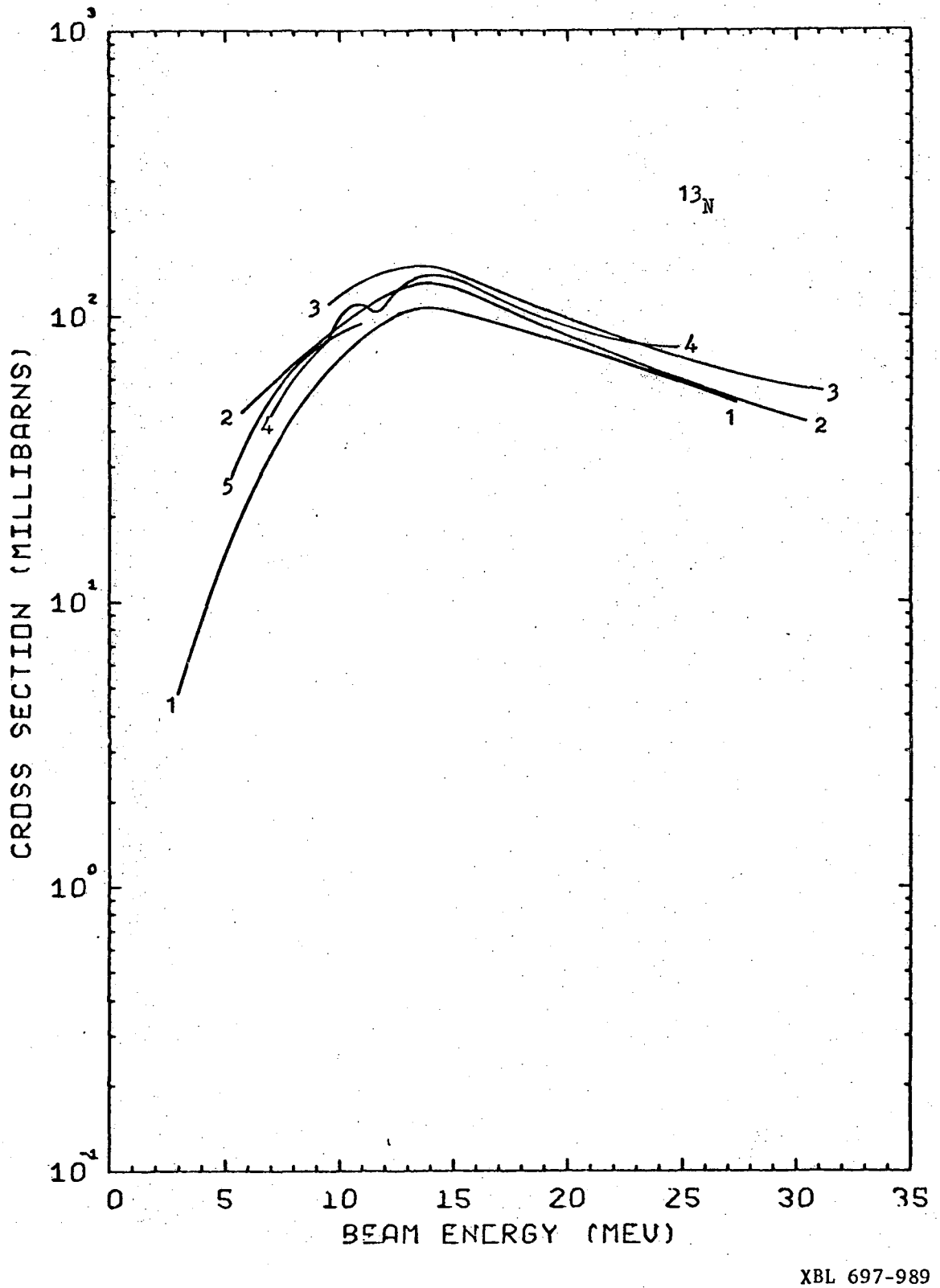

Fig. 12. Excitation function for $^{12}C(^{3}He,d)^{13}N$. The numbers refer to references given in the text.

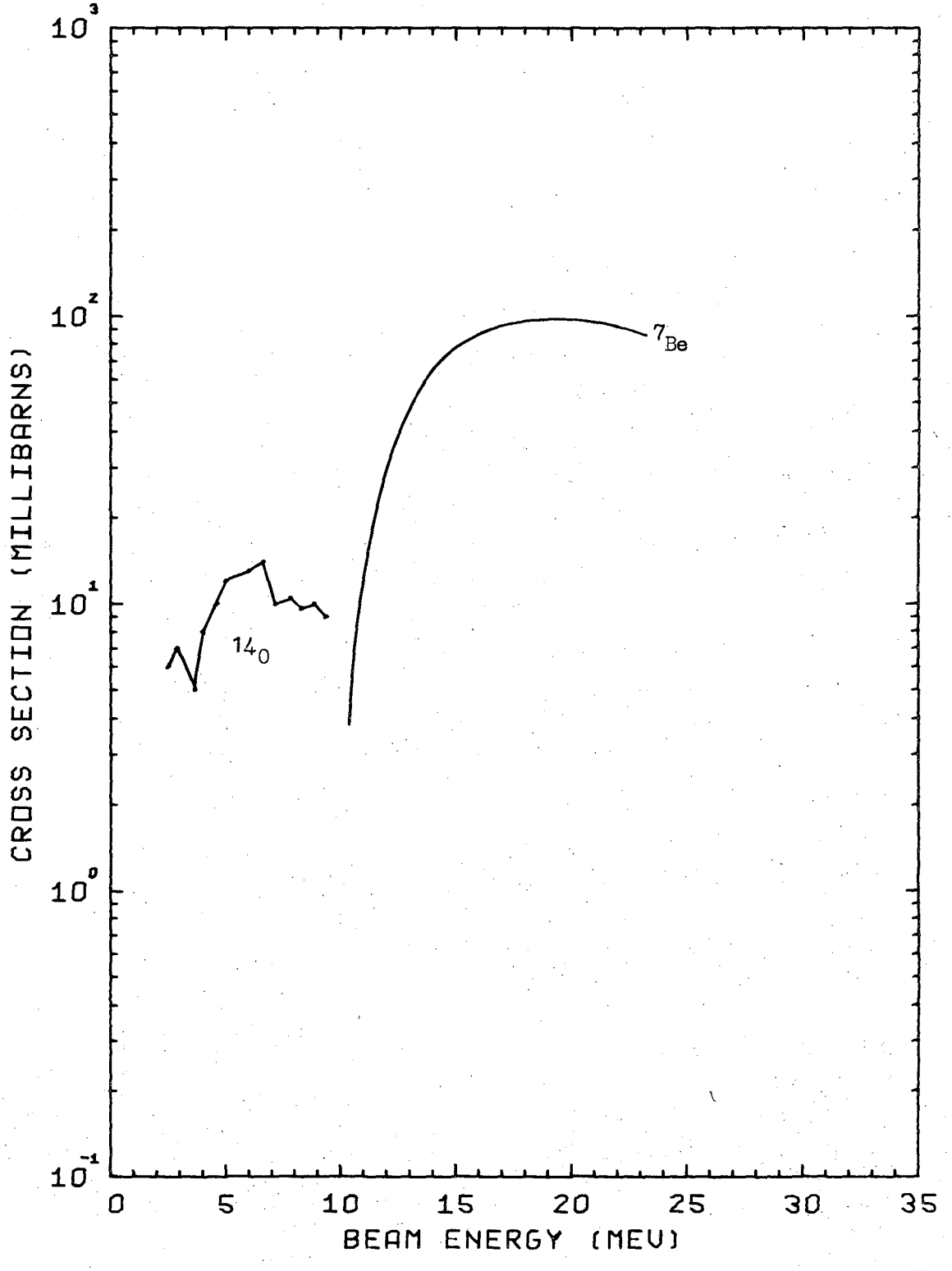

Fig. 13. Excitation functions for $^{12}C(^{3}He,n)^{14}O$ and $^{12}C(^{3}He,2\alpha)^{7}Be$. The references are given in the text.

D. NITROGEN

Figure 14

$^{14}N(^{3}He,\alpha)^{13}N$ 1. Hahn and Ricci[55]

2. Brill'[57]

$^{14}N(^{3}He,pn)^{15}O$ 3. Hahn and Ricci[55]

Estimated errors in σ are 15% for curve 1 and ^{15}O and 25% for curve 2. The data of Hahn and Ricci are calculated by numerical differentiation of thick target yields.

While curves 1 and 2 do not agree well in shape or magnitude, the trend of these excitation functions to rise through early maxima at low energy and rise again at high energy will be frequently observed in $(^{3}He,\alpha)$ reactions. There is no doubt that this shape corresponds to a change in reaction mechanism at increased energy. Brill' indicates that the principal role is probably played by inelastic scattering followed by neutron evaporation, the threshold for which is 13.8 MeV. That the preceding $^{12}C(^{3}He,\alpha)^{11}C$ excitation does not behave similarly is accounted for by the 23.4 MeV threshold for the reaction $^{3}He + {}^{14}N \rightarrow {}^{3}He + {}^{13}N + {}^{1}_{0}n$

The shape of the ^{15}O function is not similar to the $(^{3}He,d)$ functions observed in the carbon reactions. Hahn and Ricci observed that direct stripping mechanism calculations for reactions leading to states of known spin and parity in ^{15}O account for about 30% of the measured σ. It is possible that including other states might account for the remaining 70%, but it is also possible that a large contribution comes from $(^{3}He,pn)$, threshold -0.5 MeV.

Table IV. Reactions induced in N by ^{3}He ion bombardment. Isotopic abundance: ^{14}N(99.64%), ^{15}N(0.36%)

Product	Reactions	Q(MeV)[a]	$T_{1/2}$[b]	Decay[b]	Associated γ-rays[b] keV(% per decay)	Interferences[c]
^{17}F	$^{15}N(^{3}He,n)$	5.01	66.6s	β^+	511(200)	$^{16}O(^{3}He,pn)^{17}F$
						$^{17}O(^{3}He,p2n)^{17}F$
						$^{19}F(^{3}He,\alpha n)^{17}F$
^{15}O	$^{14}N(^{3}He,pn)$	-0.43	2m	β^+	511(200)	$^{13}C(^{3}He,n)^{15}O$
	$^{15}N(^{3}He,p2n)$	-11.26				$^{16}O(^{3}He,\alpha)^{15}O$
						$^{17}O(^{3}He,\alpha n)^{15}O$
^{14}O	$^{14}N(^{3}He,p2n)$	-13.64	71s	β^+	511(200), 2312(99)	$^{12}C(^{3}He,n)^{14}O$
						$^{16}O(^{3}He,\alpha n)^{14}O$
^{13}N	$^{14}N(^{3}He,\alpha)$	10.02	10m	β^+	511(200)	$^{11}B(^{3}He,n)^{13}N$
	$^{15}N(^{3}He,\alpha n)$	-0.81				$^{12}C(^{3}He,d)^{13}N$
						$^{13}C(^{3}He,p2n)^{13}N$

[a] Appendix B

[b] Reference 50

[c] Interferences are ^{3}He induced reactions with other elements which may lead to the same product at bombarding energies below about 30 MeV.

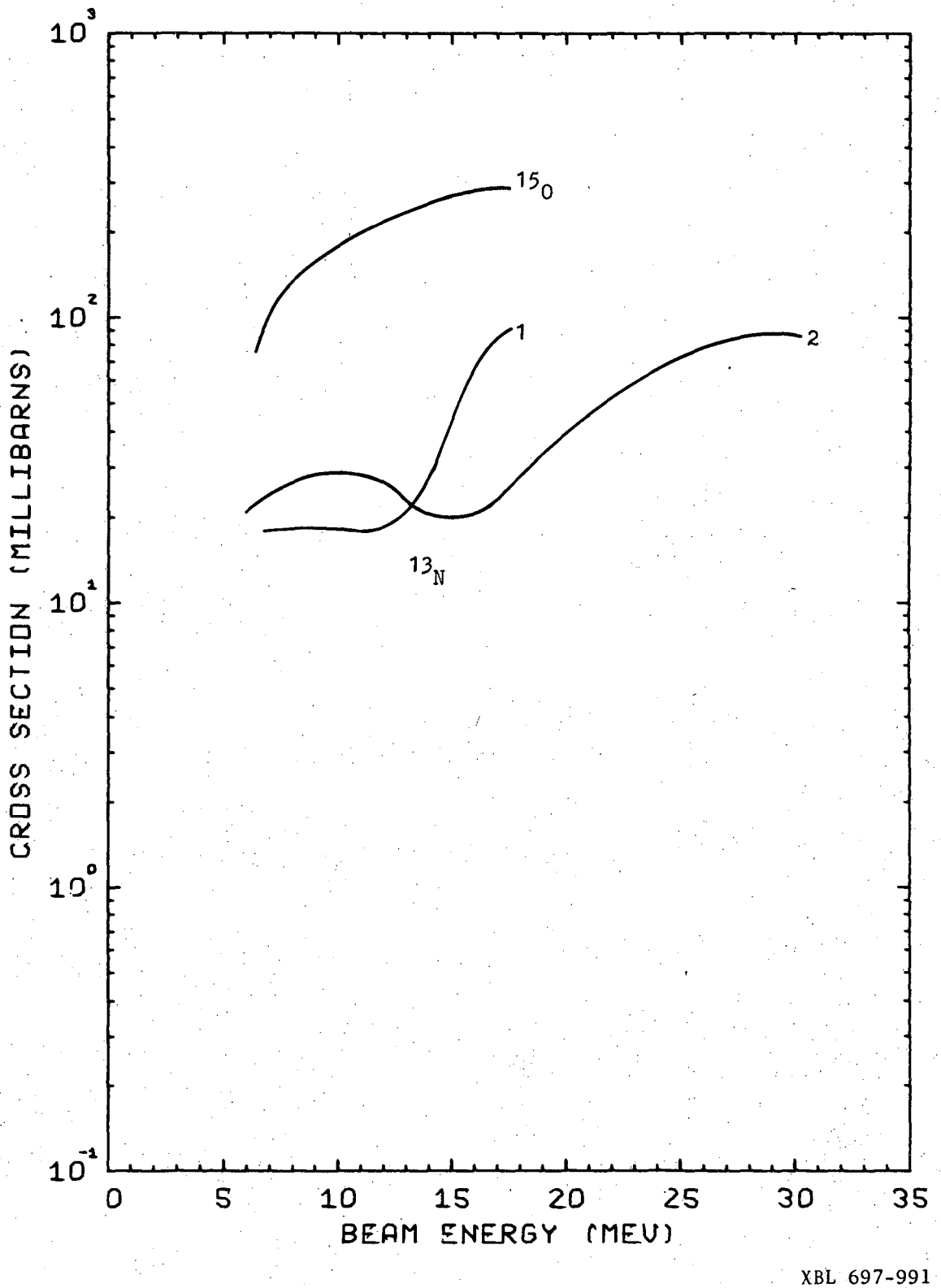

Fig. 14. Excitation functions for $^{14}N(^{3}He,pn)^{15}O$ and $^{14}N(^{3}He,\alpha)^{13}N$ (1,2). The numbers refer to references given in the text.

E. OXYGEN

Figure 15

$^{16}O(^{3}He,p)^{18}F$ +
$^{16}O(^{3}He,n)^{18}Ne \rightarrow {}^{18}F$

1. Markowitz and Mahony[10]
2. Hahn and Ricci[54]
3. Brill'[57]

Estimated errors in σ are 5% in curve 1, 10% in curve 2, and 25% in curve 3.

The ^{18}F produced in the ^{3}He activation of ^{16}O results as the sum of the two reactions shown above; direct formation and β^{+} decay of the 1.6 sec ^{18}Ne.

Figure 16

$^{16}O(^{3}He,\alpha)^{15}O$

$^{16}O(^{3}He,2\alpha)^{11}C$

1. Hahn and Ricci[54]
2. Brill'[57]

Error estimates are 10% for ^{15}O and 25% for ^{11}C. Discussion of these functions follows the presentation of our own data for the reactions induced in oxygen.

E. OXYGEN (Cont) Figure 17

$^{16}O(^{3}He,\alpha)^{15}O$ Lee, Lamb, Markowitz[62,66]

$^{16}O(^{3}He,2\alpha)^{11}C$

$^{16}O(^{3}He,p)^{18}F + {}^{16}O(^{3}He,n)^{18}Ne \rightarrow {}^{18}F$

$^{16}O(^{3}He,pn)^{17}F$

$^{16}O(^{3}He,n\alpha)^{14}O$

Systematic errors are estimated as described in Sec. III.D.3. The total propagated errors in the cross sections are less than ±8% for ^{15}O and ^{11}C, ±7% for ^{18}F and ^{17}F, AND ±10% for ^{14}O. The uncertainty in beam energy for adjustment by degrader foils depend upon uncertainties in both range-energy relationships and foil thickness measurements. The accuracy has been estimated[32] to be within ±1-MeV for an initial 30-MeV beam degraded to about 11 MeV and to decrease with degradation to about ±2-MeV at 6-MeV.

The targets used were 3.5 mg/cm^2 Ta_2O_5 prepared by anodization of tantalum foils. The anodization process is described in Sec. V.A of this report.

The targets were individually irradiated at the Hilac for 1 min at an incident beam energy of 31.2 ± 0.6 MeV and at an average current of 0.2 μA $^{3}He^{++}$. Each target was covered with a thin gold-foil backward recoil catcher which was assayed with the activated Ta_2O_5. Energy adjustment for the measurement of the excitation function was accomplished using aluminum degrader foils. The targets were protected from downstreaming recoil contamination by a thin gold foil placed behind the aluminum degraders.

The total count rates of the activation products were followed (without destruction of the target foil) for about 4 hours by counting of the 511-keV annihilation radiation from ^{18}F, ^{11}C, ^{17}F, and ^{15}O and the 2.31 MeV γ-ray from ^{14}O. A γ-ray spectrometer with a 3-in × 3-in-diameter NaI(Tl) detector was used. The complex decay curves obtained by photopeak analysis of the data were resolved using the RAD computer code[52] on the CDC 6600 computer.

The ^{18}F data in Fig. 17 agrees very well with literature values. The ^{15}O data is in fair agreement, and the agreement between the ^{11}C data of Brill' and our own data is rather poor, especially at lower energies. Brill' used BeO targets for measurement of the $^{16}O(^{3}He,2\alpha)^{11}C$ reaction, subtracting the $^{9}Be(^{3}He,n)^{11}C$ contribution calculated from measurement using beryllium metal targets. Brill's data appears to be an order of magnitude too low for the latter reaction (see Fig. 9), which would result in his $^{16}O(^{3}He,2\alpha)^{11}C$ data being too high, especially at lower energies.

Figure 18

$^{18}O(^{3}He,p)^{20}F$	Lamb, Lee, Markowitz[63]
$^{18}O(^{3}He,2p)^{19}O$	Lamb, Lee, Markowitz (unpublished)

The errors in the cross-section data are estimated to be about 13% in the ^{20}F function and about 16% for ^{19}O. The larger error in the ^{20}F data arises because of the ≈5% error in determining the decay time between the end of bombardment and the time of each count for a system whose half-life is as short as 11 sec and because of the added error in

the determination of the exact percentage of ^{18}O in the isotopically enriched target. Spectrum analysis of the ^{19}O activity incurred larger error because of the difficulty in detecting this small, 1.37-MeV photopeak amid those from other activities.

Samples of the Ta_2O_5 were prepared by anodization of tantalum foils using isotopically enriched water in the electrolyte. The ^{18}O enrichment in the Ta_2O_5 film was 49.8 ± 2.5%, verified by mass spectrometric analysis of the electrolyte. The film thickness was 1.2 mg/cm^2 oxygen.

The ^{20}F and ^{19}O functions were determined in similar but separate experiments using the gravity-track sample-holder described in Sec. III. The ^{20}F activity was measured via the 1.63 MeV γ-ray associated with β^- decay using the circuitry described in Sec. III, Fig. 7, with NaI(Tl) detectors. The time mode spectrum was resolved by computer code RAD; the background beneath the gated photopeak was treated as a component of the decay curve. The ^{19}O activities were obtained by spectrum analysis and hand-fitted decay curves.

Table V. Reactions induced in O by ^{3}He ion bombardment. Isotopic abundance: $^{16}O(99.76\%)$, $^{17}O(0.04\%)$, $^{18}O(0.20\%)$

Product	Reactions	Q(MeV)[a]	$T_{1/2}$[b]	Decay[b]	Associated γ-rays[b] keV(% per decay)	Interferences[c]
^{18}Ne	$^{16}O(^{3}He,n)$	-3.20	1.6s	β^+	511(200), 1040(7)	$^{20}Ne(^{3}He,\alpha n)^{18}Ne$
	$^{17}O(^{3}He,2n)$	-7.34				
	$^{18}O(^{3}He,3n)$	-15.38				
^{19}Ne	$^{17}O(^{3}He,n)$	4.30	17.4s	β^+	511(200)	$^{20}Ne(^{3}He,\alpha)^{19}Ne$
	$^{18}O(^{3}He,2n)$	-3.75				
^{17}F	$^{16}O(^{3}He,pn)$	-7.12	66.6s	β^+	511(200)	$^{15}N(^{3}He,n)^{17}F$
	$^{17}O(^{3}He,p2n)$	-11.26				$^{19}F(^{3}He,\alpha n)^{17}F$
^{18}F	$^{16}O(^{3}He,p)$	2.03	110m	β^+EC	511(194)	$^{19}F(^{3}He,\alpha)^{18}F$
	$^{17}O(^{3}He,pn)$	-2.11				$^{23}Na(^{3}He,2\alpha)^{18}F$
	$^{18}O(^{3}He,p2n)$	-10.16				$^{20}Ne(^{3}He,\alpha n)^{18}Ne \rightarrow {}^{18}F$
	Decay of ^{18}Ne					
^{20}F	$^{18}O(^{3}He,p)$	6.87	11.4s	β^-	1630(100)	$^{19}F(^{3}He,2p)^{20}F$
^{14}O	$^{16}O(^{3}He,\alpha n)$	-8.31	71.0s	β^+	511(200), 2312(99)	$^{12}C(^{3}He,n)^{14}O$
						$^{13}C(^{3}He,2n)^{14}O$
						$^{14}N(^{3}He,p2n)^{14}O$

Table V. (Continued)

Product	Reactions	Q(MeV)[a]	$T_{1/2}$[b]	Decay[b]	Associated γ-rays[b] keV(% per decay)	Interferences[c]
^{15}O	$^{16}O(^{3}He,\alpha)$	4.91	2.0m	β^+	511(200)	$^{13}C(^{3}He,n)^{15}O$
	$^{17}O(^{3}He,\alpha n)$	0.76				$^{14}N(^{3}He,pn)^{15}O$
						$^{15}N(^{3}He,p2n)^{15}O$
^{19}O	$^{18}O(^{3}He,2p)$	-3.76	29.1s	β^-	197(97), 1370(59)	None
^{11}C	$^{16}O(^{3}He,2\alpha)$	-5.31	20.3m	β^+,EC	511(200)	$^{9}Be(^{3}He,n)^{11}C$
						$^{10}B(^{3}He,pn)^{11}C$
						$^{11}B(^{3}He,p2n)^{11}C$
						$^{12}C(^{3}He,\alpha)^{11}C$

[a] Appendix B

[b] Reference 50

[c] Interferences are ^{3}He induced reactions with other elements which may lead to the same product at bombarding energies below about 30 MeV.

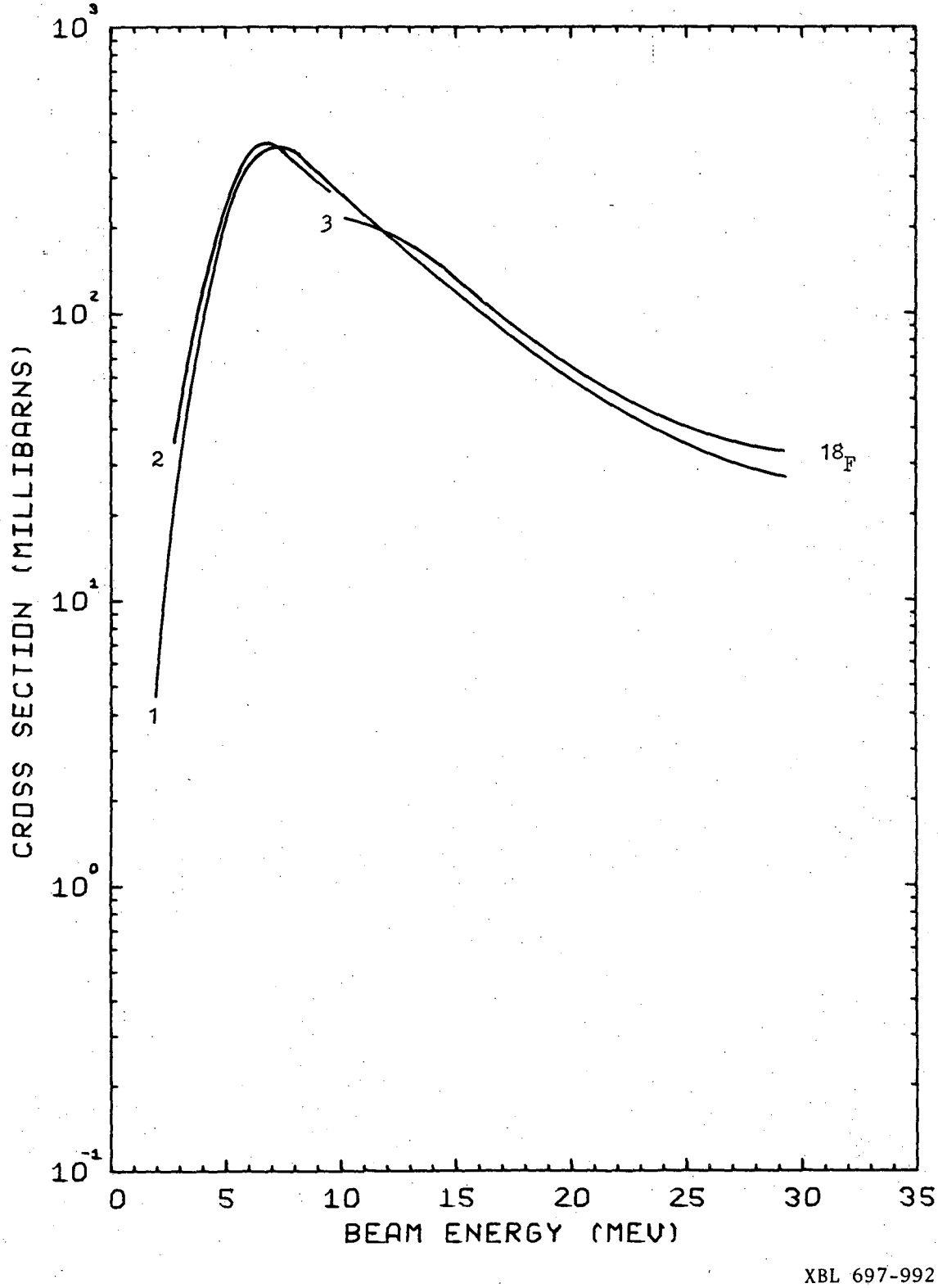

Fig. 15. Total production excitation function for $^{16}O + {}^{3}He \rightarrow {}^{18}F$. The numbers refer to references given in the text.

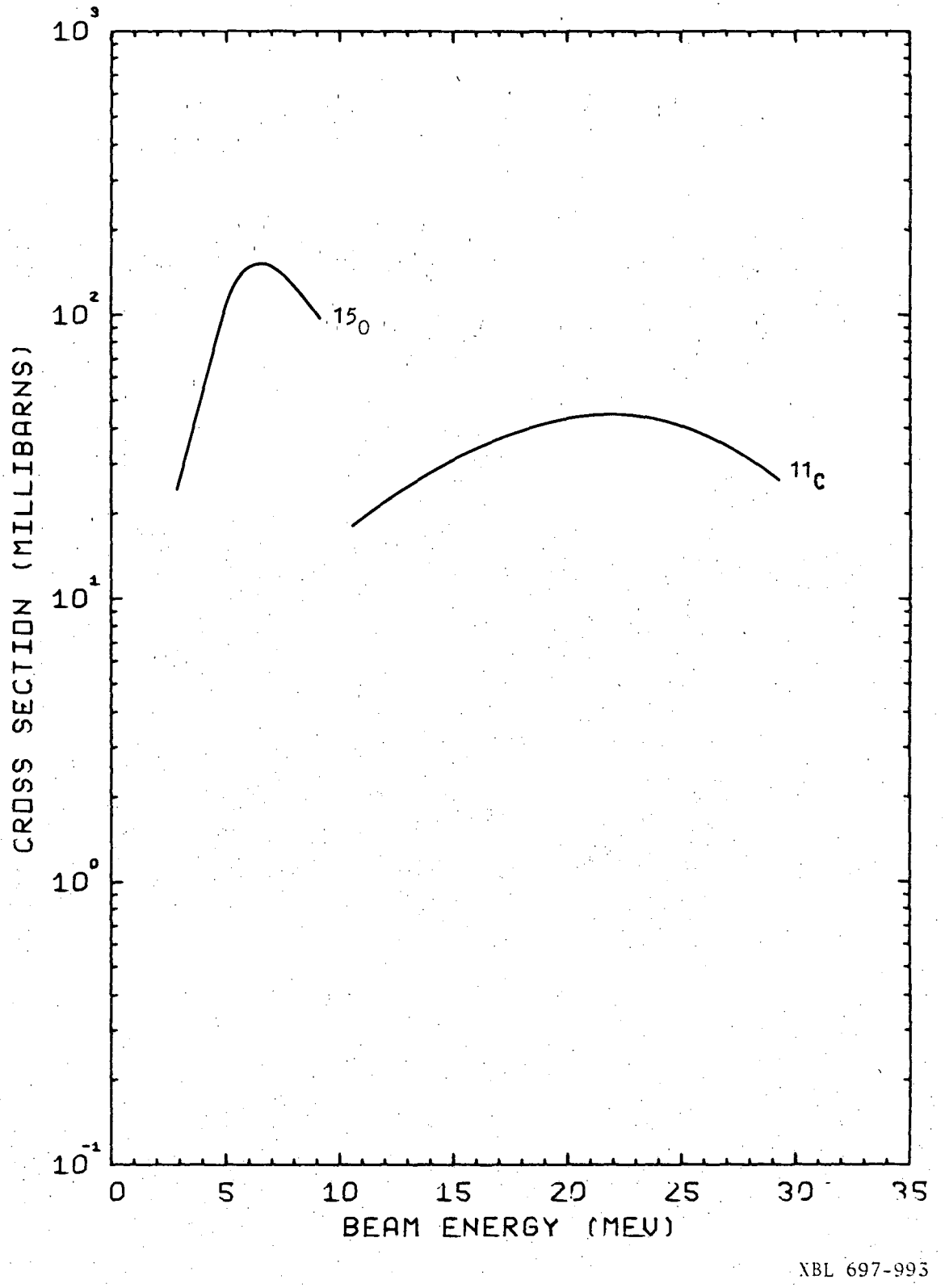

Fig. 16. Excitation functions for $^{16}O(^{3}He,\alpha)^{15}O$ and $^{16}O(^{3}He,2\alpha)^{11}C$. The references are given in the text.

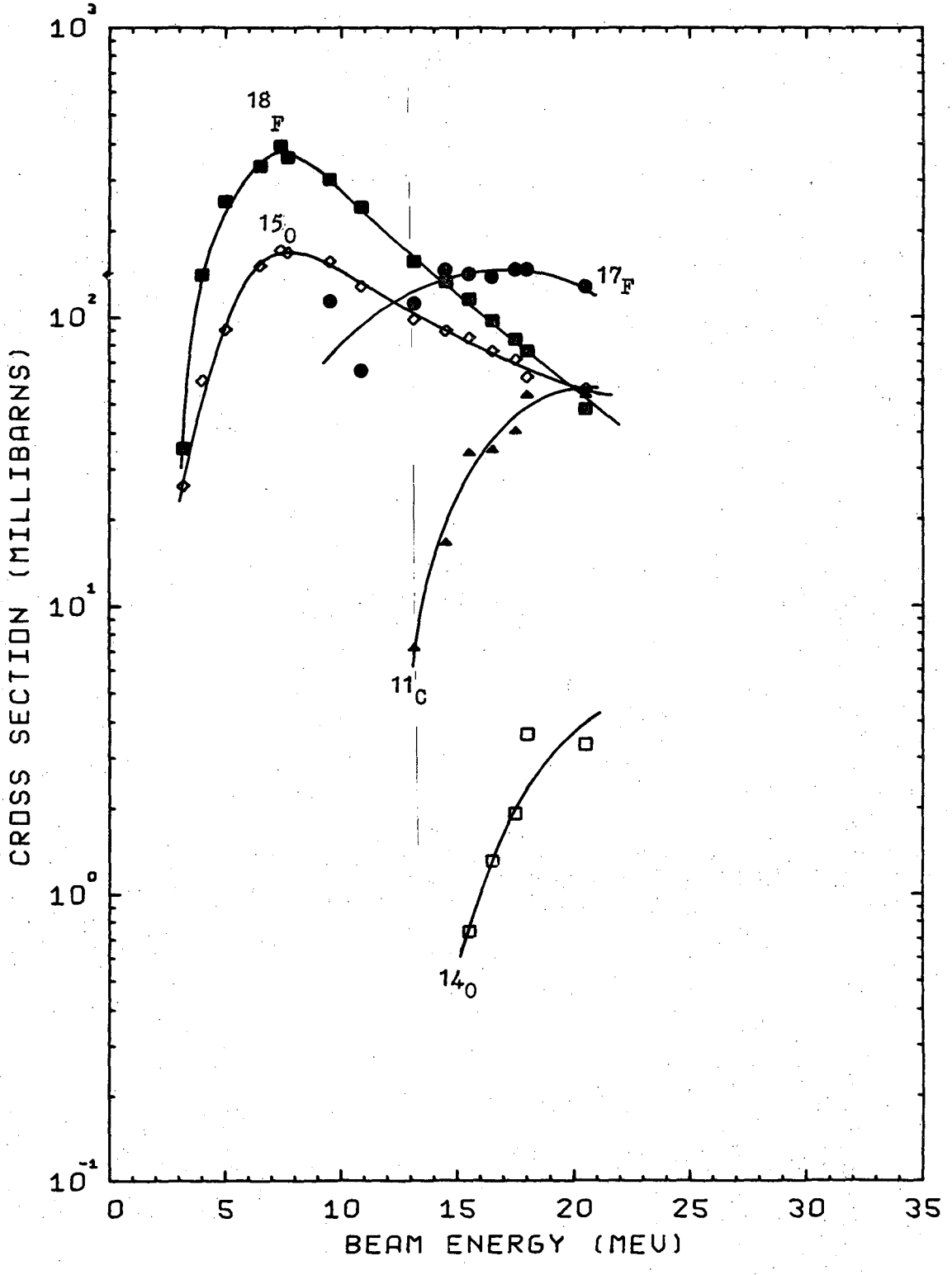

Fig. 17. Excitation functions for $^{16}O(^{3}He,\alpha)^{15}O$, $^{16}O(^{3}He,2\alpha)^{11}C$, $^{16}O(^{3}He,pn)^{17}F$, and $^{16}O(^{3}He,2\alpha)^{14}O$ and total production excitation function for $^{16}O + {}^{3}He \rightarrow {}^{18}F$.

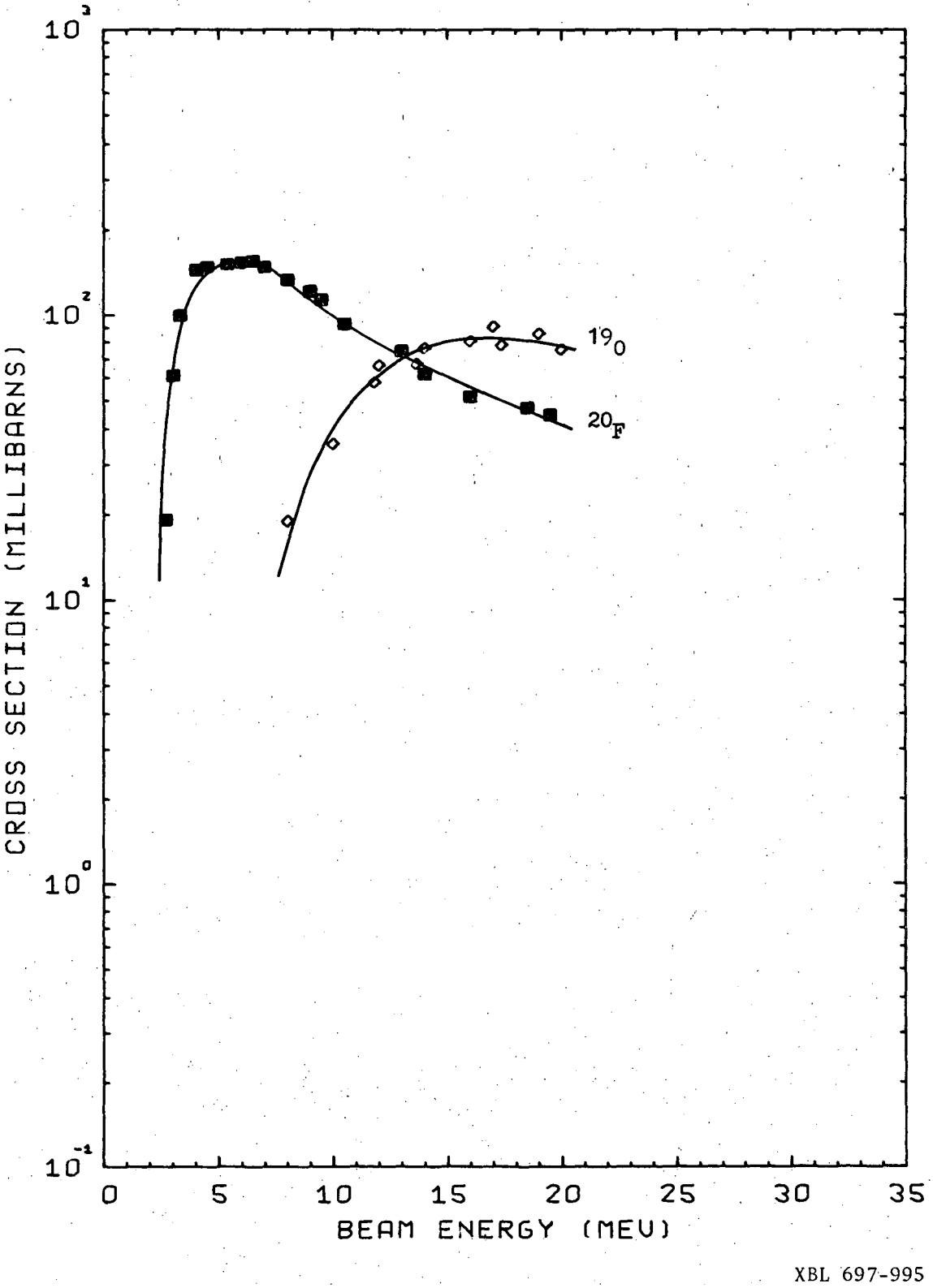

Fig. 18. Excitation functions for $^{18}O(^{3}He,p)^{20}F$ and $^{18}O(^{3}He,2p)^{19}O$.

F. FLUORINE

Figure 19

$^{19}F(^{3}He,\alpha)^{18}F$	1. Brill'[57]
	2. Mahony[64]
	3. Hahn and Ricci[54]
$^{19}F(^{3}He,\alpha n)^{17}F$	Hahn and Ricci[54]

Estimated errors in σ are 5% for curve 2, 15% for curve 3 and ^{17}F, and 25% for curve 1. Once again we note the shape of the excitation function for ^{18}F production from ^{19}F. The neutron boil-off threshold from excited ^{19}F is about 12-MeV.

Figure 20

$^{19}F(^{3}He,\alpha)^{18}F$	Lee, Lamb, Markowitz[62,66]
$^{19}F(^{3}He,2p)^{20}F$	

The errors in the cross-section data for these reactions are estimated to be about ±8% for ^{20}F and ±5% for ^{18}F.

The targets used were 1 mg/cm^2 teflon foils of approximately 1% variation in thickness uniformity. The ^{20}F activity resulting from bombardment of fluorine was detected as described in the $^{18}O(^{3}He,p)^{20}F$ reaction study. The ^{18}F activity was determined from the decay of the 511-keV annihilation radiation photopeak.

The ^{18}F excitation function presented in Fig. 20 agrees very well with the values of Mahony and Brill', remaining substantially below that of Hahn and Ricci at lower energy. It should be noted, however, that all

workers except Hahn and Ricci used degrader foils to adjust higher energy beams ($\approx$ 30-MeV) to desired bombarding energies calculated by the same, or similar range-energy relationships. Hahn and Ricci performed individual irradiations using a Van de Graaf accelerator whose beam-energy was precisely known.

Table VI. Reactions induced in F by ^{3}He ion bombardment. Isotopic abundance: ^{19}(100%)

Product	Reactions	Q(MeV)[a]	$T_{1/2}$[b]	Decay[b]	Associated γ-rays[b] keV(% per decay)	Interferences[c]
^{21}Na	$^{19}F(^{3}He,n)$	7.56	23.0s	β^+	350(2.3), 511(200)	$^{20}Ne(^{3}He,pn)^{21}Na$
						$^{21}Ne(^{3}He,p2n)^{21}Na$
						$^{23}Na(^{3}He,\alpha n)^{21}Na$
^{19}Ne	$^{19}F(^{3}He,p2n)$	-11.74	17.4s	β^+	511(200)	$^{20}Ne(^{3}He,\alpha)^{19}Ne$
						$^{21}Ne(^{3}He,\alpha n)^{19}Ne$
						$^{17}O(^{3}He,n)^{19}Ne$
						$^{18}O(^{3}He,2n)^{19}Ne$
^{17}F	$^{19}F(^{3}He,\alpha n)$	0.99	66.6s	β^+	511(200)	$^{15}N(^{3}He,n)^{17}F$
						$^{16}O(^{3}He,pn)^{17}F$
						$^{17}O(^{3}He,p2n)^{17}F$

Table VI. (Continued)

Product	Reactions	Q(MeV)[a]	$T_{1/2}$[b]	Decay[b]	Associated γ-rays[b] keV(% per decay)	Interferences[c]
^{18}F	$^{19}F(^{3}He,\alpha)$	10.14	110.0m	β^+,EC	511(194)	$^{23}Na(^{3}He,2\alpha)^{18}F$
						$^{20}Ne(^{3}He,\alpha n)^{18}Ne\rightarrow^{18}F$
						$^{16}O(^{3}He,p)^{18}F$
						$^{16}O(^{3}He,n)^{18}Ne\rightarrow^{18}F$
						$^{17}O(^{3}He,pn)^{18}F$
						$^{18}O(^{3}He,p2n)^{18}F$
^{20}F	$^{19}F(^{3}He,2p)$	-1.12	11.4s	β^-	1630(100)	$^{18}O(^{3}He,p)^{20}F$

[a] Appendix B

[b] Reference 50

[c] Interferences are ^{3}He induced reactions with other elements which may lead to the same product at bombarding energies below about 30 MeV.

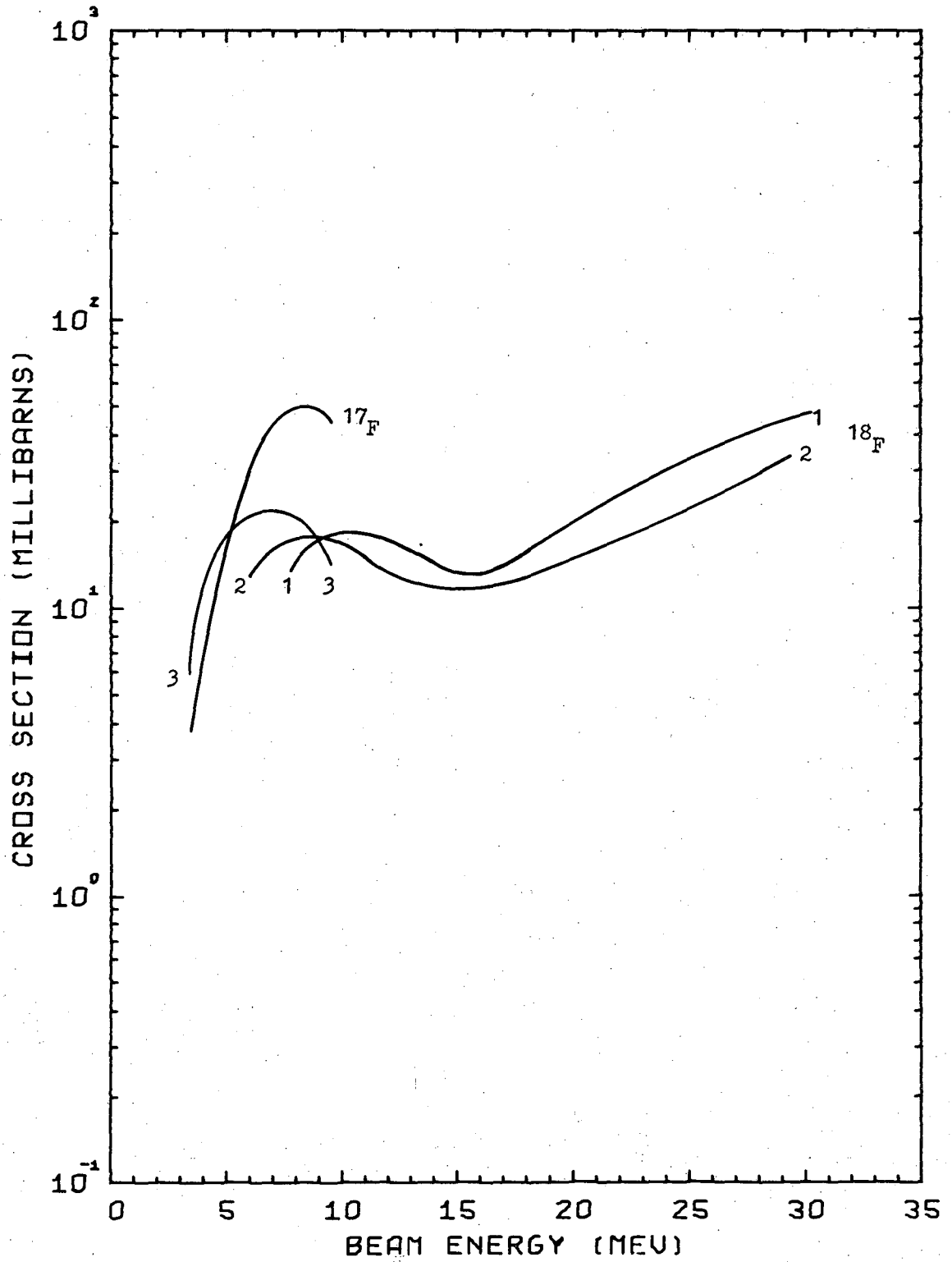

Fig. 19. Excitation functions for $^{19}F(^{3}He,\alpha)^{18}F$ (1,2,3), and $^{19}F(^{3}He,\alpha n)^{17}F$. The references are given in the text.

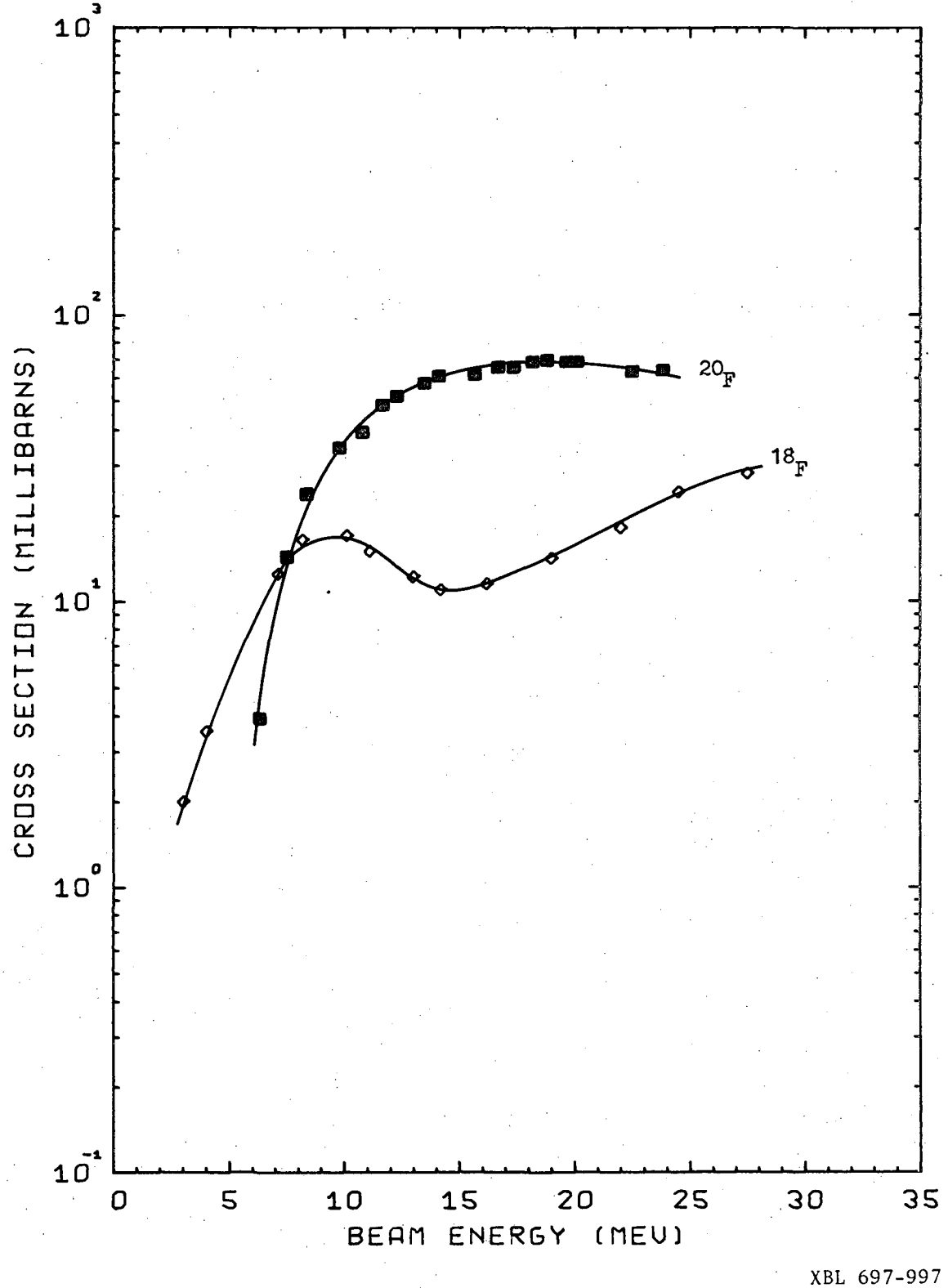

Fig. 20. Excitation functions for $^{19}F(^3He,\alpha)^{18}F$ and $^{19}F(^3He,2p)^{20}F$.

G. SODIUM Figure 21

$^{23}Na(^{3}He,2p)^{24}Na$ Hahn and Ricci[55]

The estimated cross section error for this reaction is ±15%. The excitation function was calculated by numerical differentiation of thick target yield data. The target used was NaI.

Table VII. Reactions induced in Na by ^{3}He ion bombardment. Isotopic abundance: ^{23}Na(100%)

Product	Reactions	Q(MeV)[a]	$T_{1/2}$[b]	Decay[b]	Associated γ-rays[b] keV(% per decay)	Interferences[c]
^{24}Al	$^{23}Na(^{3}He,2n)$	-10.69	2.1s	β^+	511(200), 1368(--), 2754(--)	$^{24}Mg(^{3}He,p2n)^{24}Al$
^{25}Al	$^{23}Na(^{3}He,n)$	6.26	7.2s	β^+	511(200)	$^{24}Mg(^{3}He,pn)^{25}Al$
						$^{25}Mg(^{3}He,p2n)^{25}Al$
^{23}Mg	$^{23}Na(^{3}He,p2n)$	-12.56	12.1s	β^+	440(9), 511(200)	$^{21}Ne(^{3}He,n)^{23}Mg$
						$^{22}Ne(^{3}He,2n)^{23}Mg$
						$^{24}Mg(^{3}He,\alpha)^{23}Mg$
						$^{25}Mg(^{3}He,\alpha n)^{23}Mg$
^{21}Na	$^{23}Na(^{3}He,\alpha n)$	-2.91	23.0s	β^+	350(2.3), 511(200)	$^{19}F(^{3}He,n)^{21}Na$
^{22}Na	$^{23}Na(^{3}He,\alpha)$	8.16	2.6y	β^+,EC	511(180), 1275(100)	$^{21}Ne(^{3}He,pn)^{22}Na$
						$^{22}Ne(^{3}He,p2n)^{22}Na$
						$^{24}Mg(^{3}He,\alpha n)^{22}Mg\rightarrow^{22}Na$
						$^{27}Al(^{3}He,2\alpha)^{22}Na$
^{24}Na	$^{23}Na(^{3}He,2p)$	-0.76	15.0h	β^-	1369(100), 2754(100)	$^{22}Ne(^{3}He,p)^{24}Na$

[a] Appendix B

[b] Reference 50

[c] Interferences are ^{3}He induced reactions with other elements which may lead to the same product at bombarding energies below about 30 MeV.

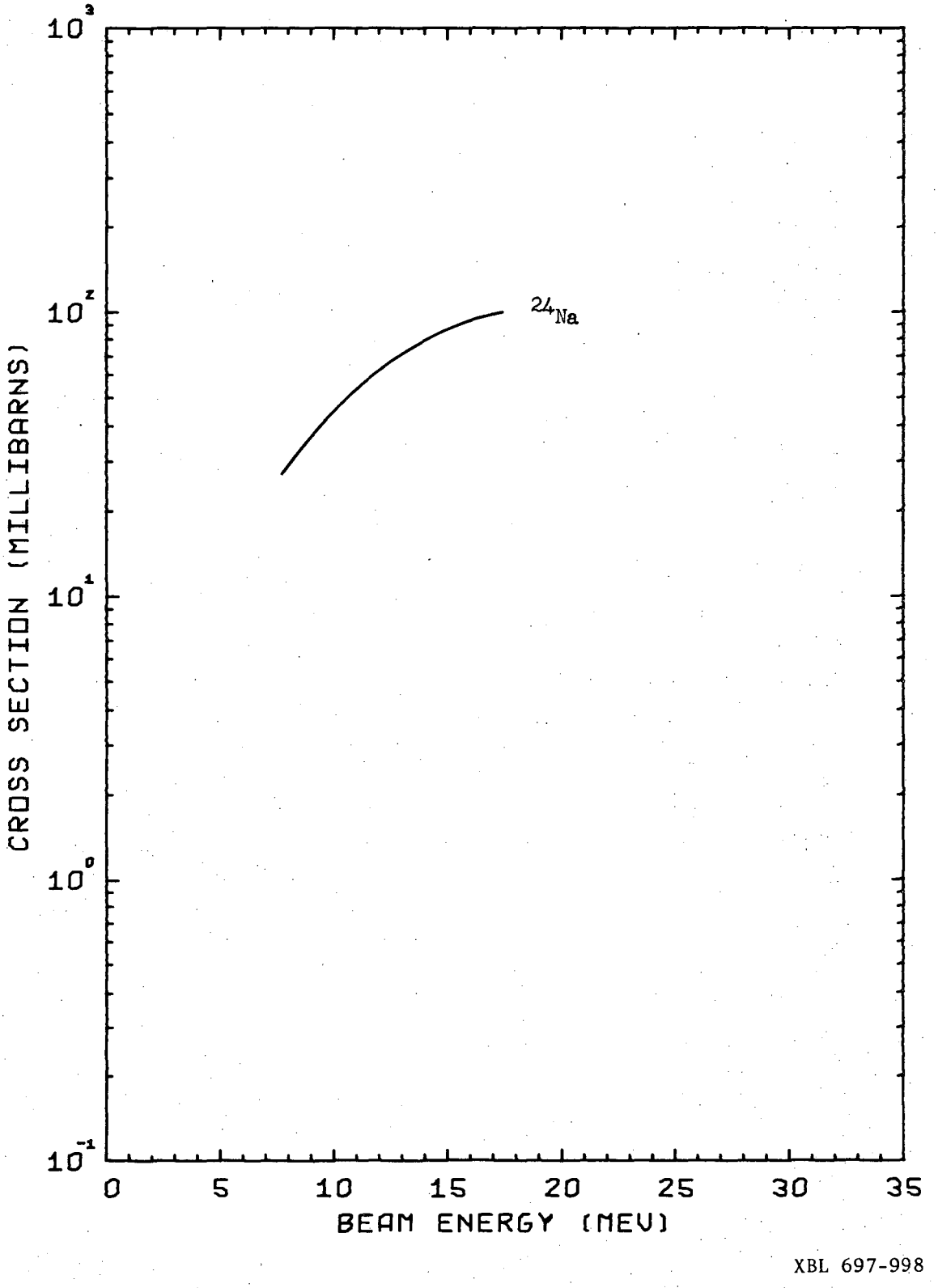

Fig. 21. Excitation function for $^{23}Na(^{3}He,2p)^{24}Na$. The reference is given in the text.

H. MAGNESIUM Figure 22

$^{26}Mg(^{3}He,p)^{28}Al$ Lamb, Lee, and Markowitz[65]

$^{26}Mg(^{3}He,2p)^{27}Mg$

Total production of ^{24}Na

The estimated errors for cross-section data are ±6% for ^{28}Al, ±7% for ^{27}Mg, and ±6% for ^{24}Na.

The targets used for these functions were magnesium metal, vacuum evaporated onto platinum foil base-plates. The mg thicknesses were about 1.5-2 mg/cm^2 and the uniformity estimated to be within about 2%. Each target was covered with 0.00013-in platinum foil.

For the ^{28}Al and ^{27}Mg excitation functions, individual target irradiations were performed using aluminum degraders to adjust the incident 31.2 MeV beam. The beam current was about 0.2 μA. For the production of ^{24}Na, a stack of these targets was bombarded at the full beam energy.

The decay of ^{28}Al and ^{24}Na were followed using NaI(Tl) detectors to measure the 1780 keV and 2750 keV γ-rays associated with the β^- decay of these two nuclides, respectively. The 840-keV γ-ray from ^{27}Mg was measured using a 16-cm^3 (active volume) Ge(Li) detector.

The excitation function for production of ^{24}Na from Mg includes no correction for isotopic abundance, as it is not clear which Mg isotopes contribute to this activity. The threshold for the $^{24}Mg(^{3}He,3p)^{24}Na$ reaction is about 14 MeV, while the $^{26}Mg(^{3}He,\alpha p)^{24}Na$ reaction threshold is about 2.9 MeV.

Table VIII. Reactions induced in Mg by ^{3}He ion bombardment. Isotopic abundance: $^{24}Mg(78.60\%)$, $^{25}Mg(10.11\%)$, $^{26}Mg(11.29\%)$

Product	Reactions	Q(MeV)[a]	$T_{1/2}$[b]	Decay[b]	Associated γ-rays[b] keV(% per decay)	Interferences[c]
^{26}Si	$^{24}Mg(^{3}He,n)$	0.06	2.1s	β^+	511(200), 820(34)	$^{28}Si(^{3}He,\alpha n)^{26}Si$
	$^{25}Mg(^{3}He,2n)$	-7.27				
	$^{26}Mg(^{3}He,3n)$	-18.36				
^{27}Si	$^{25}Mg(^{3}He,n)$	6.05	4.1s	β^+	511(200)	$^{28}Si(^{3}He,\alpha)^{27}Si$
	$^{26}Mg(^{3}He,2n)$	-5.04				$^{29}Si(^{3}He,\alpha n)^{27}Si$
						$^{27}Al(^{3}He,p2n)^{27}Si$
^{24}Al	$^{24}Mg(^{3}He,p2n)$	-22.38	2.1s	β^+	511(200), 1368(--), 2754(--)	$^{23}Na(^{3}He,2n)^{24}Al$
^{25}Al	$^{24}Mg(^{3}He,pn)$	-5.43	7.2s	β^+	511(200)	$^{27}Al(^{3}He,\alpha n)^{25}Al$
	$^{25}Mg(^{3}He,p2n)$	-12.76				$^{23}Na(^{3}He,n)^{25}Al$

Table VIII. (Continued)

Product	Reactions	Q(MeV)[a]	$T_{1/2}$[b]	Decay[b]	Associated γ-rays[b] keV(% per decay)	Interferences[c]
$^{26}Al+$	$^{25}Mg(^{3}He,pn)$	-1.41	7×10^{5}y	β^+,EC	511(170), 1120(4), 1810(100)	$^{27}Al(^{3}He,\alpha)^{26}Al$
^{26m}Al			6.4s[d]	β^+	511(200)	
	$^{26}Mg(^{3}He,p2n)$	-12.50				$^{28}Si(^{3}He,n)^{26}Si\rightarrow^{26}Al$
	Decay of ^{26}Si					
^{28}Al	$^{26}Mg(^{3}He,p)$	8.28	2.3m	β^-	1780(100)	$^{27}Al(^{3}He,2p)^{28}Al$
^{23}Mg	$^{24}Mg(^{3}He,\alpha)$	4.04	12.1s	β^+	440(9), 511(200)	$^{23}Na(^{3}He,p2n)^{23}Mg$
	$^{25}Mg(^{3}He,\alpha n)$	-3.29				$^{21}Ne(^{3}He,n)^{23}Mg$
						$^{22}Ne(^{3}He,2n)^{23}Mg$
^{27}Mg	$^{26}Mg(^{3}He,2p)$	-1.28	9.5m	β^-	180(0.7), 840(70), 1013(30)	None

[a] Appendix B

[b] Reference 50

[c] Interferences are ^{3}He induced reactions with other elements which may lead to the same product at bombarding energies below about 30 MeV.

[d] Underlined decay data indicates metastable or isomeric state.

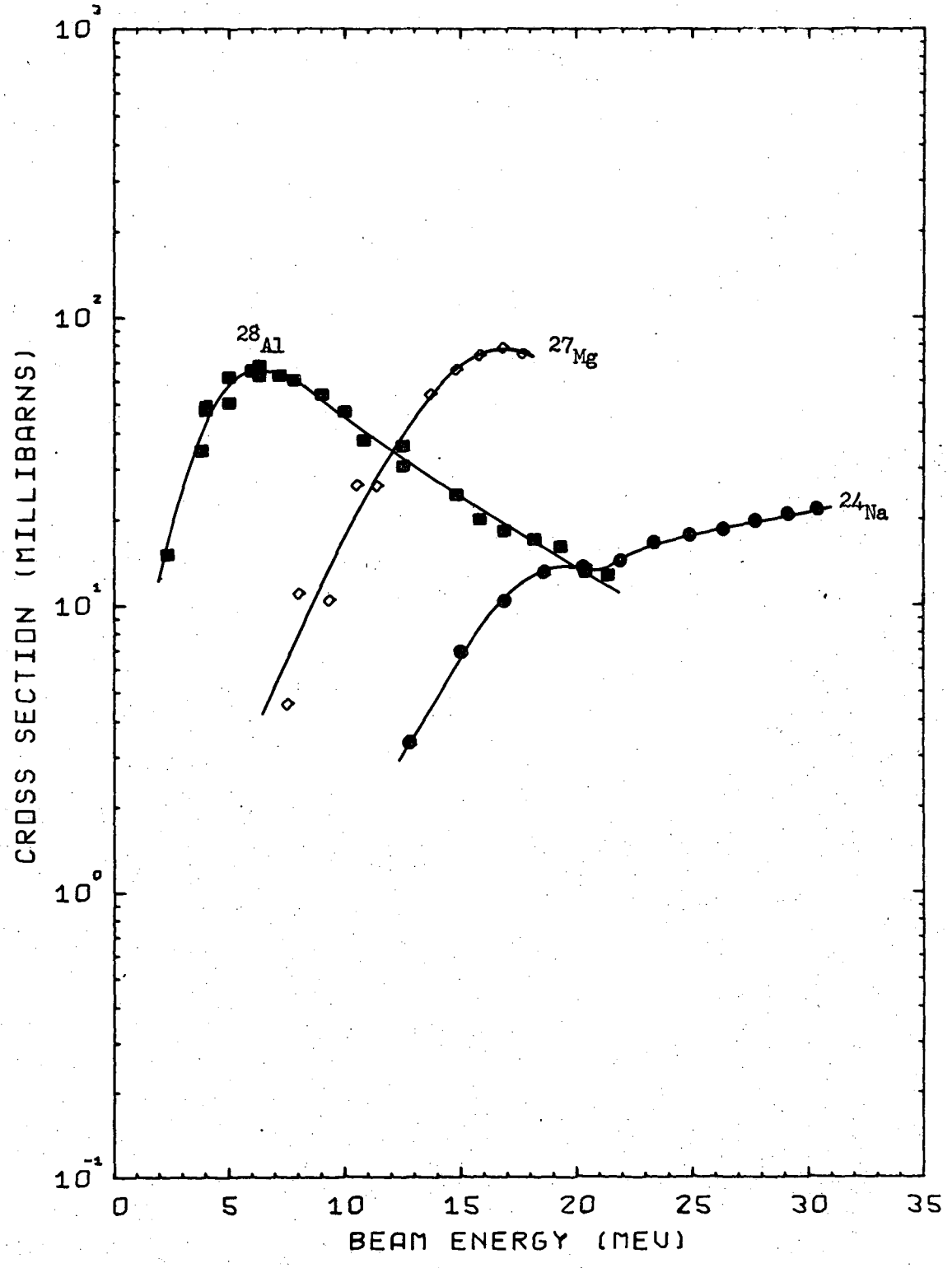

Fig. 22. Excitation functions for $^{26}Mg(^{3}He,p)^{28}Al$ and $^{26}Mg(^{3}He,2p)^{27}Mg$ and the total production excitation function for Mg + $^{3}He \rightarrow {}^{24}Na$.

I. ALUMINUM

Figure 23
Figure 24
Figure 25
Figure 26

$^{27}Al(^{3}He,2p)^{28}Al$	Brill'[57]
$^{27}Al(^{3}He,3p)^{27}Mg$	
$^{27}Al(^{3}He,3\alpha)^{18}F$	1. Markowitz and Hall[56]
	2. Cochran and Knight[60]
$^{27}Al(^{3}He,\alpha 2p)^{24}Na$	1. Markowitz and Hall[56]
	2. Brill'[57]
	3. Cochran and Knight[60]
$^{27}Al(^{3}He,2\alpha)^{22}Na$	1. Brill'[57]
	2. Markowitz and Hall[56]
	3. Cochran and Knight[60]

Estimated errors in σ for ^{27}Mg, ^{24}Na (curve 2), and ^{22}Na (curve 1) are given as ±25%. Error estimates were not given for the other reactions. The ^{28}Al data in Fig. 23 is relative but was roughly estimated to be on the order of a few tens of millibarns.

It is interesting to note the structure of the ^{18}F excitation function of Fig. 24. The peculiar low-energy (< 10 MeV appearance of ^{18}F below the $^{27}Al \rightarrow {}^{18}F$ threshold) behavior of this data was found by Markowitz and Hall to be due to surface oxide contamination on the aluminum-foil targets. This observation led Markowitz to consider use of accelerated ^{3}He ions for activation analysis. The first such analyses by Markowitz and Mahony were reported in 1962.[10]

The low-energy portion of excitation function 1, Fig. 25, for production of ^{24}Na cannot be attributed to the $^{27}Al(^{3}He,\alpha 2p)^{24}Na$ reaction because the threshold for this reaction is 12.1 MeV. This ^{24}Na activity might arise from production by $^{27}Al(n,\alpha)^{24}Na$ (Q = -3.1 MeV) initiated by the reaction-produced neutrons and secondary neutrons produced at the accelerator whose energies average a few MeV.

Figure 27

$^{27}Al(^{3}He,2p)^{28}Al$ Lee, Lamb, Markowitz (unpublished)

The estimated error in σ is ±5%.

Targets were each composed of three 0.00025-in aluminum foils individually irradiated for 2 min at a beam current of about 0.2 μA. The center foil of each target was radio-assayed using a 3-in × 3-in diameter NaI(Tl) detector to follow decay of the 1.78-MeV photopeak from ^{28}Al.

The dashed portion of the curve in Fig. 27 was obtained by superimposing the data of Brill', Fig. 23, multiplied by 10, on our own data. Brill's ^{28}Al data was given in relative units. The relative magnitude of this excitation function is supported by thick target activation data of Ricci and Hahn.[37]

Table IX. Reactions induced in Al by ^{3}He ion bombardment. Isotopic abundance: $^{27}Al(100\%)$

Product	Reactions	Q(MeV)[a]	$T_{1/2}$[b]	Decay[b]	Associated γ-rays[b] keV(% per decay)	Interferences[c]
^{29}P	$^{27}Al(^{3}He,n)$	6.61	4.5s	β^+	511(200), 1280(0.8)	$^{28}Si(^{3}He,pn)^{29}P$
						$^{29}Si(^{3}He,p2n)^{29}P$
^{27}Si	$^{27}Al(^{3}He,p2n)$	-13.31	4.1s	β^+	511(200)	$^{28}Si(^{3}He,\alpha)^{27}Si$
						$^{29}Si(^{3}He,\alpha n)^{27}Si$
						$^{25}Mg(^{3}He,n)^{27}Si$
						$^{26}Mg(^{3}He,2n)^{27}Si$
^{25}Al	$^{27}Al(^{3}He,\alpha n)$	-3.83	7.2s	β^+	511(200)	$^{24}Mg(^{3}He,pn)^{25}Al$
						$^{25}Mg(^{3}He,p2n)^{25}Al$
						$^{23}Na(^{3}He,n)^{25}Al$
$^{26}Al+$	$^{27}Al(^{3}He,\alpha)$	7.52	$7\times10^{5}y$	β^+,EC	511(170), 1120(4), 1810(100)	$^{25}Mg(^{3}He,pn)^{26}Al$
^{26m}Al			6.4s[d]	β^+	511(200)	$^{26}Mg(^{3}He,p2n)^{26}Al$
^{28}Al	$^{27}Al(^{3}He,2p)$	0.01	2.3m	β^-	1780(100)	$^{26}Mg(^{3}He,p)^{28}Al$

Table IX. (Continued)

Products	Reactions	Q(MeV)[a]	$T_{1/2}$[b]	Decay[b]	Associated γ-rays[b] keV(% per decay)	Interferences[c]
^{22}Na	$^{27}Al(^{3}He,2\alpha)$	-1.94	2.6y	β^+,EC	511(180), 1275(100)	$^{20}Ne(^{3}He,p)^{22}Na$
						$^{21}Ne(^{3}He,pn)^{22}Na$
						$^{22}Ne(^{3}He,p2n)^{22}Na$
						$^{23}Na(^{3}He,\alpha)^{22}Na$
^{24}Na	$^{27}Al(^{3}He,\alpha 2p)$	-10.85	15h	β^-	1369(100), 2754(100)	$^{22}Ne(^{3}He,p)^{24}Na$
						$^{23}Na(^{3}He,2p)^{24}Na$
^{18}F	$^{27}Al(^{3}He,3\alpha)$	-10.41	110m	β^+,EC	511(194)	$^{16}O(^{3}He,p)^{18}F$
						$^{17}O(^{3}He,pn)^{18}F$
						$^{18}O(^{3}He,p2n)^{18}F$
						$^{19}F(^{3}He,\alpha)^{18}F$

[a] Appendix B

[b] Reference 50

[c] Interferences are ^{3}He induced reactions with other elements which may lead to the same product at bombarding energies below about 30 MeV

[d] Underlined decay data indicates metastable or isomeric state.

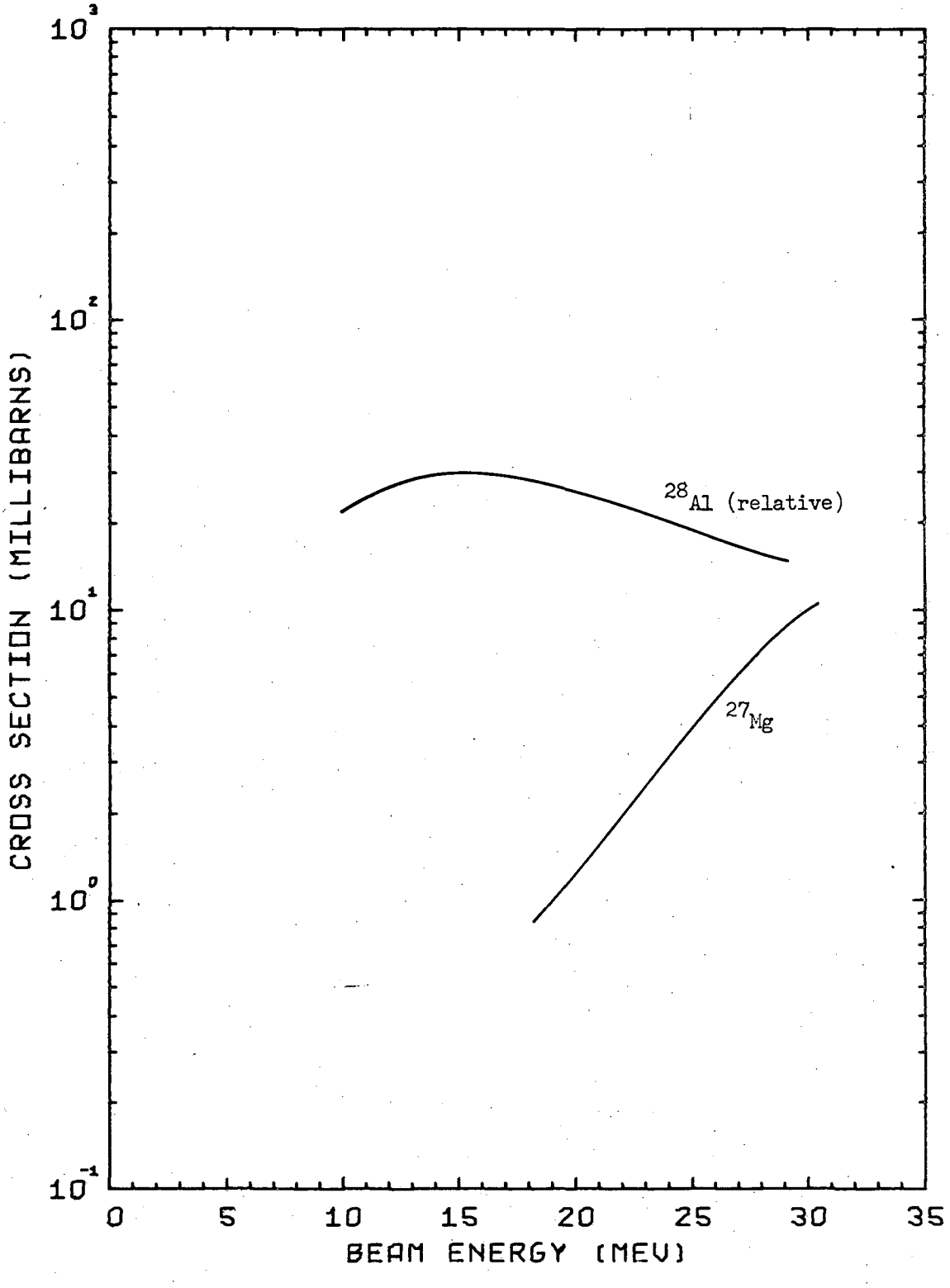

XBL 697-1000

Fig. 23. Excitation functions for $^{27}Al(^{3}He,2p)^{28}Al$ and $^{27}Al(^{3}He,3p)^{27}Mg$. The references are given in the text.

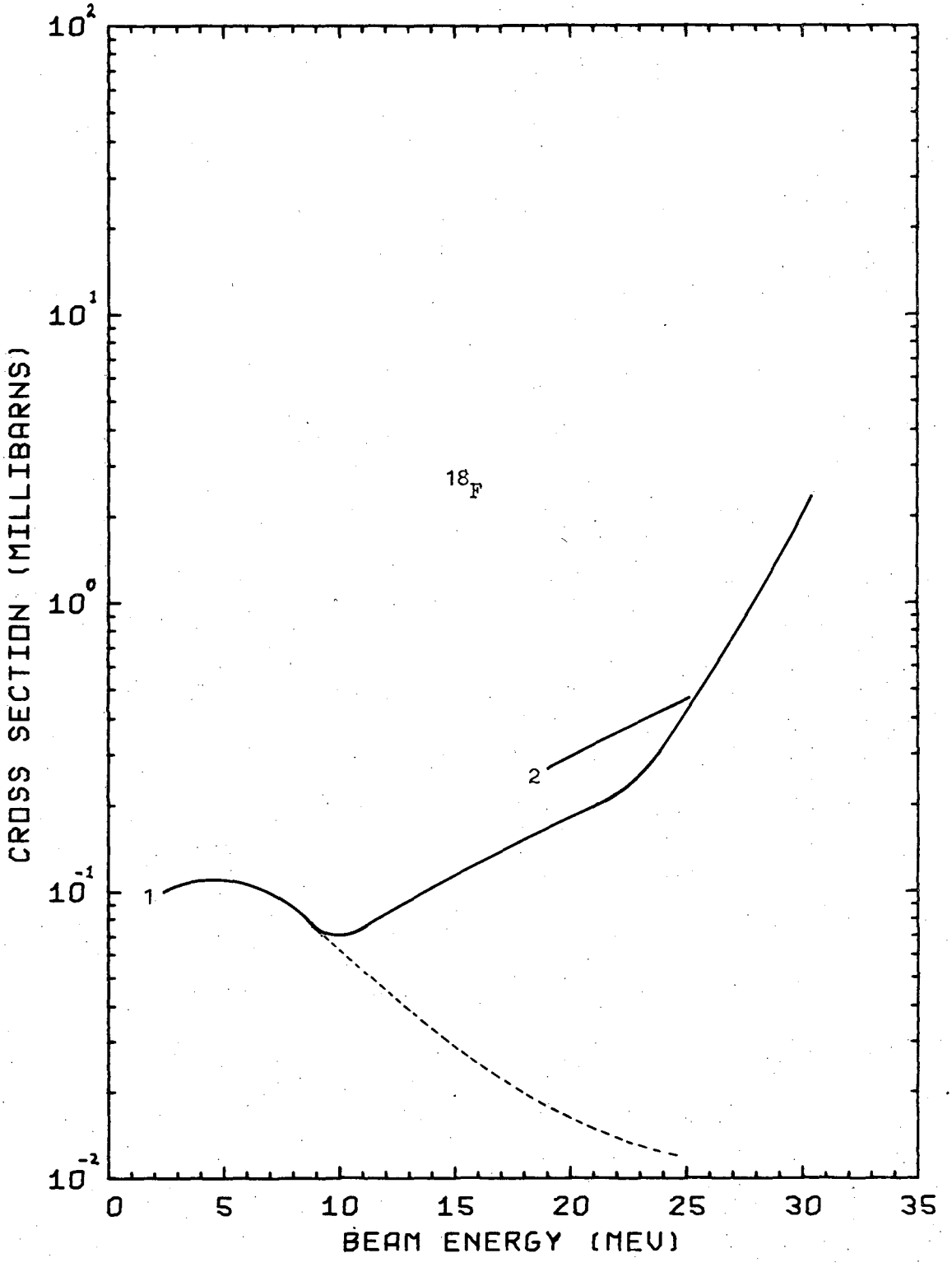

XBL 697-1001

Fig. 24. Excitation function for $^{27}Al(^3He,3\alpha)^{18}F$. The references are given in the text. Dashed line on curve 1 assumes low-energy ^{18}F due to $^{16}O(^3He,p)^{18}F$ from surface oxygen.

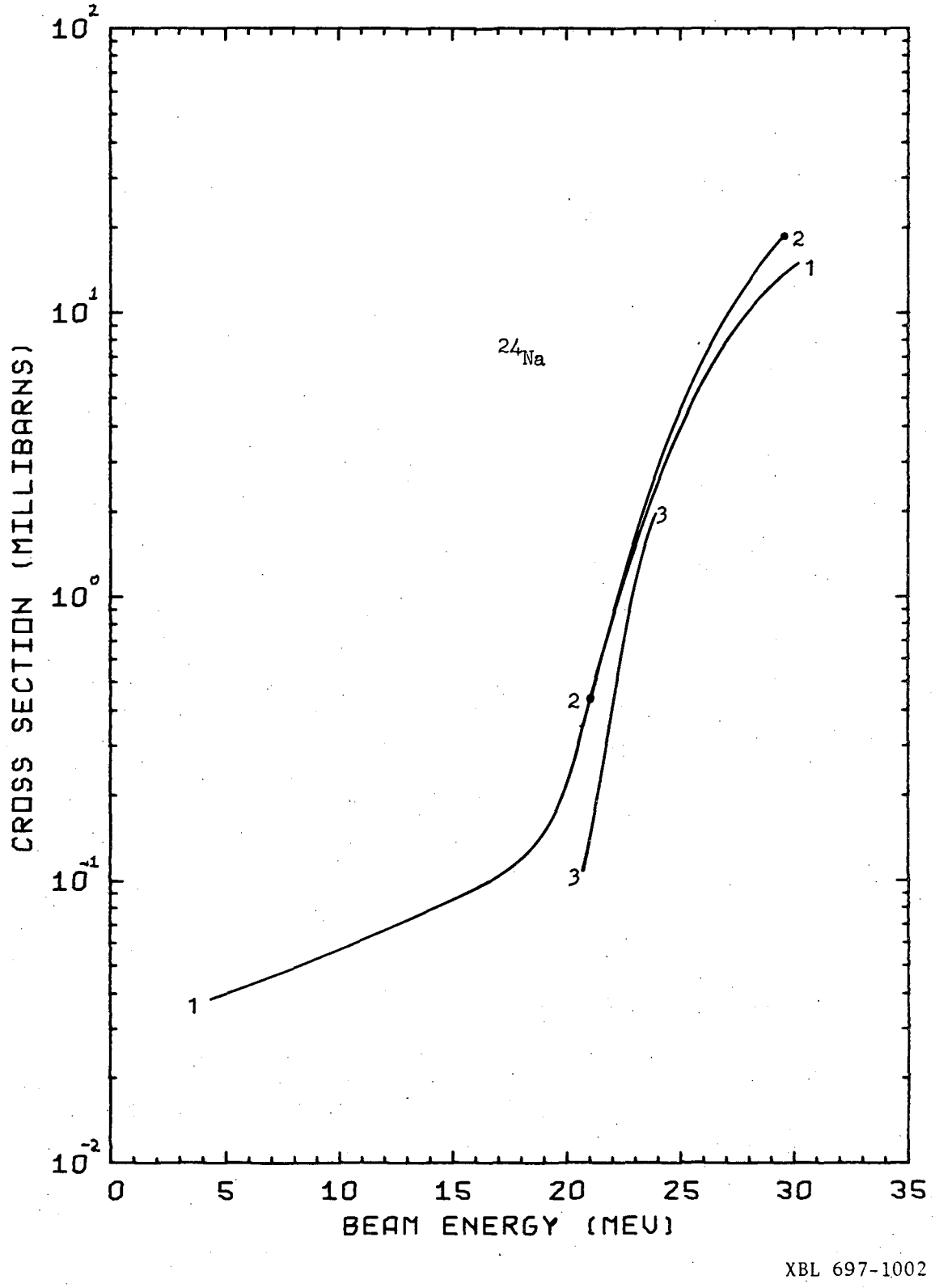

Fig. 25. Excitation function for $^{27}Al(^{3}He,\alpha 2p)^{24}Na$. The references are given in the text.

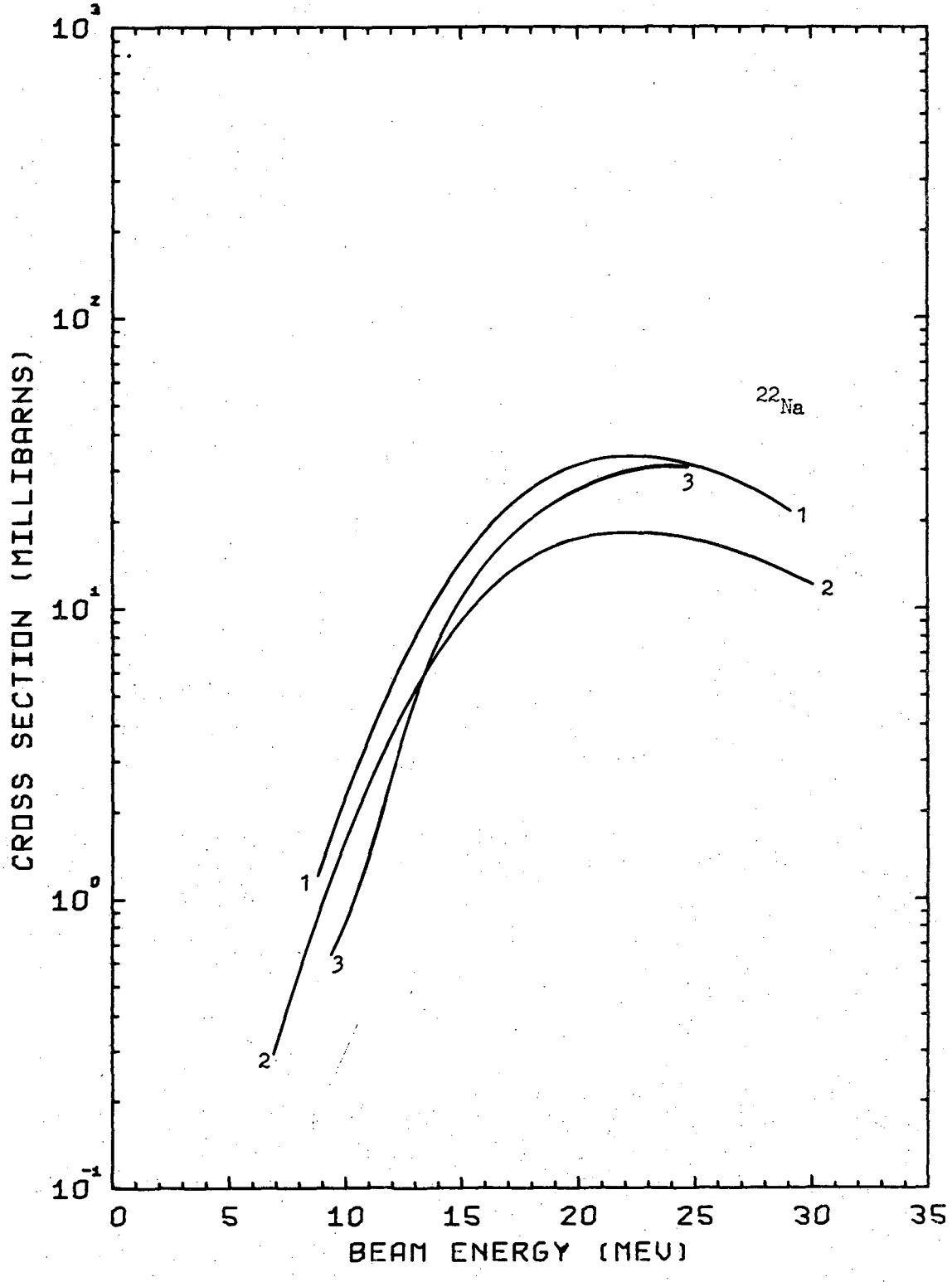

XBL 697-1003

Fig. 26. Excitation function for $^{27}Al(^{3}He,2\alpha)^{22}Na$. The references are given in the text.

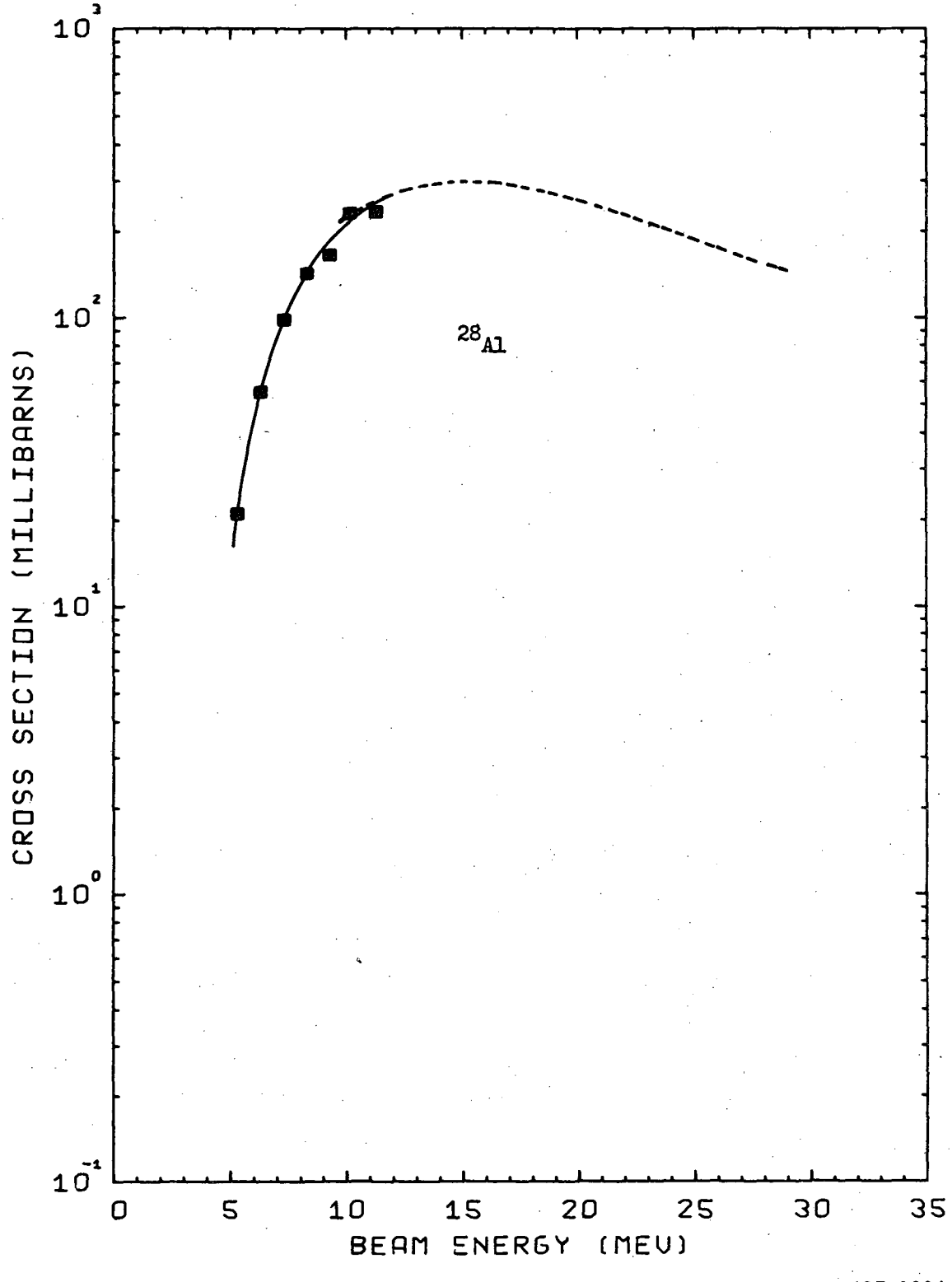

Fig. 27. Excitation function for $^{27}Al(^{3}He,2p)^{28}Al$. The dashed portion of the curve is a superimposition of the data of Brill'.[57]

J. SILICON Figure 28

$^{3}He + Si \rightarrow {}^{30}P$ Lamb, Lee, and Markowitz[62,65]

The estimated error in σ is ±14%. An error of ±10% assigned to sample uniformity accounts for most of this.

Targets were prepared by first grinding lump silicon under ether, then transferring this slurry to a sedimentation column from which the ether was allowed to evaporate, leaving finely divided silicon particles dispersed on the thick platinum backing-plate. One drop of a solution of 100 μg/ml polystyrene (C_8H_8-) in dichloroethylene was added to stabilize the deposit. The targets were covered with 13.5 mg/cm^2 tantalum foils. The target thicknesses varied from 1.7 mg/cm^2 used for lowest beam energies to 6.2 mg/cm^2 used for higher energy bombardment.

These targets were individually irradiated for 2 min at a $^{3}He^{++}$ beam current of 0.1 μA.

The 511-keV β^+ annihilation radiation from ^{30}P was followed using a 6 cm^3 (active volume) Ge(Li) detector.

Contamination in the activated sample produced by the polystyrene deposit stabilizer was not detectable in the resulting decay curves because the amount of carbon introduced was only about 1.8 μg/cm^2. Long-lived ^{18}F, produced in the $^{16}O(^{3}He,p)^{18}F + {}^{16}O(^{3}He,n)^{18}Ne \rightarrow {}^{18}F$ reactions with surface oxygen, was observed in the decay of the activated sample, but it was easily accounted for by decay curve resolution. The presence of ^{18}F, however, indicated the presence of ^{15}O also, produced in the

$^{16}O(^{3}He,\alpha)^{15}O$ reaction. The half life of ^{15}O is 2 min, inseparable from the 2.6 min ^{30}P. Using the known cross sections of these two interference reactions and the measured ^{18}F activity in the silicon targets, the contribution by ^{15}O was roughly estimated to be less than 5% of the end-of-bombardment activities.

Table X. Reactions induced in Si by ^{3}He ion bombardment. Isotopic abundance: ^{28}Si(92.18%), ^{29}Si(4.71%), ^{30}Si(3.12%)

Product	Reactions	Q(MeV)[a]	$T_{1/2}$[b]	Decay[b]	Associated γ-rays[b] keV(% per decay)	Interferences[c]
^{30}S	$^{28}Si(^{3}He,n)$	-0.57	1.4s	β^+	511(200), 687(80)	$^{32}Si(^{3}He,\alpha n)^{30}S$
	$^{29}Si(^{3}He,2n)$	-9.05				
	$^{30}Si(^{3}He,3n)$	-19.66				
^{31}S	$^{29}Si(^{3}He,n)$	3.96	2.7s	β^+	511(200), 1270(1.1)	$^{32}S(^{3}He,\alpha)^{31}S$
	$^{30}Si(^{3}He,2n)$	-6.66				$^{33}S(^{3}He,\alpha n)^{31}S$
						$^{31}P(^{3}He,p2n)^{31}S$
^{29}P	$^{28}Si(^{3}He,pn)$	-4.97	4.5s	β^+	511(200), 1280(0.8) 2430(0.2)	$^{31}P(^{3}He,\alpha n)^{29}P$
	$^{29}Si(^{3}He,p2n)$	-13.45				$^{27}Al(^{3}He,n)^{29}P$
^{30}P	$^{28}Si(^{3}He,p)$	6.35	2.5m	β^+	511(200), 2230(0.5)	$^{31}P(^{3}He,\alpha)^{30}P$
	$^{29}Si(^{3}He,pn)$	-2.13				
	$^{30}Si(^{3}He,p2n)$	-12.74				

Table X. (Continued)

Product	Reactions	Q(MeV)[a]	$T_{1/2}$[b]	Decay[b]	Associated γ-rays[b] keV(% per decay)	Interferences[c]
^{32}P	$^{30}Si(^{3}He,p)$	7.51	14.3d	β^-	No γ-rays	$^{31}P(^{3}He,2p)^{32}P$
^{26}Si	$^{28}Si(^{3}He,\alpha n)$	-9.93	2.1s	β^+	511(200), 820(34)	$^{24}Mg(^{3}He,n)^{26}Si$
						$^{25}Mg(^{3}He,2n)^{26}Si$
						$^{26}Mg(^{3}He,3n)^{26}Si$
^{27}Si	$^{28}Si(^{3}He,\alpha)$	3.40	4.1s	β^+	511(200)	$^{27}Al(^{3}He,p2n)^{27}Si$
	$^{29}Si(^{3}He,\alpha n)$	-5.07				$^{25}Mg(^{3}He,n)^{27}Si$
						$^{26}Mg(^{3}He,2n)^{27}Si$
^{31}Si	$^{30}Si(^{3}He,2p)$	-1.12	2.6h	β^-	1260(0.07)	None

[a] Appendix B

[b] Reference 50

[c] Interferences are ^{3}He induced reactions with other elements which may lead to the same product at bombarding energies below about 30 MeV.

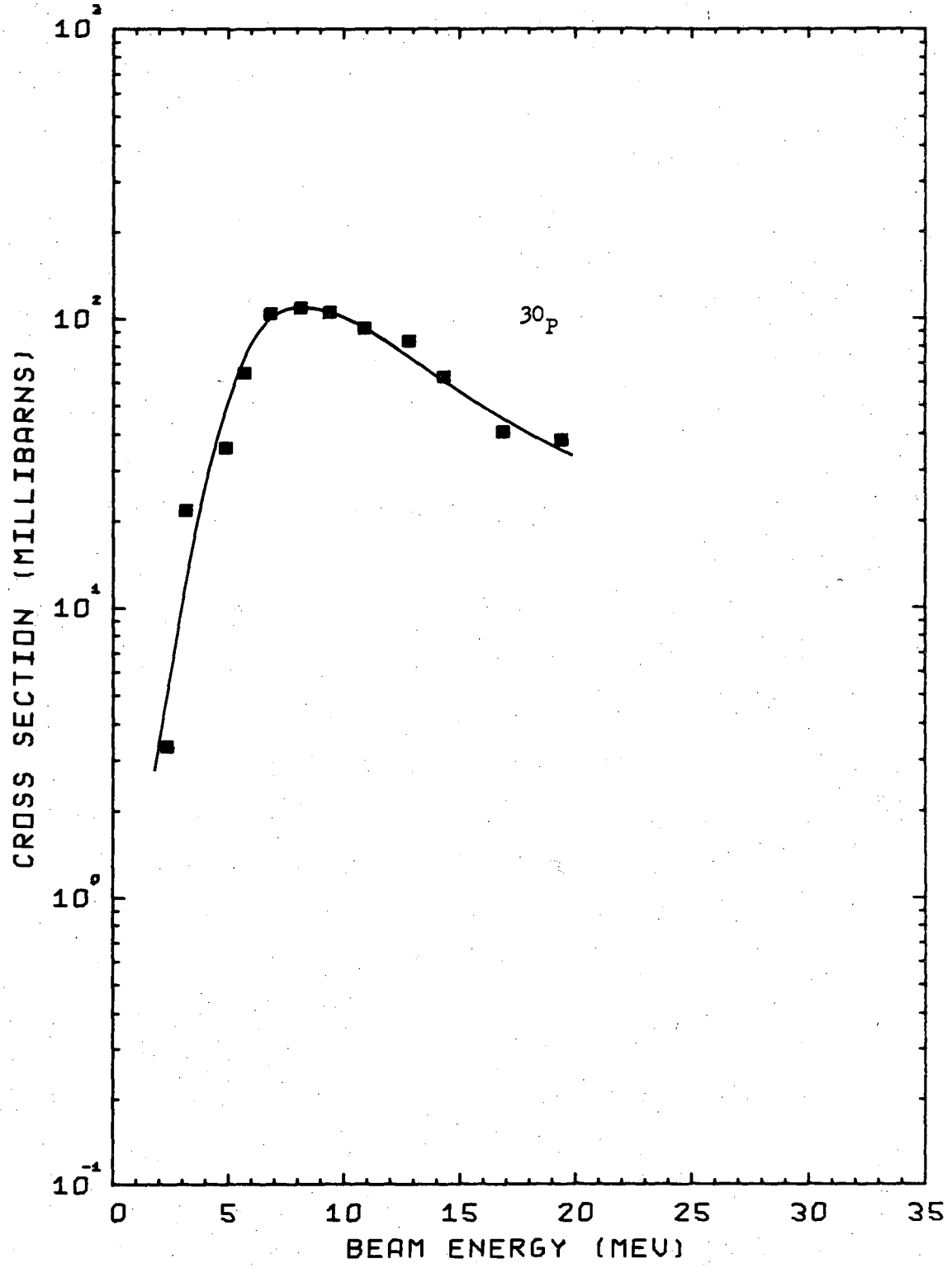

XBL 697-1005

Fig. 28. Total production excitation function for Si + ^{3}He → ^{30}P.

K. CALCIUM

Figure 29

$^{40}Ca(^{3}He,p)^{42m}Sc$ Lamb, Lee, and Markowitz[65]

Estimated error in σ is ±13%, including an uncertainty of ≈10% in photopeak analysis because the ^{42m}Sc γ-ray detected was superimposed on the Compton distribution below the 511-keV β^+ annihilation photopeak.

The targets used were prepared by vacuum-depositing calcium onto gold backing-plates and then depositing a thin film of gold over the calcium to minimize oxidation. The thicknesses of the calcium targets were determined by standard analytical procedures after irradiation and assay. The thickness of calcium on each target was about 0.9 mg/cm^2.

The activity of ^{42m}Sc was measured using a 6 cm^3 Ge(Li) detector to follow the decay of the 438-keV γ-ray photopeak. No other activities induced in Ca could be detected non-destructively.

The excitation function shown in Fig. 29 may be considered entirely attributable to the $^{40}Ca(^{3}He,p)^{42m}Sc$ because the threshold of the only other possible reaction, $^{42}Ca(^{3}He,p2n)$, is about 16 MeV.

Table XI. Reactions induced in Ca by ^{3}He ion bombardment. Isotopic abundance: $^{40}Ca(96.97\%)$, $^{42}Ca(0.64\%)$, $^{43}Ca(0.15\%)$, $^{44}Ca(2.06\%)$, $^{46}Ca(0.003\%)$, $^{48}Ca(0.18\%)$

Product	Reactions	Q(MeV)[a]	$T_{1/2}$[b]	Decay[b]	Associated γ-rays[b] keV(% per decay)	Interferences[c]
^{44}Ti	$^{42}Ca(^{3}He,n)$	5.98	48y	EC	68(90), 78(98)	$^{46}Ti(^{3}He,\alpha n)^{44}Tl$
	$^{43}Ca(^{3}He,2n)$	-1.95				
	$^{44}Ca(^{3}He,3n)$	-13.08				
^{45}Ti	$^{43}Ca(^{3}He,n)$	7.47	3.1h	β^{+},EC	511(170), 718(0.4) 1408(0.3)	$^{46}Ti(^{3}He,\alpha)^{45}Ti$
	$^{44}Ca(^{3}He,2n)$	-3.67				$^{47}Ti(^{3}He,\alpha n)^{45}Ti$
						$^{45}Sc(^{3}He,p2n)^{45}Ti$
^{42}Sc+	$^{40}Ca(^{3}He,p)$	4.90	0.7s	β^{+}	511(200)	$^{40}K(^{3}He,n)^{42}Sc$
^{42m}Sc	$^{42}Ca(^{3}He,p2n)$	-14.93	60.6s[d]	β^{+}	438(100), 511(200), 1220(100), 1520(100)	$^{41}K(^{3}He,2n)^{42}Sc$
^{43}Sc	$^{42}Ca(^{3}He,pn)$	-2.80	3.9h	β^{+},EC	375(22), 511(176)	$^{45}Sc(^{3}He,\alpha n)^{43}Sc$
	$^{43}Ca(^{3}He,p2n)$	-10.72				$^{41}K(^{3}He,n)^{43}Sc$
^{44}Sc+	$^{42}Ca(^{3}He,p)$	6.92	3.9h	β^{+},EC	511(188), 1159(100)	$^{45}Sc(^{3}He,\alpha)^{44}Sc$
^{44m}Sc	$^{43}Ca(^{3}He,pn)$	-1.01	2.4d	IT,EC	2.71(86), 1020(1.3), 1140(2.7)	
	$^{44}Ca(^{3}He,p2n)$	-12.15				
^{46}Sc+	$^{44}Ca(^{3}He,p)$	7.94	84d	β^{-}	889(100), 1120(100)	$^{45}Sc(^{3}He,2p)^{44}Sc$
^{46m}Sc	$^{46}Ca(^{3}He,p2n)$	-9.88	20s	IT	142(100)	
^{47}Sc	$^{46}Ca(^{3}He,pn)$	0.76	3.4d	β^{-}	160(73)	None

Table XI. (Continued)

Product	Reactions	Q(MeV)[a]	$T_{1/2}$[b]	Decay[b]	Associated γ-rays[b] keV(% per decay)	Interferences[c]
^{48}Sc	$^{46}Ca(^{3}He,p)$	9.01	1.8d	β^-	175(6), 983(100) 1040(100), 1314(100)	None
	$^{48}Ca(^{3}He,p2n)$	-8.21				
^{49}Sc	$^{48}Ca(^{3}He,pn)$	1.90	57.5m	β^-	1760(0.03)	None
$^{50}Sc+$	$^{48}Ca(^{3}He,p)$	8.39	1.7m	β^-	520(100), 1120(100), 1550(100)	None
$\underline{^{50m}Sc}$			$\underline{0.4s}$	$\underline{IT}$	$\underline{258(100)}$	
^{39}Ca	$^{40}Ca(^{3}He,\alpha)$	4.95	0.9s	β^+	511(200)	$^{38}Ar(^{3}He,2n)^{39}Ca$
						$^{39}K(^{3}He,p2n)^{39}Ca$
^{41}Ca	$^{40}Ca(^{3}He,2p)$	0.63	$8\times10^{4}y$	EC	No γ-rays	$^{40}Ar(^{3}He,2n)^{41}Ca$
	$^{42}Ca(^{3}He,\alpha)$	9.09				$^{40}K(^{3}He,pn)^{41}Ca$
						$^{41}K(^{3}He,p2n)^{41}Ca$

Table XI. (Continued)

Product	Reactions	Q(MeV)[a]	$T_{1/2}$[b]	Decay[b]	Associated γ-rays[b] keV(% per decay)	Interferences[c]
^{45}Ca	$^{44}Ca(^{3}He,2p)$	−0.30	165d	β^-	No γ-rays	None
	$^{46}Ca(^{3}He,\alpha)$	10.17				
^{47}Ca	$^{46}Ca(^{3}He,2p)$	-.44	4.5d	β^-	490(5), 815(5), 1308(74)	None
	$^{48}Ca(^{3}He,\alpha)$	10.63				
^{49}Ca	$^{48}Ca(^{3}He,2p)$	-2.57	8.8m	β^-	3100(89), 4100(10)	None

[a] Appendix B

[b] Reference 50

[c] Interferences are ^{3}He induced reactions with other elements which may lead to the same product at bombarding energies below about 30 MeV.

[d] Underlined decay data indicates metastable or isomeric state.

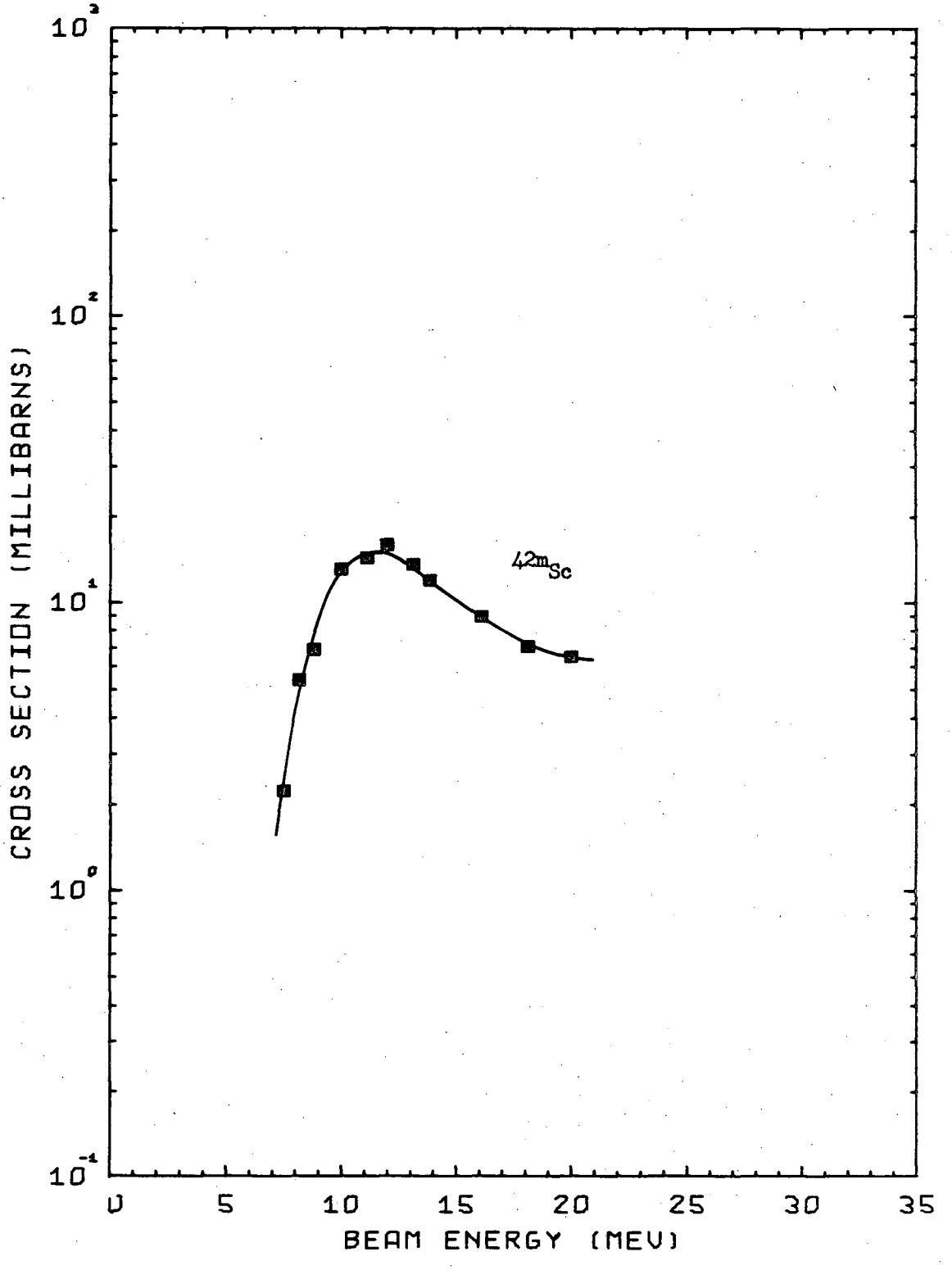

Fig. 29. Excitation function for $^{40}Ca(^{3}He,p)^{42m}Sc$.

L. TITANIUM

Figure 30

$^{3}He + Ti \rightarrow {}^{49}Cr$

$^{3}He + Ti \rightarrow {}^{48}V$

$^{3}He + Ti \rightarrow {}^{48}Cr$

Lamb, Lee, Markowitz[65]

Estimated errors in σ are ±7% for ^{49}Cr, ±14% for ^{48}V, and ±9% for ^{48}Cr. The ^{48}V excitation function has errors compounded from measurements of ^{48}V activity and its parent, ^{48}Cr.

Targets for these experiments were 0.00025-in thick titanium foils. The ^{49}Cr data were obtained by individual 5 min bombardment of three foils, of which only the center foil was radio-assayed. The ^{48}Cr and ^{48}V data were obtained in a stacked foil experiment with a bombardment time of 1 hour. The beam currents were about 0.2 μA for each experiment.

The activities of the products were measured using a 6 cm^3 Ge(Li) detector. For the ^{49}Cr excitation function, the decay of the 153-keV γ-ray line was followed. The decay of the 116-keV photopeak was followed for the ^{48}Cr function. The activity of ^{48}V in irradiated titanium arose from direct production and from decay of ^{48}Cr. The ^{48}V activity was followed via the 983-keV γ-ray, the contribution from ^{48}Cr decay calculated from the ^{48}Cr activities obtained in the same run, and directly produced ^{48}V obtained as the difference.

None of the excitation functions shown in Fig. 30 have been corrected for isotopic abundances. The ^{49}Cr curve represents the sum of $(^{3}He,n)$, $(^{3}He,2n)$, and $(^{3}He,3n)$ reactions with the various stable isotopes of titanium. The shape of the function suggests that the contribution from

single neutron emission is small. Go has predicted a maximum cross section of only 7 mb for the $^{47}Ti(^{3}He,n)^{49}Cr$ reaction.[67] Because natural Ti is about 74% ^{48}Ti, and because the threshold for the $^{49}Ti(^{3}He,3n)^{49}Cr$ reaction is about 13.3 MeV, it may be assumed that this ^{49}Cr production excitation function is almost entirely due to $^{48}Ti(^{3}He,2n)^{49}Cr$. The ^{48}V curve is composed of contributions from $(^{3}He,p)$, $(^{3}He,pn)$, and $(^{3}He,p2n)$. Of these three reactions, the (p2n) emission (threshold = 13.3 MeV) is predominant because of the high relative abundance of ^{48}Ti. The ^{48}Cr function shows contributions from at least two of the possible three neutron boil-off reactions.

Table XII. Reactions induced in Ti by ^{3}He ion bombardment. Isotopic abundance: $^{46}Ti(7.99\%)$, $^{47}Ti(7.32\%)$, $^{48}Ti(73.99\%)$, $^{49}Ti(5.46\%)$, $^{50}Ti(5.25\%)$

Product	Reactions	Q(MeV)[a]	$T_{1/2}$[b]	Decay[b]	Associated γ-rays[b] keV(% per decay)	Interferences[c]
^{48}Cr	$^{46}Ti(^{3}He,n)$	5.81	23h	EC	116(98), 310(99)	$^{50}Cr(^{3}He,\alpha n)^{48}Cr$
	$^{47}Ti(^{3}He,2n)$	-3.07				
	$^{48}Ti(^{3}He,3n)$	-14.70				
^{49}Cr	$^{47}Ti(^{3}He,n)$	7.32	41.9m	β^{+},EC	63(14), 91(28), 153(13), 511(186)	$^{50}Cr(^{3}He,\alpha)^{49}Cr$
	$^{48}Ti(^{3}He,2n)$	-4.30				
	$^{49}Ti(^{3}He,3n)$	-12.45				
^{51}Cr	$^{49}Ti(^{3}He,n)$	9.75	27.8d	EC	320(9)	$^{50}Cr(^{3}He,2p)^{51}Cr$
	$^{50}Ti(^{3}He,2n)$	-1.19				$^{52}Cr(^{3}He,\alpha)^{51}Cr$
						$^{53}Cr(^{3}He,\alpha n)^{51}Cr$
						$^{51}V(^{3}He,p2n)^{51}Cr$
^{47}V	$^{46}Ti(^{3}He,pn)$	-2.54	33m	β^{+},EC	511(192),1550(0.7), 1800(0.5), 2160(0.2)	$^{45}Sc(^{3}He,n)^{47}V$
	$^{47}Ti(^{3}He,p2n)$	-11.42				
^{48}V	$^{46}Ti(^{3}He,p)$	7.99	16d	β^{+},EC	511(100), 945(10), 983(100), 1312(97) 2241(3)	Decay of ^{48}Cr
	$^{47}Ti(^{3}He,pn)$	-.089				
	$^{48}Ti(^{3}He,p2n)$	-12.51				
	Decay of ^{48}Cr					

Table XII (Continued)

Product	Reactions	Q(MeV)[a]	$T_{1/2}$[b]	Decay[b]	Associated γ-rays[b] keV(% per decay)	Interferences[c]
^{49}V	$^{47}Ti(^{3}He,p)$	10.67	330d	EC	No -rays	$^{51}V(^{3}He,\alpha n)^{49}V$
	$^{48}Ti(^{3}He,pn)$	-0.96				
	$^{49}Ti(^{3}He,p2n)$	-9.10				
	Decay of ^{49}Cr					
^{52}V	$^{50}Ti(^{3}He,p)$	7.65	3.8m	β^-	1434(100)	$^{51}V(^{3}He,2p)^{52}V$
^{45}Ti	$^{46}Ti(^{3}He,\alpha)$	7.38	3.1h	β^+,EC	511(170), 718(0.4) 1408(0.3)	$^{43}Ca(^{3}He,n)^{45}Ti$
	$^{47}Ti(^{3}He,\alpha n)$	-1.49				$^{44}Ca(^{3}He,2n)^{45}Ti$
						$^{45}Sc(^{3}He,p2n)^{45}TI$
^{51}Ti	$^{50}Ti(^{3}He,2p)$	-1.34	5.8m	β^-	320(95), 605(1.5), 928(5)	None

[a] Appendix B

[b] Reference 50

[c] Interferences are ^{3}He induced reactions with other elements which may lead to the same product at bombarding energies below about 30 MeV.

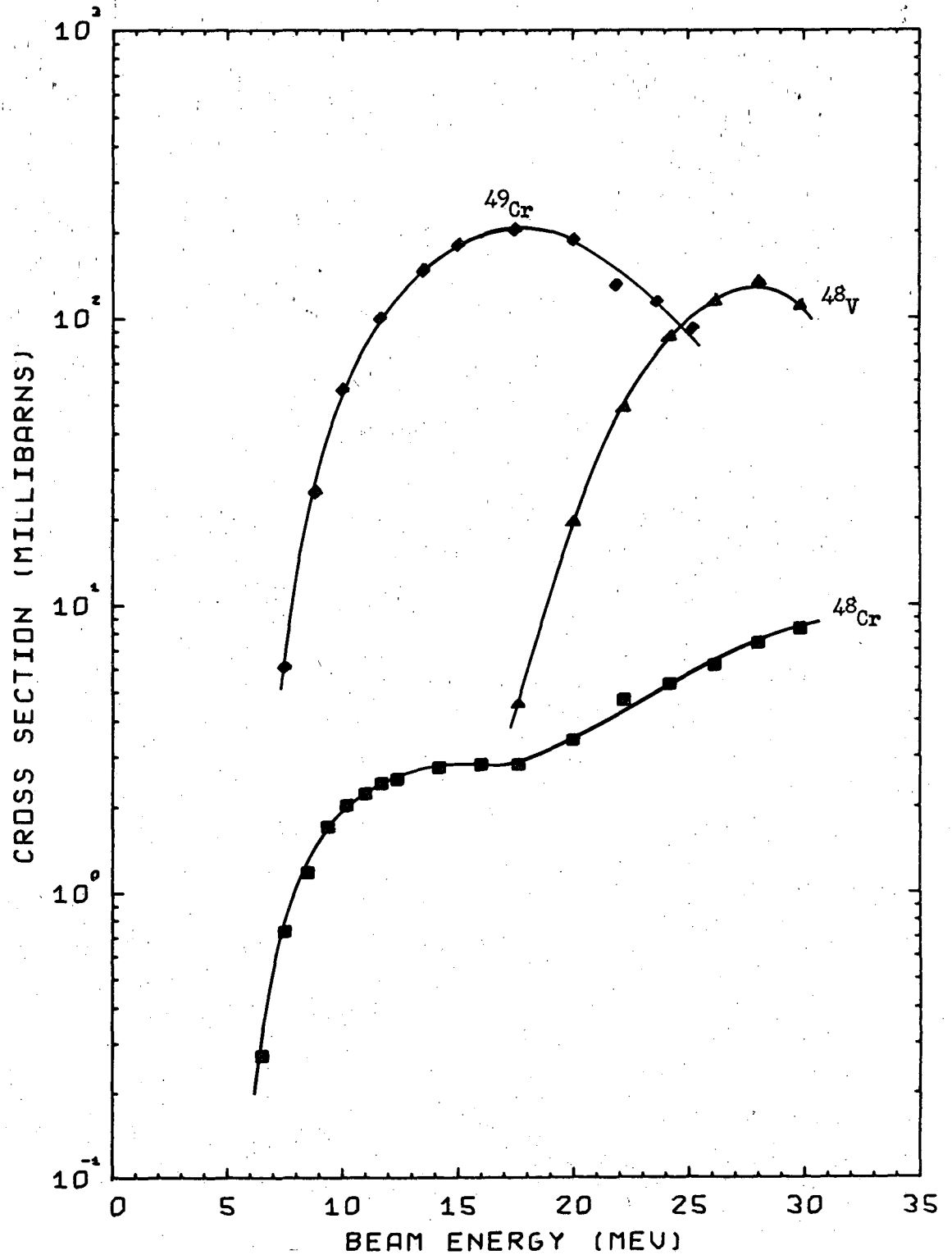

Fig. 30. Total production excitation functions for Ti + $^{3}He \rightarrow {}^{49}Cr$, ^{48}V, ^{48}Cr.

M. IRON Figure 31

$^{56}Fe(^{3}He,pn)^{57}Co$ Hazan and Blann[32]

$^{56}Fe(^{3}He,p2n)^{56}Co$

$^{56}Fe(^{3}He,p)^{58}Co$

$^{56}Fe(^{3}He,n)^{57}Ni$

$^{56}Fe(^{3}He,3n)^{56}Ni$

Estimated errors in σ are ±20% in ^{57}Co, ±25% in ^{56}Co, ±25-30% in ^{58}Co, ±20% in ^{57}Ni and ±25% in ^{56}Ni.

Table XIII. Reactions induced in Fe by ^{3}He ion bombardment. Isotopic abundance: $^{54}Fe(5.84\%)$, $^{56}Fe(91.68\%)$, $^{57}Fe(2.17\%)$, $^{58}Fe(0.31\%)$

Product	Reactions	Q(MeV)[a]	$T_{1/2}$[b]	Decay[b]	Associated γ-rays[b] keV(% per decay)	Interferences[c]
^{56}Ni	$^{54}Fe(^{3}He,n)$	4.53	6.1d	EC	163(99), 276(31) 472(35), 748(48), 812(85), 1560(14)	$^{58}Ni(^{3}He,\alpha n)^{56}Ni$
	$^{56}Fe(^{3}He,3n)$	-15.97				
^{57}Ni	$^{56}Fe(^{3}He,2n)$	-5.71	36h	EC,β^+	127(14), 511(92) 1370(86), 1890(14)	$^{58}Ni(^{3}He,\alpha)^{57}Ni$
	$^{57}Fe(^{3}He,3n)$	-13.35				
^{55}Co	$^{54}Fe(^{3}He,pn)$	-2.66	18.2h	β^+,EC	480(12), 511(160), 930(80), 1410(13)	$^{55}Mn(^{3}He,3n)^{55}Co$
^{56}Co	$^{54}Fe(^{3}He,p)$	7.43	77.3d	EC,β^+	511(40), 847(100), 1040(15), 1240(66), 1760(15), 2020(11), 2600(17), 3260(13)	$^{55}Mn(^{3}He,2n)^{56}Co$
	$^{56}Fe(^{3}He,p2n)$	-13.07				$^{58}Ni(^{3}He,\alpha n)^{56}Ni\rightarrow^{56}Co$
	Decay of ^{56}Ni					
^{57}Co	$^{56}Fe(^{3}He,pn)$	-1.70	270d	EC	14(9), 122(87), 136(11), 692(0.14)	$^{55}Mn(^{3}He,n)^{57}Co$
	$^{57}Fe(^{3}He,p2n)$	-9.34				$^{59}Co(^{3}He,\alpha n)^{57}Co$
	Decay of ^{57}Ni					$^{58}Ni(^{3}He,\alpha)^{57}Ni\rightarrow^{57}Co$
^{58}Co	$^{56}Fe(^{3}He,p)$	6.87	71.3d	EC,β^+	511(30), 810(99), 865(1.4), 1670(0.6)	$^{59}Co(^{3}He,\alpha)^{58}Co$
^{58m}Co	$^{57}Fe(^{3}He,pn)$	-0.77	9.2h[d]	IT	No γ-rays	
	$^{58}Fe(^{3}He,p2n)$	-10.81				

Table XIII. (Continued)

Product	Reactions	Q(MeV)[a]	$T_{1/2}$[b]	Decay[b]	Associated γ-rays[b] keV(% per decay)	Interferences[c]
^{60}Co	$^{58}Fe(^{3}He,p)$	7.15	5.3y	β^-	1173(100), 1332(100)	$^{59}Co(^{3}He,2p)^{60}Co$
$\underline{^{60m}Co}$			<u>10.5m</u>	<u>IT,β^-</u>	<u>59(2.1), 1330(.25)</u>	
^{52}Fe	$^{54}Fe(^{3}He,\alpha n)$	-3.49	8.2h	β^+,EC	165(100), 511(112)	$^{50}Cr(^{3}He,n)^{52}Fe$
						$^{52}Cr(^{3}He,3n)^{52}Fe$
^{53}Fe	$^{54}Fe(^{3}He,\alpha)$	6.95	8.5m	β^+,EC	380(32), 511(196)	$^{52}Cr(^{3}He,2n)^{53}Fe$
^{55}Fe	$^{54}Fe(^{3}He,2p)$	1.58	2.6y	EC	No γ-rays	$^{53}Cr(^{3}He,n)^{55}Fe$
	$^{56}Fe(^{3}He,\alpha)$	9.37				$^{54}Cr(^{3}He,2n)^{55}Fe$
	$^{57}Fe(^{3}He,\alpha n)$	1.73				$^{55}Mn(^{3}He,p2n)^{55}Fe$
	Decay of ^{55}Co					
^{59}Fe	$^{58}Fe(^{3}He,2p)$	-1.13	45d	β^-	143(0.8), 192(2.8), 1095(56), 1292(44)	None

[a] Appendix B

[b] Reference 50

[c] Interferences are ^{3}He induced reactions with other elements which may lead to the same product at bombarding energies below about 30 MeV.

[d] Underlined decay data indicates metastable or isomeric state.

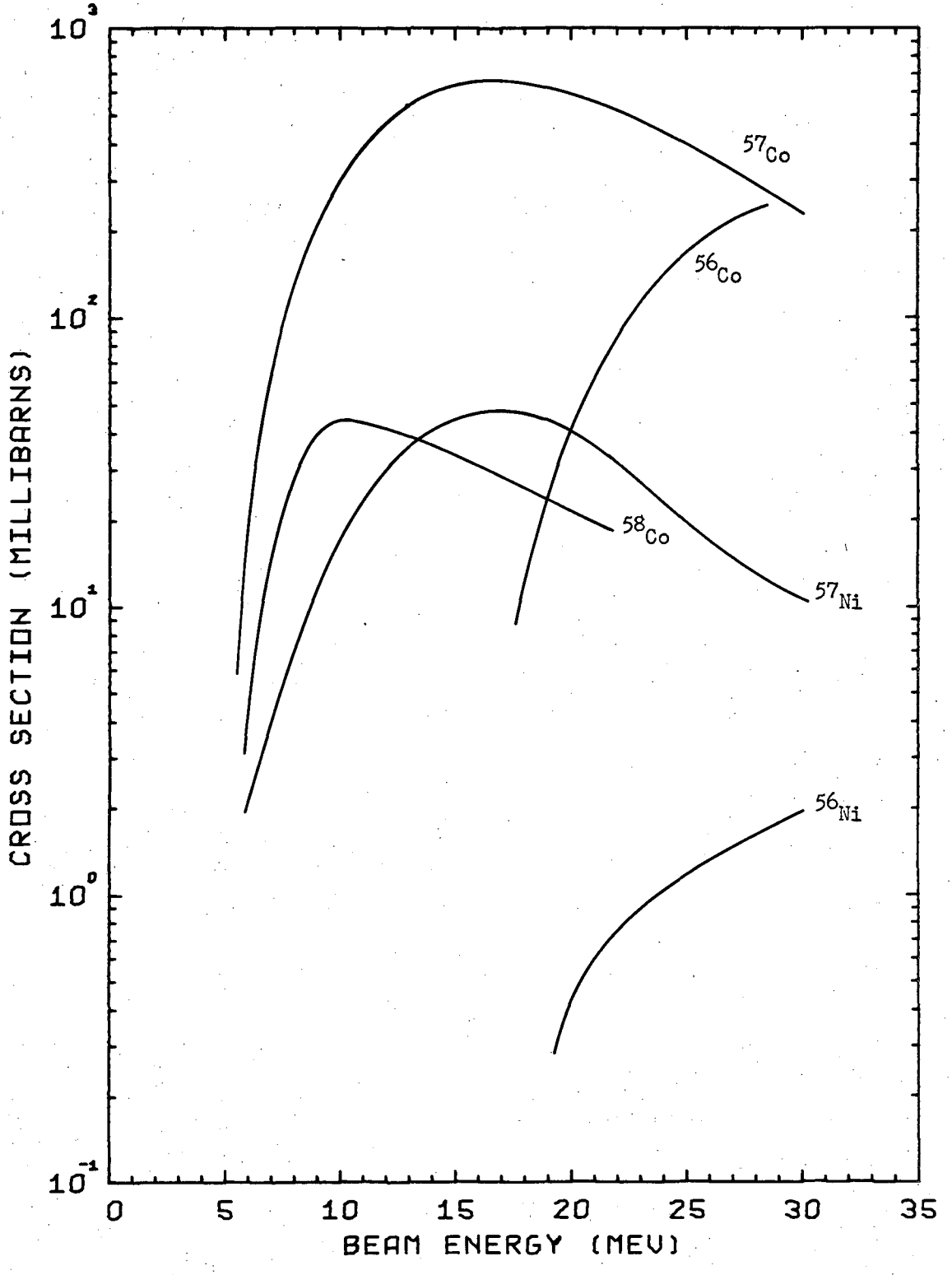

Fig. 31. Excitation functions for $^{56}Fe(^{3}He,pn)^{57}Co$, $^{56}Fe(^{3}He,p2n)^{56}Co$, $^{56}Fe(^{3}He,p)^{58}Co$, $^{56}Fe(^{3}He,2n)^{57}Ni$, and $^{56}Fe(^{3}He,3n)^{56}Ni$. The reference is given in the text.

N. NICKEL Figure 32

$^{61}Ni(^{3}He,pn)^{62}Cu$ Smith[85]

$^{61}Ni(^{3}He,2n)^{62}Zn$

$^{61}Ni(^{3}He,n)^{63}Zn$

The estimated errors in σ are 7% for ^{63}Zn, 4% for ^{62}Zn, and 8% for ^{62}Cu. The data were obtained using targets isotopically enriched in ^{61}Ni, having 79.4% ^{61}Ni and from approximately 3.5 to 7.5% of the other natural Ni isotopes. Natural Ni has only 1.25% ^{61}Ni. The data for the $^{61}Ni(^{3}He,n)^{62}Zn$ reaction includes a contribution from $^{62}Ni(^{3}He,2n)^{63}Zn$.

N. NICKEL (Cont) Figure 33

$^{3}He + Ni \rightarrow {}^{61}Cu$ Lamb, Lee, and Markowitz[65]

$^{3}He + Ni \rightarrow {}^{60}Cu$

$^{3}He + Ni \rightarrow {}^{59}Cu$

$^{3}He + Ni \rightarrow {}^{57}Ni$

$^{3}He + Ni \rightarrow {}^{56}Ni$

$^{3}He + Ni \rightarrow {}^{62}Zn$

Estimated errors in σ are ±15%.

Two sets of Ni targets were irradiated. The first set, for determination of the short-lived activities of ^{60}Cu and ^{59}Cu, were prepared by sandwiching 1.2 mg/cm^2 Ni foil targets between two 6 mg/cm^2 Au recoil catcher foils which were, in turn, protected from contamination by an additional Au foil on either side. Individual irradiations were performed at 0.25 μA, and the nickel foil was radio-assayed together with the recoil catchers (inner two Au foils) using a 16 cm^3 Ge(Li) detector. The second target, a stack composed of 1.2 mg/cm^2 and 3.0 mg/cm^2 Ni foils, was bombarded with 0.25 μA of 31.2 MeV $^{3}He^{++}$ ions for 40 minutes. Selected foils were assayed using the 16 cm^3 Ge(Li) detector.

The activities of the products were obtained by following the decay of convenient γ-ray photopeaks in the spectra. These were: 284 keV for ^{61}Cu, 1332 keV for ^{60}Cu, 872 keV for ^{59}Cu, 1370 keV for ^{57}Ni, 163 keV for ^{56}Ni, and 590 keV for ^{62}Zn.

The excitation functions shown in Fig. 33 are total production curves, uncorrected for isotopic abundance.

The ^{61}Cu activity results directly via (^{3}He,pn) and (^{3}He,p2n) reactions and from decay of ^{61}Zn produced by (^{3}He,2n) and (^{3}He,3n) reactions. Because of unfavorable decay characteristics, ^{61}Zn activity was not determined. The ^{59}Cu activity may be attributed entirely to (^{3}He,pn), the ^{56}Ni entirely to (^{3}He,αn) and the ^{57}Ni entirely to (^{3}He,α), all reactions with 67.8% abundant ^{58}Ni. The activity of ^{60}Cu results from the summed (^{3}He,n) and (^{3}He,p) on ^{58}Ni and from ^{60}Ni(^{3}He,p2n)^{60}Cu. The threshold for the last reaction, 15.4 MeV, corresponds very well with the higher-energy behavior of the ^{60}Cu excitation funtion. ^{62}Zn may arise from (^{3}He,n), (^{3}He,2n), and (^{3}He,3n) reactions. The last two reactions involve minor constituents of natural nickel, while the first involves the 26.2% ^{60}Ni. The behavior of the function at low energy suggests that the contribution from (^{3}He,n) is predominant, while at higher energies the multiple neutron boil-off is observed.

Table XIV. Reactions induced in Ni by ^{3}He ion bombardment. Isotopic abundance: $^{58}Ni(67.76\%)$, $^{60}Ni(26.16\%)$, $^{61}Ni(1.25\%)$, $^{62}Ni(3.66\%)$, $^{64}Ni(1.16\%)$

Product	Reactions	Q(MeV)[a]	$T_{1/2}$[b]	Decay[b]	Associated γ-ray[b] keV(% per decay)	Interferences[c]
^{60}Zn	$^{58}Ni(^{3}He,n)$	---	2.1m	EC,β^+	--	None
	$^{60}Ni(^{3}He,3n)$	---				
^{61}Zn	$^{60}Ni(^{3}He,2n)$	-9.10	1.5m	β^+,EC	480(11), 511(198), 980(3), 1640(6)	None
	$^{61}Ni(^{3}He,3n)$	-16.92				
^{62}Zn	$^{60}Ni(^{3}He,n)$	3.51	9.1h	EC,β^+	42(20), 511(47), 590(22)	$^{64}Zn(^{3}He,\alpha n)^{62}Zn$
	$^{61}Ni(^{3}He,2n)$	-4.31				
	$^{62}Ni(^{3}He,3n)$	-14.91				
^{63}Zn	$^{61}Ni(^{3}He,n)$	4.86	38.4m	β^+,EC	511(186), 669(8), 962(6), 1420(0.9)	$^{64}Zn(^{3}He,\alpha)^{63}Zn$
	$^{62}Ni(^{3}He,2n)$	5.74				$^{63}Cu(^{3}He,p2n)^{63}Zn$
^{65}Zn	$^{64}Ni(^{3}He,2n)$	-2.40	245d	EC,β^+	511(3.4), 1115(49),	$^{63}Cu(^{3}He,p)^{65}Zn$
						$^{65}Cu(^{3}He,p2n)^{65}Zn$
						$^{64}Zn(^{3}He,2p)^{65}Zn$
						$^{66}Zn(^{3}He,\alpha)^{65}Zn$
						$^{67}Zn(^{3}He,\alpha n)^{65}Zn$
						$^{64}Zn(^{3}He,pn)^{65}Ga\rightarrow^{65}Zn$

Table XIV. (Continued)

Product	Reactions	Q(MeV)[a]	$T_{1/2}$[b]	Decay[b]	Associated γ-rays[b] keV(per decay)	Interferences[c]
^{58}Cu	$^{58}Ni(^{3}He,p2n)$	-17.07	3.2s	β^+	511(200)	None
^{59}Cu	$^{58}Ni(^{3}He,pn)$	-4.30	81.5s	β^+	343(5), 463(5), 511(197), 872(9), 1305(11), 1700(1)	$^{59}Co(^{3}He,3n)^{59}Cu$
^{60}Cu	$^{58}Ni(^{3}He,p)$	5.76	23.4m	β^+,EC	511(186), 850(15), 1332(80), 1760(52), 2130(6), 2640(5)	$^{59}Co(^{3}He,2n)^{60}Cu$
	$^{60}Ni(^{3}He,p2n)$	-14.63				
	Decay of ^{60}Zn					
^{61}Cu	$^{60}Ni(^{3}He,pn)$	-2.92	3.3h	β^+,EC	67(4), 284(12), 380(3), 511(120), 580(1.5), 660(11), 940(1.5), 1150(1), 1220(5)	$^{59}Co(^{3}He,n)^{61}Cu$
	$^{61}Ni(^{3}He,p2n)$	-10.74				
	Decay of ^{61}Zn					
^{62}Cu	$^{60}Ni(^{3}He,p)$	5.98	9.8m	β^+,EC	511(195), 880(0.3), 1170(0.5)	$^{63}Cu(^{3}He,\alpha)^{62}Cu$
	$^{61}Ni(^{3}He,pn)$	-1.84				$^{64}Zn(^{3}He,\alpha n)^{62}Zn\rightarrow^{62}Cu$
	$^{62}Ni(^{3}He,p2n)$	-12.44				
	Decay of ^{62}Zn					
^{64}Cu	$^{62}Ni(^{3}He,p)$	6.32	12.8h	EC,$\beta^-\beta^+$	511(30), 1340(0.5)	$^{63}Cu(^{3}He,2p)^{64}Cu$
	$^{64}Ni(^{3}He,p2n)$	-10.18				$^{65}Cu(^{3}He,\alpha)^{64}Cu$
^{66}Cu	$^{64}Ni(^{3}He,p)$	6.79	5.1m	β^-	1039(9)	$^{65}Cu(^{3}He,2p)^{66}Cu$

Table XIV. (Continued)

Product	Reactions	Q(MeV)[a]	$T_{1/2}$[b]	Decay[b]	Associated -rays[b] keV(% per decay)	Interferences[c]
^{56}Ni	$^{58}Ni(^{3}He,\alpha n)$	-1.88	6.1d	EC	163(99), 276(31), 472(35), 748(48) 812(85), 1560(14)	$^{54}Fe(^{3}He,n)^{56}Ni$ $^{56}Fe(^{3}He,3n)^{56}Ni$
^{57}Ni	$^{58}Ni(^{3}He,\alpha)$	8.38	36h	EC,β^+	127(14), 511(92), 1370(86), 1890(14)	$^{56}Fe(^{3}He,2n)^{57}Ni$ $^{57}Fe(^{3}He,3n)^{57}Ni$
^{59}Ni	$^{58}Ni(^{3}He,2p)$	1.29	8×10^{4}y	EC	No γ-rays	$^{57}Fe(^{3}He,n)^{59}Ni$
	$^{60}Ni(^{3}He,\alpha)$	9.19				$^{58}Fe(^{3}He,2n)^{59}Ni$
	$^{61}Ni(^{3}He,\alpha n)$	1.37				$^{59}Co(^{3}He,p2n)^{59}Ni$
	Decay of ^{59}Cu					$^{59}Co(^{3}He,3n)^{59}Cu\rightarrow^{59}Ni$
^{63}Ni	$^{62}Ni(^{3}He,2p)$	-0.88	92y	β^-	No γ-rays	None
	$^{64}Ni(^{3}He,\alpha)$	10.91				
^{65}Ni	$^{64}Ni(^{3}He,2p)$	-1.62	2.6h	β^-	368(4.5), 1115(16), 1481(25)	None

[a] Appendix B

[b] Reference 50

[c] Interferences are ^{3}He induced reactions with other elements which may lead to the same product at bombarding energies below about 30 MeV.

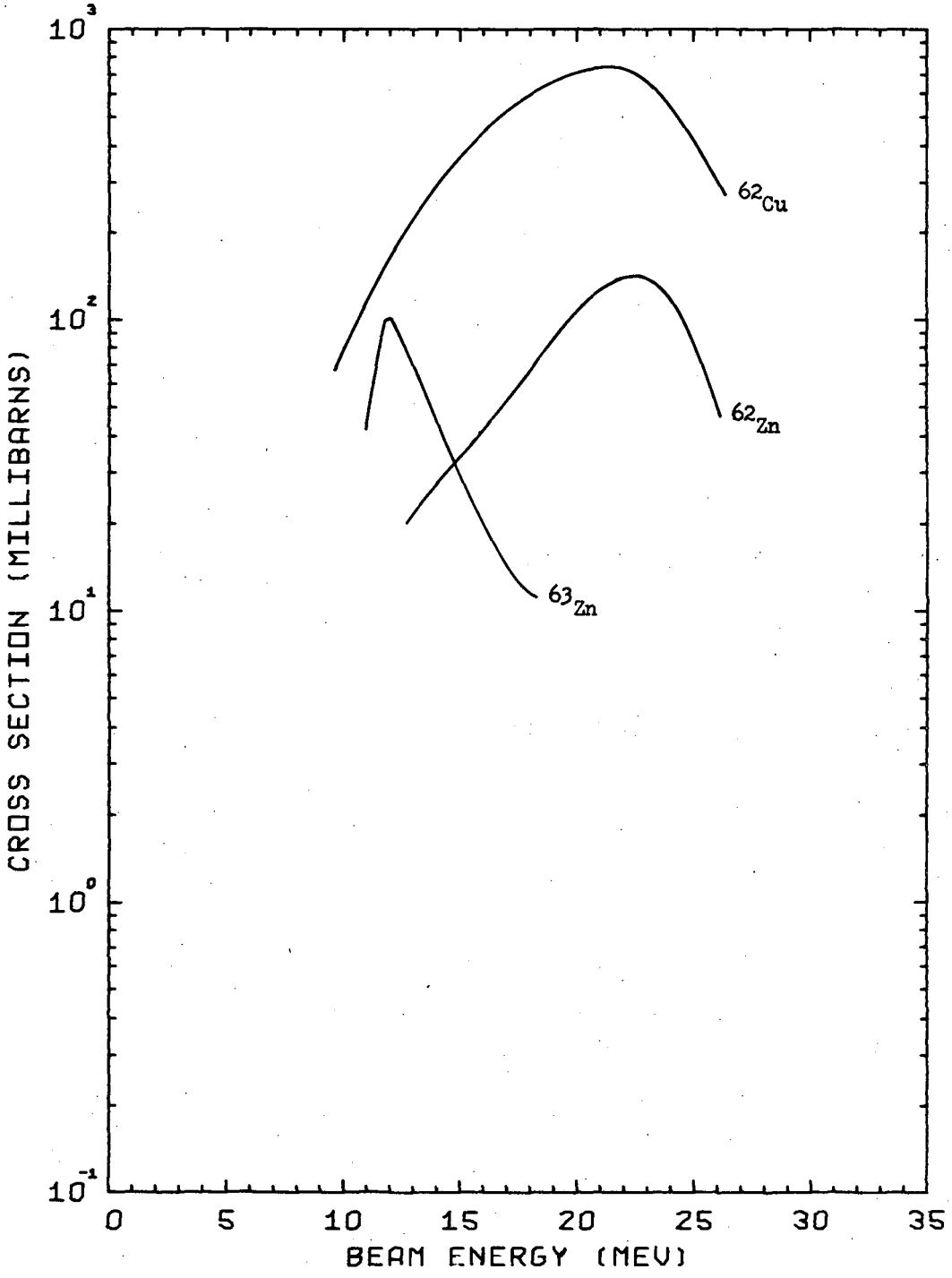

Fig. 32. Excitation functions for the reactions $^{61}Ni(^{3}He,pn)^{62}Cu$, $^{61}Ni(^{3}He,2n)^{62}Zn$, and $^{61}Ni(^{3}He,n)^{63}Zn$. The reference is given in the text.

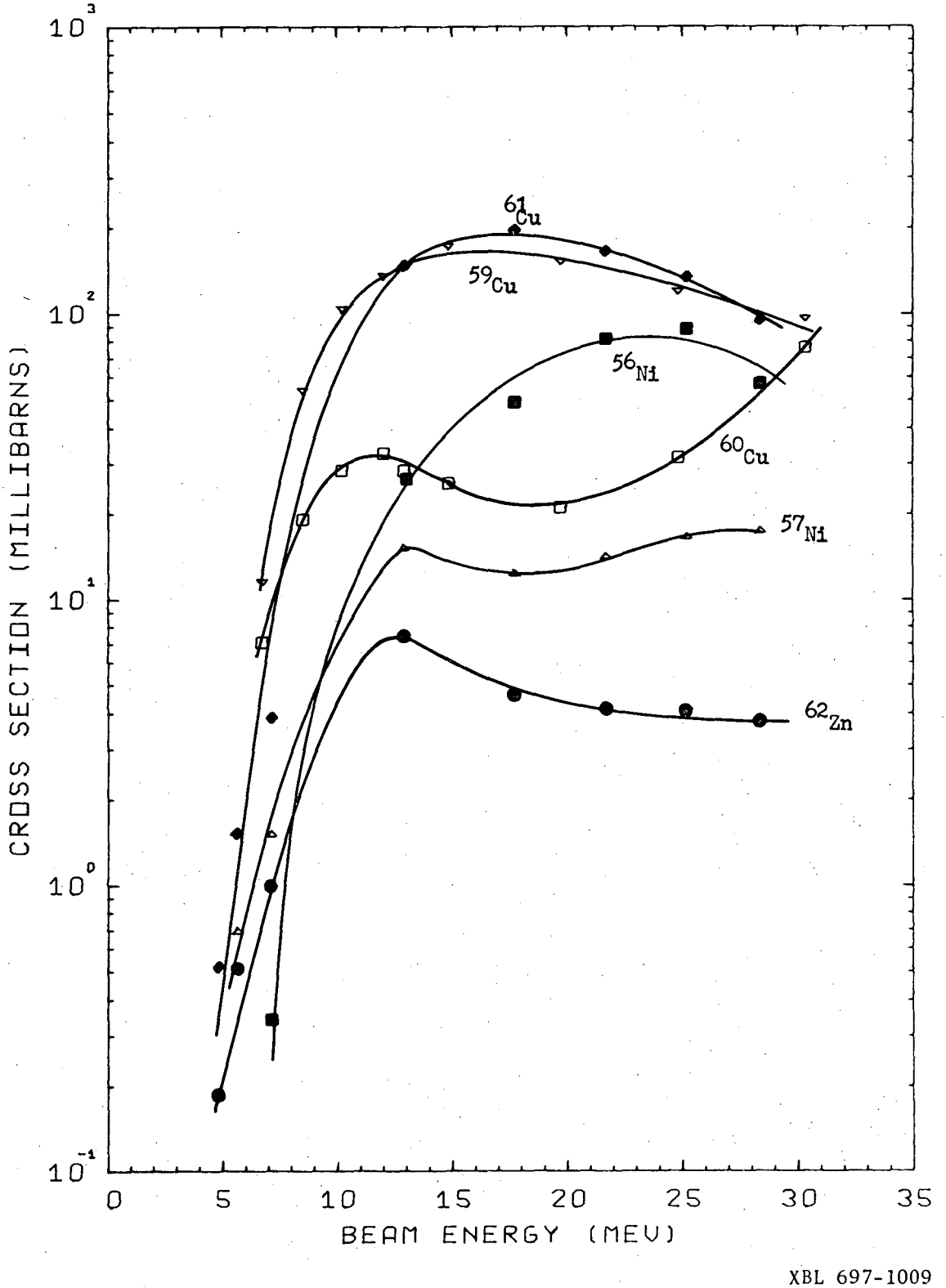

Fig. 33. Total production excitation functions for Ni + $^{3}He \rightarrow {}^{61}Cu$, ^{59}Cu, ^{56}Ni, ^{60}Cu, ^{57}Ni, ^{62}Zn.

O. COPPER

Figure 34

$^{63}Cu(^{3}He,p3n)^{62}Zn$ Bryant, Cochran, and Knight[31]

$^{63}Cu(^{3}He,n)^{65}Ga$

$^{63}Cu(^{3}He,2\alpha)^{58}Co$

$^{63}Cu(^{3}He,p)^{65}Zn$

$^{63}Cu(^{3}He,\alpha)^{62}Cu$

$^{63}Cu(^{3}He,\alpha n)^{61}Cu$

$^{63}Cu(^{3}He,2p)^{64}Cu$

$^{63}Cu(^{3}He,p2n)^{63}Zn + {}^{63}Cu(^{3}He,3n)^{63}Ga \rightarrow {}^{63}Zn$

Figure 35

$^{65}Cu(^{3}He,n)^{67}Ga$ Bryant, Cochran, and Knight[31]

$^{65}Cu(^{3}He,\alpha p)^{63}Ni$

$^{65}Cu(^{3}He,3n)^{65}Ga$

$^{65}Cu(^{3}He,2n)^{66}Ga$

$^{65}Cu(^{3}He,p2n)^{65}Zn$

$^{65}Cu(^{3}He,\alpha)^{64}Cu$ Saha and Porile[33]

The estimated errors in σ for the data of Bryant, Cochran and Knight are less than 15-18% for all reactions except $^{65}Cu(^{3}He, p)^{63}Ni$ (±36%). The data of Saha and Porile are correct to an estimated ±15-20%.

The excitation functions shown in Fig. 34 and Fig. 35 were corrected for ambiguities resulting from formation of the same product from more than one target isotope by using isotopically enriched targets where necessary. Only the ^{63}Zn retains such unresolved ambiguities and these are believed to contribute less than 10% to the total σ even at the highest energies studied.

Table XV. Reactions induced in Cu by ^{3}He ion bombardment. Isotopic abundance: $^{63}Cu(69.1\%)$, $^{65}Cu(30.9\%)$

Product	Reactions	Q(MeV)[a]	$T_{1/2}$[b]	Decay[b]	Associated γ-rays[b] keV(% per decay)	Interferences[c]
^{63}Ga	$^{63}Cu(^{3}He,3n)$	-17.87	33s	β^{+},EC	---	None
^{64}Ga	$^{63}Cu(^{3}He,2n)$	-7.87	2.6m	β^{+},EC	511(196), 800(15), 992(43), 1250(7), 1380(14), 1560(7), 1780(5), 2180(11), 2340(9), 3320(18)	$^{64}Zn(^{3}He,p2n)^{64}Ga$
^{65}Ga	$^{63}Cu(^{3}He,n)$	3.93	15.2m	β^{+},EC	54(8), 61(12), 115(55), 152(10), 206(4), 511(180), 750(10), 930(3)	$^{64}Zn(^{3}He,pn)^{65}Ga$
	$^{65}Cu(^{3}He,3n)$	-13.89				$^{64}Zn(^{3}He,2n)^{65}Ge\rightarrow^{65}Ga$
^{66}Ga	$^{65}Cu(^{3}He,2n)$	-4.77	9.5h	β^{+},EC	511(114), 828(5) 1039(37), 1910(3), 2183(5), 2748(25)	$^{64}Zn(^{3}He,p)^{66}Ga$
						$^{66}Zn(^{3}He,p2n)^{66}Ga$
						$^{64}Zn(^{3}He,n)^{66}Ge\rightarrow^{66}Ga$
^{67}Ga	$^{65}Cu(^{3}He,n)$	6.46	77.9h	EC	93(40), 184(24), 296(22), 388(7)	$^{66}Zn(^{3}He,pn)^{67}Ga$
						$^{67}Zn(^{3}He,p2n)^{67}Ga$
						$^{69}Ga(^{3}He,\alpha n)^{67}Ga$
						$^{66}Zn(^{3}He,2n)^{67}Ge\rightarrow^{67}Ga$
						$^{67}Zn(^{3}He,3n)^{67}Ge\rightarrow^{67}Ga$
^{63}Zn	$^{63}Cu(^{3}He,p2n)$	-11.87	38.4m	β^{+},EC	511(186), 669(8), 962(6), 1420(0.9)	$^{61}Ni(^{3}He,n)^{63}Zn$
						$^{62}Ni(^{3}He,2n)^{63}Zn$
						$^{64}Zn(^{3}He,\alpha)^{63}Zn$

Table XV. (Continued)

Product	Reactions	Q(MeV)[a]	$T_{1/2}$[b]	Decay[b]	Associated γ-rays[b] keV(% per decay)	Interferences[c]
^{65}Zn	$^{63}Cu(^{3}He,p)$	7.98	245d	EC,β^+	511(3.4),1115(49)	$^{64}Ni(^{3}He,2n)^{65}Zn$
	$^{65}Cu(^{3}He,p2n)$	-9.85				$^{64}Zn(^{3}He,2p)^{65}Zn$
	Decay of ^{65}Ga					$^{66}Zn(^{3}He,\alpha)^{65}Zn$
						$^{67}Zn(^{3}He,\alpha n)^{65}Zn$
						$^{64}Zn(^{3}He,pn)^{65}Ga\rightarrow^{65}Zn$
^{61}Cu	$^{63}Cu(^{3}He,\alpha n)$	0.83	3.3h	β^+,EC	67(4), 284(12), 380(3), 511(120) 580(1.5), 660(11) 940(1.5), 1150(1), 1220(5)	$^{59}Co(^{3}He,n)^{61}Cu$
						$^{60}Ni(^{3}He,pn)^{61}Cu$
						$^{61}Ni(^{3}He,p2n)^{61}Cu$
						$^{60}Ni(^{3}He,2n)^{61}Zn\rightarrow^{61}Cu$
						$^{61}Ni(^{3}He,3n)^{61}Zn\rightarrow^{61}Cu$
^{62}Cu	$^{63}Cu(^{3}He,\alpha)$	9.73	9.8m	β^+,EC	511(195), 880(0.3), 1170(0.5)	$^{60}Ni(^{3}He,p)^{62}Cu$
						$^{61}Ni(^{3}He,pn)^{62}Cu$
						$^{62}Ni(^{3}He,p2n)^{62}Cu$
						$^{60}Ni(^{3}He,n)^{62}Zn\rightarrow^{62}Cu$
						$^{61}Ni(^{3}He,2n)^{62}Zn\rightarrow^{62}Cu$
						$^{62}Ni(^{3}He,3n)^{62}Zn\rightarrow^{62}Cu$
						$^{64}Zn(^{3}He,\alpha n)^{62}Zn\rightarrow^{62}Cu$

Table XV. (Continued)

Product	Reactions	Q(MeV)[a]	$T_{1/2}$[b]	Decay[b]	Associated γ-rays[b] keV(% per decay)	Interferences[c]
^{64}Cu	$^{63}Cu(^{3}He,2p)$	0.20	12.8h	EC,β^-,β^+	511(38), 1340(0.5)	$^{62}Ni(^{3}He,p)^{64}Cu$
	$^{65}Cu(^{3}He,\alpha)$	10.66				$^{64}Ni(^{3}He,p2n)^{64}Cu$
^{66}Cu	$^{65}Cu(^{3}He,2p)$	-0.66	5.1m	β^-	1039(9)	$^{64}Ni(^{3}He,p)^{66}Cu$

[a] Appendix B

[b] Reference 50

[c] Interferences are ^{3}He induced reactions with other elements which may lead to the same product at bombarding energies below about 30 MeV.

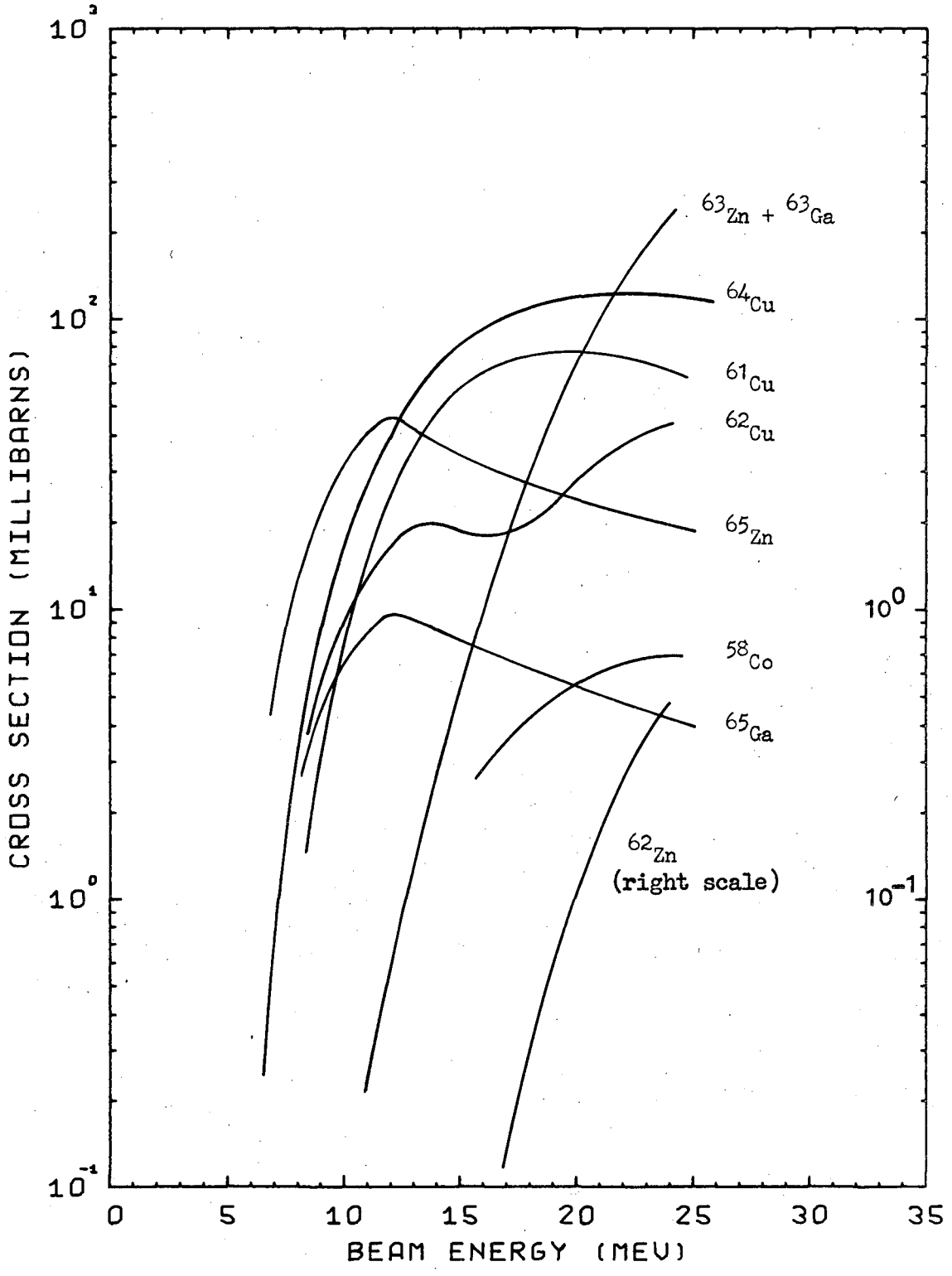

XBL 697-1010

Fig. 34. Excitation functions for $^{63}Cu(^{3}He,p3n)^{62}Zn$, $^{63}Cu(^{3}He,n)^{65}Ga$, $^{63}Cu(^{3}He,2\alpha)^{58}Co$, $^{63}Cu(^{3}He,p)^{65}Zn$, $^{63}Cu(^{3}He,\alpha)^{62}Cu$, $^{63}Cu(^{3}He,\alpha n)^{61}Cu$, $^{63}Cu(^{3}He,2p)^{64}Cu$, and $^{63}Cu(^{3}He,p2n)^{63}Zn + ^{63}Cu(^{3}He,3n)^{63}Ga \rightarrow ^{63}Zn$. The reference is given in the text.

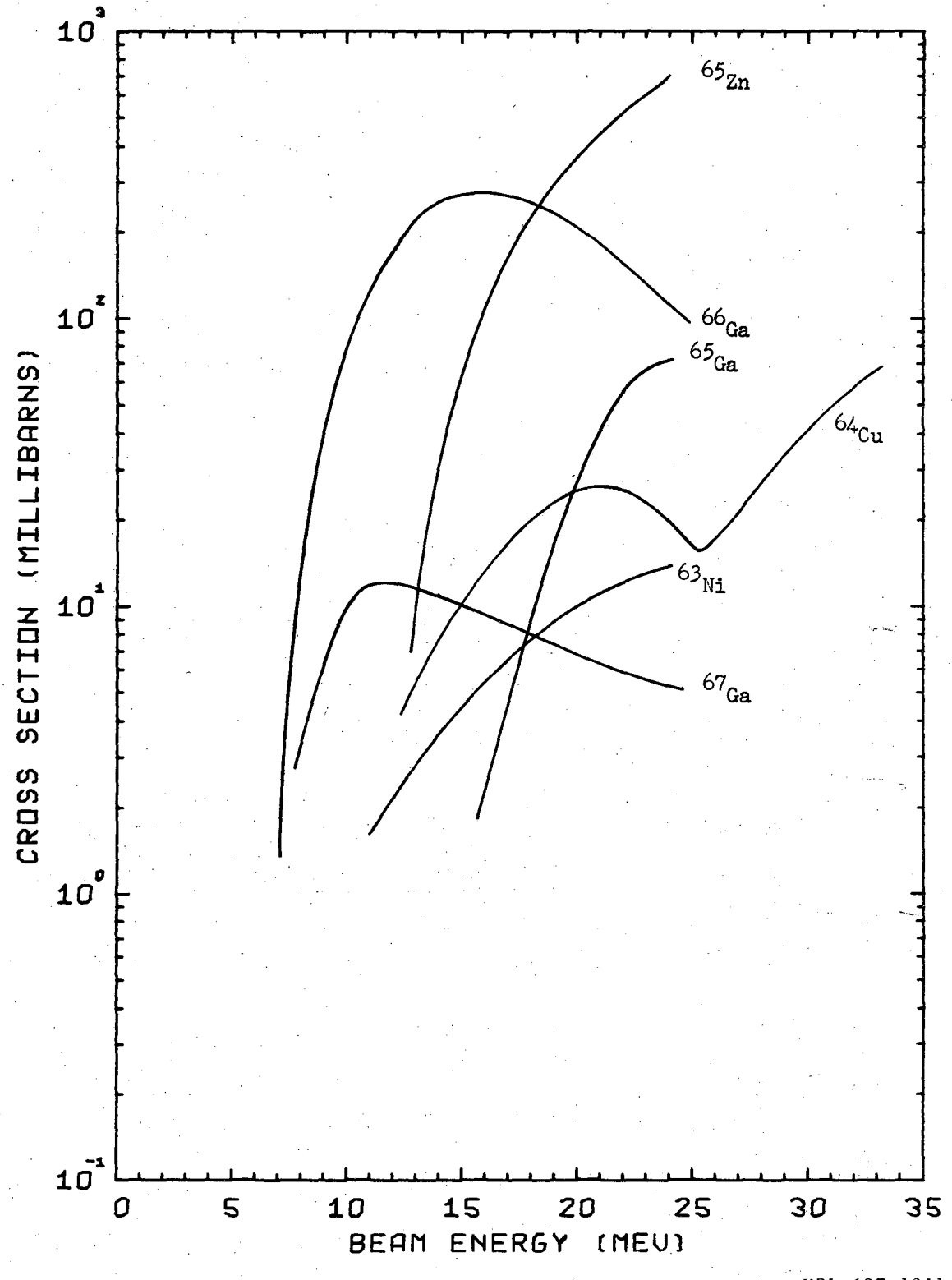

XBL 697-1011

Fig. 35. Excitation functions for $^{65}Cu(^{3}He,n)^{67}Ga$, $^{65}Cu(^{3}He,\alpha p)^{63}Ni$, $^{65}Cu(^{3}He,3n)^{65}Ga$, $^{65}Cu(^{3}He,2n)^{66}Ga$, $^{65}Cu(^{3}He,p2n)^{65}Zn$, and $^{65}Cu(^{3}He,\alpha)^{64}Cu$. The reference is given in the text.

P. GERMANIUM Figure 36

$^{3}He + Ge \rightarrow {}^{75}Se$ Lamb, Lee, amd Markowitz[62,65]

$^{3}He + Ge \rightarrow {}^{71}As$

$^{3}He + Ge \rightarrow {}^{74}As$

Estimated errors in σ are ±8% for ^{71}As, ±12% for ^{75}Se, and ±25% for ^{74}As.

Germanium targets were prepared by vacuum evaporating the metal onto thick, platinum backing-foils. Each target was covered with a 6 mg/cm^2 Au-foil recoil-catcher. Individual 30-min bombardments were carried out at a beam current of about 0.2 μA.

The activated targets were counted non-destructively using a 6 cm^3 Ge(Li) detector over a period of several weeks. Because of the extreme complexity of the resulting spectra only three of the twenty possible reaction products were measured. The γ-ray lines followed were 175-keV for ^{71}As, 136-keV for ^{75}Se, and 596-keV for ^{74}As. The presence of a large oxygen contaminant and the nine possible β^+ emitters among the products precluded accurate early measurements of γ-rays whose energies were less than 511-keV. The excitation functions which appear in Fig. 36 were not corrected for isotopic abundances in the targets.

Table XVI. Reactions induced in Ge by ^{3}He ion bombardment. Isotopic abundance: $^{70}Ge(20.55\%)$, $^{72}Ge(27.37\%)$, $^{73}Ge(7.67\%)$, $^{74}Ge(36.74\%)$, $^{76}Ge(7.67\%)$

Product	Reactions	Q(MeV)[a]	$T_{1/2}$[b]	Decay	Associated γ-rays[b] keV(% per decay)	Interferences[c]
^{70}Se	$^{70}Ge(^{3}He,3n)$	---	44m	β^{+},EC	511(--)	None
^{71}Se	$^{70}Ge(^{3}He,2n)$	-8.28	4.5m	β^{+},EC	160(--), 511(195)	None
^{72}Se	$^{70}Ge(^{3}He,n)$	3.92	8.4d	EC	46(59)	$^{74}Se(^{3}He,\alpha n)^{72}Se$
	$^{72}Ge(^{3}He,3n)$	-14.24				
^{73}Se	$^{72}Ge(^{3}He,2n)$	-5.62	7.1h	β^{+},EC	66(65), 359(99), 511(130)	$^{74}Se(^{3}He,\alpha)^{73}Se$
	$^{73}Ge(^{3}He,3n)$	-12.40				
^{75}Se	$^{73}Ge(^{3}He,n)$	7.73	120d	EC	66(1), 97(3.3), 121(17), 136(57) 265(60), 280(25) 401(12)	$^{74}Se(^{3}He,2p)^{75}Se$
	$^{74}Ge(^{3}He,2n)$	-2.46				$^{76}Se(^{3}He,\alpha)^{75}Se$
						$^{77}Se(^{3}He,\alpha n)^{75}Se$
						$^{75}As(^{3}He,p2n)^{75}Se$
$\underline{^{77m}Se}$	$^{76}Ge(^{3}He,2n)$	0.02	$\underline{17.5s}$[d]	$\underline{IT}$	$\underline{161(50)}$	$^{76}Se(^{3}He,2p)^{77m}Se$
						$^{78}Se(^{3}He,\alpha)^{77m}Se$
						$^{75}As(^{3}He,p)^{77m}Se$
^{70}As	$^{70}Ge(^{3}He,p2n)$	-14.74	52m	β^{+},EC	511(183), 600(23), 670(25), 750(23), 910(17), 1040(78), 1120(23), 1360(12), 1420(10), 1540(7), 1710(22), 1800(6), 2030(19)	$^{69}Ga(^{3}He,2n)^{70}As$
	Decay of ^{70}Se					

Table XVI. (Continued)

Product	Reactions	Q(MeV)[a]	$T_{1/2}$[b]	Decay[b]	Associated γ-rays[b] keV(% per decay)	Interferences[c]
^{71}As	$^{70}Ge(^{3}He,pn)$	-3.09	62h	EC,β^+	175(90), 511(60)	$^{69}Ga(^{3}He,n)^{71}As$
	Decay of ^{71}Se					
^{72}As	$^{70}Ge(^{3}He,p)$	5.30	26h	EC,β^+	511(150), 630(8), 835(78)	$^{71}Ga(^{3}He,2n)^{72}As$
	$^{72}Ge(^{3}He,p2n)$	-12.86				$^{74}Se(^{3}He,\alpha n)^{72}Se\rightarrow^{72}As$
	Decay of ^{72}Se					
^{73}As	$^{72}Ge(^{3}He,pn)$	-2.09	80.3d	EC	54(9)	$^{71}Ga(^{3}He,n)^{73}As$
	$^{73}Ge(^{3}He,p2n)$	-8.87				$^{75}As(^{3}He,\alpha n)^{73}As$
	Decay of ^{73}Se					$^{74}Se(^{3}He,\alpha)^{73}Se\rightarrow^{73}As$
^{74}As+	$^{72}Ge(^{3}He,p)$	5.92	17.9d	EC,β^-,β^+	511(59), 596(61), 635(14)	$^{75}As(^{3}He,\alpha)^{74}As$
$\underline{^{74m}As}$	$^{73}Ge(^{3}He,pn)$	-0.87	<u>8s</u>	<u>IT</u>	<u>283(100)</u>	
	$^{74}Ge(^{3}He,p2n)$	-11.06				
^{76}As	$^{74}Ge(^{3}He,p)$	6.51	26.4h	β^-	559(43), 657(6), 1220(5)	$^{75}As(^{3}He,2p)^{76}As$
	$^{76}Ge(^{3}He,p2n)$	-9.42				
^{77}As	$^{76}Ge(^{3}He,pn)$	0.28	38.7h	β^-	86(0.1), 239(2.5), 522(0.8)	None
^{78}As	$^{76}Ge(^{3}He,p)$	7.18	91m	β^-	614(42), 700(15), 830(8), 1310(11)	None

Table XVI. (Continued)

Product	Reactions	Q(MeV)[a]	$T_{1/2}$[b]	Decay[b]	Associated γ-rays[b] keV(% per decay)	Interferences
^{68}Ge	$^{70}Ge(^{3}He,\alpha n)$	0.44	275d	EC	No γ-rays	$^{66}Zn(^{3}He,n)^{68}Ge$
						$^{67}Zn(^{3}He,2n)^{68}Ge$
						$^{68}Zn(^{3}He,3n)^{68}Ge$
^{69}Ge	$^{70}Ge(^{3}He,\alpha)$	9.05	36h	EC,β^{+}	511(68), 573(13), 872(10), 1107(28), 1335(3)	$^{67}Zn(^{3}He,n)^{69}Ge$
						$^{68}Zn(^{3}He,2n)^{69}Ge$
						$^{69}Ga(^{3}He,p2n)^{69}Ge$
						$^{69}Ga(^{3}He,3n)^{69}As\rightarrow^{69}Ge$
^{71}Ge	$^{70}Ge(^{3}He,2p)$	-0.31	11.4d	EC	No γ-rays	$^{70}Zn(^{3}He,2n)^{71}Ge$
	$^{72}Ge(^{3}He,\alpha)$	9.82				$^{69}Ga(^{3}He,p)^{71}Ge$
	$^{73}Ge(^{3}He,\alpha n)$	3.04				$^{71}Ga(^{3}He,p2n)^{71}Ge$

Table XVI. (Continued)

Product	Reactions	Q(MeV)[a]	$T_{1/2}$[b]	Decay[b]	Associated γ-rays[b] keV(% per decay)	Interferences[c]
^{75}Ge+	^{74}Ge(^{3}He,2p)	-1.23	82m	β^-	66(0.3), 199(1.4), 265(11), 427(0.3), 477(0.3), 628(0.1)	None
<u>^{75m}Ge</u>	^{76}Ge(^{3}He,α)	11.13	<u>48s[d]</u>	<u>IT</u>	<u>139(34)</u>	
^{77}Ge+	^{76}Ge(^{3}He,2p)	-1.69	11.3h	β^-	210(61), 263(45), 368(15), 417(25), 563(18), 632(11), 730(14), 800(6), 930(5), 1090(6)	None
^{77m}Ge	Decay of ^{77}As		<u>54.0s</u>	<u>β^-,IT</u>	<u>159(12), 215(21)</u>	

[a] Appendix B

[b] Reference 50

[c] Interferences are ^{3}He induced reactions with other elements which may lead to the same product at bombarding energies below about 30 MeV

[d] Underlined decay data indicates metastable or isomeric state.

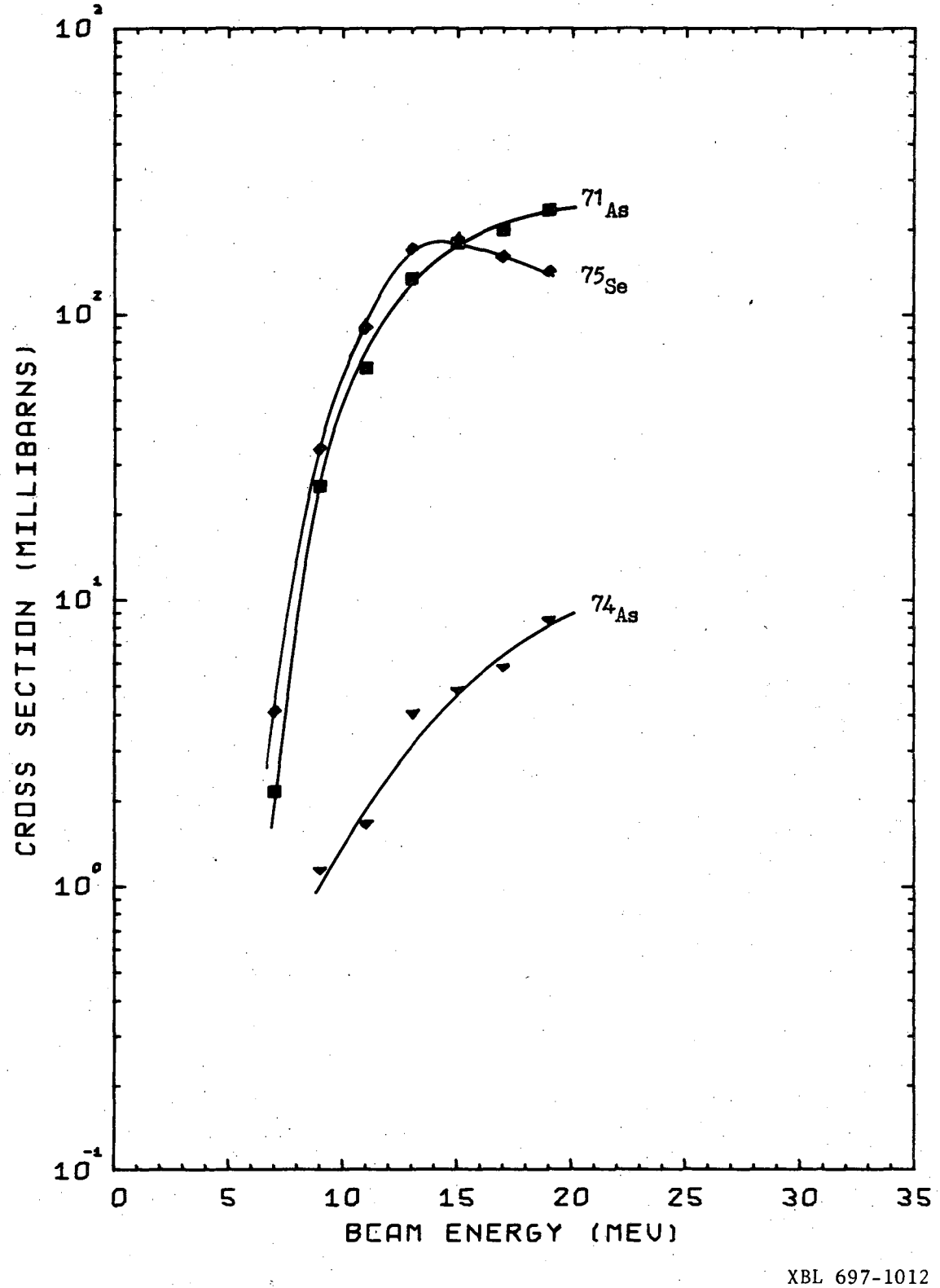

XBL 697-1012

Fig. 36. Total production excitation functions for Ge + ^{3}He → ^{71}As, ^{74}As, ^{75}Se.

Q. TANTALUM

Figure 37

$^{181}Ta(^{3}He,4n)^{180}Re$ Lamb. Lee, and Markowitz[65]

$^{181}Ta(^{3}He,3n)^{181}Re$

Estimated errors in σ are ±8% for ^{180}Re and ^{181}Re.

The targets, composed of three 23.5 mg/cm^2 Ta foils, were irradiated individually for 2 min at a beam current of about 0.1 μA. The resulting activity of ^{180}Re in the center foils were measured using a 6 cm^3 Ge(Li) detector to follow the decay of the 104-keV γ-ray. The activity of ^{181}Re in the center foils was measured after several hours using a NaI(Tl) detector to follow its 18-hour decays via the 365-keV γ-rays.

Many γ-rays are associated with the decay of both ^{180}Re and ^{181}Re, but the relative intensities are not known. The excitation functions, therefore, are calculated without correction for the number of γ-rays per disintegration.

Table XVII. Reactions induced in Ta by ^{3}He bombardment. Isotopic abundance: $^{180}Ta(0.012\%)$, $^{181}Ta(99.988\%)$

Product	Reactions	Q(MeV)[a]	$T_{1/2}$[b]	Decay[b]	Associated γ-rays[b] keV(% per decay)	Interferences[c]
^{180}Re+	$^{180}Ta(^{3}He,3n)$	---	2.4m	β^{+},EC	110(--), 511(--), 880(--)	$^{180}W(^{3}He,p2n)^{180}Re$
^{180}Re[d]	$^{181}Ta(^{3}He,4n)$	---	20h	β^{+},EC	511(--)	
^{181}Re	$^{180}Ta(^{3}He,2n)$	---	18h	EC	365(--) others	$^{180}W(^{3}He,pn)^{181}Re$
	$^{181}Ta(^{3}He,3n)$	---				$^{180}W(^{3}He,2n)^{181}Os\rightarrow^{181}Re$
^{182}Re	$^{180}Ta(^{3}He,n)$	3.29	12.7h	EC,β^{+}	68(--), 100(--), 1122(--), 1189(--) others	$^{180}W(^{3}He,p)^{182}Re$
^{182}Re[d]	$^{181}Ta(^{3}He,2n)$	-4.35	64h	EC	68(--), 100(--) others	$^{182}W(^{3}He,p2n)^{182}Re$
						$^{180}W(^{3}He,n)^{182}Os\rightarrow^{182}Re$
						$^{182}W(^{3}He,3n)^{182}Os\rightarrow^{182}Re$
						$^{184}Os(^{3}He,\alpha n)^{182}Os\rightarrow^{182}Re$
^{183}Re	$^{181}Ta(^{3}He,n)$	3.83	71d	EC	46(--), 53(--), 109(--), 209(--), others	$^{182}W(^{3}He,pn)^{183}Re$
						$^{183}W(^{3}He,2pn)^{183}Re$
						$^{182}W(^{3}He,2n)^{183}Os\rightarrow^{183}Re$
						$^{183}W(^{3}He,3n)^{183}Os\rightarrow^{183}Re$
						$^{184}Os(^{3}He,\alpha)^{183}Os\rightarrow^{183}Re$

Table XVII. (Continued)

Product	Reactions	Q(MeV)[a]	$T_{1/2}$[b]	Decay[b]	Associated γ-rays[b] keV(%per decay)	Interferences[c]
^{181}W	$^{180}Ta(^{3}He,pn)$	-1.05	140d	EC	136(0.1), 152(0.1)	$^{179}Hf(^{3}He,n)^{181}W$
	$^{181}Ta(^{3}He,p2n)$	-8.69				$^{180}Hf(^{3}He,2n)^{181}W$
						$^{180}W(^{3}He,2p)^{181}W$
						$^{182}W(^{3}He,\alpha)^{181}W$
						$^{183}W(^{3}He,\alpha n)^{181}W$
						$^{180}W(^{3}He,pn)^{181}Re\rightarrow^{181}W$
$^{178}Ta+$ ^{178}Ta[d]	$^{180}Ta(^{3}He,\alpha n)$	5.93	9.4m	EC,β^+	93(100), 511(10), 1100(11), 1180(4), 1350(46), 1450(9),	$^{176}Hf(^{3}He,p)^{178}Ta$
						$^{177}Hf(^{3}He,pn)^{178}Ta$
			2.1h	EC	89(54), 93(14), 214(75), 328(120 complex), 427(97)	$^{178}Hf(^{3}He,p2n)^{178}Ta$
						$^{176}Hf(^{3}He,n)^{178}W\rightarrow^{178}Ta$
						$^{177}Hf(^{3}He,2n)^{178}W\rightarrow^{178}Ta$
						$^{178}Hf(^{3}He,3n)^{178}W\rightarrow^{178}Ta$
						$^{180}W(^{3}He,\alpha n)^{178}W\rightarrow^{178}Ta$

Table XVII. (Continued)

Product	Reactions	Q(MeV)[a]	$T_{1/2}$[b]	Decay[b]	Associated γ-rays[b] keV(% per decay)	Interferences[c]
^{179}Ta	$^{180}Ta(^{3}He,\alpha)$	13.79	600d	EC	No γ-rays	$^{177}Hf(^{3}He,p)^{179}Ta$
	$^{181}Ta(^{3}He,\alpha n)$	6.15				$^{178}Hf(^{3}He,pn)^{179}Ta$
						$^{179}Hf(^{3}He,p2n)^{179}Ta$
						$^{177}Hf(^{3}He,n)^{179}W \rightarrow ^{179}Ta$
						$^{178}Hf(^{3}He,2n)^{179}W \rightarrow ^{179}Ta$
						$^{179}Hf(^{3}He,3n)^{179}W \rightarrow ^{179}Ta$
						$^{180}W(^{3}He,\alpha)^{179}W \rightarrow ^{179}Ta$
$\underline{180m}Ta$	$^{181}Ta(^{3}He,\alpha)$	12.70	8.1e	EC, β^-	93(4), 103(0.6)	$^{178}Hf(^{3}He,p)^{180m}Ta$
						$^{179}Hf(^{3}He,pn)^{180m}Ta$
						$^{180}Hf(^{3}He,p2n)^{180m}Ta$

Table XVII. (Continued)

Product	Reactions	Q(MeV)[a]	$T_{1/2}$[b]	Decay[b]	Associated γ-rays[b] keV(% per decay)	Interferences[c]
^{182}Ta	$^{181}Ta(^{3}He,2p)$	-1.73	115d	--	68(42), 100(14), 152(7), 222(8), 1122(34), 1189(16), 1222(27), 1231(13), others	$^{180}Hf(^{3}He,p)^{182}Ta$
$\underline{^{182m}Ta}$			16.5m	IT	147(40), 172(40), 184(20), 319(5), 356(0.3)	

[a] Appendix B

[b] Reference 50

[c] Interferences are ^{3}He induced reactions with other elements which may lead to the same product at bombarding energies below about 30 MeV.

[d] The isomeric relationship between the two states of this nuclide is not known.

[e] Underlined decay data indicates metastable or isomeric state.

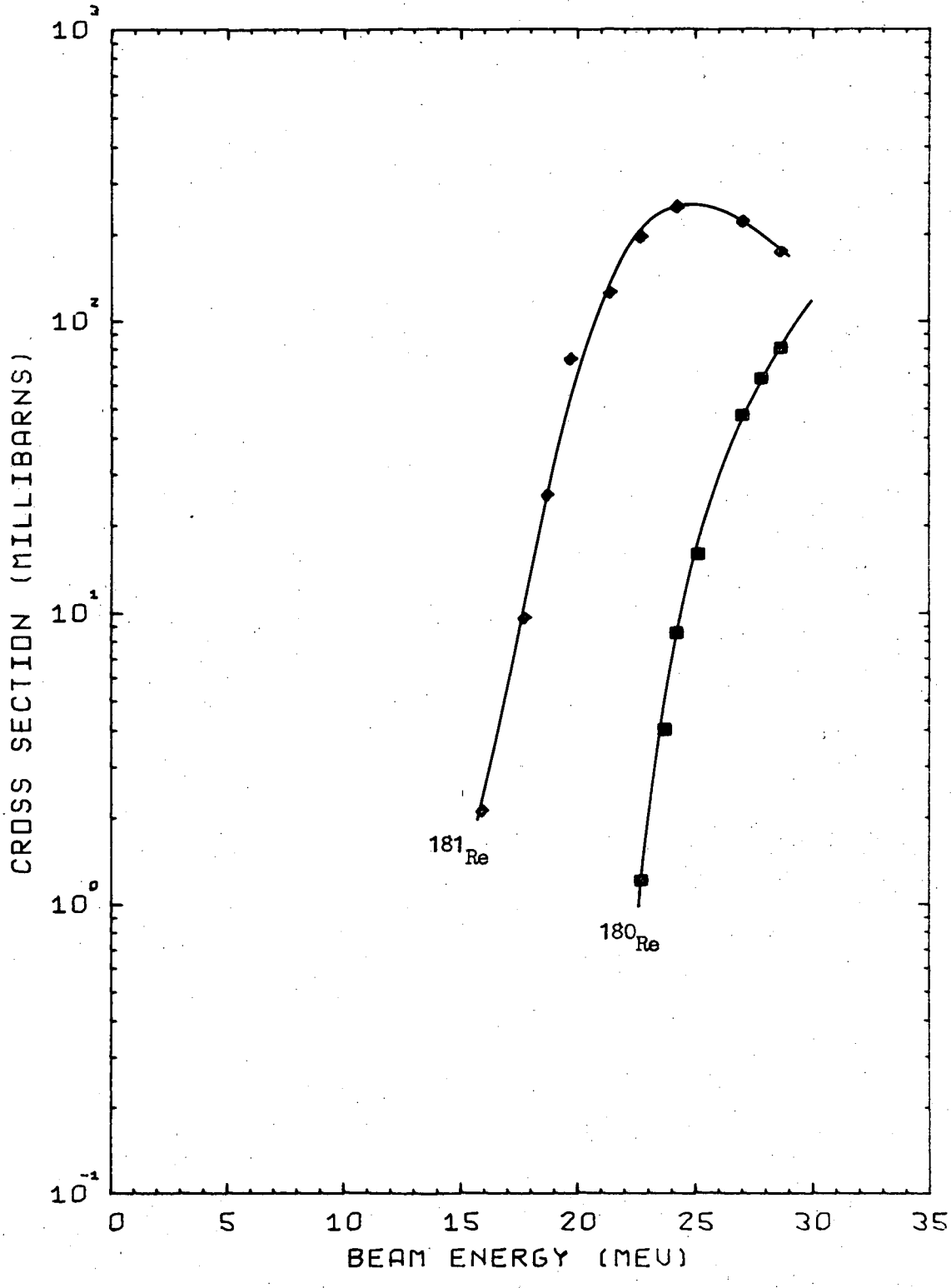

XBL 697-1013

Fig. 37. Excitation functions for $^{181}Ta(^{3}He,4n)^{180}Re$ and $^{181}Ta(^{3}He,3n)^{181}Re$. The cross sections were calculated assuming 1 γ-ray per disintegration.

R. GOLD Figure 38

$^{197}Au(^{3}He,3n)^{197}Tl$ Lamb, Lee, and Markowitz (unpublished)

$^{197}Au(^{3}He,\alpha)^{196}Au$

$^{197}Au(^{3}He,2p)^{198}Au$

$^{197}Au(^{3}He,p2n)^{197m}Hg + {}^{197}Au(^{3}He,3n)^{197}Tl \rightarrow {}^{197m}Hg$

Estimated errors are ±8% for ^{196}Au and ^{198}Au and ±12% for ^{197}Tl and ^{197m}Hg.

A stack of 4.6 mg/cm^2 Au foils was irradiated for 30 min at 2.0 μA. Selected foils were counted using the 16 cm^3 Ge(Li) detector. The γ-rays which were measured for each product were 359-keV for ^{196}Au, 134-keV for ^{197m}Hg, 310-keV for ^{197}Tl, and 412-keV for ^{198}Au.

All excitation functions shown involve only one reaction except the production of ^{197m}Hg. This function could not be corrected for the (^{3}He,3n) contribution because γ-ray relative intensities for ^{197}Tl are unknown. The excitation functions for ^{196}Au and ^{198}Au, only, are absolute functions.

The excitation function for ^{196}Au provides an example of the high-energy portion, only, of a (^{3}He,α) reaction. The high Coulomb barrier of the ^{197}Au nucleus and the high Q-value (12.5 MeV) preclude observation of the low-energy porition.

That the calculation of a Coulomb barrier from a rigid sphere approximation (r_0 = 1.5f, Fig. 2) cannot be considered an accurate threshold for reaction is demonstrated by these reactions of Au. Significant activation occurs 5-6 MeV below the calculated 21-MeV Coulomb barrier.

Table XVIII. Reactions induced in Au by ^{3}He ion bombardment. Isotopic abundance: $^{197}Au(100\%)$

Product	Reactions	Q(MeV)[a]	$T_{1/2}$[b]	Decay[b]	Associated γ-rays[b] keV(% per decay)	Interferences[c]
^{197}Tl+ ^{197m}Tl	$^{197}Au(^{3}He,3n)$	-12.23	2.8h	EC	152(--), 426(--)	$^{196}Hg(^{3}He,pn)^{197}Tl$
			0.5s[d]	IT	222(40), 385(90)	
^{198}Tl+ ^{198m}Tl	$^{197}Au(^{3}He,2n)$	-4.87	5.3h	EC,β^{+}	412(90), 650(40), 1200(21), 1420(24), 2010(15), 2450(5), 2780(2)	$^{196}Hg(^{3}He,p)^{198}Tl$
						$^{198}Hg(^{3}He,p2n)^{198}Tl$
			1.9h	IT,EC	283(30), 412(45), 586(35), 635(35)	$^{198}Hg(^{3}He,3n)^{198}Pb\rightarrow^{198}Tl$
^{199}Tl	$^{197}Au(^{3}He,n)$	4.14	7.4h	EC	158(5), 208(12) 247(9), 455(14)	$^{198}Hg(^{3}He,pn)^{199}Tl$
						$^{199}Hg(^{3}He,p2n)^{199}Tl$
						$^{198}Hg(^{3}He,2n)^{199}Pb\rightarrow^{199}Tl$
						$^{199}Hg(^{3}He,3n)^{199}Pb\rightarrow^{199}Tl$
^{197}Hg+ ^{197m}Hg	$^{197}Au(^{3}He,p2n)$	-9.26	65h	EC	77(18), 191(2), 268(0.15)	$^{195}Pt(^{3}He,n)^{197}Hg$
	Decay of ^{197}Tl		24h	IT,EC	134(42), 279(7)	$^{196}Pt(^{3}He,2n)^{197}Hg$
						$^{196}Hg(^{3}He,2p)^{197}Hg$
						$^{198}Hg(^{3}He,\alpha)^{197}Hg$
						$^{199}Hg(^{3}He,\alpha n)^{197}Hg$
						$^{196}Hg(^{3}He,pn)^{197}Tl\rightarrow^{197}Hg$

Table XVIII. (Continued)

Product	Reactions	Q(MeV)[a]	$T_{1/2}$[b]	Decay[b]	Associated γ-rays[b] keV(% per decay)	Interferences[c]
^{199m}Hg	$^{197}Au(^{3}He,p)$	6.02	43m	IT	158(53), 375(15)	$^{198}Pt(^{3}He,2n)^{199m}Hg$
	Decay of ^{199}Tl					$^{198}Hg(^{3}He,2p)^{199m}Hg$
						$^{200}Hg(^{3}He,\alpha)^{199m}Hg$
						$^{201}Hg(^{3}He,\alpha n)^{199m}Hg$
						$^{198}Hg(^{3}He,pn)^{199}Tl\rightarrow^{199m}Hg$
						$^{199}Hg(^{3}He,p2n)^{199}Tl\rightarrow^{199m}Hg$
$^{195}Au+$ ^{195m}Au	$^{197}Au(^{3}He,\alpha n)$	5.81	183d 30.6s	EC IT	99(10), 129(1) 261(77)	$^{193}Ir(^{3}He,n)^{195}Au$
						$^{194}Pt(^{3}He,pn)^{195}Au$
						$^{195}Pt(^{3}He,p2n)^{195}Au$
						$^{194}Pt(^{3}He,2n)^{195}Hg\rightarrow^{195}Au$
						$^{195}Pt(^{3}He,3n)^{195}Hg\rightarrow^{195}Au$
						$^{196}Hg(^{3}He,\alpha)^{195}Hg\rightarrow^{195}Au$

Table XVIII. (Continued)

Product	Reactions	Q(MeV)[a]	$T_{1/2}$[b]	Decay	Associated γ-rays[b] keV(% per decay)	Interferences[c]
^{196}Au+	^{197}Au(^{3}He,α)	12.49	6.2d	EC,β^-	333(25), 356(94), 426(6), 1091(0.2)	^{194}Pt(^{3}He,p)^{196}Au
<u>^{196m}Au</u>			<u>9.7h</u>	<u>IT</u>	<u>148(42), 188(32), 285(5), 316(5)</u>	^{195}Pt(^{3}He,pn)^{196}Au
<u>^{197m}Au</u>	Decay of ^{197}Hg		<u>7.2s</u>	<u>IT</u>	<u>130(8), 279(75)</u>	See ^{197}Hg
^{198}Au	^{197}Au(^{3}He,2p)	-1.22	2.7d	β^-	412(95), 676(1), 1088(0.2)	^{196}Pt(^{3}He,p)^{198}Au
						^{198}Pt(^{3}He,p2n)^{198}Au

[a] Appendix B

[b] Reference 50

[c] Interferences are ^{3}He induced reactions with other elements which may lead to the same product at bombarding energies below about 30 MeV.

[d] Underlined decay data indicates metastable or isomeric state.

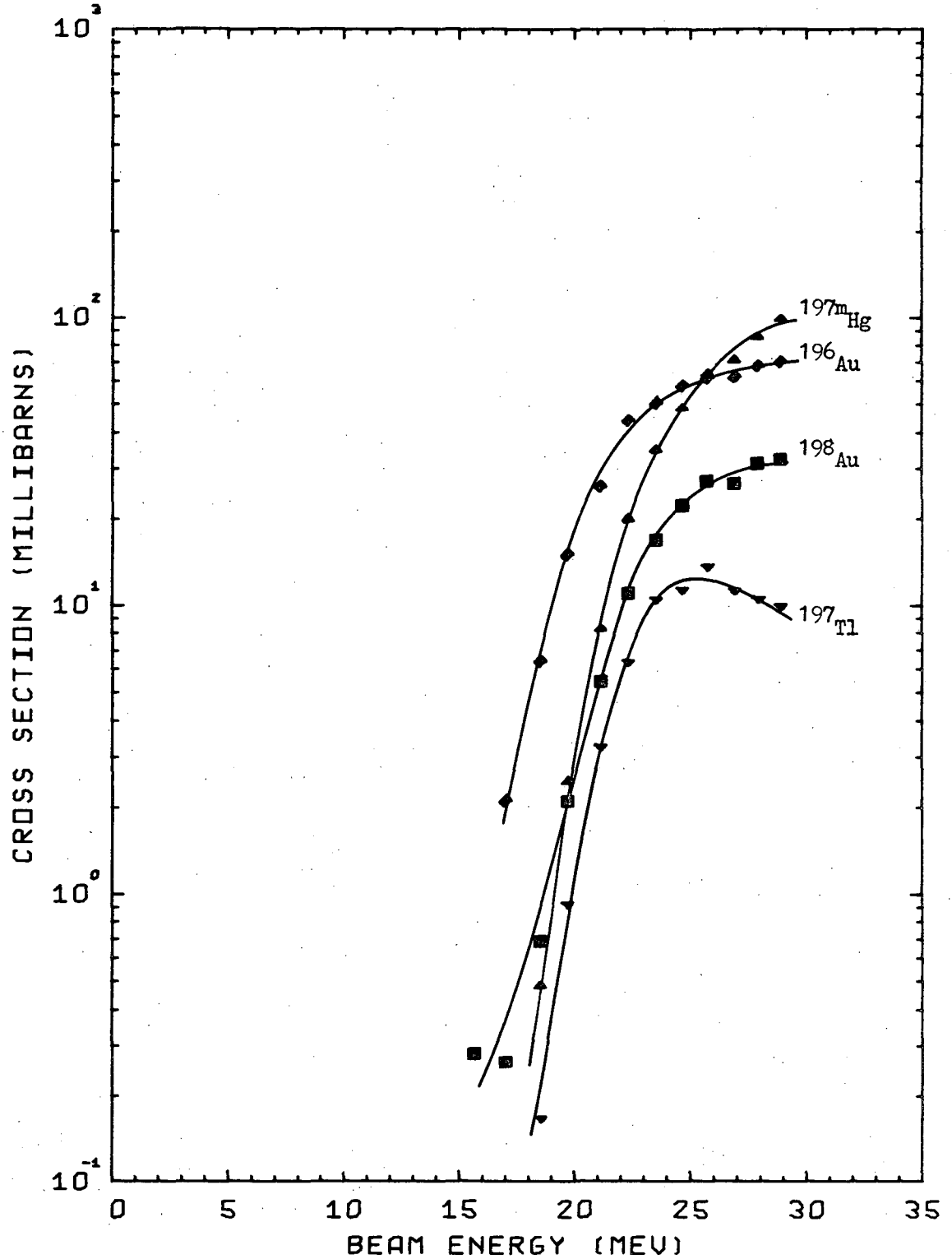

Fig. 38. Excitation functions for $^{197}Au(^{3}He,3n)^{197}Tl$, $^{197}Au(^{3}He,\alpha)^{196}Au$, $^{197}Au(^{3}He,2p)^{198}Au$, and $^{197}Au(^{3}He,p2n)^{197m}Hg$ + $^{197}Au(^{3}He,3n)^{197}Tl \rightarrow {}^{197m}Hg$. The cross sections for ^{197}Tl and ^{196m}Hg were calculated assuming 1 γ-ray per disintegration.

S. Discussion of Excitation Functions

Nuclear reaction excitation functions are of paramount importance in charged particle activation analysis because they enable the analyst to optimize the systematic variables of beam energy, length of bombardment, and radiation detection procedure so as to enhance the measurement of desired products while minimizing the effects of interferences. In this section the recognizable trends in the previously presented excitation functions will be discussed in relation to ^{3}He activation analysis for the prupose of estimating the applicability of the system to elements for which experimental ^{3}He induced reaction data are not available. These trends may also be useful for approximating sensitivities of, and interferences to, such analyses.

The discussion is ordered as the number of particles emitted from the compound system ^{3}He + target nucleus. Unless otherwise noted only those excitation functions are included which result from a single reaction of a particular target nuclide.

1. Single particle emission.

The $(^{3}He,n)$ excitation functions for reactions induced in ^{9}Be, ^{11}B, ^{12}C, ^{63}Cu, and ^{65}Cu are re-drawn in Fig. 39 for comparison. The data for the reactions shown (with the exception of ^{9}Be) and our failure to observe significant $(^{3}He,n)$ contributions among the reaction products in the nondestructive measurements in this work support the generalization of Brill'[57] that $(^{3}He,n)$ cross sections seldom exceed 10-20 mb. The cross sections decrease with increasing beam energy after an early maximum near the Coulomb barrier. The relative importance of $(^{3}He,n)$ among the

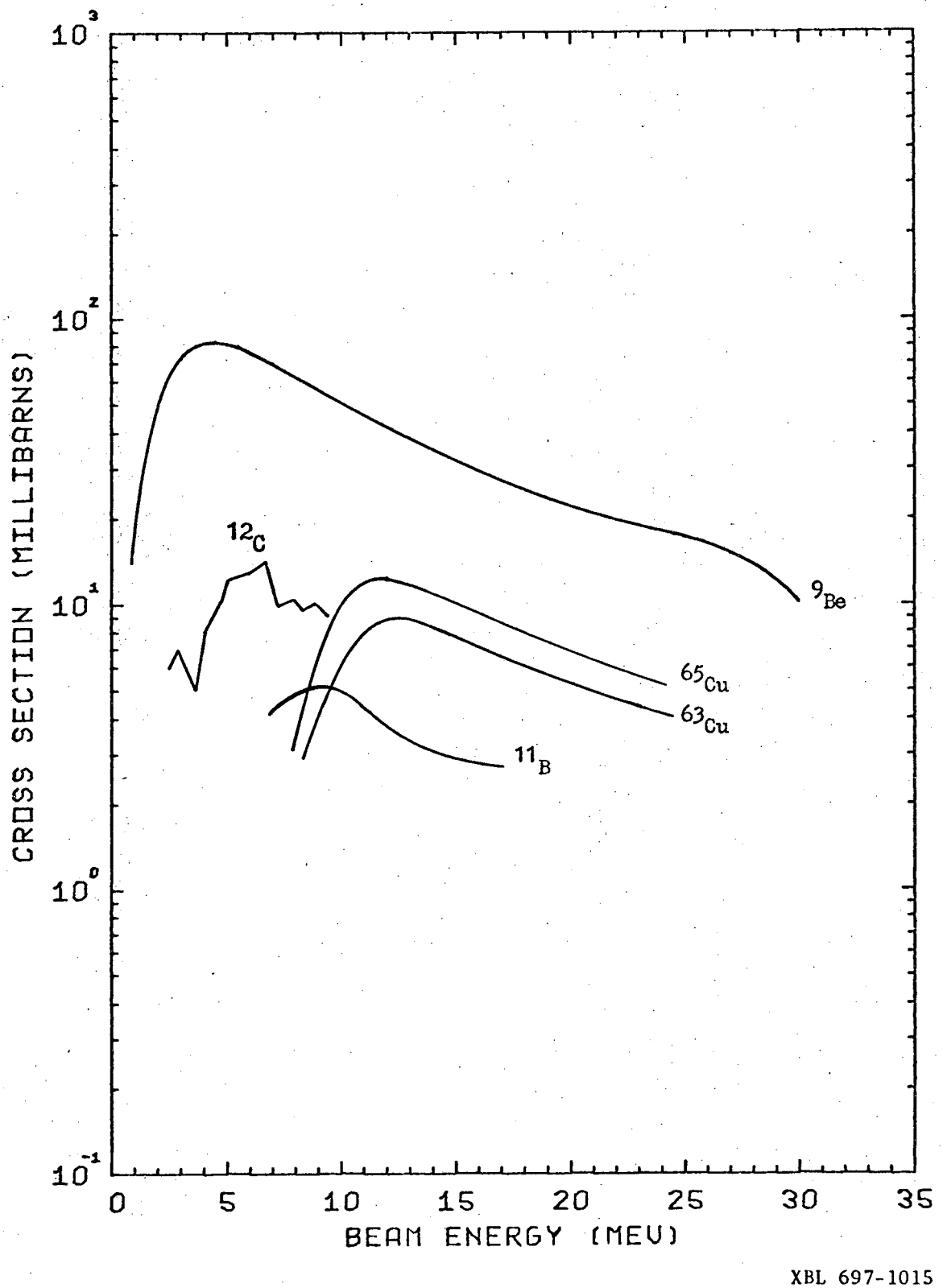

Fig. 39. Comparison of (^{3}He,n) reactions of various targets.

reactions induced in a target may be expected to decrease for targets having Coulomb barriers greater than about 10 MeV.

The (^{3}He,p) excitation functions for ^{18}O, ^{26}Mg, ^{40}Ca, ^{56}Fe, and ^{63}Cu and the (^{3}He,p) + (^{3}He,n) sum functions of oxygen and silicon are shown in Fig. 40. The ^{40}Ca function represents production of isomeric ^{42m}Sc only so that a low isomeric ratio probably accounts for its small magnitude. The data shown for the (^{3}He,p) reaction reveals that the excitation functions have shapes similar to the (^{3}He,n) functions but are generally larger. A large apparent (^{3}He,p) reaction often results as a sum of (^{3}He,p) and decay of the neutron deficient (^{3}He,n) product also produced. These neutron deficient nuclides are frequently very short lived, reaching saturation activity quickly during bombardment with resultant feeding of the (^{3}He,p) product by their positron and electron capture decays. Because the (^{3}He,p) and (^{3}He,n) excitation functions reach their maximum cross sections at low bombarding energies, an analysis of light elements may often be accomplished nondestructively in a heavier sample matrix using a beam whose energy is below that necessary to overcome the Coulomb barrier of the matrix.

The (^{3}He,α) reactions of ^{12}C, ^{16}O, ^{14}N, ^{19}F, ^{63}Cu, ^{65}Cu, ^{58}Ni, and ^{197}Au are shown in Fig. 41. For most of the reactions shown contributions from more than one reaction or reaction mechanism can be seen. The low energy (< 15 MeV) portions of the curves of Fig. 41 are attributable to the (^{3}He,α) reaction which has a positive Q-value for all stable target nuclides. The cross section increase at higher energies has been variously interpreted as a change to predominant (^{3}He,2p2n)[81] and as inelastic

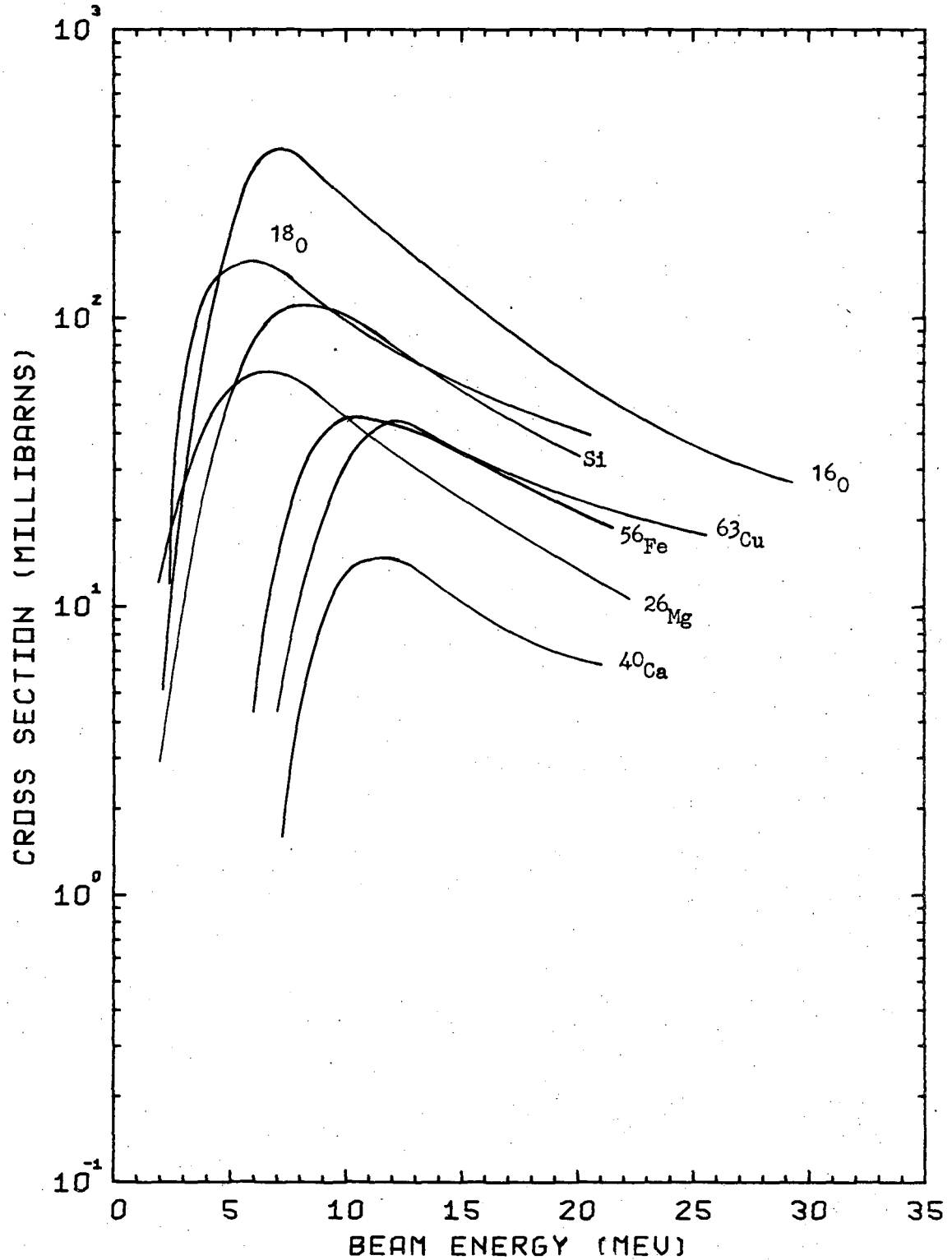

XBL 697-1016

Fig. 40. Comparison of (^{3}He,p) reactions of various targets.

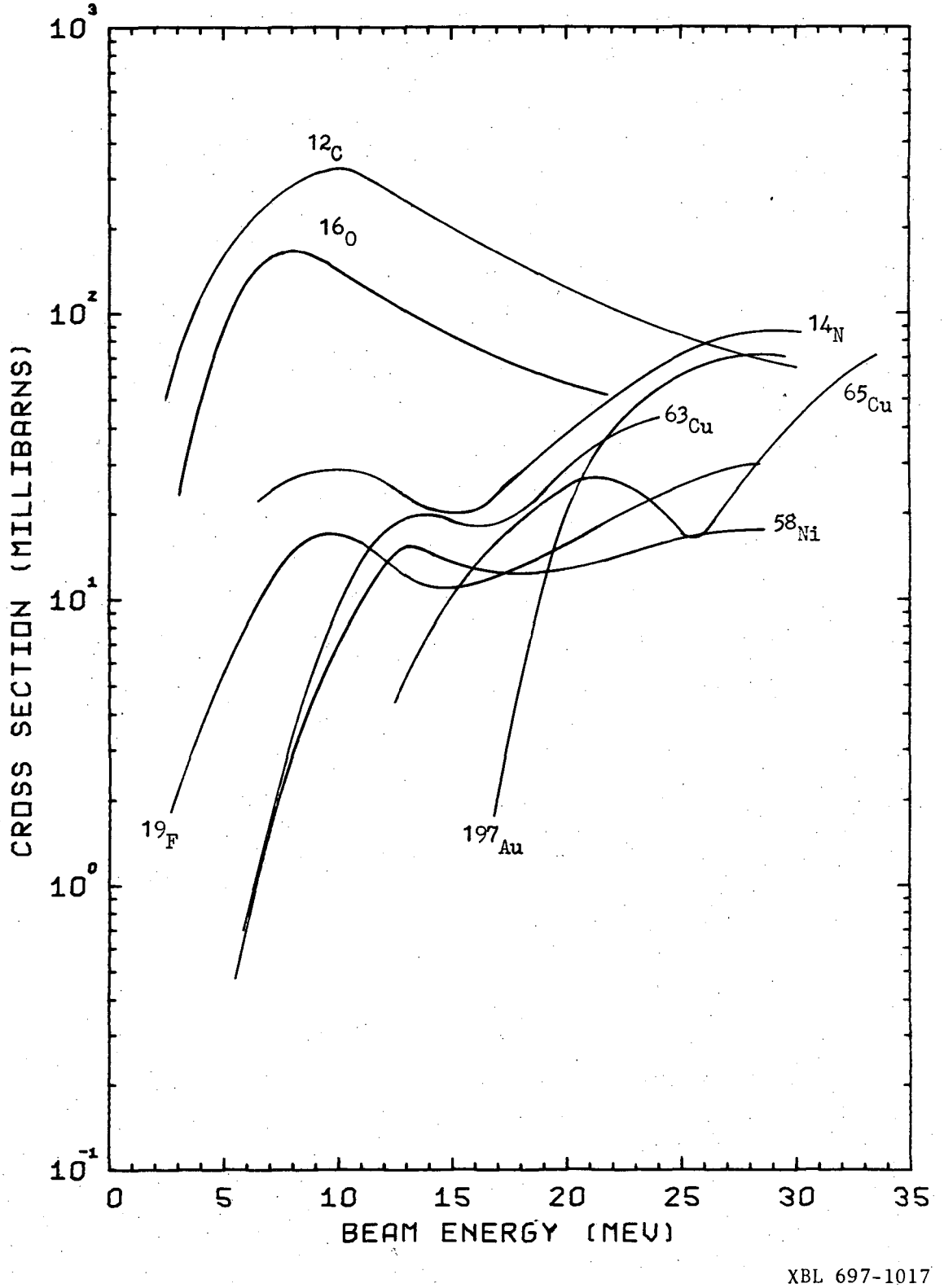

Fig. 41. Comparison of (^{3}He,α) reactions of various targets.

scattering followed by neutron evaporation,[57] either of which has a negative Q-value for each reaction shown. The threshold for both of these reactions is so high as to preclude their observation in the data for ^{12}C and ^{16}O. The Coulomb barrier for ^{197}Au is too high to permit observation of low energy $^{197}Au(^{3}He,\alpha)^{196}Au$.

2. Emission of two particles.

The $(^{3}He,2n)$ excitation functions of ^{65}Cu and ^{56}Fe and the $(^{3}He,2p)$ reactions of ^{27}Al, ^{63}Cu, ^{23}Na, ^{18}O, ^{19}F, ^{26}Mg, and ^{197}Au are shown in Fig. 42 and Fig. 43, respectively. Among the light elements the $(^{3}He,2n)$ reaction has been seldom observed because multiple neutron emission usually leads to unknown products or products whose half-lives are very short. The $(^{3}He,2p)$ and $(^{3}He,2n)$ excitation functions are observed to be slowly varying with energy near the cross section maxima which are comparatively large. The $(^{3}He,2p)$ reaction, however, leads to the same product as the (n,γ) reaction so that contributions form the latter reaction induced by reaction and accelerator-produced neutrons are sometimes difficult to assess. Among the light elements this effect is often minimized by very low neutron capture cross sections.

The $(^{3}He,pn)$ and $(^{3}He,d)$ excitation functions for ^{56}Fe, ^{14}N, ^{10}B, ^{16}O, and ^{12}C are shown in Fig. 44. These reactions have been included among two particle emissions because their shapes resemble multiple particle emissions more than single particle emissions shown in this report. Also, statistical model predictions for particle evaporation from excited copper nuclei[82] estimate bound deuteron and triton evaporation probabilities of only a few percent or less of the evaporation

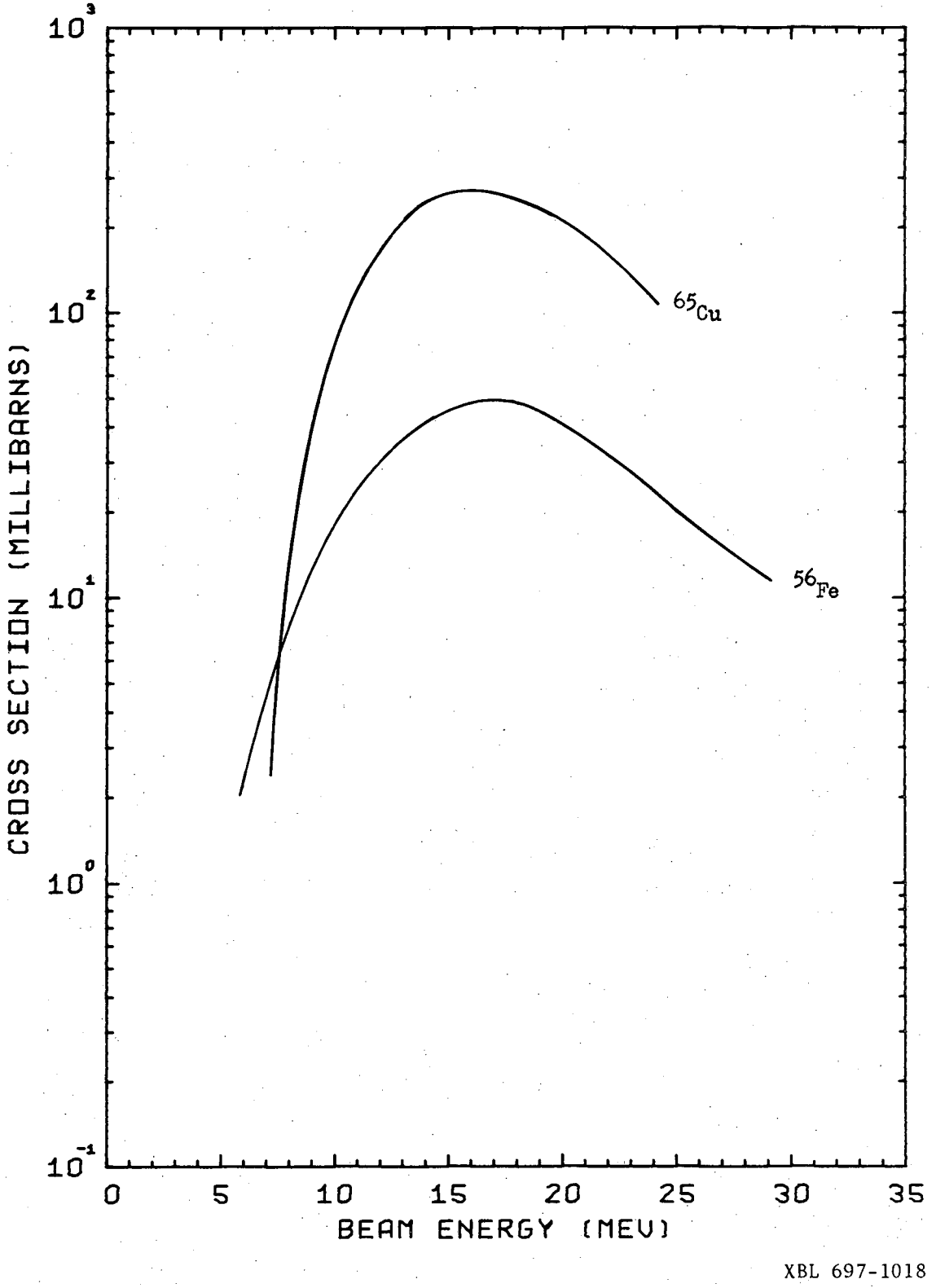

Fig. 42. Comparison of (^{3}He,2n) reactions of various targets.

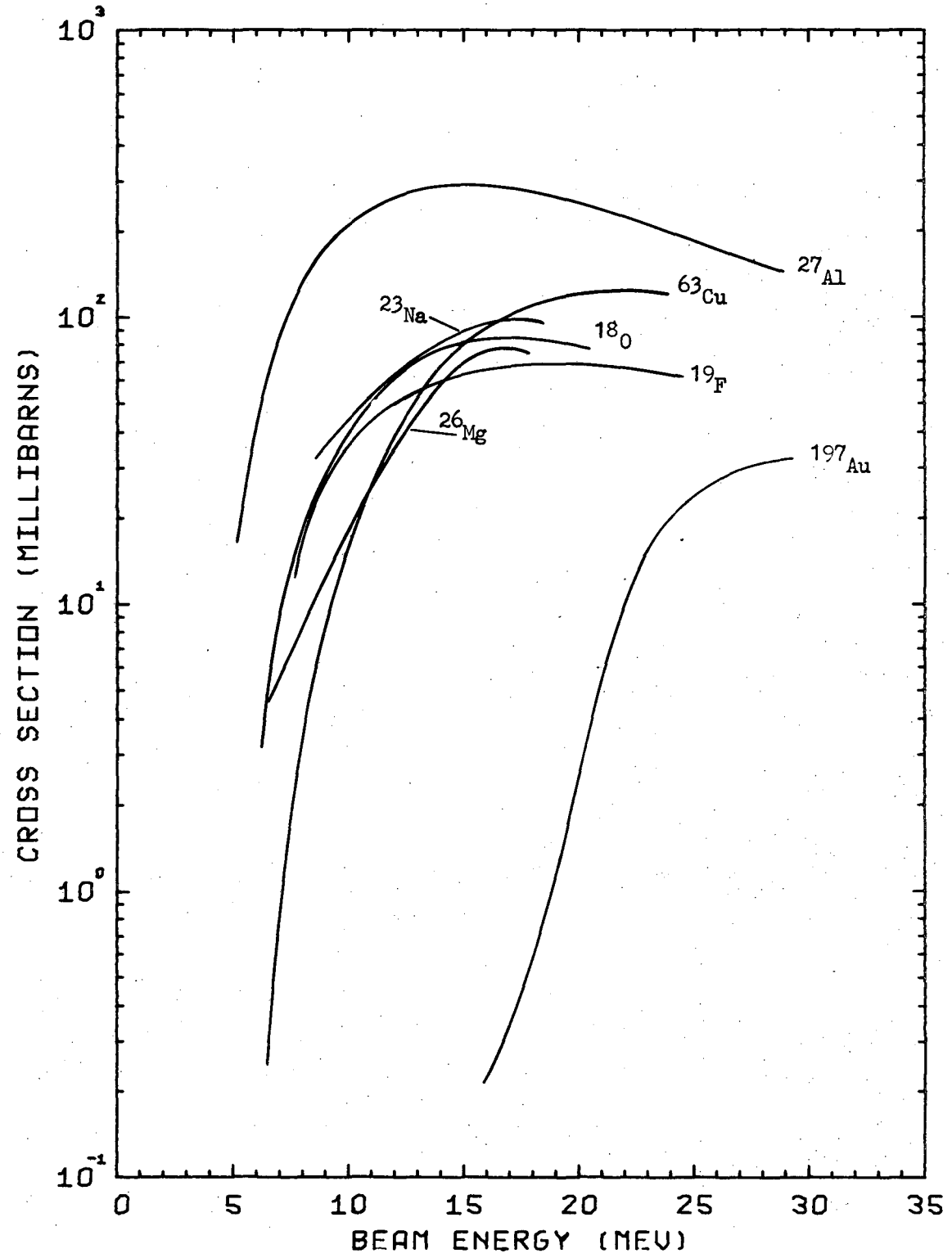

Fig. 43. Comparison of (^{3}He,2p) reactions of various targets.

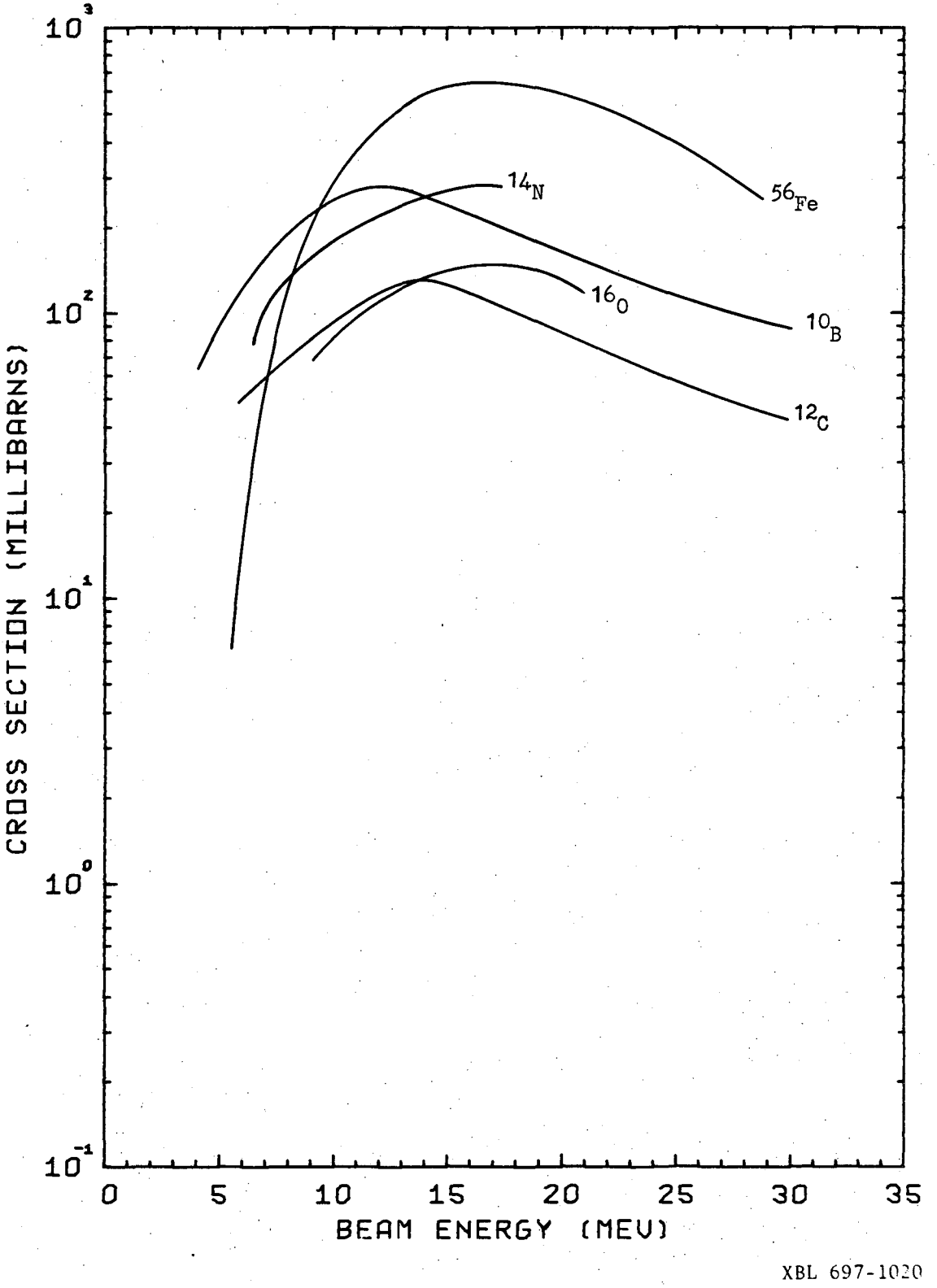

Fig. 44. Comparison of (^{3}He,pn) and (^{3}He,d) reactions of various targets.

probabilities of neutrons and protons at excitations of about 30-MeV. The relative probabilities of deuteron and triton evaporation decrease rapidly with decreasing excitation. The relative contributions of bound deuterons and tritons among the ^{3}He induced reaction products is of interest in avtivation analysis because the reaction thresholds are about 2.2-MeV and 8.5-MeV lower than the corresponding (pn) and (p2n) reactions respectively. The $(^{3}He,pn)$ + $(^{3}He,d)$ reaction products may often be enhanced through decay of short lived, neutron deficient $(^{3}He,2n)$ products as described for the $(^{3}He,p)$ reactions.

The $(^{3}He,2\alpha)$ reactions of ^{12}C, ^{16}O, ^{27}Al, and ^{63}Cu, the $(^{3}He,\alpha p)$ reaction of ^{63}Ni and the $(^{3}He,\alpha n)$ reactions of ^{19}F, ^{63}Cu, and ^{56}Ni are shown together in Fig. 45. The data are too few and too scattered for any general trends to stand out other than the smooth, slowly varying shapes of the curves near the cross section maxima characteristic of the other two particle emission reactions.

3. Emission of three or more particles.

The three particle emission excitation functions re-drawn together in Fig. 46 are the $(^{3}He,3n)$ reactions of ^{181}Ta, ^{197}Au, ^{65}Cu, and ^{56}Fe, the $(^{3}He,p2n)$ reactions of ^{65}Cu, ^{56}Fe, and ^{11}B, and the $(^{3}He,3p)$, $(^{3}He,\alpha 2p)$, and $(^{3}He,3\alpha)$ reactions of ^{27}Al. The $^{181}Ta(^{3}He,4n)^{180}Re$ and the $^{63}Cu(^{3}He,p3n)^{62}Zn$ reactions are shown in Fig. 47. The relative magnitudes of the $(^{3}He,3n)$ curves are not significant because a relative intensity of 1 γ-ray per decay was used for the unknown values for the the activities induced in Au and Ta.

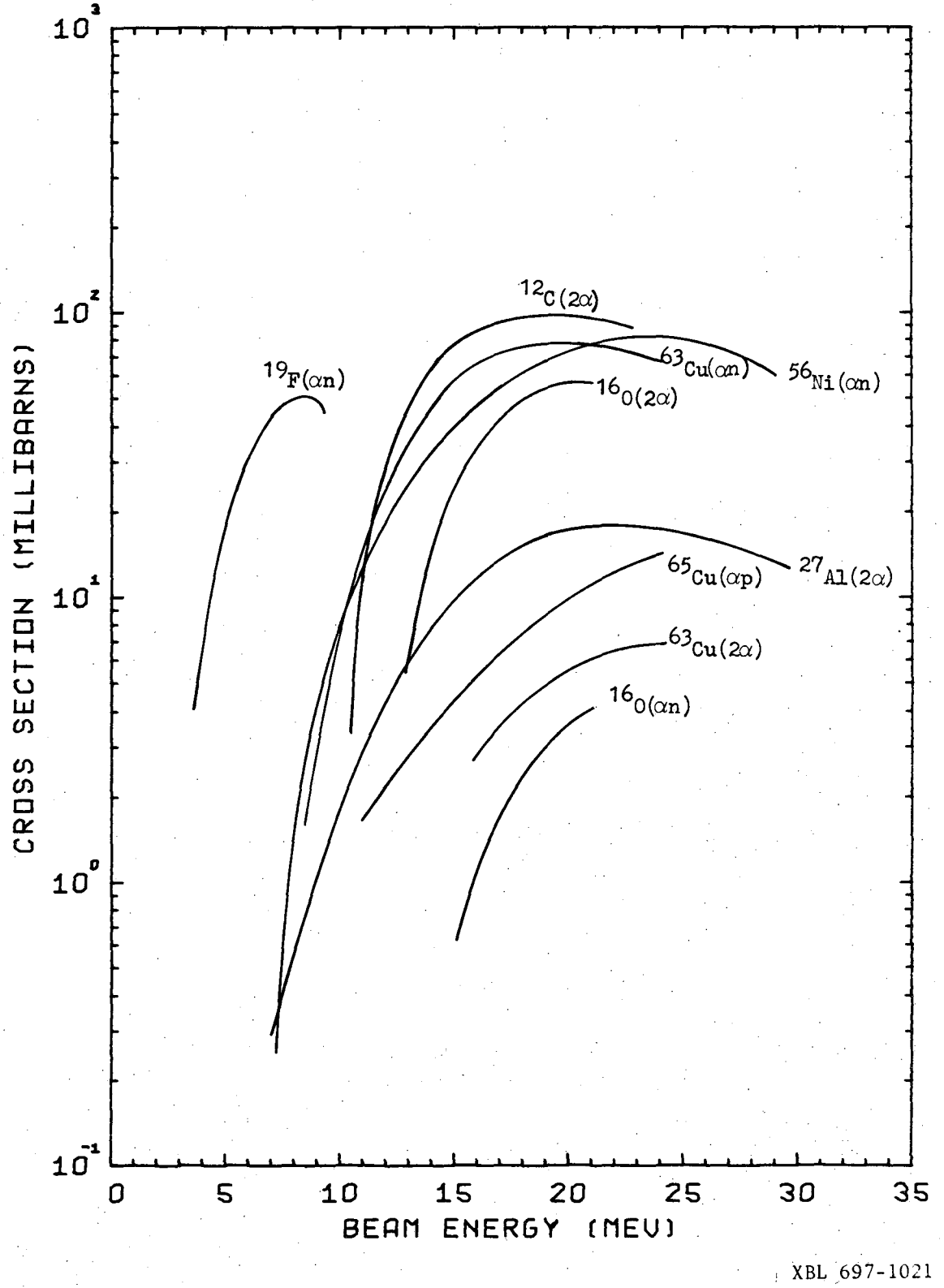

Fig. 45. Comparison of (^{3}He,2α), (^{3}He,αn), and (^{3}He,αp) reactions of various targets.

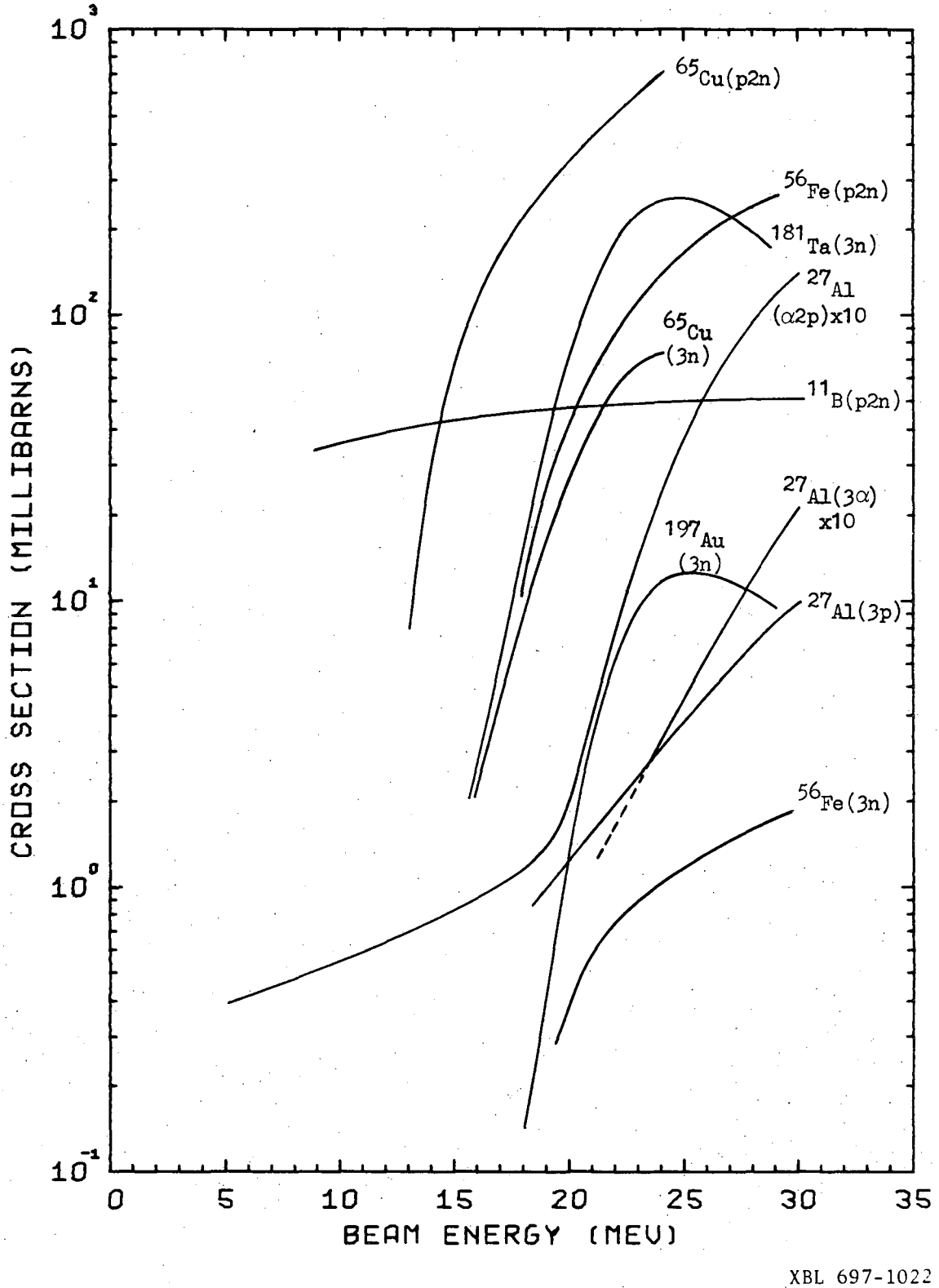

Fig. 46. Comparison of (^{3}He,3n), (^{3}He,3p), (^{3}He,3α), (^{3}He,p2n) and (^{3}He,α2p) reactions of various targets.

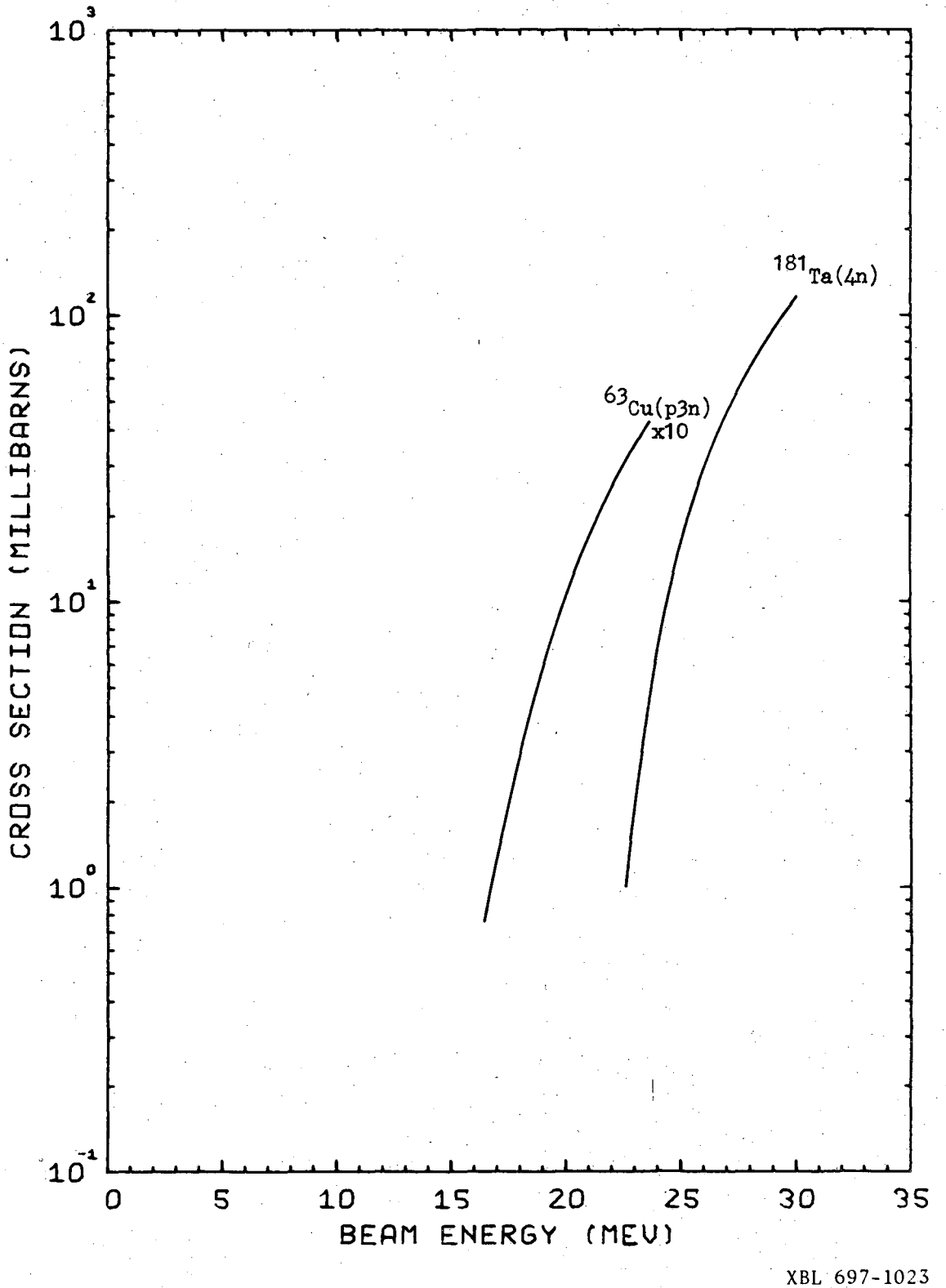

Fig. 47. Comparison of (^{3}He,4n) and (^{3}He,p3n) reactions of various targets.

It is interesting to note that the cross sections for these multiple particle emissions tend to be quite high, even at bombarding energies well below the Coulomb barriers. Production of activity will be possible, therefore, from almost all elements using modest beam energies of 15-20 MeV. Furthermore, discrimination of unwanted activation is clearly possible on the basis of reaction threshold and Coulomb barrier.

V. SPECIAL METHODS AND APPLICATIONS

A. Simultaneous Isotopic Analysis of ^{16}O : ^{18}O.[63]

Charged particle activation analysis affords the sometimes unique opportunity to measure isotopic compositions of various light elements by nuclear methods. In the case of ^{16}O and ^{18}O, analysis by ^{3}He activation is simultaneous for the isotopes, fast, fairly sensitive, and non-destructive. The only general interference may be fluorine, which, upon bombardment, yields products identical with those of oxygen.

Isotopic analysis of oxygen is more difficult than that of most other elements because of the problems encountered in preparing standards of accurately known composition. Oxygen, enriched in ^{18}O, is available in the form of O_2 gas, H_2O, and several prepared compounds, most of which have constituents which themselves activate when bombarded with $^{3}He^{++}$ ions. Practical samples for which an isotopic analysis is desired may not be available in sufficient quantity for preparation of a thick target, and methods of preparation of uniform thin targets often alter chemical composition. For intermediate thickness targets, comparison standards of identical beam-degrading power are most useful.

We have developed a method for preparing isotopic oxygen standards from ^{18}O-enriched water by anodic oxidation of tantalum foils. These targets may be used to produce any degree of beam energy attenuation, from negligible to complete degradation of incident 10 MeV ^{3}He ions, and the target matrix does not, itself, activate.

Anodization of tantalum[70] is usually performed in a dilute electrolyte-solution of salt or acid concentration of about 0.1% by weight, with either a constant current or a constant potential applied across the electrolytic cell, the anode of which is a tantalum foil. In the constant-voltage method, the potential is maintained at the desired level while the current decreases as the oxide film thickens. Theoretically, a film of any thickness may be prepared by this method; but, in practice, the current is so low after a few minutes anodization that further thickening is impractical. In the constant-current method the current is held constant while the potential rises as the film thickness increases. The thickness of oxide film obtained depends upon the final voltage. The limiting voltage which may be applied has been described[70] as characterized by sparking, oxygen evolution, and the formation of a thick, discolored film.

The films which have been prepared as described above are a maximum of a few thousand Angstroms thick, brightly colored, and amorphous, having a density of 8 g/cm^3,[71] as opposed to the crystalline Ta_2O_5 density of 8.7 g/cm^3. Davies, et al,[72] have found that the anodization mechanism involves mobility of both tantalum and oxygen ions through the oxide film. Vermilyea[73] has described the effects of various

surface treatments of the Ta foils on the uniformity of the film produced and Thompson[74] has described a film-thickness determination based on proton activation.

Our method of standard preparation[69] is a constant-current anodization at increased temperature by which films as thick as 36 mg/cm^2 Ta_2O_5 have been produced.

The electrolytic cell, shown in Fig. 48, is made of teflon with an aluminum base and is fitted with a small reflux condenser to minimize loss of the isotopically enriched electrolyte. This electrolyte is prepared by adding KCl to ^{18}O-enriched H_2O to make a 0.1% solution. A manually-operated DC power supply is used, with the current and voltage measured by a milliammeter and voltmeter in the external circuit. The current is held at 40 mA throughout each anodization with the cathode 1 cm from the Ta foil anode. Immediately before each anodization the electrolyte is brought to the boiling point. During the process, cell temperature is maintained near the boiling point by directing an air stream on the aluminum cell-base to carry off the power-deposited heat. The behavior of the voltage applied over a 160 min anodization period is shown in Fig. 49.

It must be noted that some sparking does occur briefly as the voltage passes through its maximum value after about 4 min of plating and continues for 3 or 4 minutes until the voltage has fallen to about 380 V. The sparks appear as tiny light flashes over the surface of the film. Foils removed from the cell during this time are a uniform gray color with tiny white spots evenly distributed over the surface. These spots

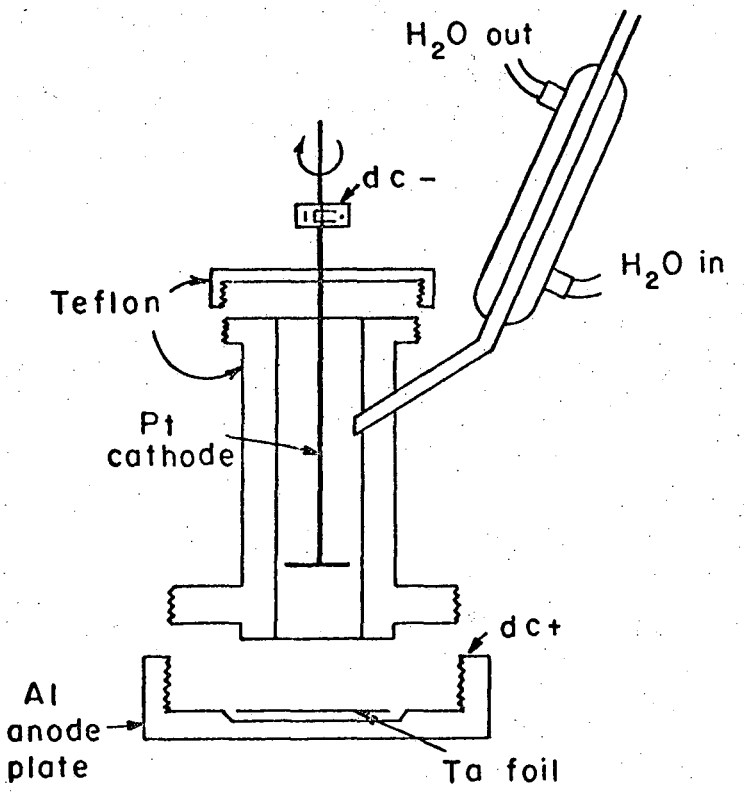

XBL671-345

Fig. 48. Electrolytic cell for anodization of tantalum metal foils at the electrolyte boiling point ($\approx 100^{\circ}C$).

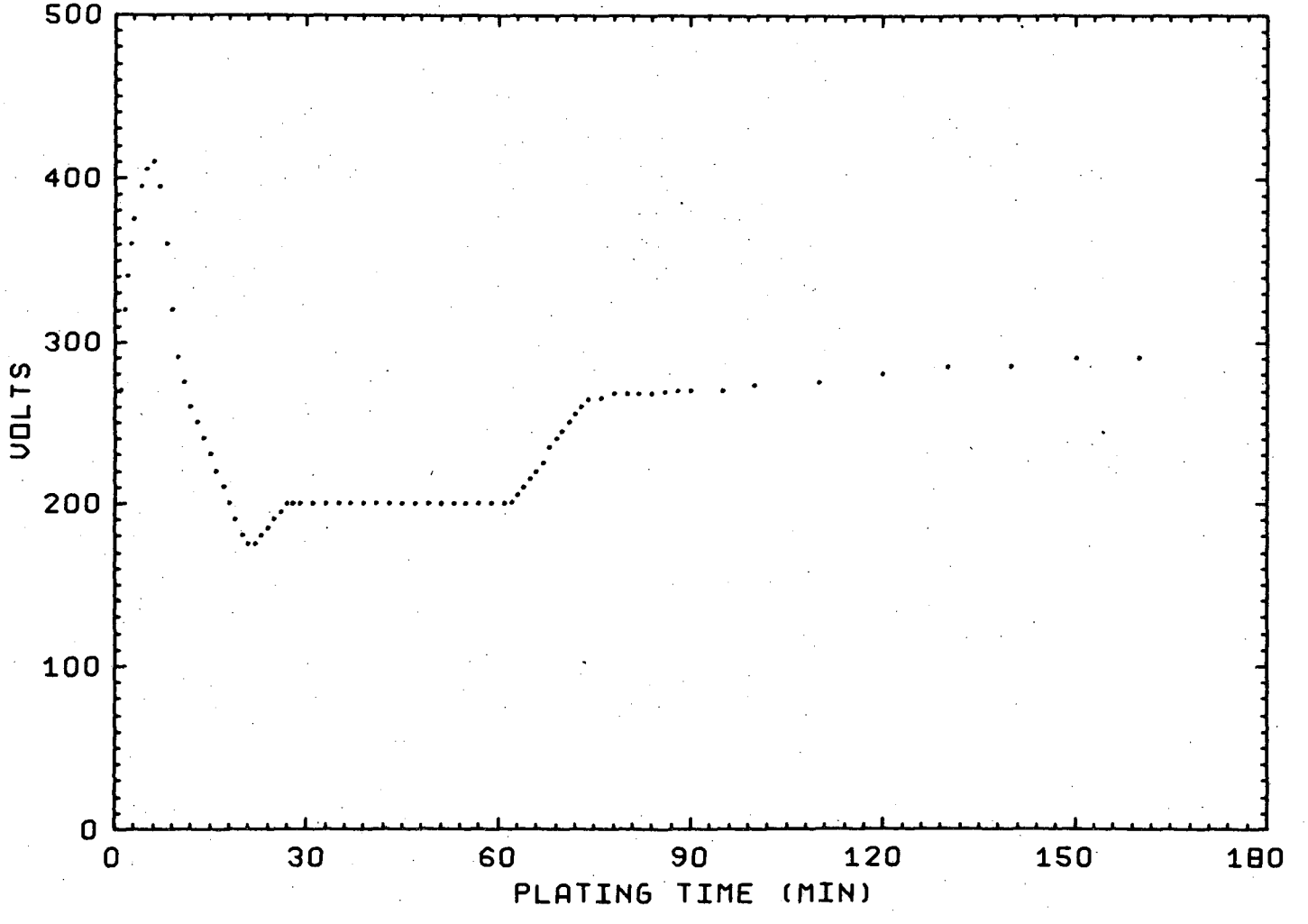

XBL 697-1032

Fig. 49. Variation in the applied voltage during boiling point anodization of Ta metal foil. Current = 40 mA, temperature $\approx 100^{\circ}$C.

are undoubtedly small, local non-uniformities in the film caused by sparking, but their even distribution should average over the area of the collimated bombarding ion beam. After 15 min of plating the entire surface of the oxide film is white and appears uniform to visual inspection.

The amounts of oxygen in the anodized foils, obtained directly by weight difference, are shown as a function of anodization-time in Fig. 50. These preliminary anodizations were performed with natural H_2O in the electrolyte. The reproducibility of this data has been demonstrated in the preparation of 25-30 targets in which the predicted oxide thicknesses have been correct to within 2-5%.

The relative thicknesses of these targets have also been measured by ^3He activation analysis via the $^{16}O(^3He,p)^{18}F$ reaction. These data are shown in Fig. 51. The ordinate is a relative scale expressed as ^{18}F activity per unit-beam-current normalized to the cross section for ^{18}F production at 10 MeV. The excitation function of Markowitz and Mahony in Sec. IV.E, Fig. 15, was used for normalization. The dashed line represents the maximum thick-target yield at the bombarding energy of 10 MeV.

Isotopic standards prepared as described above were used to measure the $^3He + ^{18}O$ excitation functions described in Sec. IV.E, and as standards for the ^3He activation analysis of samples of glycine and KH_2PO_4 of various ^{18}O enrichments. The ^{18}O enriched samples, obtained from the Weizmann Institute,[75] were prepared by isotopic exchange in ^{18}O enriched aqueous solution, with the degree of enrichment determined

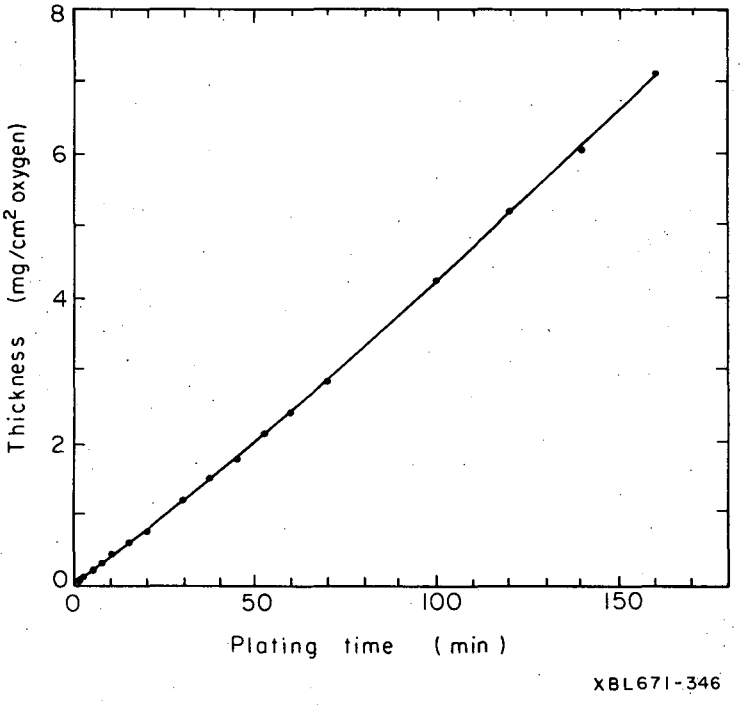

Fig. 50. Thickness of oxide coating produced by anodization of Ta foils in 0.1% KCl at the boiling point. Current = 40 mA, temperature ≈ 100° C.

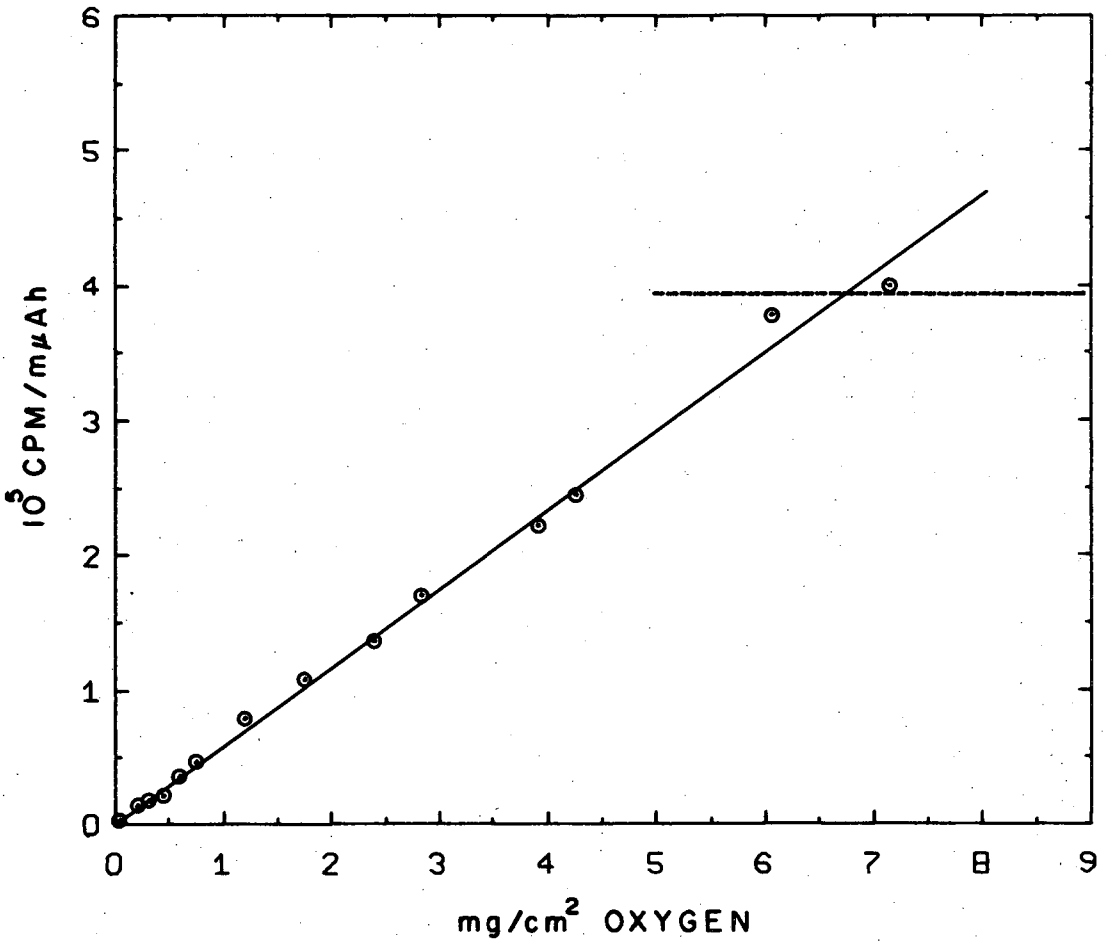

XBL 698-1276

Fig. 51. Activation of ^{16}O in the Ta_2O_5 films by the $^{16}O(^3He,p \text{ and } n)^{18}F$ reaction using 10-MeV $^3He^{++}$ ions. The dashed line represents the approximate thick target activity normalized to 10-MeV.

from mass spectrometric analysis of the solution before and after equilibration. Targets of these materials were prepared by sedimentation of the finely-ground crystals onto a platinum base-plate from an ether suspension. The powder targets were stabilized by adding one drop of a solution of 100 μg/ml polystyrene (C_8H_{8-}) in dichloroethylene. Several dilutions of ^{18}O-enriched H_2O were also analyzed as "unknowns" using the anodization method to prepare the targets. The standards were prepared from an aqueous KCl solution of 9.4 atom % ^{18}O, verified by mass spectrometric analysis. Each sample was irradiated for 10 sec with 10 MeV $^3He^{++}$ ions at a beam current of about 0.1 μA. The ^{18}O was determined through the $^{18}O(^3He,p)^{20}F$ reaction by counting the 1.63 MeV γ-ray from ^{20}F decay using the time-mode scaler apparatus described in Sec. III.C. The ^{16}O was determined through the $^{16}O(^3He,p)^{18}F$ reaction via the 511 keV annihilation radiation from the positron decay of ^{18}F. The ^{18}O content was calculated from the measured ^{16}O : ^{18}O ratio of the samples and standards. The results of the analyses are shown in Table XIX.

B. Surface Profile Analysis: Oxygen in Silicon

One of the main advantages gained through use of charged particles for activation analysis is the ability to differentiate between surface and bulk constituents. This advantage is accentuated with the use of ^3He as the activating particle because the low binding energy of the ^3He nucleus allows reactions to take place at lower energy, minimizing recoil-distortion of the surface profile.

Table XIX. Non-destructive analysis of ^{18}O by ^{3}He activation

Sample	% ^{18}O Quoted	% ^{18}O Found
KH_2PO_4	40.0	44.8 ± 1.4
KH_2PO_4	8.7	7.7 ± 0.5
KH_2PO_4	1.6	1.9 ± 0.1
Glycine	10.0	11.5 ± 1.7
Ta_2O_5	0.204	0.24± 0.01
Ta_2O_5	3.13	3.3 ± 0.1
Ta_2O_5	9.4	standard

The energy with which a product of a nuclear reaction recoils from the target is dependent upon the reaction mechanism. The maximum recoil energy will be obtained in pure compound-nucleus reactions in which the incident particle and the target nucleus are fused into an intermediate product having the total-system linear momentum. This compound nucleus then de-excites, predominantly by particle emission which is symmetric in the forward and backward directions. The averaged result is almost total linear momentum transfer to the recoiling product. ^{3}He reactions among light elements have been shown to proceed in part by compound nucleus mechanisms and in part by direct mechanisms in which the incident ion and the target nucleus transfer nucleons from one to the other. The linear momentum transferred to the recoiling product is much smaller in the latter case. The recoil energy of product nuclides is often a good test of mechanism.[76,32,33]

For ^{3}He activation analysis it will be practical to assume complete linear-momentum transfer and to calculate the recoil energy, E_r, from[77]

$$E_r = \frac{A_I \; A_P}{(A_I + A_T)^2} \; E_I \qquad (24)$$

where A_I is the mass number of incident ^{3}He ion, A_P is the mass number of the product nucleus, A_T is the mass number of the target, and E_I is the incident beam energy. Using this calculated value of recoil energy, it is possible to estimate the maximum recoil range for reaction products in various target and absorbing media. For example, the recoil energy of ^{18}F produced in the $^{16}O(^{3}He,p)^{18}F$ reaction is

$$E_r = 0.15\ E_I. \qquad (25)$$

Figure 52 shows the theoretical ranges of ^{18}F recoiling subsequent to reactions induced by 1-35 MeV $^{3}He^{++}$ ions, in various target materials, calculated by the method of Steward.[29]

An experimental illustration of the ^{18}F recoil in aluminum is given in Figs. 53 and 54. The targets were composed of 5 upstream aluminum catcher foils, a 1 mg/cm^2 mylar foil (33% O, 63% C), and 14 downstream aluminum catcher foils. The aluminum foils, each 100 μg/c m^2, were held in place in 0.005-in aluminum envelopes with 1-in-diameter center holes. The total thickness of this target stack, when held in place in the Faraday cup-sample holder, was about 1 cm. The total thickness of the catcher foils and mylar through which the beam passed was 2.9 mg/cm^2. The targets were bombarded for 20 minutes at a beam-current of about 0.05 μA at 5, 10, 20, and 25 MeV. The ^{18}F activity of each foil was determined via 511-keV β^+ annihilation radiation using a NaI(Tl) detector. The activities for a typical bombardment at 10 MeV are shown in Fig. 53. After subtracting the ^{18}F activity in each foil arising from the natural oxide coating (determined by averaging the activities of the last five foils), the percentage of forward recoils which passed through each catcher foil was calculated. This is shown in Fig. 54 for all bombarding energies.

Because the thickness of the mylar foil was too large with respect to the recoil energy, an average recoil range may not be accurately

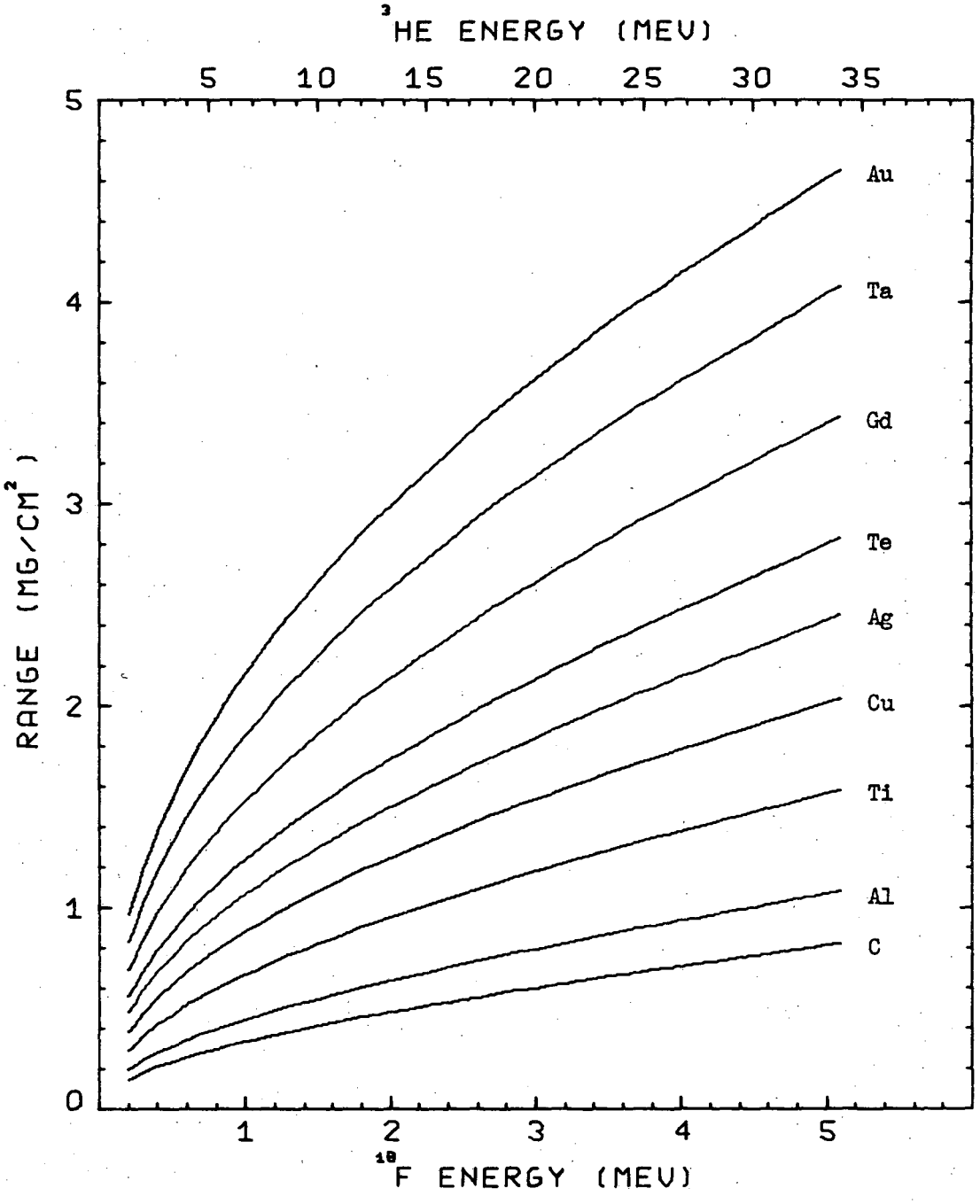

XBL 697-1024

Fig. 52. Theoretical ranges of recoiling ^{18}F produced by ^3He bombardment of ^{16}O. Total momentum transfer is assumed.

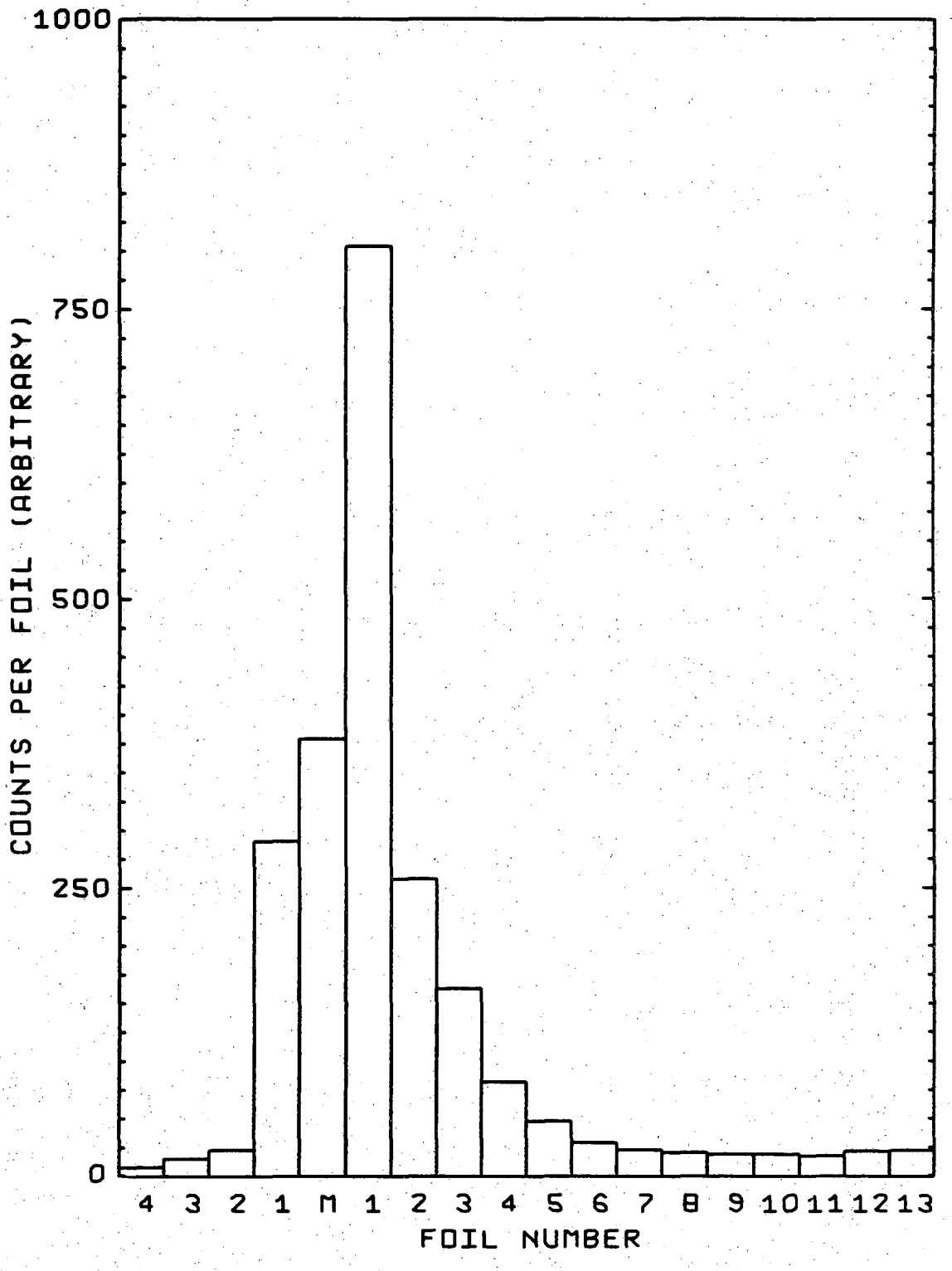

XBL 697-1025

Fig. 53. Activities of ^{18}F recoiling upstream and downstream from a mylar foil target irradiated with 10-MeV ^{3}He ions. The foil numbers refer to 100 μg/cm^2 Al catcher foils.

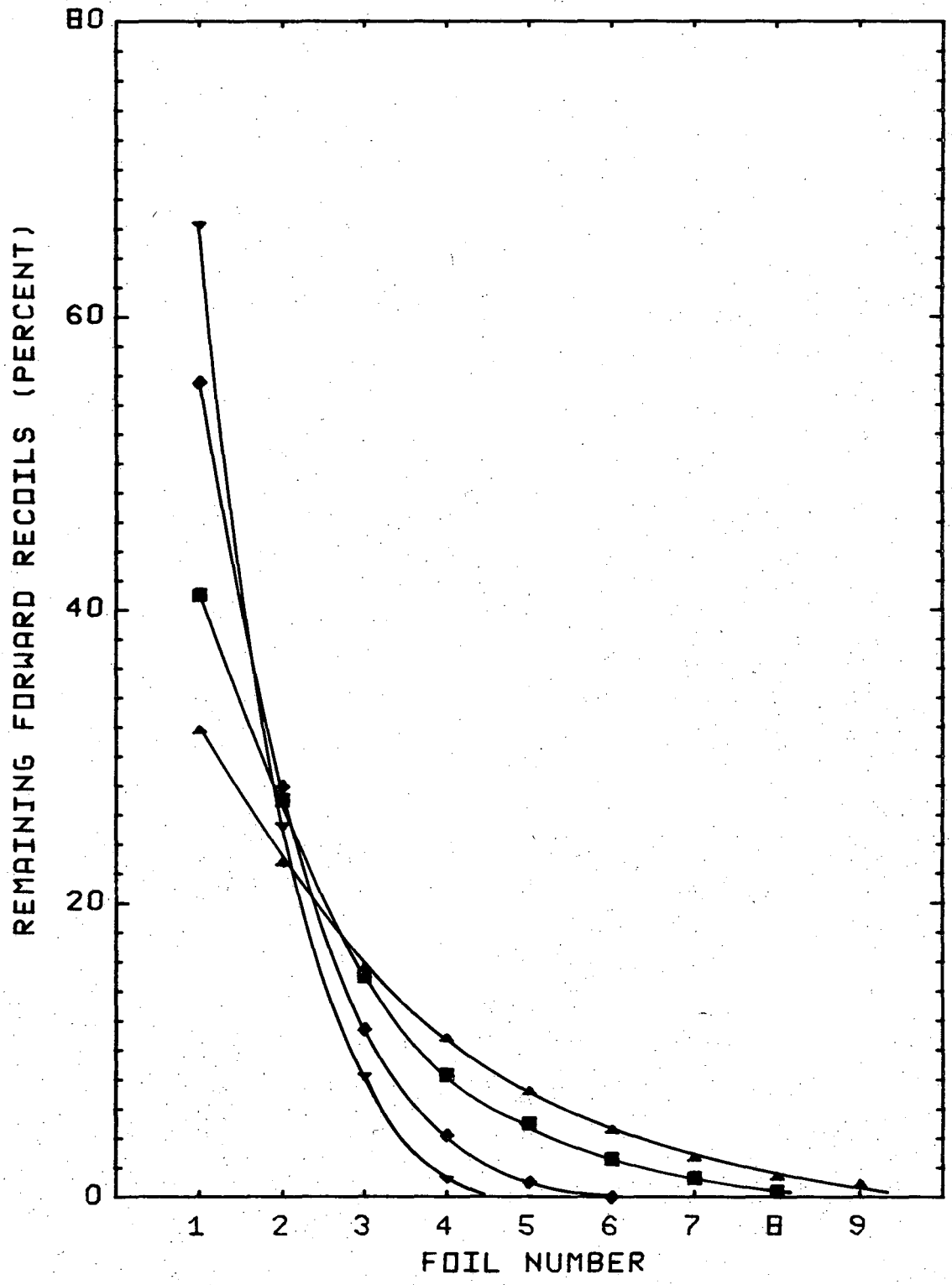

XBL 697-1026

Fig. 54. Percentage of forward recoiling ^{18}F which passed through each Al catcher foil. ▼ = 5-MeV, ◆ = 10-MeV, ■ = 20-MeV, ▲ = 25 MeV.

calculated from this data. It is meaningless to apply thick-target range calculations[76] because the assumption of isotropic particle emission is not valid for the $^{16}O(^{3}He,p)^{18}F$ reaction.[61] The data do, however, give a practical quantitative estimate of recoil range of ^{3}He activation analysis because the 1 mg/cm^2 mylar may be considered a "thin target" at these bombarding energies. From Fig. 52 we may estimate the maximum range of recoiling ^{18}F in aluminum for each experimental energy. These ranges are approximately 0.9 mg/cm^2, 0.8 mg/cm^2, 0.6 mg/cm^2, and 0.4 mg/cm^2 at 25, 20, 10, and 5 MeV, respectively. The maximum experimental recoil ranges are roughly obtained from Fig. 54 by adding the weights of successive foils, each 0.1 mg/cm^2.

A surprisingly high recoiling ^{18}F activity was observed in the backward direction. This is shown in Fig. 53 for the 10 MeV bombardment by foils 4, 3, 2, and 1, which were upstream from the mylar foil, M. The percentages of total recoils found in the upstream foils for the various bombardments were

25 MeV --- 7.4%

20 MeV --- 12.7%

10 MeV --- 17.6%

5 MeV --- 24.2%.

Almost all of this activity was found in the upstream catcher-foil nearest the mylar at the lower energies, while a small but significant amount was found in the second upstream foil at 20 and 25 MeV. This result was later verified by M. K. Go,[79] who obtained a backward recoil of 12% of the total ^{18}F activity produced in bombardment of a thinly anodized Ta_2O_5 target at a bombarding energy of 12 MeV. In that experiment,

significant ^{18}F activity was found to a depth of several $\mu g/cm^2$ in the aluminum catcher-foils. The explanation for these results remains to be explored.

The utility of recoil-range data in surface analysis is demonstrated by the analysis of oxygen on the surface of high-purity silicon. Mahony[64] has obtained the total oxygen content of some silicon samples by ^3He activation and Saito, et al.,[80] have determined surface oxygen using α-particle activation.

A 1-in diameter silicon disc, 800 mg/cm^2 thick, prepared from zone refined silicon for fabrication of a semiconductor particle detector, was ground flat on a glass plate using 600 mesh silicon carbide powder and washed with water and ethanol immediately before irradiation. The surface was protected from downstreaming contamination by a thin gold foil. The sample was irradiated for 45 minutes at 8 MeV at a current of 0.1 μA $^3He^{++}$ and the decay of the total activity in the irradiated sample followed via the 511-keV β^+ annihilation radiation using a NaI(Tl) detector until all short-lived activities had decayed to a negligible level, leaving only the 110 min activity of ^{18}F produced in the $^{16}O(^3He,p)^{18}F$ reaction. A thin layer of silicon was removed by surface grinding on a glass plate, its thickness determined by weight difference, and the activity on the remaining silicon disc re-determined. This process was repeated, using fresh grinding compound each time, until the activity per mg of Si removed remained constant.

The effective range of the 8 MeV $^3He^{++}$ ion in silicon is about 12.6 mg/cm^2. If the target is thought of as being composed of a stack

of thin layers up to this thickness, then the total integrated cross-section for ^{18}F production, measured from the front face of each layer, decreases with each successive layer. The variation in the average cross-section, however, is less than about 10% over the first 2.5 mg/cm Si. Because this variation in σ is small, the apparent concentration of oxygen in the Si disc was obtained after each surface grinding by comparison with a thick Ta_2O_5 standard irradiated for 5 min under the same conditions (8 MeV and 0.1 μA). Shown in Fig. 55 as a function of depth from the surface is the oxygen concentration calculated as though the oxygen were uniform over the silicon disc remaining after grinding.

If ^{18}F nuclei produced by ^{3}He bombardment did not recoil from the original positions occupied by oxygen atoms, Fig. 55 would be an exact surface profile. Instead, the profile must be deduced by comparison with the recoil range. From Fig. 54 it may be seen that only a few percent of recoils produced from oxygen at 10 MeV bombarding energy penetrate to a depth greater than about 0.5 mg/cm^2 in aluminum. Because of the close similarity of the range of ^{18}F in silicon and aluminum, little recoiling activity would be expected at depths below about 0.5 mg/cm^2 in the silicon target if all the oxygen were contained in a very thin surface layer. The data in Fig. 55 illustrate that the surface oxygen is, indeed, a thin layer. It should be noted that the silicon disc was ground by hand in this experiment with resulting non-uniformity in the layers removed. An accurate mechanical grinder should produce surface profile data sufficient to deduce fairly accurate surface-film thicknesses.

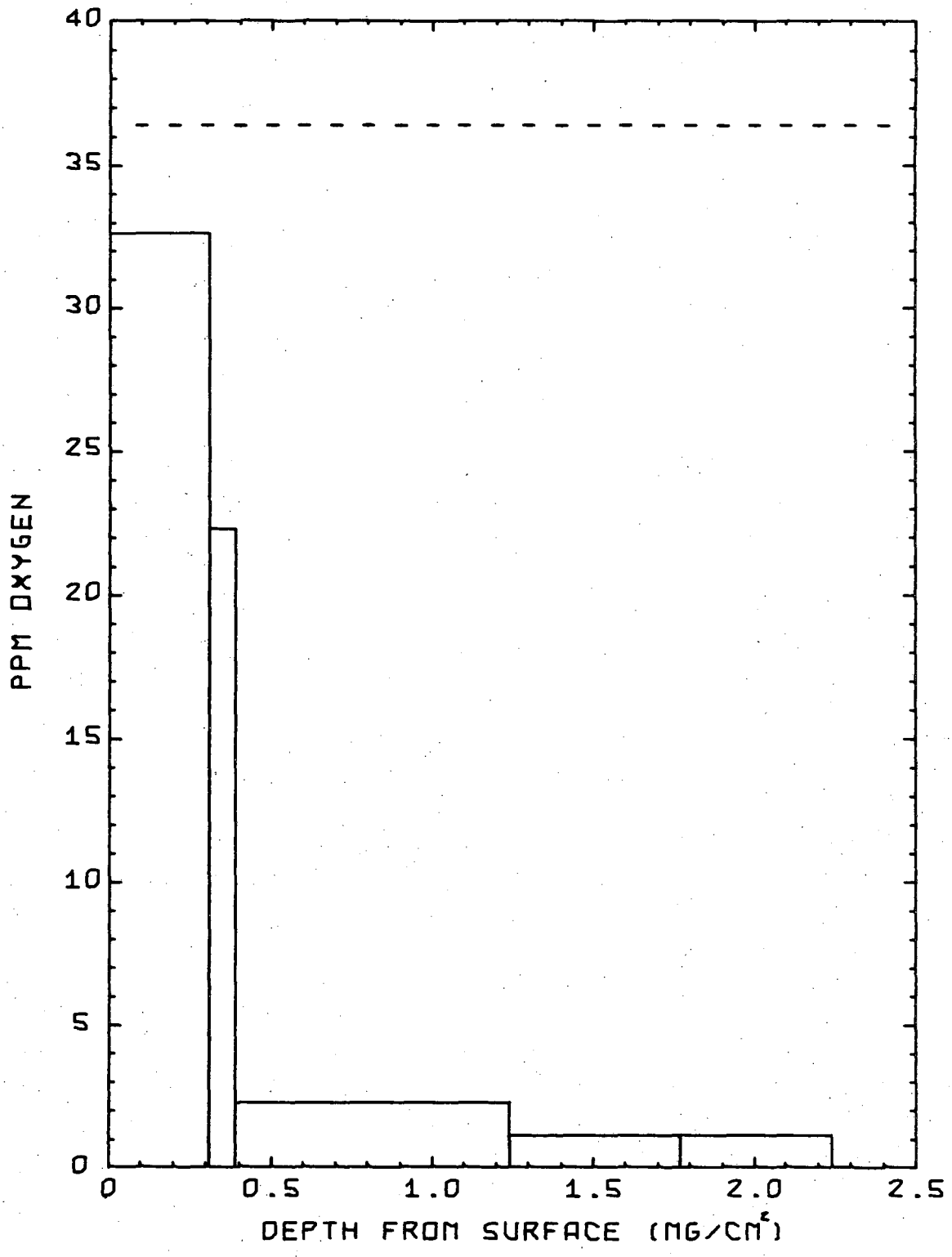

XBL 697-1027

Fig. 55. Surface profile of high-purity silicon obtained by ^{3}He activation analysis. The dashed line represents the apparent oxygen concentration before surface grinding.

Chemical etching, is of little use because the etchant attacks the silicon surface preferentially over the beam damaged areas. The oxygen profile description is completed by the activity of ^{18}F present at depths greater than about 1 mg/cm^2 Si. This represents the oxygen content in bulk (non-surface) high purity silicon. This concentration, 1.2 ppm, is comparable to the data of Saito, et al.,[80] who found by α-particle activation analysis that bulk silicon contained from a few tenths to several ppm, among different samples.

C. The Self Standard Method

Sample matrix activation may be used as an internal normalization standard in the comparative determination of contaminants in samples of very similar composition. The relative oxygen analysis of a number of samples of high-purity iron and nickel was used as an illustrative example.

The production of activities by ^3He-ion bombardment of iron and nickel, shown in Figs. 31 and 33, is appreciable even below about 7 MeV when compared with activity produced by a parts-per-million oxygen impurity, even though the cross-section (Fig 15) for the $^{16}O(^3He,p)^{18}F$ reaction is many times higher than the cross section for matrix activation. Use of lower bombarding energies to reduce matrix activation is limited by loss of sensitivity, and, in fact, matrix activation of iron and nickel is observable below about 5 MeV. This would be of small concern were it not for the unfortunate circumstance that most of the product activities decay by positron emission. The result is a multi-

component β^+ or 511-keV annihilation radiation decay-curve which may be difficult to resolve nondestructively. If matrix activation is appreciable, but not large compared to the activity induced in the impurity, then long-lived components may be used to provide a normalization between samples from which impurity contributions may be calculated without solving the decay curve.

Several samples of thick iron and nickel foil were obtained (from the Low Temperature Group of this Laboratory) whose anomalous behavior in magnetic fields at very low temperature was thought to result from variations in oxygen content produced by difference surface treatment. The extent of the variation, rather than the absolute oxygen content, was desired. These foils and several untreated pure-metal-foil standards were washed with ethanol and covered with a high-purity gold foil before irradiation. The targets were individually bombarded for 20 min at 5 MeV beam energy at a current of 0.2 μA $^3He^{++}$ and the induced positron activity followed via the 511-keV annihilation radiation using a NaI(Tl) detector.

The induced activities in the foils are shown in Fig. 56 for Ni and Fig. 57 for Fe plotted as a function of time after bombardment. The 3-4 hours which elapsed between the end of bombardment and the time of the first count allowed short-lived activities to decay to a negligible level.

All bombardments were of the same duration and performed at the same beam energy so that any differences in matrix activation could arise only from variations in beam intensity, which is a multiplicative term in the radioactivation equation. Assuming that the long-lived components

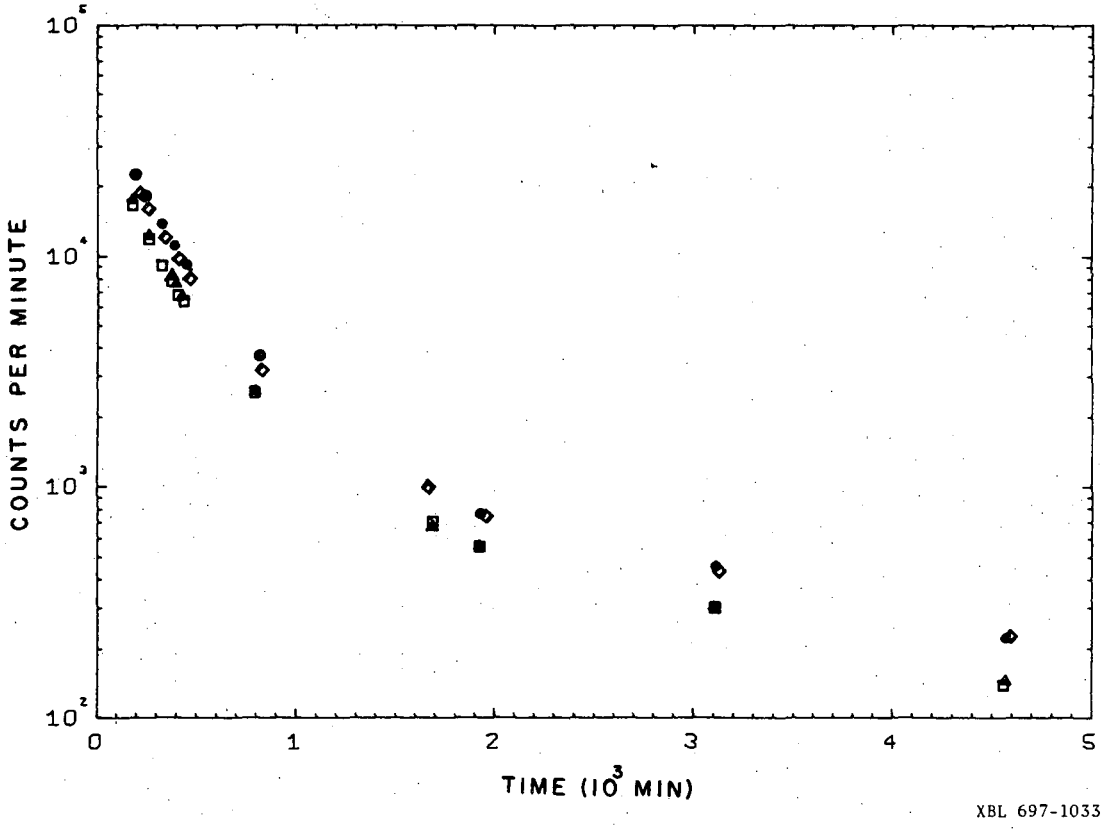

Fig. 56. Positron annihilation radiation activity of Ni irradiated for 20 min with 5-MeV ^{3}He ions. ● = Ni(I), ◇ =std(1), □ = std(2), △ = std(3).

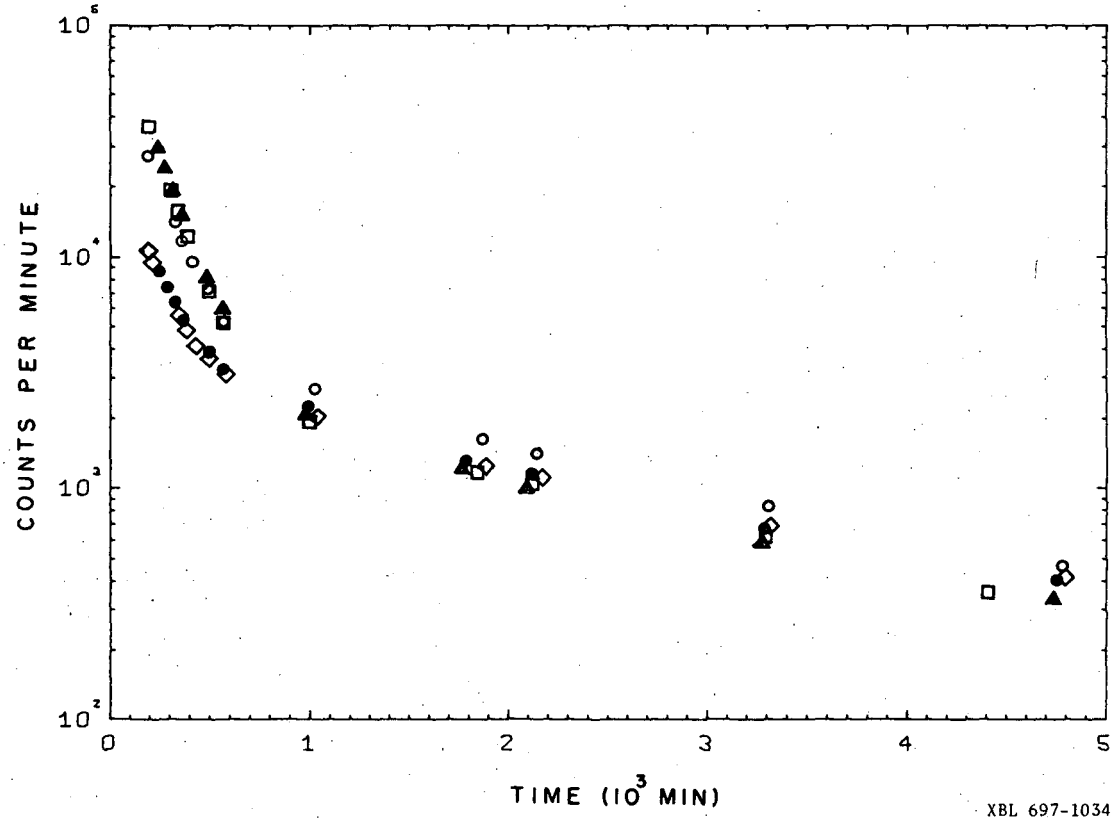

Fig. 57. Positron annihilation radiation activity of Fe irradiated for 20 min with 5-MeV ^{3}He ions. O = Fe(I), ● = Fe(II), ◇ = std(1), □ = std(2), △ = std(3).

in the decay curves of Figs. 56 and 57 resulted entirely from matrix activation, superposition of the data beyond about ten half-life of ^{18}F (10 × 110 min) would effectively normalize the curves. Variations in the curves at shorter times might then be interpreted as resulting from differences in impurities. This is shown in Fig. 58 for Ni. The result is completely superimposable curves for samples and standards. The sensitivity of the method is illustrated by the dashed line, which represents a hypothetical sample 20% richer in oxygen impurity. A rough decay-curve resolution approximating the complex long-lived components as a pure exponential decay yielded an approximate oxygen concentration of several $\mu g/cm^2$ over the effective beam range in Ni (the oxygen distribution is considered homogeneous).

Figure 59 shows the result of a similar superposition of long-lived components in the decay of activated Fe. That this difference is attributable to variations in oxygen content may be shown by a semilog plot of the differences between the curves. The data were first smoothed and then the differences, Fe(I) −std(1) and std(2) −std(1), calculated. These differences are shown in Fig. 60 as a function of time. The half-lives of the curves are 110 min; the correct value for ^{18}F.

If we interpret the activity difference in terms of a difference in surface oxidation, an approximate difference in oxygen content of 3 $\mu g/cm^2$ is found between std(1) and Fe(I), with the calculation based upon the cross section for the $^{16}O(^3He,p)^{18}F$ reaction at 5 MeV.

A further complication in the data interpretation arises from the large difference found in the oxygen content of the three standards.

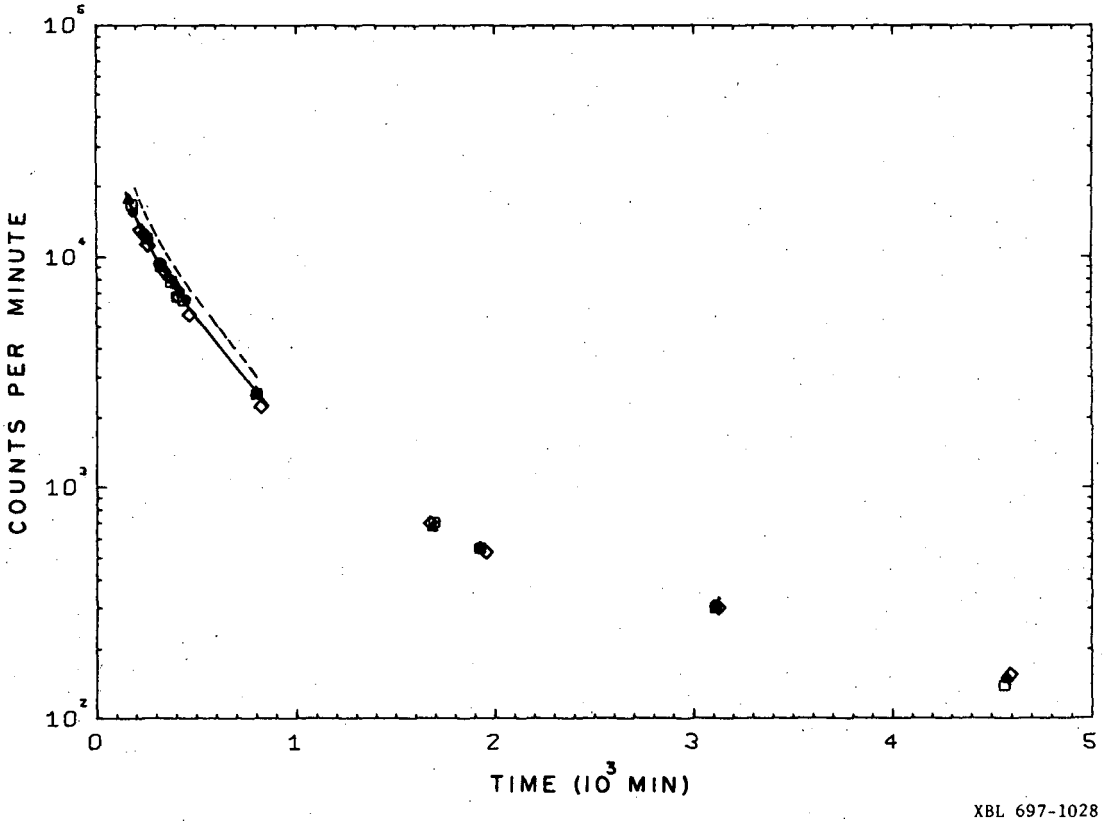

Fig. 58. Normalization of Ni activation data (Fig.55) obtained by superimposing long-lived matrix activities. The dashed line represents a hypothetical sample 20% richer in oxygen.

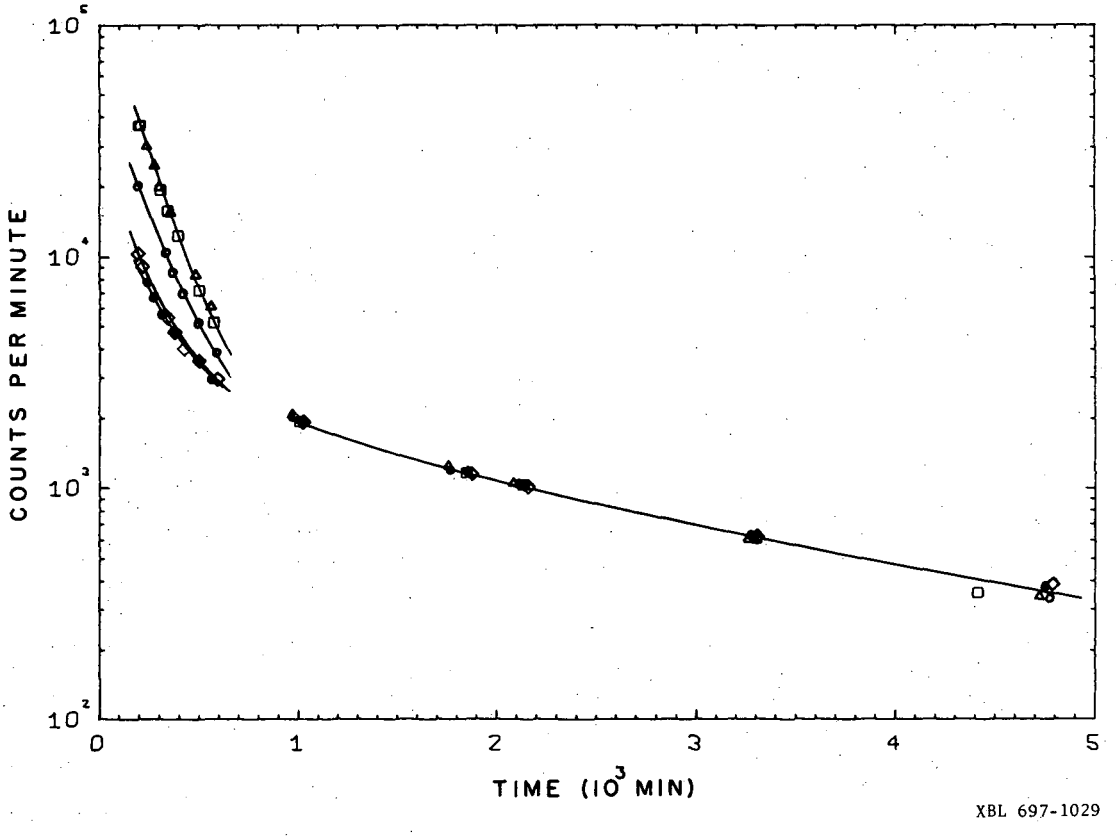

Fig. 59. Normalization of Fe activation data (Fig. 56) obtained by superimposing long-lived matrix activities.

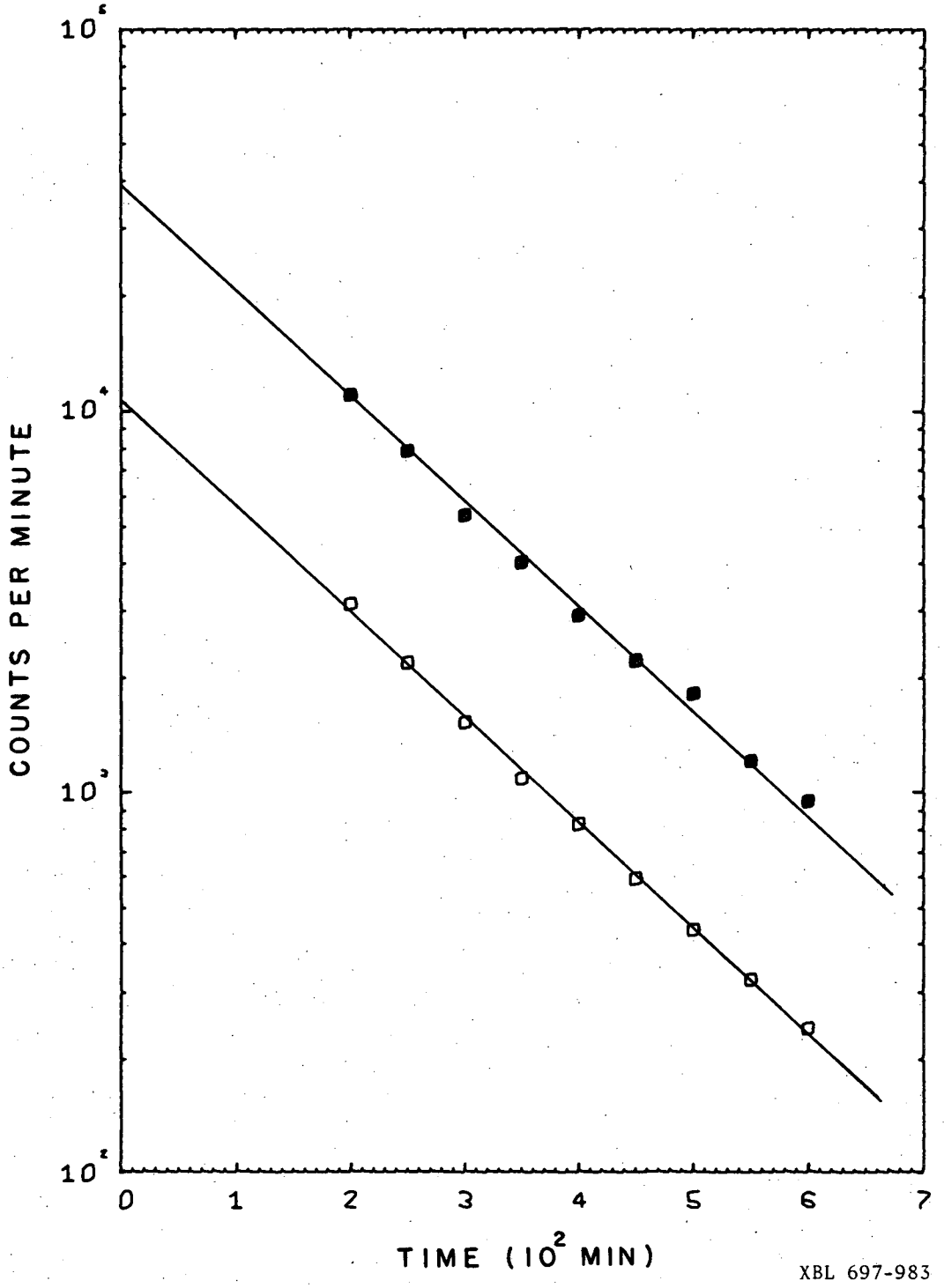

Fig. 60. Decay curves of the activity differences between Fe standards and samples. ■ = Fe(I) - std(1), □ = (std(2)-std(1) × 10^{-1}.

Of these, std(1) was obtained at the same time as the two samples Fe(I) and Fe(II). The other two standards, std(2) and std(3), were obtained later, cut from the same, or similar, pure-metal foil. It is possible that the methods of surface pretreatment for the various samples and standards were not identical.

The differences in oxygen content between these samples may or may not explain any anomalous properties of the metals, but it does demonstrate that the self standard method of charged particle activation analysis is fairly sensitive, accurate, and much easier than resolution of complex decay curves.

D. Tantalum, Platinum, and Gold as Target Supports and Cover Foils

A few excitation functions for ^{3}He induced reactions in tantalum and gold were presented in Sec. IV. The γ-ray spectra of targets irradiated at about 20 MeV were too complex to allow non-destructive measurement of all reactions. Samples of platinum were also irradiated at various energies with resulting spectra even more complicated because of the greater number of stable platinum isotopes. Reactions were observed in all three materials commencing at about 15 MeV. The approximate Coulomb barriers, shown in Fig. 2, are near 20 MeV. Of the heavy elements which might be used as cover foils or as support foils for samples to be irradiated, these three materials are most readily available and are structurally most suitable. The choice between then, then, depends upon interferences produced by activation of trace impurities, notably carbon and oxygen. Mahony[64] and Ryan, et al.[83] analyzed gold foil by ^{3}He activation, obtaining about 0.006% ^{16}O and 0.01% ^{12}C.

Foil stacks of platinum (7.3 mg/cm^2) and gold (6 mg/cm^2) were prepared by decking together five foils, the second and fourth of which were considered targets and the others as recoil compensators. The second foil and the surfaces of the compenstaor foils facing the second foil were surface etched in aqua regia, briefly, two hours before irradiation. All foil surfaces were then cleaned in acetone. The foil stacks were bombarded for 30 min each at 11 MeV and a beam current of about 0.25 μA. The 511-keV β^+ annihilation radiation from each target foil was followed for 4 hours using a NaI(Tl) detector.

The activities of ^{11}C, ^{13}N, and ^{18}F from the resolved decay curves were used with the experimental cross-sections of Mahony[64] to calculate the ^{12}C and ^{16}O content of the foils, assuming uniform distribution of these impurities. The results for gold were 0.005% carbon and 0.002% oxygen, accurate to within about ±20%. No differences were found between etched and unetched foils. The results for platinum were 0.002% oxygen and 0.006% carbon.

Tantalum foils (12.6 mg/cm^2), treated in the same manner, were analyzed for oxygen only. The results indicated an oxygen content of about 0.015%. Most of this oxygen content may be assumed to be surface contamination because tantalum is unstable to oxidation in air.

VI. CONCLUSION

The usefulness and practicality of an analytical system depends upon four factors: the extent of applicability, limitations imposed by interference, obtainable analytical sensitivity, and benefits derived from any unique features. In this section each of these factors will be summarized.

A. Applicability

An analysis by radioactivation is applicable to the estimation of a particular element if a nuclear reaction with a reasonable reaction cross-section can be induced by the method which leads to formation of a convenient product nuclide. The 2 proton-1 neutron configuration of the ^{3}He nucleus and its low binding energy allow formation of nine different reaction products (plus a few other less common ones) from a single target isotope at bombarding energies less than 20-30 MeV. From these possible products, at least one can usually be selected for detection whose half-life, decay characteristics, and formation cross-section are convenient. Among the light elements, the predominance of neutron deficient products induced by $^{3}He^{++}$ ion activation permits detection of activities through positron annihilation radiation where no conveniently detectable decay-associated γ-rays are emitted. The cross-sections of the ^{3}He induced reactions are comparatively quite high at low bombarding energies, many of them characteristically in hundreds of millibarns. The trends in the excitation functions allow reasonable estimates of cross-sections for reactions which have not, as yet, been studied.

Because more than one isotope of an element can often react with an incident ^{3}He ion to yield the same nuclear reaction products, total production cross-sections are frequently observed which are very high. Another factor which increases apparent production cross sections of (^{3}He,p) and (^{3}He,pn) reactions is the decay feeding by simultaneously induced (^{3}He,n) and (^{3}He,2n) products which characteristically decay by positron emission and electron capture. The total cross-sections for ^{3}He induced reactions generally increase with the size of the nucleus so that among the various reaction products induced in heavier nuclei by 15-20 MeV $^{3}He^{++}$ ions some convenient reaction products will usually be found.

B. Interferences

The same factors which are responsible for the wide range of applicability of ^{3}He activation analysis may also lead to increased interferences. The most severe interference results from formation of the same reaction product by more than one element, usually a neighbor in atomic number. The interferences listed in Table I through XVIII are of this type. It is sometimes possible to minimize these interferences by adjustment of bombarding energies. For example, in the simultaneous determination of carbon and oxygen the ^{18}F produced by $^{16}O(^{3}He,p)^{18}F$ is unambiguous, but the most convenient detectable product of ^{3}He + C is ^{11}C, produced by both $^{16}O(^{3}He,2\alpha)^{11}C$ and by $^{12}C(^{3}He,\alpha)^{11}C$. Reference to Fig. 17 shows that adjustment of the incident beam energy to less than about 12 MeV will eliminate the ambiguity in ^{11}C production. In

many practical situations, however, this procedure may not work. Sometimes the extent of interference can be assessed by bombarding standards prepared from the interfering element. If at least one other unambiguous detectable activity can be induced in the standard, then the extent of interference to detection of the activity in question can be estimated.

A second type of interference results from complication of the spectra of emitted radiations. The use of high resolution Ge(Li) detectors and the development of computer codes for spectrum analysis have minimized the effects of many closely spaced γ-rays in the same spectrum, and the use of these systems, coupled with chemical separations, virtually eliminates any interferences. There is one type of spectral interference, however, which cannot be so easily eliminated. This is the production of two or more activities which must be assayed by measuring radiation of the same energy. This situation is encountered in the analysis of many of the light elements whose reaction products decay by positron emission directly to the ground state of a stable daughter. The resulting detectable radiations are either the positrons themselves or the 511-keV radiation from positron annihilation. Measurement of the radiations emitted from complex activated samples almost always results in very complex decay curves. These may be treated by decay-curve resolution computer codes with the successful solution depending upon the relative half-lives and activities of the components. The most severe limitation to this procedure is that the ratio of the half-lives of any two components must be about 2 or more. An example of this interference is the analysis of silicon in glass. While ^{28}Si produces ^{30}P unambiguously,

the non-destructive measurement of detectable radiation yields 511-keV annihilation radiation decay curves among whose components are 2.6 min ^{30}P and 2 min ^{15}O. Accurate separation of these two activities is not possible. If, however, the atomic number (and therefore the Coulomb barrier) of the interfering element is sufficiently larger than that of the element sought, or if the interference reaction has a higher reaction threshold, then spectral interferences can be minimized by beam energy manipulation.

A further interference which arises because of the preponderance of β^+ emitting products from ^3He induced reactions is the masking of γ-rays whose energies are less than 511-keV by the enormous Compton distribution from incomplete photoelectric absorption of the annihilation radiation in the detector. The low-energy γ-rays are superimposed over a high background with resultant loss in detection sensitivity. Anticoincidence counting methods as described in Sec. III produce some reduction of this effect and can increase the analytical sensitivity (see Sec. VI.C).

C. Sensitivity

The sensitivity of an analytical method is a measure of the smallest amount or concentration of a species sought that can be detected within some acceptable limits of accuracy under the specified conditions. In activation analysis, because the count rates of the induced activities are low near the sensitivity limits, the theoretical limiting error is usually expressed as the counting statistical error. All other error

sources are considered small in comparison. The representation of the counting statistical uncertainty is given in Sec. III.D.3. For spectral analysis the sensitivity may be expressed in terms of the amount of material which must be bombarded under specified conditions to result in N_p detected photopeak counts,[8]

$$N_p = \frac{1}{2K^2}\left[1 + \sqrt{1 + 8K^2 N_b}\right], \tag{26}$$

where K is the desired accuracy limit and N_b is the spectral background count beneath the photopeak. This representation applies equally to analytical procedures involving chemical separations of product activities and to non-destructive methods in which the spectral background may be the dominating source of counting statistical error.

Because there are factors such as counting methods, interferences, and target restrictions encountered in practical analytical situations, which cannot be parameterized in the fashion of the systematic variables beam current, incident beam energy, length of bombardment, etc., sensitivity estimates were not included in the reaction data of Sec. IV. There are such estimates in the literature, giving thick-target sensitivities[37] and thick-target activity yields[65] for most of the light elements, however. These sensitivity estimates are really nothing more than relative measurements of the average cross-sections for total production of various activities by ^{3}He bombardment of thick targets.

In this author's opinion, the measured excitation functions and the trends observable in them, together with reaction and decay data

such as that tabulated in Sec. IV, will serve the purpose of sensitivity estimation. Comparison between sensitivities obtainable in ^{3}He activation analysis and other highly sensitive methods is better understood by comparing systematic parameters directly.

The cross-sections for reactions induced by thermal neutrons are generally higher than those induced by 0-30 MeV charged particles except in the light elements, for which the cross-sections of ^{3}He induced reactions are often higher. In very few instances are the neutron cross-sections more than about an order of magnitude higher than the larger ^{3}He induced reaction cross-sections, even among the heavier elements. Available reactor neutron fluxes are typically 10^{14} - 10^{15} neutrons/cm^{2}min while the beam current from small cyclotrons is about the same number of $^{3}He^{++}$ ions per minute for 1-10 μA beams. The length of bombardment may, of course, be the same for both methods except for extremely long bombardments. Samples may be irradiated in the thermal facility of a reactor for many days while such long bombardment using a particle accelerator is impractical.

The only other parametric variable is the sample thickness. While the amount of material which can be irradiated with thermal neutrons is often limited only by physical dimensions of the reactor facility, the short range of the ^{3}He ion in a sample material permits effective irradiation of only 10^{21}-10^{22} target nuclei at about 20 MeV incident energy. The number of nuclei "seen" by the neutron flux is often hundreds or even thousands of times greater. Of course, in practical analyses using reactor neutrons, analysis of a massive sample may be complicated by self-

absorption of neutrons in the sample and by inhomogenieties in the flux over the sample area.

We may then conclude that for analyses in which the sample size is restricted to a few hundred mg/cm^2, ^{3}He activation provides the most sensitive method for the light elements, in general, and is comparable to thermal neutron activation for many heavier elements.

D. Unique Features

The ability of the ^{3}He ion to induce many different nuclear reactions with high relative cross-sections increases the opportunity for isotopic analysis. Such analysis can be performed simultaneously and non-destructively, as in the case of ^{16}O : ^{18}O. This feature is shared by α-particle activation, which requires acceleration to much higher energies, and to a limited extent by p, d, and t bombardments, which induce fewer probable reactions.

Charged particle activation analysis also provides a highly sensitive method for surface and surface-profile analysis. The recoil ranges of the activation products are fairly short at low activating energies, causing little distortion of the depth distribution of a sample's surface constituents. ^{3}He ions are more suitable than other particles because of their ability to induce many reactions at low bombarding energies. The recoiling reaction-products resulting from ^{3}He activation of the surface oxide on high-purity silicon, for example, were completely contained within the first few hundred μg/cm^2 of the surface whereas the same products were found to a depth of almost 10 mg/cm^2 after α-particle activation.

Another interesting feature of charged particle activation analysis results from taking advantage of the Coulomb barrier differences between the constituents sought and the elements of the sample matrix. Interference can sometimes be eliminated completely by reducing the beam energy below the threshold for such reactions. It has been demonstrated that even in situations in which the Coulomb barrier difference between the trace and major sample constituents are not sufficient for exclusion of matrix activation the low reaction cross-sections encountered far below the barrier provide a convenient point of normalization for comparative analysis. This analytical procedure, termed the self standard method, could provide a rapid method of quality control for oxygen concentration in various high-purity metals requiring little or no mathematical treatment of the data.

ACKNOWLEDGMENTS

It is my great pleasure to acknowledge the encouragement and assistance I have received from so many people during my years at the University of California at Berkeley. I wish to extend particular thanks to Professor Samuel S. Markowitz who directed my work with such kindness, patience, and understanding and to Professor Stanley G. Prussin whose advice and friendship have so often been my support.

Throughout this work I have benefited from the cooperation of my research associate, Mrs. Diana M. Lee, for which I am deeply grateful. I am grateful, too, for the tireless efforts of the Lawrence Radiation Laboratory staff, the electronics group, particularly M. N. Firth, F. S. Duarte, K. B. Russell, and M. K. Lee and the staff of the Hilac, particularly J. N. Heieck, W. P. Kimlinger, and A. F. Schlosser. I also wish to thank C. A. Corum and D. B. Fong for their aid in designing the bombardment apparatus used in this work and Dr. J. M. Hollander for his guidance during my first years at this Laboratory.

My association with Drs. A. J. Haverfield, R. L. Watson, J. A. Cooper, F. M. Bernthal, J. B. Wilhelmy, A. Gilbert, M. D. Holtz, and E. Hoyle has been a most rewarding experience.

My wife, Ann, stands beside me at this moment as she has for so many years, through so many moments so much more difficult. Together, we offer our thanks to our children and our families for their patience, help, and understanding which has made possible this realization of our dream.

FOOTNOTES AND REFERENCES

1. W. E. Burcham, Nuclear Physics (McGraw-Hill Book Co., Great Britain, 1963).

2. G. Hevesy and H. Levi, Kgl. Danske Videnskab. Selskab, Mat.-Fys. Medd. 14, No. 5(1963).

3. G. T. Seaborg and J. J. Livingood, J. Am. Chem. Soc. 60, 1784 (1938).

4. G. E. Boyd, Anal. Chem. 21, 335 (1949).

5. R. E. Connolly, M. B. LeBoeuf, Anal. Chem. 25, 1095 (1953).

6. S. G. Prussin, J. A. Harris, and J. M. Hollander, Anal. Chem. 37, 1127 (1965).

7. F. Girardi, G. Guzzi, and J. Pauly, Radiochim. Acta 4, 109 (1965).

8. J. F. Lamb, S. G. Prussin, J. A. Harris, and J. M. Hollander, Anal. Chem. 38, 813 (1966).

9. G. L. Schroeder, H. W. Kraner, and R. D. Evans, Science 151, 815 (1966).

10. S. S. Markowitz and J. D. Mahony, Anal. Chem. 34, 329 (1962).

11. R. M. Main, M. R. Curtis, R. Garzier, P. B. Kennedy, B. H. Smith, and D. A. Spence, 1967 Particle Accelerator Conf., Washington, D.C., UCRL-17274 (1967).

12. The sensitivity for oxygen analysis by ^{3}He activation is estimated to be about 1 ppb using a 1-μA beam (Ref. 10).

13. G. Amsel and D. Samule, Anal. Chem. 39, 1689 (1967).

14. T. B. Pierce, P. F. Peck, and W. M. Henry, Nature 204, 571 (1964).

15. M. Peisach and D. O. Poole, Anal. Chem. 38, 1345 (1966).

16. E. Ricci and R. L. Hahn, Anal. Chem. 37, 742 (1965).

17. R. C. Koch, Activation Analysis Handbook (Academic Press, New York 1960).

18. H. J. M. Brown and D. Gibbons, Radioactivation Analysis (Oxford Univ. Press, London, 1963).

19. P. Albert, L'analyse par Radioactivation, (Gauthier-Villars and Cie, Paris, 1964).

20. R. S. Tilbury, NAS-NRC Nuclear Science Series, NAS-NS 3110 (1966).

21. E. Odeblad, Acta Radiol. 45, 396 (1956).

22. L. C. Bate, Nucleonics 21, 72 (1963).

23. P. Albert, Proceedings of the 1961 International Conf. on Modern Trends in Activation Anal., College Station, Texas, 78 (1961).

24. B. W. Hoffman and S. B. Van Camerik, Anal. Chem. 39, 1198(1967).

25. C. F. Williamson, J. P. Boujot, and J. Picard, Commissariat a' l'Energie Atomique Report No. CEA-R3042 (1966).

26. A. C. Demildt, Lawrence Radiation Laboratory Report UCRL-11618 (1964).

27. W. H. Barkas and M. J. Berger, NAS-NRC 1133, 103 (1964).

28. H. Bichsel, Lawrence Radiation Laboratory Report UCRL-17538 (1967).

29. P. G. Steward, Lawrence Radiation Laboratory Report UCRL-18127, Ph. D. Thesis, (1968).

30. C. Maples, G. W. Goth, and J. Cerny, Nuclear Data 2, 429 (1966).

31. E. A. Bryant, D. R. F. Cochran, and J. D. Knight, Phys. Rev. 130, 1512 (1963).

32. J. P. Hazan and M. Blann, Phys. Rev. 137, B1202 (1964).

33. G. B. Saha and N. T. Porile, Phys. Rev. 151, 907 (1966).

34. D. R. Osgood, J. R. Patterson, and E. W. Titterton, Nucl. Phys. 60, 503 (1964).

35. S. P. Cirilov, J. O. Newton, and J. P. Schapira, Nucl. Phys. 77, 472 (1965).

36. R. S. Blake, D. J. Jacobs, J. O. Newton, and J. P. Schapira, Nucl. Phys. 77, 254 (1965).

37. E. Ricci and R. L. Hahn, Anal. Chem. 39, 794 (1967).

38. E. L. Kelly, Nucl. Instr. Methods 18, 19, 33 (1962).

39. E. L. Hubbard, W. R. Baker, K. W. Ehlers, H. S. Gordon, R. M. Main, N. J. Norris, R. Peters, L. Smith, C. M. Van Atta, F. Voelker, C. E. Anderson, R. Beringer, R. L. Gluckstern, W. J. Knox, M. J. Malkin, A. R. Quinton, L. Schwarcz, and G. W. Wheeler, Rev. Sci. Instr. 32, 621 (1961).

40. D. A. Landis, Lawrence Radiation Laboratory Instr. No. 11X4160P-1.

41. F. S. Goulding, Nucl. Instr. Methods 43, 1 (1965).

42. J. M. Hollander, Nucl. Instr. Methods 43, 65 (1966).

43. G. T. Ewan and A. J. Tavendale, Can. J. Phys. 42, 2286 (1964).

44. F. S. Goulding and D. A. Landis, Proceedings of the Conf. on Instrumentation Techniques in Nuclear Pulse Analysis, Monterey, April 1963, NAS-NRC 1184.

45. Manufactured by Radiation Instruments Development Laboratories, Inc., Melrose Park, Illinois.

46. Manufactured by Northern Scientific, Inc., Madison, Wisconsin.

47. K. B. Russell, Lawrence Radiation Laboratory Instr. No. 15X8410.

48. International Atomic Energy Agency, Vienna, Austria.

49. A. J. Haverfield, Lawrence Radiation Laboratory Report UCRL-16969, Ph. D. Thesis (1966).

50. C. M. Lederer, J. M. Hollander, and I. Perlman, Table of Isotopes, Sixth Edition (John Wiley and Sons, New York, 1967).

51. J. Routti and S. G. Prussin, Lawrence Radiation Laboratory Report UCRL-17672 (1968).

52. Program RAD is a modification by C. Rugge, Lawrence Radiation Laboratory, of the Los Alamos least squares package, LA-2367.

53. J. B. Cumming, NAS-NRC Nuclear Science Series NAS-NS-3107, 25 (1963).

54. R. L. Hahn and E. Ricci, Phys. Rev. 146, 650 (1966).

55. R. L. Hahn and E. Ricci, Nucl. Phys. A101, 353 (1967).

56. S. S. Markowitz and J. M. Hall, Bull. Am. Phys. Soc. 4, 8 (1959).

57. O. D. Brill', Sov. J. Nucl. Phys. 1, 37 (1965).

58. J. R. Patterson, J. M. Poate, E. W. Titterton, and B. A. Robson, Proc. Phys. Soc. 86, 1297 (1965).

59. G. U. Din and J. L. Weil, Nucl. Phys. 86, 509 (1966).

60. D. R. F. Cochran and J. D. Knight, Phys. Rev. 128, 1281 (1962).

61. N. F. Mangelson, Lawrence Radiation Laboratory Report UCRL-17732, Ph. D. Thesis (1967).

62. J. F. Lamb, D. M. Lee, and S. S. Markowitz, 143rd National Meeting of the American Chemical Society, San Francisco, 1968. UCRL-18053A (1968).

63. J. F. Lamb, D. M. Lee, and S. S. Markowitz, Proc. of the Second Conf. on Practical Aspects of Activation Analysis with Charged Particles, Leige, Belgium, 1967, Euratom, 225 (1968).

64. J. D. Mahony, Lawrence Radiation Laboratory Report UCRL-11780, Ph. D. Thesis (1965).

65. J. F. Lamb, D. M. Lee, and S. S. Markowitz, Lawrence Radiation Laboratory Report UCRL-18667 (1968).

66. D. M. Lee, J. F. Lamb, and S. S. Markowitz, Lawrence Radiation Laboratory Report UCRL-17989 (1967).

67. M. K. Go and S. S. Markowitz, Lawrence Radiation Laboratory Report UCRL-18667 (1968).

68. S. Gorodetzky, A. Pape, A. Chevallier, J. C. Sens, and R. Armbruster, Nucl. Instr. Methods 42, 269 (1966).

69. J. F. Lamb, D. M. Lee, and S. S. Markowitz, Lawrence Radiation Laboratory Report UCRL-17299 (1966).

70. L. Young, Anodic Oxide Films (Academic Press, London, 1961).

71. J. Klerer, J. Electrochem. Soc. 112(9), 896 (1965).

72. J. A. Davies, B. Domeij, J. P. S. Pringle, and F. Brown, J. Electrochem. Soc. 112(7), 675 (1965).

73. D. A. Vermilyea, J. Electrochem. Soc. 110(4), 250 (1963).

74. B. A. Thompson, Anal. Chem. 33, 585 (1961).

75. Weizmann Institute of Science, Rehovoth, Israel.

76. B. G. Harvey, Ann. Rev. of Nucl. Sci. 10, 235 (1960).

77. L. Winsberg and J. M. Alexander, Phys. Rev. 121, 518 (1961).

78. F. M. Bernthal, Lawrence Radiation Laboratory Report UCRL-18651 Ph. D. Thesis (1969).

79. M. K. Go, Private communication, 1969.

80. K. Saito, T. Nozaki, S. Tanaka, M. Furukawa, and Hwasheng Cheng, Intl. J. Appl. Rad. Isotope 14, 357 (1963).

81. N. T. Porile, Purdue Univ. Dept. of Chem. Progress Rept. May 1967-April 1968, 11 (1968).

82. M. Blann, Phys. Rev. 133, B707 (1963).

83. V. A. Ryan, J. L. Green, and E. H. Lowenhaupt, Lawrence Radiation Laboratory Report UCRL-11618 (1964).

84. D. M. Lee, J. F. Lamb, and S. S. Markowitz, unpublished result.

85. C. F. Smith, Lawrence Radiation Laboratory Report, UCRL-11862, Ph. D. Thesis (1965).

APPENDIX A

Range-Energy Table for ^3He Ions

Total pathlength ranges of 0-35 MeV ^3He ions in nongaseous targets are given for elements 1 through 96. Also included are ^3He ranges in the compounds Ta_2O_5, KH_2PO_4, $PbCl_2$, and Glycine and the plastics Mylar and Teflon. The range data were calculated using the computer program of P. G. Steward.[29]

The computer code uses a combination of experimenta data, the nuclear and electronic stopping-power theory developed by Lindhard et al., and Bethe's theory for ions at high energy.

HE-3 IONS INCIDENT ON NONGASEOUS TARGETS

ENERGY	RANGE (MG/SQCM)					
MEV	H	HE	LI	BE	B	C
.5	.10	.36	.41	.44	.44	.43
1.0	.19	.62	.70	.77	.77	.74
1.5	.30	.92	1.05	1.14	1.14	1.10
2.0	.44	1.28	1.45	1.57	1.58	1.52
2.5	.61	1.70	1.93	2.09	2.10	2.01
3.0	.80	2.14	2.43	2.63	2.64	2.53
3.5	1.04	2.71	3.08	3.33	3.34	3.20
4.0	1.29	3.29	3.73	4.04	4.04	3.86
4.5	1.53	3.86	4.39	4.74	4.74	4.53
5.0	1.85	4.59	5.21	5.62	5.63	5.38
5.5	2.16	5.31	6.02	6.50	6.51	6.21
6.0	2.48	6.03	6.84	7.39	7.39	7.05
6.5	2.89	6.96	7.90	8.52	8.51	8.13
7.0	3.30	7.89	8.95	9.65	9.64	9.20
7.5	3.71	8.82	10.01	10.79	10.77	10.27
8.0	4.12	9.76	11.06	11.92	11.90	11.35
8.5	4.53	10.69	12.12	13.05	13.03	12.42
9.0	4.94	11.62	13.18	14.18	14.16	13.50
9.5	5.46	12.80	14.52	15.62	15.58	14.85
10.0	5.98	13.99	15.87	17.05	17.01	16.20
10.5	6.51	15.18	17.21	18.49	18.43	17.56
11.0	7.03	16.36	18.55	19.92	19.86	18.91
11.5	7.55	17.54	19.90	21.36	21.29	20.26
12.0	8.07	18.73	21.24	22.79	22.71	21.62
13.0	9.34	21.60	24.50	26.26	26.15	24.88
14.0	10.61	24.48	27.76	29.73	29.59	28.14
15.0	11.88	27.35	31.02	33.19	33.02	31.40
16.0	13.49	30.98	35.15	37.56	37.35	35.49
17.0	15.10	34.62	39.28	41.93	41.67	39.58
18.0	16.71	38.25	43.41	46.30	45.99	43.68
19.0	18.32	41.88	47.54	50.67	50.32	47.77
20.0	19.92	45.52	51.66	55.04	54.64	51.86
21.0	21.53	49.15	55.79	59.40	58.96	55.96
22.0	23.68	53.98	61.28	65.18	64.66	61.34
23.0	25.82	58.81	66.77	70.96	70.37	66.73
24.0	27.96	63.64	72.26	76.73	76.07	72.12
25.0	30.10	68.47	77.75	82.51	81.77	77.50
26.0	32.24	73.29	83.24	88.29	87.47	82.89
27.0	34.39	78.12	88.73	94.06	93.17	88.28
28.0	36.53	82.95	94.22	99.84	98.88	93.67
29.0	38.67	87.78	99.70	105.61	104.58	99.05
30.0	40.81	92.60	105.19	111.39	110.28	104.44
31.0	43.30	98.21	111.57	118.08	116.88	110.67
32.0	45.98	104.21	118.40	125.24	123.93	117.32
33.0	48.68	110.28	125.30	132.47	131.05	124.04
34.0	51.38	116.34	132.20	139.70	138.17	130.76
35.0	54.09	122.41	139.11	146.93	145.30	137.48

HE-3 IONS INCIDENT ON NONGASEOUS TARGETS

ENERGY MEV	RANGE (MG/SQCM) N	O	F	NE	NA	MG
.5	.44	.45	.50	.52	.56	.56
1.0	.76	.78	.88	.90	.97	.97
1.5	1.13	1.15	1.30	1.33	1.44	1.44
2.0	1.56	1.59	1.79	1.83	1.98	1.98
2.5	2.07	2.11	2.37	2.42	2.61	2.61
3.0	2.59	2.64	2.97	3.04	3.27	3.26
3.5	3.28	3.34	3.75	3.83	4.12	4.10
4.0	3.97	4.03	4.53	4.62	4.97	4.95
4.5	4.65	4.73	5.31	5.42	5.82	5.79
5.0	5.51	5.60	6.28	6.41	6.88	6.84
5.5	6.37	6.47	7.26	7.39	7.94	7.89
6.0	7.23	7.34	8.23	8.38	9.00	8.93
6.5	8.32	8.44	9.47	9.63	10.33	10.25
7.0	9.42	9.55	10.71	10.89	11.67	11.58
7.5	10.51	10.66	11.94	12.14	13.01	12.90
8.0	11.61	11.77	13.18	13.39	14.35	14.22
8.5	12.70	12.88	14.42	14.64	15.68	15.54
9.0	13.80	13.99	15.65	15.89	17.02	16.86
9.5	15.18	15.38	17.20	17.46	18.68	18.50
10.0	16.56	16.78	18.75	19.02	20.35	20.15
10.5	17.94	18.17	20.30	20.58	22.01	21.79
11.0	19.32	19.57	21.85	22.14	23.68	23.43
11.5	20.70	20.97	23.40	23.70	25.34	25.07
12.0	22.08	22.36	24.95	25.27	27.00	26.72
13.0	25.40	25.71	28.67	29.00	30.97	30.63
14.0	28.72	29.07	32.38	32.73	34.94	34.54
15.0	32.04	32.42	36.09	36.46	38.90	38.45
16.0	36.20	36.62	40.73	41.10	43.83	43.30
17.0	40.36	40.82	45.37	45.73	48.75	48.14
18.0	44.52	45.02	50.00	50.37	53.68	52.99
19.0	48.68	49.22	54.64	55.01	58.60	57.84
20.0	52.84	53.42	59.28	59.65	63.53	62.69
21.0	57.01	57.62	63.91	64.29	68.45	67.54
22.0	62.47	63.14	69.97	70.33	74.84	73.82
23.0	67.94	68.66	76.04	76.37	81.24	80.10
24.0	73.41	74.17	82.10	82.41	87.63	86.39
25.0	78.88	79.69	88.16	88.45	94.02	92.67
26.0	84.35	85.20	94.22	94.48	100.42	98.96
27.0	89.82	90.72	100.28	100.52	106.81	105.24
28.0	95.29	96.23	106.34	106.56	113.20	111.52
29.0	100.76	101.75	112.40	112.60	119.59	117.81
30.0	106.22	107.26	118.46	118.63	125.99	124.09
31.0	112.54	113.63	125.45	125.57	133.33	131.30
32.0	119.29	120.43	132.90	132.98	141.15	138.98
33.0	126.10	127.30	140.43	140.45	149.05	146.74
34.0	132.92	134.17	147.95	147.92	156.95	154.50
35.0	139.74	141.04	155.48	155.40	164.85	162.26

HE-3 IONS INCIDENT ON NONGASEOUS TARGETS

ENERGY	RANGE (MG/SQCM)					
MEV	AL	SI	P	S	CL	AR
.5	.57	.59	.63	.63	.68	.75
1.0	.99	1.02	1.09	1.09	1.16	1.28
1.5	1.47	1.51	1.60	1.60	1.71	1.87
2.0	2.01	2.07	2.19	2.18	2.33	2.55
2.5	2.65	2.73	2.88	2.87	3.06	3.34
3.0	3.32	3.41	3.59	3.58	3.81	4.16
3.5	4.17	4.28	4.51	4.48	4.77	5.20
4.0	5.02	5.15	5.43	5.39	5.74	6.24
4.5	5.88	6.02	6.34	6.29	6.69	7.28
5.0	6.93	7.10	7.47	7.41	7.88	8.57
5.5	7.99	8.18	8.61	8.53	9.07	9.85
6.0	9.05	9.26	9.74	9.65	10.25	11.14
6.5	10.39	10.62	11.16	11.06	11.74	12.74
7.0	11.73	11.98	12.58	12.46	13.22	14.35
7.5	13.06	13.34	14.00	13.86	14.71	15.95
8.0	14.40	14.69	15.43	15.27	16.19	17.56
8.5	15.74	16.05	16.85	16.67	17.68	19.17
9.0	17.08	17.41	18.27	18.07	19.16	20.77
9.5	18.75	19.09	20.03	19.81	21.00	22.75
10.0	20.41	20.78	21.79	21.54	22.83	24.73
10.5	22.09	22.46	23.55	23.28	24.66	26.71
11.0	23.76	24.14	25.31	25.01	26.50	28.69
11.5	25.43	25.83	27.07	26.75	28.33	30.67
12.0	27.10	27.51	28.83	28.49	30.16	32.65
13.0	31.09	31.51	33.01	32.60	34.51	37.34
14.0	35.08	35.51	37.19	36.71	38.85	42.03
15.0	39.07	39.50	41.36	40.83	43.19	46.71
16.0	44.04	44.45	46.53	45.90	48.55	52.49
17.0	49.00	49.39	51.69	50.98	53.90	58.26
18.0	53.97	54.34	56.85	56.06	59.26	64.03
19.0	58.94	59.29	62.01	61.14	64.61	69.80
20.0	63.91	64.23	67.17	66.21	69.96	75.57
21.0	68.88	69.18	72.33	71.29	75.32	81.34
22.0	75.37	75.57	78.99	77.84	82.21	88.76
23.0	81.86	81.96	85.65	84.38	89.10	96.18
24.0	88.35	88.35	92.31	90.92	95.99	103.60
25.0	94.84	94.74	98.97	97.47	102.88	111.02
26.0	101.33	101.13	105.63	104.01	109.77	118.44
27.0	107.82	107.53	112.29	110.55	116.66	125.86
28.0	114.31	113.92	118.95	117.10	123.56	133.28
29.0	120.80	120.31	125.61	123.64	130.45	140.70
30.0	127.29	126.70	132.27	130.18	137.34	148.12
31.0	134.77	134.02	139.90	137.67	145.22	156.60
32.0	142.74	141.82	148.02	145.64	153.60	165.62
33.0	150.79	149.69	156.22	153.69	162.07	174.73
34.0	158.83	157.57	164.42	161.73	170.54	183.84
35.0	166.88	165.45	172.62	169.78	179.01	192.95

HE-3 IONS INCIDENT ON NONGASEOUS TARGETS

ENERGY MEV	RANGE (MG/SQCM) K	CA	SC	TI	V	CR
.5	.72	.72	.80	.84	.89	.90
1.0	1.22	1.23	1.35	1.42	1.49	1.51
1.5	1.78	1.79	1.96	2.06	2.15	2.17
2.0	2.43	2.43	2.66	2.78	2.91	2.92
2.5	3.17	3.17	3.47	3.62	3.78	3.79
3.0	3.95	3.94	4.31	4.49	4.68	4.69
3.5	4.93	4.91	5.37	5.59	5.81	5.82
4.0	5.92	5.89	6.43	6.69	6.95	6.95
4.5	6.90	6.87	7.49	7.78	8.08	8.08
5.0	8.11	8.06	8.79	9.13	9.47	9.46
5.5	9.32	9.26	10.10	10.47	10.86	10.83
6.0	10.53	10.46	11.40	11.81	12.25	12.21
6.5	12.05	11.96	13.02	13.49	13.97	13.92
7.0	13.56	13.45	14.64	15.16	15.70	15.63
7.5	15.07	14.95	16.26	16.83	17.42	17.34
8.0	16.58	16.44	17.88	18.50	19.15	19.05
8.5	18.10	17.94	19.50	20.17	20.87	20.76
9.0	19.61	19.43	21.12	21.84	22.59	22.47
9.5	21.47	21.27	23.11	23.90	24.71	24.56
10.0	23.33	23.11	25.10	25.95	26.82	26.66
10.5	25.20	24.95	27.09	28.00	28.94	28.75
11.0	27.06	26.79	29.09	30.05	31.05	30.85
11.5	28.92	28.63	31.08	32.11	33.17	32.94
12.0	30.78	30.47	33.07	34.16	35.28	35.04
13.0	35.19	34.81	37.77	39.00	40.26	39.97
14.0	39.59	39.16	42.47	43.84	45.25	44.90
15.0	44.00	43.50	47.17	48.68	50.23	49.84
16.0	49.41	48.84	52.95	54.62	56.34	55.88
17.0	54.83	54.18	58.72	60.56	62.45	61.92
18.0	60.25	59.52	64.49	66.49	68.56	67.96
19.0	65.67	64.86	70.26	72.43	74.67	74.00
20.0	71.09	70.20	76.04	78.37	80.78	80.04
21.0	76.51	75.55	81.81	84.31	86.88	86.08
22.0	83.46	82.39	89.21	91.91	94.69	93.80
23.0	90.42	89.24	96.60	99.51	102.50	101.51
24.0	97.38	96.09	104.00	107.11	110.31	109.23
25.0	104.33	102.94	111.39	114.71	118.12	116.94
26.0	111.29	109.79	118.79	122.30	125.93	124.66
27.0	118.25	116.64	126.18	129.90	133.73	132.37
28.0	125.21	123.49	133.58	137.50	141.54	140.09
29.0	132.16	130.34	140.97	145.10	149.35	147.80
30.0	139.12	137.19	148.37	152.70	157.16	155.51
31.0	147.06	145.00	156.80	161.36	166.05	164.30
32.0	155.52	153.32	165.78	170.58	175.52	173.64
33.0	164.05	161.71	174.83	179.88	185.06	183.06
34.0	172.59	170.11	183.89	189.18	194.61	192.49
35.0	181.12	178.51	192.95	198.48	204.16	201.92

HE-3 IONS INCIDENT ON NONGASEOUS TARGETS

ENERGY MEV	RANGE (MG/SQCM) MN	FE	CO	NI	CU	ZN
.5	.95	.96	1.02	1.02	1.08	1.09
1.0	1.58	1.60	1.68	1.68	1.77	1.78
1.5	2.27	2.29	2.40	2.39	2.52	2.54
2.0	3.05	3.07	3.21	3.18	3.36	3.39
2.5	3.95	3.96	4.14	4.09	4.32	4.35
3.0	4.88	4.89	5.09	5.02	5.32	5.35
3.5	6.04	6.04	6.29	6.19	6.55	6.60
4.0	7.21	7.20	7.48	7.35	7.78	7.84
4.5	8.37	8.36	8.68	8.52	9.02	9.08
5.0	9.79	9.76	10.13	9.93	10.51	10.59
5.5	11.21	11.17	11.57	11.34	12.00	12.09
6.0	12.62	12.58	13.02	12.75	13.50	13.59
6.5	14.38	14.32	14.81	14.49	15.34	15.44
7.0	16.14	16.05	16.60	16.23	17.18	17.30
7.5	17.89	17.79	18.39	17.97	19.02	19.15
8.0	19.65	19.53	20.18	19.72	20.86	21.00
8.5	21.41	21.27	21.97	21.46	22.70	22.85
9.0	23.16	23.01	23.76	23.20	24.54	24.71
9.5	25.32	25.14	25.95	25.32	26.79	26.96
10.0	27.47	27.27	28.13	27.45	29.03	29.22
10.5	29.62	29.39	30.32	29.57	31.28	31.48
11.0	31.77	31.52	32.51	31.69	33.52	33.73
11.5	33.92	33.65	34.69	33.82	35.77	35.99
12.0	36.07	35.78	36.88	35.94	38.01	38.25
13.0	41.13	40.78	42.02	40.93	43.28	43.54
14.0	46.19	45.78	47.16	45.92	48.55	48.84
15.0	51.25	50.78	52.30	50.91	53.82	54.13
16.0	57.44	56.90	58.58	57.01	60.25	60.58
17.0	63.64	63.02	64.86	63.10	66.68	67.04
18.0	69.83	69.13	71.13	69.19	73.10	73.49
19.0	76.02	75.25	77.41	75.28	79.53	79.95
20.0	82.22	81.37	83.69	81.37	85.96	86.40
21.0	88.41	87.48	89.97	87.46	92.39	92.85
22.0	96.31	95.28	97.96	95.21	100.55	101.05
23.0	104.21	103.07	105.96	102.96	108.72	109.24
24.0	112.11	110.87	113.95	110.71	116.89	117.44
25.0	120.01	118.66	121.94	118.46	125.06	125.63
26.0	127.91	126.46	129.94	126.21	133.23	133.83
27.0	135.81	134.26	137.93	133.96	141.40	142.02
28.0	143.71	142.05	145.93	141.71	149.57	150.22
29.0	151.61	149.85	153.92	149.46	157.74	158.42
30.0	159.51	157.64	161.91	157.21	165.91	166.61
31.0	168.50	166.51	171.00	166.02	175.19	175.92
32.0	178.06	175.94	180.66	175.37	185.05	185.80
33.0	187.71	185.45	190.41	184.82	195.00	195.78
34.0	197.36	194.96	200.16	194.26	204.95	205.76
35.0	207.01	204.48	209.91	203.71	214.91	215.73

HE-3 IONS INCIDENT ON NONGASEOUS TARGETS

ENERGY MEV	RANGE (MG/SQCM) GA	GE	AS	SE	BR	KR
.5	1.13	1.15	1.16	1.20	1.19	1.23
1.0	1.86	1.90	1.92	1.98	1.97	2.03
1.5	2.65	2.70	2.74	2.83	2.81	2.90
2.0	3.54	3.61	3.65	3.78	3.75	3.87
2.5	4.55	4.64	4.70	4.86	4.84	4.98
3.0	5.59	5.71	5.78	5.98	5.95	6.13
3.5	6.89	7.04	7.13	7.37	7.33	7.56
4.0	8.19	8.36	8.47	8.76	8.71	8.99
4.5	9.49	9.69	9.81	10.15	10.10	10.41
5.0	11.06	11.29	11.44	11.84	11.77	12.13
5.5	12.63	12.90	13.06	13.52	13.44	13.86
6.0	14.20	14.50	14.68	15.20	15.11	15.58
6.5	16.14	16.47	16.68	17.26	17.16	17.69
7.0	18.07	18.44	18.67	19.32	19.21	19.80
7.5	20.00	20.42	20.67	21.39	21.26	21.92
8.0	21.94	22.39	22.67	23.45	23.31	24.03
8.5	23.87	24.36	24.66	25.51	25.36	26.14
9.0	25.80	26.33	26.66	27.58	27.41	28.25
9.5	28.16	28.73	29.09	30.09	29.90	30.82
10.0	30.51	31.13	31.51	32.59	32.39	33.38
10.5	32.87	33.53	33.94	35.10	34.88	35.94
11.0	35.22	35.93	36.36	37.61	37.37	38.50
11.5	37.58	38.33	38.79	40.11	39.86	41.06
12.0	39.93	40.73	41.22	42.62	42.35	43.63
13.0	45.45	46.35	46.90	48.49	48.17	49.62
14.0	50.97	51.98	52.58	54.35	53.99	55.61
15.0	56.49	57.60	58.26	60.22	59.81	61.60
16.0	63.21	64.44	65.17	67.35	66.89	68.87
17.0	69.94	71.29	72.09	74.49	73.96	76.14
18.0	76.66	78.13	79.00	81.62	81.03	83.42
19.0	83.39	84.97	85.91	88.75	88.11	90.69
20.0	90.11	91.82	92.82	95.89	95.18	97.96
21.0	96.83	98.66	99.73	103.02	102.25	105.24
22.0	105.36	107.34	108.49	112.05	111.20	114.43
23.0	113.89	116.02	117.24	121.07	120.14	123.62
24.0	122.43	124.69	126.00	130.10	129.09	132.81
25.0	130.96	133.37	134.75	139.13	138.04	142.01
26.0	139.49	142.05	143.51	148.16	146.98	151.20
27.0	148.02	150.72	152.26	157.19	155.93	160.39
28.0	156.55	159.40	161.02	166.21	164.87	169.58
29.0	165.08	168.08	169.77	175.24	173.82	178.77
30.0	173.61	176.75	178.53	184.27	182.77	187.97
31.0	183.29	186.60	188.46	194.51	192.91	198.38
32.0	193.58	197.05	199.00	205.37	203.67	209.43
33.0	203.96	207.60	209.64	216.34	214.53	220.58
34.0	214.34	218.15	220.28	227.30	225.39	231.74
35.0	224.72	228.70	230.92	238.27	236.25	242.89

HE-3 IONS INCIDENT ON NONGASEOUS TARGETS

ENERGY	RANGE (MG/SQCM)					
MEV	RB	SR	Y	ZR	NB	MO
.5	1.23	1.24	1.23	1.25	1.25	1.26
1.0	2.03	2.05	2.04	2.06	2.07	2.09
1.5	2.91	2.93	2.92	2.95	2.96	3.00
2.0	3.88	3.91	3.91	3.95	3.96	4.02
2.5	5.00	5.04	5.04	5.09	5.11	5.18
3.0	6.15	6.21	6.20	6.27	6.29	6.38
3.5	7.58	7.65	7.65	7.73	7.76	7.87
4.0	9.02	9.10	9.09	9.19	9.23	9.36
4.5	10.45	10.54	10.54	10.65	10.69	10.85
5.0	12.18	12.29	12.28	12.41	12.46	12.64
5.5	13.90	14.03	14.02	14.17	14.23	14.43
6.0	15.63	15.77	15.76	15.93	16.00	16.22
6.5	17.75	17.91	17.89	18.09	18.16	18.41
7.0	19.87	20.04	20.02	20.24	20.32	20.60
7.5	21.98	22.18	22.16	22.39	22.48	22.79
8.0	24.10	24.31	24.29	24.54	24.63	24.98
8.5	26.22	26.45	26.42	26.70	26.79	27.16
9.0	28.34	28.58	28.55	28.85	28.96	29.35
9.5	30.90	31.17	31.13	31.46	31.57	32.00
10.0	33.47	33.76	33.71	34.06	34.18	34.64
10.5	36.04	36.34	36.29	36.66	36.79	37.29
11.0	38.61	38.93	38.87	39.27	39.40	39.93
11.5	41.17	41.51	41.45	41.87	42.01	42.57
12.0	43.74	44.10	44.04	44.48	44.62	45.22
13.0	49.74	50.14	50.06	50.56	50.71	51.38
14.0	55.73	56.18	56.08	56.63	56.80	57.55
15.0	61.73	62.22	62.11	62.71	62.89	63.71
16.0	69.01	69.55	69.41	70.07	70.27	71.17
17.0	76.29	76.87	76.71	77.44	77.64	78.63
18.0	83.57	84.20	84.01	84.80	85.01	86.09
19.0	90.85	91.52	91.31	92.16	92.39	93.54
20.0	98.12	98.85	98.61	99.52	99.76	101.00
21.0	105.40	106.17	105.91	106.88	107.13	108.46
22.0	114.59	115.41	115.12	116.16	116.42	117.85
23.0	123.79	124.66	124.33	125.44	125.70	127.24
24.0	132.98	133.90	133.54	134.72	134.99	136.62
25.0	142.17	143.15	142.74	144.00	144.27	146.01
26.0	151.36	152.39	151.95	153.27	153.56	155.40
27.0	160.55	161.64	161.16	162.55	162.85	164.78
28.0	169.75	170.88	170.37	171.83	172.13	174.17
29.0	178.94	180.12	179.57	181.11	181.42	183.56
30.0	188.13	189.37	188.78	190.39	190.70	192.95
31.0	198.54	199.83	199.20	200.88	201.20	203.56
32.0	209.59	210.94	210.26	212.02	212.34	214.81
33.0	220.73	222.14	221.41	223.25	223.58	226.17
34.0	231.88	233.35	232.57	234.49	234.82	237.53
35.0	243.03	244.56	243.73	245.73	246.06	248.89

HE-3 IONS INCIDENT ON NONGASEOUS TARGETS

ENERGY MEV	RANGE (MG/SQCM) TC	RU	RH	PD	AG	CD
.5	1.29	1.29	1.30	1.32	1.32	1.37
1.0	2.14	2.15	2.16	2.20	2.20	2.28
1.5	3.06	3.08	3.10	3.16	3.16	3.27
2.0	4.10	4.13	4.15	4.24	4.24	4.38
2.5	5.29	5.33	5.36	5.47	5.48	5.66
3.0	6.52	6.57	6.60	6.74	6.75	6.97
3.5	8.04	8.11	8.15	8.32	8.33	8.60
4.0	9.57	9.64	9.69	9.90	9.92	10.23
4.5	11.09	11.17	11.23	11.47	11.49	11.86
5.0	12.92	13.02	13.09	13.37	13.39	13.81
5.5	14.75	14.86	14.94	15.26	15.29	15.76
6.0	16.58	16.71	16.80	17.15	17.18	17.71
6.5	18.82	18.96	19.06	19.46	19.49	20.09
7.0	21.05	21.21	21.32	21.77	21.80	22.47
7.5	23.29	23.46	23.58	24.07	24.11	24.84
8.0	25.52	25.71	25.84	26.38	26.42	27.22
8.5	27.76	27.96	28.10	28.69	28.73	29.59
9.0	30.00	30.21	30.36	30.99	31.03	31.97
9.5	32.69	32.93	33.09	33.78	33.82	34.83
10.0	35.39	35.64	35.82	36.56	36.60	37.69
10.5	38.09	38.36	38.54	39.34	39.38	40.55
11.0	40.79	41.08	41.27	42.12	42.16	43.41
11.5	43.49	43.79	44.00	44.90	44.94	46.27
12.0	46.19	46.51	46.72	47.68	47.72	49.13
13.0	52.48	52.84	53.07	54.15	54.19	55.78
14.0	58.77	59.16	59.42	60.62	60.66	62.43
15.0	65.06	65.49	65.76	67.09	67.13	69.08
16.0	72.67	73.13	73.43	74.90	74.94	77.10
17.0	80.27	80.78	81.10	82.71	82.75	85.13
18.0	87.88	88.42	88.77	90.53	90.55	93.15
19.0	95.49	96.07	96.44	98.34	98.36	101.17
20.0	103.09	103.72	104.11	106.15	106.17	109.20
21.0	110.70	111.36	111.77	113.96	113.98	117.22
22.0	120.27	120.97	121.41	123.77	123.78	127.28
23.0	129.83	130.58	131.04	133.58	133.57	137.34
24.0	139.40	140.19	140.68	143.39	143.37	147.40
25.0	148.97	149.81	150.31	153.20	153.17	157.46
26.0	158.54	159.42	159.94	163.01	162.97	167.52
27.0	168.10	169.03	169.58	172.82	172.76	177.59
28.0	177.67	178.64	179.21	182.63	182.56	187.65
29.0	187.24	188.25	188.85	192.44	192.36	197.71
30.0	196.81	197.86	198.48	202.25	202.15	207.77
31.0	207.62	208.72	209.36	213.32	213.21	219.12
32.0	219.09	220.24	220.90	225.06	224.94	231.16
33.0	230.65	231.85	232.53	236.91	236.76	243.30
34.0	242.23	243.47	244.17	248.76	248.59	255.44
35.0	253.80	255.09	255.82	260.61	260.42	267.58

HE-3 IONS INCIDENT ON NONGASEOUS TARGETS

ENERGY	RANGE (MG/SQCM)					
MEV	IN	SN	SB	TE	I	XE
.5	1.39	1.43	1.46	1.52	1.51	1.56
1.0	2.31	2.38	2.42	2.53	2.50	2.58
1.5	3.32	3.41	3.47	3.62	3.58	3.69
2.0	4.44	4.56	4.65	4.84	4.78	4.92
2.5	5.73	5.88	5.99	6.23	6.15	6.33
3.0	7.06	7.24	7.37	7.66	7.57	7.77
3.5	8.71	8.92	9.07	9.43	9.31	9.56
4.0	10.35	10.60	10.78	11.20	11.05	11.34
4.5	12.00	12.28	12.49	12.97	12.79	13.13
5.0	13.97	14.30	14.53	15.09	14.88	15.26
5.5	15.94	16.31	16.57	17.21	16.96	17.40
6.0	17.91	18.33	18.62	19.33	19.05	19.53
6.5	20.31	20.77	21.10	21.90	21.58	22.12
7.0	22.70	23.22	23.58	24.47	24.11	24.71
7.5	25.10	25.67	26.06	27.04	26.64	27.30
8.0	27.50	28.12	28.55	29.62	29.17	29.89
8.5	29.89	30.57	31.03	32.19	31.70	32.48
9.0	32.29	33.02	33.51	34.76	34.23	35.07
9.5	35.18	35.96	36.50	37.85	37.27	38.18
10.0	38.06	38.91	39.48	40.94	40.30	41.29
10.5	40.95	41.85	42.47	44.04	43.34	44.39
11.0	43.83	44.80	45.45	47.13	46.38	47.50
11.5	46.72	47.74	48.43	50.22	49.42	50.61
12.0	49.60	50.69	51.42	53.31	52.46	53.72
13.0	56.31	57.53	58.35	60.48	59.51	60.93
14.0	63.01	64.37	65.28	67.66	66.56	68.14
15.0	69.72	71.22	72.21	74.83	73.61	75.35
16.0	77.80	79.46	80.56	83.47	82.10	84.02
17.0	85.88	87.71	88.91	92.11	90.58	92.70
18.0	93.97	95.95	97.26	100.75	99.07	101.37
19.0	102.05	104.20	105.61	109.39	107.55	110.05
20.0	110.14	112.45	113.96	118.03	116.04	118.72
21.0	118.22	120.69	122.31	126.67	124.53	127.40
22.0	128.35	131.02	132.76	137.49	135.14	138.24
23.0	138.49	141.35	143.22	148.30	145.76	149.09
24.0	148.62	151.68	153.67	159.11	156.37	159.93
25.0	158.75	162.01	164.12	169.92	166.99	170.77
26.0	168.89	172.34	174.58	180.73	177.60	181.62
27.0	179.02	182.67	185.03	191.55	188.22	192.46
28.0	189.15	193.00	195.49	202.36	198.83	203.31
29.0	199.28	203.34	205.94	213.17	209.44	214.15
30.0	209.42	213.66	216.39	223.98	220.06	225.00
31.0	220.85	225.31	228.18	236.17	232.02	237.21
32.0	232.96	237.66	240.67	249.08	244.69	250.15
33.0	245.19	250.12	253.27	262.11	257.48	263.21
34.0	257.41	262.57	265.87	275.13	270.26	276.26
35.0	269.63	275.03	278.47	288.16	283.05	289.32

HE-3 IONS INCIDENT ON NONGASEOUS TARGETS

ENERGY MEV	RANGE (MG/SQCM) CS	BA	LA	CE	PR	ND
.5	1.57	1.62	1.64	1.65	1.66	1.70
1.0	2.60	2.68	2.70	2.72	2.73	2.79
1.5	3.71	3.82	3.85	3.87	3.88	3.96
2.0	4.95	5.09	5.13	5.15	5.16	5.26
2.5	6.36	6.54	6.58	6.60	6.60	6.73
3.0	7.82	8.03	8.07	8.09	8.10	8.25
3.5	9.61	9.86	9.91	9.93	9.93	10.10
4.0	11.40	11.69	11.74	11.76	11.76	11.96
4.5	13.19	13.52	13.58	13.60	13.59	13.82
5.0	15.32	15.71	15.77	15.79	15.77	16.03
5.5	17.46	17.90	17.96	17.98	17.95	18.25
6.0	19.60	20.09	20.15	20.17	20.13	20.46
6.5	22.20	22.74	22.81	22.82	22.77	23.14
7.0	24.79	25.39	25.47	25.48	25.41	25.81
7.5	27.38	28.04	28.12	28.13	28.06	28.49
8.0	29.98	30.70	30.78	30.78	30.70	31.17
8.5	32.57	33.35	33.43	33.43	33.34	33.85
9.0	35.16	36.00	36.09	36.08	35.98	36.53
9.5	38.28	39.18	39.27	39.26	39.14	39.73
10.0	41.39	42.36	42.45	42.44	42.31	42.93
10.5	44.50	45.54	45.64	45.62	45.47	46.14
11.0	47.61	48.72	48.82	48.79	48.63	49.35
11.5	50.72	51.90	52.00	51.97	51.79	52.55
12.0	53.83	55.09	55.18	55.15	54.96	55.76
13.0	61.05	62.46	62.56	62.51	62.28	63.18
14.0	68.26	69.83	69.93	69.87	69.60	70.59
15.0	75.48	77.20	77.31	77.23	76.93	78.01
16.0	84.16	86.06	86.17	86.07	85.72	86.92
17.0	92.83	94.93	95.03	94.91	94.51	95.83
18.0	101.51	103.79	103.90	103.75	103.31	104.73
19.0	110.19	112.65	112.76	112.59	112.10	113.64
20.0	118.87	121.52	121.62	121.43	120.89	122.54
21.0	127.54	130.38	130.48	130.27	129.69	131.45
22.0	138.39	141.45	141.55	141.30	140.65	142.55
23.0	149.23	152.52	152.61	152.33	151.62	153.65
24.0	160.07	163.58	163.67	163.36	162.59	164.75
25.0	170.91	174.65	174.73	174.39	173.55	175.85
26.0	181.75	185.72	185.80	185.42	184.52	186.95
27.0	192.60	196.79	196.86	196.45	195.49	198.05
28.0	203.44	207.86	207.92	207.48	206.45	209.15
29.0	214.28	218.93	218.99	218.51	217.42	220.26
30.0	225.12	229.99	230.05	229.54	228.39	231.36
31.0	237.33	242.46	242.50	241.95	240.73	243.84
32.0	250.27	255.66	255.69	255.10	253.79	257.07
33.0	263.32	268.97	269.00	268.36	266.97	270.40
34.0	276.36	282.29	282.30	281.62	280.15	283.74
35.0	289.41	295.61	295.61	294.88	293.33	297.08

HE-3 IONS INCIDENT ON NONGASEOUS TARGETS

ENERGY	RANGE (MG/SQCM)					
MEV	PM	SM	EU	GD	TB	DY
.5	1.73	1.77	1.79	1.86	1.88	1.93
1.0	2.84	2.90	2.93	3.03	3.07	3.14
1.5	4.03	4.11	4.15	4.29	4.33	4.42
2.0	5.34	5.45	5.49	5.67	5.72	5.83
2.5	6.83	6.96	7.01	7.23	7.28	7.43
3.0	8.36	8.51	8.57	8.83	8.90	9.07
3.5	10.24	10.42	10.48	10.80	10.86	11.06
4.0	12.12	12.32	12.39	12.76	12.83	13.06
4.5	14.00	14.23	14.30	14.72	14.80	15.06
5.0	16.23	16.50	16.57	17.05	17.13	17.43
5.5	18.47	18.76	18.84	19.38	19.47	19.80
6.0	20.70	21.03	21.12	21.71	21.81	22.17
6.5	23.41	23.77	23.86	24.53	24.63	25.03
7.0	26.11	26.51	26.61	27.34	27.45	27.89
7.5	28.81	29.25	29.35	30.16	30.27	30.75
8.0	31.52	31.99	32.09	32.97	33.09	33.61
8.5	34.22	34.73	34.84	35.79	35.91	36.46
9.0	36.92	37.47	37.58	38.60	38.73	39.32
9.5	40.16	40.75	40.86	41.97	42.10	42.74
10.0	43.39	44.02	44.14	45.33	45.47	46.15
10.5	46.63	47.30	47.42	48.69	48.84	49.57
11.0	49.86	50.58	50.71	52.06	52.20	52.98
11.5	53.10	53.85	53.99	55.42	55.57	56.39
12.0	56.33	57.13	57.27	58.79	58.94	59.81
13.0	63.82	64.71	64.85	66.56	66.73	67.70
14.0	71.30	72.29	72.44	74.34	74.51	75.58
15.0	78.79	79.87	80.03	82.11	82.30	83.47
16.0	87.77	88.96	89.12	91.43	91.63	92.92
17.0	96.75	98.05	98.22	100.75	100.95	102.37
18.0	105.73	107.14	107.32	110.07	110.28	111.81
19.0	114.71	116.24	116.41	119.39	119.61	121.26
20.0	123.69	125.33	125.51	128.72	128.94	130.71
21.0	132.68	134.42	134.61	138.03	138.27	140.16
22.0	143.86	145.74	145.93	149.63	149.87	151.90
23.0	155.06	157.07	157.26	161.23	161.47	163.65
24.0	166.24	168.39	168.58	172.83	173.07	175.39
25.0	177.44	179.71	179.90	184.43	184.68	187.14
26.0	188.62	191.03	191.23	196.02	196.28	198.89
27.0	199.81	202.36	202.55	207.62	207.88	210.63
28.0	211.01	213.68	213.87	219.22	219.48	222.38
29.0	222.19	225.00	225.20	230.81	231.09	234.12
30.0	233.39	236.32	236.52	242.41	242.69	245.87
31.0	245.97	249.06	249.25	255.45	255.73	259.07
32.0	259.29	262.53	262.73	269.24	269.52	273.03
33.0	272.73	276.13	276.32	283.16	283.44	287.11
34.0	286.17	289.72	289.91	297.07	297.35	301.19
35.0	299.61	303.32	303.50	310.99	311.27	315.28

HE-3 IONS INCIDENT ON NONGASEOUS TARGETS

ENERGY	RANGE (MG/SQCM)					
MEV	HO	ER	TM	YB	LU	HF
.5	1.96	2.00	2.03	2.09	2.12	2.17
1.0	3.19	3.24	3.28	3.37	3.42	3.50
1.5	4.49	4.55	4.60	4.72	4.78	4.88
2.0	5.91	5.99	6.05	6.19	6.26	6.39
2.5	7.52	7.61	7.68	7.85	7.93	8.09
3.0	9.18	9.28	9.35	9.56	9.65	9.83
3.5	11.19	11.31	11.38	11.62	11.73	11.93
4.0	13.20	13.33	13.42	13.69	13.80	14.04
4.5	15.21	15.36	15.45	15.76	15.88	16.14
5.0	17.60	17.76	17.86	18.21	18.34	18.63
5.5	19.99	20.16	20.26	20.66	20.80	21.12
6.0	22.37	22.57	22.67	23.11	23.25	23.61
6.5	25.25	25.46	25.57	26.05	26.21	26.61
7.0	28.13	28.36	28.47	29.00	29.17	29.60
7.5	31.01	31.25	31.37	31.95	32.12	32.59
8.0	33.88	34.14	34.27	34.90	35.08	35.59
8.5	36.76	37.04	37.17	37.84	38.04	38.58
9.0	39.64	39.93	40.07	40.79	40.99	41.57
9.5	43.08	43.39	43.53	44.30	44.52	45.14
10.0	46.51	46.84	46.99	47.82	48.04	48.70
10.5	49.94	50.29	50.45	51.33	51.57	52.27
11.0	53.38	53.75	53.91	54.85	55.09	55.84
11.5	56.82	57.20	57.37	58.36	58.61	59.40
12.0	60.25	60.65	60.83	61.87	62.14	62.97
13.0	68.18	68.63	68.81	69.98	70.27	71.20
14.0	76.12	76.60	76.79	78.09	78.40	79.42
15.0	84.05	84.58	84.78	86.20	86.53	87.64
16.0	93.55	94.12	94.33	95.90	96.25	97.48
17.0	103.05	103.67	103.88	105.59	105.97	107.31
18.0	112.55	113.21	113.44	115.29	115.69	117.14
19.0	122.05	122.76	122.99	124.99	125.41	126.97
20.0	131.55	132.30	132.54	134.69	135.14	136.81
21.0	141.05	141.85	142.10	144.39	144.86	146.64
22.0	152.85	153.70	153.96	156.43	156.92	158.83
23.0	164.66	165.56	165.82	168.47	168.98	171.03
24.0	176.46	177.42	177.69	180.51	181.05	183.22
25.0	188.27	189.28	189.55	192.55	193.11	195.42
26.0	200.07	201.14	201.41	204.59	205.17	207.61
27.0	211.88	212.99	213.27	216.63	217.23	219.81
28.0	223.68	224.85	225.14	228.66	229.30	232.01
29.0	235.49	236.71	237.00	240.70	241.36	244.20
30.0	247.29	248.56	248.86	252.74	253.42	256.40
31.0	260.55	261.88	262.18	266.26	266.96	270.08
32.0	274.58	275.97	276.27	280.55	281.28	284.56
33.0	288.73	290.18	290.49	294.97	295.72	299.15
34.0	302.88	304.38	304.69	309.39	310.17	313.75
35.0	317.04	318.60	318.91	323.81	324.61	328.35

HE-3 IONS INCIDENT ON NONGASEOUS TARGETS

ENERGY MEV	RANGE (MG/SQCM) TA	W	RE	OS	IR	PT
.5	2.22	2.27	2.32	2.39	2.43	2.49
1.0	3.56	3.63	3.70	3.80	3.86	3.95
1.5	4.96	5.06	5.14	5.27	5.35	5.45
2.0	6.49	6.60	6.70	6.86	6.95	7.07
2.5	8.20	8.33	8.44	8.63	8.73	8.88
3.0	9.95	10.10	10.23	10.45	10.56	10.73
3.5	12.07	12.25	12.39	12.64	12.76	12.95
4.0	14.19	14.39	14.54	14.83	14.96	15.17
4.5	16.32	16.53	16.70	17.02	17.16	17.39
5.0	18.82	19.06	19.24	19.60	19.76	20.01
5.5	21.33	21.59	21.79	22.18	22.35	22.62
6.0	23.84	24.12	24.33	24.76	24.94	25.23
6.5	26.85	27.15	27.38	27.86	28.05	28.37
7.0	29.86	30.19	30.44	30.96	31.15	31.50
7.5	32.87	33.23	33.49	34.06	34.26	34.63
8.0	35.88	36.27	36.55	37.15	37.37	37.77
8.5	38.89	39.31	39.60	40.25	40.48	40.90
9.0	41.91	42.34	42.65	43.35	43.59	44.03
9.5	45.49	45.96	46.29	47.03	47.28	47.76
10.0	49.08	49.58	49.92	50.72	50.98	51.48
10.5	52.67	53.19	53.56	54.40	54.67	55.20
11.0	56.25	56.81	57.19	58.09	58.37	58.93
11.5	59.84	60.42	60.83	61.77	62.07	62.65
12.0	63.43	64.04	64.46	65.46	65.76	66.38
13.0	71.70	72.38	72.84	73.95	74.28	74.95
14.0	79.97	80.71	81.22	82.44	82.79	83.53
15.0	88.24	89.05	89.59	90.93	91.30	92.11
16.0	98.12	99.01	99.59	101.06	101.47	102.34
17.0	108.01	108.97	109.60	111.20	111.63	112.58
18.0	117.89	118.92	119.60	121.34	121.79	122.81
19.0	127.77	128.88	129.61	131.47	131.95	133.05
20.0	137.66	138.84	139.61	141.61	142.12	143.28
21.0	147.54	148.80	149.61	151.75	152.28	153.52
22.0	159.80	161.14	162.01	164.30	164.86	166.19
23.0	172.05	173.49	174.40	176.86	177.44	178.85
24.0	184.31	185.83	186.80	189.41	190.02	191.52
25.0	196.56	198.17	199.19	201.97	202.61	204.19
26.0	208.81	210.52	211.59	214.52	215.19	216.86
27.0	221.07	222.86	223.98	227.07	227.77	229.52
28.0	233.32	235.20	236.38	239.63	240.35	242.19
29.0	245.58	247.55	248.77	252.19	252.94	254.86
30.0	257.83	259.89	261.17	264.74	265.52	267.52
31.0	271.58	273.74	275.07	278.82	279.62	281.72
32.0	286.12	288.38	289.76	293.70	294.53	296.73
33.0	300.78	303.14	304.59	308.71	309.57	311.87
34.0	315.45	317.91	319.41	323.72	324.61	327.01
35.0	330.11	332.68	334.24	338.73	339.65	342.15

HE-3 IONS INCIDENT ON NONGASEOUS TARGETS

ENERGY MEV	RANGE (MG/SQCM) AU	HG	TL	PB	BI	PO
.5	2.55	2.62	2.70	2.78	2.84	2.90
1.0	4.02	4.13	4.24	4.34	4.43	4.50
1.5	5.54	5.67	5.82	5.94	6.04	6.13
2.0	7.17	7.33	7.50	7.65	7.76	7.85
2.5	8.98	9.17	9.37	9.54	9.66	9.75
3.0	10.84	11.06	11.29	11.47	11.61	11.70
3.5	13.07	13.32	13.58	13.79	13.93	14.02
4.0	15.31	15.58	15.87	16.10	16.25	16.34
4.5	17.54	17.84	18.16	18.41	18.57	18.66
5.0	20.16	20.50	20.85	21.12	21.28	21.38
5.5	22.78	23.15	23.54	23.82	24.00	24.09
6.0	25.40	25.80	26.23	26.53	26.71	26.80
6.5	28.54	28.98	29.44	29.77	29.96	30.04
7.0	31.69	32.16	32.66	33.01	33.20	33.29
7.5	34.83	35.34	35.87	36.25	36.45	36.53
8.0	37.97	38.51	39.09	39.49	39.70	39.77
8.5	41.11	41.69	42.31	42.73	42.94	43.01
9.0	44.25	44.87	45.52	45.97	46.19	46.25
9.5	47.98	48.64	49.34	49.81	50.04	50.10
10.0	51.72	52.42	53.16	53.66	53.90	53.95
10.5	55.45	56.19	56.98	57.51	57.75	57.79
11.0	59.19	59.97	60.80	61.35	61.61	61.64
11.5	62.92	63.75	64.62	65.20	65.46	65.49
12.0	66.65	67.52	68.44	69.05	69.31	69.33
13.0	75.25	76.21	77.23	77.89	78.18	78.18
14.0	83.84	84.90	86.02	86.74	87.04	87.02
15.0	92.44	93.59	94.81	95.59	95.90	95.87
16.0	102.70	103.95	105.30	106.14	106.46	106.41
17.0	112.95	114.32	115.78	116.69	117.03	116.94
18.0	123.20	124.68	126.26	127.23	127.59	127.48
19.0	133.46	135.05	136.74	137.78	138.15	138.02
20.0	143.71	145.41	147.22	148.33	148.71	148.56
21.0	153.97	155.77	157.70	158.88	159.27	159.10
22.0	166.65	168.59	170.66	171.91	172.32	172.11
23.0	179.34	181.41	183.62	184.95	185.37	185.13
24.0	192.03	194.23	196.57	197.99	198.42	198.15
25.0	204.72	207.05	209.53	211.02	211.47	211.16
26.0	217.40	219.87	222.49	224.06	224.52	224.18
27.0	230.09	232.69	235.45	237.10	237.57	237.19
28.0	242.78	245.50	248.41	250.14	250.62	250.21
29.0	255.46	258.32	261.37	263.17	263.67	263.23
30.0	268.15	271.14	274.33	276.21	276.73	276.24
31.0	282.37	285.50	288.84	290.81	291.34	290.82
32.0	297.40	300.68	304.19	306.24	306.78	306.22
33.0	312.55	315.99	319.66	321.81	322.36	321.75
34.0	327.71	331.30	335.13	337.37	337.93	337.28
35.0	342.87	346.61	350.61	352.93	353.51	352.81

HE-3 IONS INCIDENT ON NONGASEOUS TARGETS

ENERGY MEV	RANGE (MG/SQCM) AT	RN	FR	RA	AC	TH
.5	2.95	3.17	3.25	3.36	3.45	3.61
1.0	4.56	4.88	4.98	5.13	5.24	5.45
1.5	6.19	6.61	6.71	6.89	7.01	7.27
2.0	7.91	8.43	8.54	8.74	8.87	9.18
2.5	9.81	10.43	10.55	10.77	10.91	11.25
3.0	11.75	12.48	12.60	12.85	12.99	13.37
3.5	14.06	14.91	15.03	15.30	15.44	15.87
4.0	16.37	17.34	17.46	17.75	17.90	18.37
4.5	18.68	19.77	19.89	20.21	20.35	20.87
5.0	21.38	22.61	22.73	23.06	23.20	23.77
5.5	24.07	25.44	25.56	25.91	26.05	26.67
6.0	26.77	28.28	28.39	28.77	28.91	29.57
6.5	29.99	31.66	31.77	32.17	32.31	33.03
7.0	33.21	35.05	35.15	35.58	35.70	36.48
7.5	36.43	38.43	38.53	38.98	39.10	39.93
8.0	39.66	41.82	41.91	42.39	42.50	43.39
8.5	42.88	45.20	45.29	45.79	45.90	46.84
9.0	46.10	48.59	48.67	49.20	49.30	50.30
9.5	49.92	52.60	52.67	53.23	53.33	54.39
10.0	53.74	56.61	56.68	57.27	57.36	58.48
10.5	57.56	60.63	60.69	61.30	61.38	62.58
11.0	61.39	64.64	64.69	65.34	65.41	66.67
11.5	65.21	68.65	68.70	69.37	69.44	70.76
12.0	69.03	72.67	72.70	73.41	73.47	74.85
13.0	77.81	81.89	81.91	82.68	82.72	84.25
14.0	86.60	91.12	91.12	91.95	91.97	93.64
15.0	95.39	100.34	100.32	101.22	101.22	103.04
16.0	105.85	111.33	111.28	112.25	112.23	114.22
17.0	116.31	122.32	122.24	123.28	123.24	125.40
18.0	126.78	133.30	133.20	134.31	134.24	136.58
19.0	137.24	144.29	144.16	145.34	145.25	147.76
20.0	147.70	155.27	155.12	156.38	156.26	158.93
21.0	158.17	166.26	166.08	167.41	167.27	170.11
22.0	171.09	179.82	179.61	181.02	180.84	183.90
23.0	184.01	193.38	193.13	194.63	194.42	197.68
24.0	196.93	206.94	206.66	208.24	208.00	211.46
25.0	209.85	220.50	220.18	221.85	221.57	225.24
26.0	222.77	234.06	233.71	235.46	235.15	239.02
27.0	235.70	247.62	247.23	249.07	248.72	252.81
28.0	248.62	261.18	260.76	262.68	262.30	266.59
29.0	261.54	274.74	274.28	276.29	275.88	280.37
30.0	274.46	288.31	287.81	289.90	289.45	294.16
31.0	288.93	303.49	302.94	305.13	304.64	309.57
32.0	304.21	319.52	318.93	321.22	320.69	325.86
33.0	319.62	335.69	335.06	337.44	336.86	342.28
34.0	335.03	351.86	351.18	353.67	353.04	358.70
35.0	350.45	368.04	367.31	369.90	369.22	375.12

HE-3 IONS INCIDENT ON NONGASEOUS TARGETS

ENERGY	RANGE (MG/SQCM)					
MEV	PA	U	NP	PU	AM	CM
.5	3.69	3.90	4.00	4.22	4.39	4.64
1.0	5.54	5.83	5.94	6.23	6.43	6.74
1.5	7.36	7.71	7.83	8.16	8.38	8.73
2.0	9.25	9.67	9.77	10.15	10.38	10.77
2.5	11.32	11.79	11.89	12.31	12.55	12.97
3.0	13.43	13.96	14.05	14.51	14.75	15.21
3.5	15.90	16.51	16.57	17.07	17.32	17.82
4.0	18.38	19.05	19.09	19.64	19.89	20.42
4.5	20.86	21.59	21.62	22.21	22.46	23.02
5.0	23.73	24.54	24.53	25.17	25.42	26.02
5.5	26.60	27.48	27.45	28.14	28.39	29.02
6.0	29.48	30.43	30.37	31.10	31.35	32.01
6.5	32.89	33.93	33.84	34.63	34.87	35.57
7.0	36.31	37.44	37.31	38.15	38.39	39.13
7.5	39.73	40.94	40.78	41.67	41.90	42.68
8.0	43.15	44.44	44.24	45.19	45.42	46.24
8.5	46.57	47.95	47.71	48.72	48.94	49.80
9.0	49.99	51.45	51.18	52.24	52.46	53.35
9.5	54.04	55.60	55.29	56.41	56.62	57.56
10.0	58.09	59.75	59.39	60.58	60.78	61.77
10.5	62.14	63.89	63.50	64.74	64.94	65.97
11.0	66.19	68.04	67.60	68.91	69.10	70.18
11.5	70.24	72.19	71.71	73.08	73.26	74.39
12.0	74.29	76.34	75.82	77.25	77.43	78.59
13.0	83.58	85.86	85.24	86.81	86.97	88.24
14.0	92.88	95.38	94.66	96.37	96.52	97.89
15.0	102.18	104.90	104.08	105.94	106.07	107.53
16.0	113.23	116.22	115.28	117.30	117.41	118.99
17.0	124.29	127.54	126.48	128.67	128.75	130.45
18.0	135.35	138.86	137.68	140.03	140.09	141.91
19.0	146.40	150.19	148.88	151.40	151.44	153.37
20.0	157.46	161.51	160.09	162.77	162.78	164.83
21.0	168.52	172.83	171.28	174.13	174.12	176.29
22.0	182.15	186.78	185.08	188.13	188.09	190.40
23.0	195.77	200.73	198.88	202.13	202.05	204.50
24.0	209.40	214.68	212.68	216.12	216.02	218.61
25.0	223.03	228.63	226.48	230.12	229.98	232.71
26.0	236.66	242.58	240.27	244.12	243.95	246.82
27.0	250.29	256.53	254.07	258.12	257.92	260.92
28.0	263.91	270.48	267.87	272.11	271.88	275.03
29.0	277.54	284.43	281.67	286.11	285.85	289.14
30.0	291.17	298.38	295.47	300.11	299.81	303.24
31.0	306.41	313.98	310.89	315.76	315.42	319.01
32.0	322.51	330.45	327.19	332.28	331.91	335.65
33.0	338.74	347.07	343.61	348.94	348.52	352.43
34.0	354.98	363.68	360.04	365.61	365.14	369.22
35.0	371.21	380.29	376.47	382.27	381.77	386.00

HE-3 IONS INCIDENT ON NONGASEOUS TARGETS

ENERGY MEV	RANGE (MG/SQCM) TA2O5	GLYCINE	KH_2PO_4	MYLAR	TEFLON	PBCL2
.5	1.34	.36	.51	.38	.48	1.57
1.0	2.22	.63	.89	.66	.84	2.59
1.5	3.19	.94	1.31	.99	1.24	3.68
2.0	4.28	1.32	1.81	1.38	1.72	4.88
2.5	5.52	1.76	2.39	1.85	2.27	6.25
3.0	6.80	2.23	3.00	2.33	2.85	7.66
3.5	8.39	2.83	3.78	2.96	3.60	9.40
4.0	9.98	3.44	4.56	3.58	4.35	11.14
4.5	11.57	4.04	5.34	4.21	5.10	12.87
5.0	13.49	4.81	6.32	5.00	6.04	14.96
5.5	15.42	5.57	7.29	5.79	6.97	17.04
6.0	17.34	6.33	8.26	6.58	7.91	19.12
6.5	19.69	7.31	9.49	7.59	9.11	21.66
7.0	22.04	8.29	10.73	8.60	10.30	24.20
7.5	24.39	9.26	11.96	9.61	11.49	26.73
8.0	26.74	10.24	13.19	10.62	12.68	29.26
8.5	29.08	11.22	14.42	11.63	13.88	31.80
9.0	31.43	12.20	15.65	12.64	15.07	34.33
9.5	34.27	13.43	17.19	13.92	16.57	37.38
10.0	37.10	14.67	18.73	15.20	18.06	40.42
10.5	39.93	15.90	20.26	16.47	19.56	43.46
11.0	42.77	17.13	21.80	17.75	21.06	46.51
11.5	45.60	18.37	23.34	19.03	22.56	49.55
12.0	48.43	19.61	24.88	20.30	24.05	52.60
13.0	55.03	22.58	28.55	23.38	27.65	59.66
14.0	61.62	25.56	32.22	26.46	31.24	66.72
15.0	68.22	28.54	35.90	29.53	34.83	73.79
16.0	76.19	32.28	40.47	33.40	39.32	82.29
17.0	84.15	36.03	45.04	37.26	43.81	90.79
18.0	92.12	39.77	49.61	41.13	48.31	99.29
19.0	100.09	43.52	54.18	45.00	52.80	107.79
20.0	108.06	47.26	58.75	48.86	57.29	116.30
21.0	116.03	51.01	63.32	52.73	61.78	124.80
22.0	126.03	55.95	69.28	57.83	67.66	135.43
23.0	136.05	60.89	75.23	62.92	73.54	146.06
24.0	146.06	65.83	81.18	68.02	79.43	156.70
25.0	156.06	70.77	87.14	73.11	85.31	167.33
26.0	166.07	75.70	93.09	78.21	91.19	177.97
27.0	176.09	80.64	99.04	83.30	97.07	188.60
28.0	186.10	85.58	104.99	88.40	102.96	199.23
29.0	196.10	90.52	110.95	93.50	108.84	209.86
30.0	206.11	95.46	116.90	98.59	114.72	220.50
31.0	217.42	101.18	123.74	104.49	121.50	232.48
32.0	229.41	107.29	131.05	110.79	128.74	245.18
33.0	241.50	113.46	138.42	117.15	136.06	257.98
34.0	253.59	119.63	145.79	123.51	143.37	270.79
35.0	265.69	125.80	153.16	129.88	150.69	283.59

APPENDIX B

^{3}He Reaction Q-Values

Reaction Q-values are given for ^{3}He induced nuclear reactions with stable or naturally occurring targets Z = 3 through Z = 92. The mass data were taken from Maples, Goth, and Cerny.[30] In the tables a reaction leading to a non-existent product is designated "NR", and a reaction which results in a product whose mass is unknown has "MU" in place of the Q-value. All Q-values are given in MeV. Q-values are given for the following reactions:

1. (^{3}He,n)
2. (^{3}He,2n)
3. (^{3}He,3n)
4. (^{3}He,p)
5. (^{3}He,2p)
6. (^{3}He,pn)
7. (^{3}He,p2n)
8. (^{3}He,α)
9. (^{3}He,αn)

HE-3 REACTION Q-VALUES

TARGET	N	2N	3N	P	2P	P,N	P,2N	HE4	HE4,N
HE-4	BE-6	BE-5	NR	LI-6	HE-5	LI-5	LI-4	NR	NR
	-9.09	MU	--	-4.02	-8.68	-9.68	MU	--	--
LI-6	B-8	B-7	NR	BE-8	LI-7	BE-7	BE-6	LI-5	LI-4
	-1.97	MU	--	16.79	-.47	-2.11	-12.79	14.91	MU
LI-7	B-9	B-8	B-7	BE-9	LI-8	BE-8	BE-7	LI-6	LI-5
	9.35	-9.23	MU	11.20	-5.69	9.53	-9.36	13.32	7.66
BE-9	C-11	C-10	NR	B-11	BE-10	B-10	B-9	BE-8	BE-7
	7.56	-5.52	--	10.33	-.90	-1.13	-9.57	18.91	.01
B-10	N-12	N-11	NR	C-12	B-11	C-11	C-10	B-9	B-8
	1.56	MU	--	19.69	3.74	.97	-12.11	12.14	-6.44
B-11	N-13	N-12	N-11	C-13	B-12	C-12	C-11	B-10	B-9
	10.18	-9.89	MU	13.19	-4.35	8.24	-10.48	9.12	.68
C-12	O-14	O-13	NR	N-14	C-13	N-13	N-12	C-11	C-10
	-1.15	-24.32	--	4.78	-2.77	-5.77	-25.85	1.85	-11.23
C-13	O-15	O-14	O-13	N-15	C-14	N-14	N-13	C-12	C-11
	7.12	-6.09	-29.27	10.67	.46	-.17	-10.72	15.63	-3.09
N-14	F-16	F-15	NR	O-16	N-15	O-15	O-14	N-13	N-12
	-.96	MU	--	15.24	3.12	-.43	-13.64	10.02	-10.05
N-15	F-17	F-16	F-15	O-17	N-16	O-16	O-15	N-14	N-13
	5.01	-11.80	MU	8.55	-5.23	4.41	-11.26	9.74	-.81
O-16	NE-18	NE-17	NR	F-18	O-17	F-17	F-16	O-15	O-14
	-3.20	-22.46	--	2.03	-3.58	-7.12	-23.92	4.91	-8.31
O-17	NE-19	NE-18	NE-17	F-19	O-18	F-18	F-17	O-16	O-15
	4.30	-7.34	-26.60	8.32	.33	-2.11	-11.26	16.43	.76
O-18	NE-20	NE-19	NE-18	F-20	O-19	F-19	F-18	O-17	O-16
	13.12	-3.75	-15.38	6.87	-3.76	.27	-10.16	12.53	8.39
F-19	NA-21	NA-20	NA-19	NF-21	F-20	NE-20	NE-19	F-18	F-17
	7.56	-9.68	MU	11.89	-1.12	5.13	-11.74	10.14	.99
NE-20	MG-22	MG-21	MG-20	NA-22	NE-21	NA-21	NA-20	NE-19	NE-18
	.20	-18.87	-32.32	5.78	-.96	-5.29	-22.52	3.71	-7.93
NE-21	MG-23	MG-22	MG-21	NA-23	NE-22	NA-22	NA-21	NE-20	NE-19
	6.60	-6.56	-25.63	11.44	2.65	-.98	-12.05	13.81	-3.05
NE-22	MG-24	MG-23	MG-22	NA-24	NE-23	NA-23	NA-22	NE-21	NE-20
	12.77	-3.76	-16.93	8.04	-2.52	1.07	-11.34	10.21	3.45
NA-23	AL-25	AL-24	AL-23	MG-25	NA-24	MG-24	MG-23	NA-22	NA-21
	6.26	-10.69	MU	11.30	-.76	3.98	-12.56	8.16	-2.91
MG-24	SI-26	SI-25	NR	AL-26	MG-25	AL-25	AL-24	MG-23	MG-22
	.06	-19.14	--	5.92	-.39	-5.43	-22.38	4.04	-9.12

HE-3 REACTION Q-VALUES

TARGET	N	2N	3N	P	2P	P,N	P,2N	HE4	HE4,N
MG-25	SI-27	SI-26	SI-25	AL-27	MG-26	AL-26	AL-25	MG-24	MG-23
	6.05	-7.27	-26.47	11.65	3.38	-1.41	-12.76	13.24	-3.29
MG-26	SI-28	SI-27	SI-26	AL-28	MG-27	AL-27	AL-26	MG-25	MG-24
	12.14	-5.04	-18.36	8.28	-1.28	.55	-12.50	9.48	2.15
AL-27	P-29	P-28	NR	SI-29	AL-28	SI-28	SI-27	AL-26	AL-25
	6.61	-11.26	--	12.34	.01	3.86	-13.31	7.52	-3.83
SI-28	S-30	S-29	NR	P-30	SI-29	P-29	P-28	SI-27	SI-26
	-.57	-19.80	--	6.35	.76	-4.97	-12.84	3.40	-9.93
SI-29	S-31	S-30	S-29	P-31	SI-30	P-30	P-29	SI-28	SI-27
	3.96	-9.05	-28.28	10.19	2.90	-2.13	-13.45	12.10	-5.07
SI-30	S-32	S-31	S-30	P-32	SI-31	P-31	P-30	SI-29	SI-28
	8.43	-6.66	-19.66	7.51	-1.12	-.43	-12.74	9.96	1.48
P-31	CL-33	CL-32	NR	S-33	P-32	S-32	S-31	P-30	P-29
	3.44	-12.39	--	9.79	.22	1.15	-13.95	8.26	-3.06
S-32	AR-34	AR-33	NR	CL-34	S-33	CL-33	CL-32	S-31	S-30
	-.76	-17.62	--	6.08	.92	-5.43	-21.26	5.48	-7.52
S-33	AR-35	AR-34	AR-33	CL-35	S-34	CL-34	CL-33	S-32	S-31
	3.33	-9.40	-26.27	10.07	3.70	-2.56	-14.07	11.93	-3.16
S-34	AR-36	AR-35	AR-34	CL-36	S-35	CL-35	CL-34	S-33	S-32
	7.16	-8.09	-20.82	7.23	-.73	-1.35	-13.98	9.15	.51
S-36	AR-38	AR-37	AR-36	CL-38	S-37	CL-37	CL-36	S-35	S-34
	10.92	-.92	-9.71	6.79	-3.30	.68	-9.64	10.69	3.71
CL-35	K-37	K-36	NR	AR-37	CL-36	AR-36	AR-35	CL-34	CL-33
	2.64	-13.50	--	9.58	.86	.79	-14.46	7.94	-3.57
CL-37	K-39	K-38	K-37	AR-39	CL-38	AR-38	AR-37	CL-36	CL-35
	8.90	-4.19	-16.25	9.12	-1.61	2.52	-9.31	10.26	1.68
AR-36	CA-38	CA-37	NR	K-38	AR-37	K-37	K-36	AR-35	AR-34
	-1.68	-18.20	--	6.20	1.07	-5.86	-22.00	5.32	-7.41
AR-38	CA-40	CA-39	CA-38	K-40	AR-39	K-39	K-38	AR-37	AR-36
	6.99	-8.63	-22.31	6.46	-1.13	-1.34	-14.43	8.74	-.05
AR-40	CA-42	CA-41	CA-40	K-42	AR-41	K-41	K-40	AR-39	AR-38
	10.36	-1.12	-9.47	7.62	-1.62	.08	-10.01	10.70	4.11
K-39	SC-41	SC-40	NR	CA-41	K-40	CA-40	CA-39	K-38	K-37
	1.69	-14.49	--	8.96	.08	.62	-15.00	7.49	-4.57
K-40	SC-42	SC-41	SC-40	CA-42	K-41	CA-41	CA-40	K-39	K-38
	5.44	-6.11	-22.29	12.66	2.37	1.16	-7.19	12.77	-.32
K-41	SC-43	SC-42	SC-41	CA-43	K-42	CA-42	CA-41	K-40	K-39
	7.48	-4.65	-16.20	10.49	-.18	2.56	-8.93	10.48	2.68

HE-3 REACTION Q-VALUES

TARGET	N	2N	3N	P	2P	P,N	P,2N	HE4	HE4,N
CA-40	TI-42	TI-41	NR	SC-42	CA-41	SC-41	SC-40	CA-39	CA-38
	-2.87	-20.23	--	4.90	.63	-6.65	-22.83	4.95	-8.73
CA-42	TI-44	TI-43	TI-42	SC-44	CA-43	SC-43	SC-42	CA-41	CA-40
	5.98	-10.41	-22.70	6.92	.21	-2.80	-14.93	9.09	.74
CA-43	TI-45	TI-44	TI-43	SC-45	CA-44	SC-44	SC-43	CA-42	CA-41
	7.47	-1.95	-18.34	10.31	3.42	-1.01	-10.72	12.65	1.16
CA-44	TI-46	TI-45	TI-44	SC-46	CA-45	SC-45	SC-44	CA-43	CA-42
	9.52	-3.67	-13.08	7.94	-.30	-.83	-12.15	9.44	1.51
CA-46	TI-48	TI-47	TI-46	SC-48	CA-47	SC-47	SC-46	CA-45	CA-44
	12.20	.58	-8.30	9.01	-.44	.76	-9.88	10.17	2.75
CA-48	TI-50	TI-49	TI-48	SC-50	CA-49	SC-49	SC-48	CA-47	CA-46
	14.07	3.13	-5.02	8.39	-2.57	1.90	-8.21	10.63	3.35
SC-45	V-47	V-46	NR	TI-47	SC-46	TI-46	TI-45	SC-44	SC-43
	7.81	-5.20	--	11.51	1.05	2.63	-10.56	9.25	-.46
TI-46	CR-48	CR-47	CR-46	V-48	TI-47	V-47	V-46	TI-45	TI-44
	5.81	MU	MU	7.99	1.16	-2.54	-15.55	7.38	-2.03
TI-47	CR-49	CR-48	CR-47	V-49	TI-48	V-48	V-47	TI-46	TI-45
	7.32	-3.07	MU	10.67	3.91	-.89	-11.42	11.70	-1.49
TI-48	CR-50	CR-49	CR-48	V-50	TI-49	V-49	V-48	TI-47	TI-46
	8.63	-4.30	-14.70	8.38	.43	-.96	-12.51	8.95	.07
TI-49	CR-51	CR-50	CR-49	V-51	TI-50	V-50	V-49	TI-48	TI-47
	9.75	.48	-12.45	11.28	3.23	.23	-9.10	12.43	.80
TI-50	CR-52	CR-51	CR-50	V-52	TI-51	V-51	V-50	TI-49	TI-48
	10.84	-1.19	-10.46	7.65	-1.34	.34	-10.71	9.63	1.48
V-50	MN-52	MN-51	MN-50	CR-52	V-51	CR-51	CR-50	V-49	V-48
	8.35	-2.17	-15.88	13.84	3.34	1.80	-7.47	11.24	-.31
V-51	MN-53	MN-52	MN-51	CR-53	V-52	CR-52	CR-51	V-50	V-49
	9.34	-2.71	-13.22	10.72	-.41	2.78	-9.25	9.52	.19
CR-50	FE-52	FE-51	NR	MN-52	CR-51	MN-51	MN-50	CR-49	CR-48
	4.94	MU	--	8.10	1.55	-2.42	-16.13	7.64	-2.75
CR-52	FE-54	FE-53	FE-52	MN-54	CR-53	MN-53	MN-52	CR-51	CR-50
	7.69	-5.92	-16.37	7.78	.22	-1.16	-13.21	8.54	-.73
CR-53	FE-55	FE-54	FE-53	MN-55	CR-54	MN-54	MN-53	CR-52	CR-51
	9.05	-.25	-13.87	10.07	2.00	-.16	-9.10	12.63	.60
CR-54	FE-56	FE-55	FE-54	MN-56	CR-55	MN-55	MN-54	CR-53	CR-52
	10.53	-.67	-9.97	7.62	-1.46	.35	-9.88	10.85	2.91
MN-55	CO-57	CO-56	CO-55	FE-57	MN-56	FE-56	FE-55	MN-54	MN-53
	8.49	-2.89	-12.97	10.11	-.45	2.47	-8.73	10.35	1.41

HE-3 REACTION Q-VALUES

TARGET	N	2N	3N	P	2P	P,N	P,2N	HE4	HE4,N
FE-54	NI-56	NI-55	NR	CO-56	FE-55	CO-55	CO-54	FE-53	FE-52
	4.53	MU	--	7.43	1.58	-2.66	-16.75	6.95	-3.49
FE-56	NI-58	NI-57	NI-56	CO-58	FE-57	CO-57	CO-56	FE-55	FE-54
	6.48	-5.71	-15.97	6.87	-.08	-1.70	-13.07	9.37	.07
FE-57	NI-59	NI-58	NI-57	CO-59	FE-58	CO-58	CO-57	FE-56	FE-55
	7.84	-1.16	-13.35	9.70	2.32	-.77	-9.34	12.93	1.73
FE-58	NI-60	NI-59	NI-58	CO-60	FE-59	CO-59	CO-58	FE-57	FE-56
	9.18	-2.20	-11.20	7.15	-1.13	-.34	-10.81	10.53	2.89
CO-59	CU-61	CU-60	CU-59	NI-61	CO-60	NI-60	NI-59	CO-58	CO-57
	6.61	-5.10	-15.16	9.63	-.23	1.81	-9.57	10.11	1.54
NI-58	ZN-60	ZN-59	NR	CU-60	NI-59	CU-59	CU-58	NI-57	NI-56
	MU	MU	--	5.76	1.29	-4.30	-17.07	8.38	-1.88
NI-60	ZN-62	ZN-61	ZN-60	CU-62	NI-61	CU-61	CU-60	NI-59	NI-58
	3.51	-9.10	MU	5.98	.10	-2.92	-14.63	9.19	.19
NI-61	ZN-63	ZN-62	ZN-61	CU-63	NI-62	CU-62	CU-61	NI-60	NI-59
	4.86	-4.31	-16.92	9.01	2.88	-1.84	-10.74	12.75	1.37
NI-62	ZN-64	ZN-63	ZN-62	CU-64	NI-63	CU-63	CU-62	NI-61	NI-60
	6.11	-5.74	-14.91	6.32	-.88	-1.59	-12.44	9.97	2.15
NI-64	ZN-66	ZN-65	ZN-64	CU-66	NI-65	CU-65	CU-64	NI-63	NI-62
	8.63	-2.40	-10.39	6.79	-1.62	-.27	-10.18	10.91	4.07
CU-63	GA-65	GA-64	GA-63	ZN-65	CU-64	ZN-64	ZN-63	CU-62	CU-61
	3.93	-7.87	-17.87	7.98	.20	-.01	-11.87	9.73	.83
CU-65	GA-67	GA-66	GA-65	ZN-67	CU-66	ZN-66	ZN-65	CU-64	CU-63
	6.46	-4.77	-13.89	8.24	-.66	1.19	-9.85	10.66	2.75
ZN-64	GE-66	GE-65	NR	GA-66	ZN-65	GA-65	GA-64	ZN-63	ZN-62
	1.60	-10.95	--	5.35	.27	-3.77	-15.57	8.72	-.45
ZN-66	GE-68	GE-67	GE-66	GA-68	ZN-67	GA-67	GA-66	ZN-65	ZN-64
	4.55	-7.63	-17.42	5.84	-.66	-2.45	-13.68	9.54	1.55
ZN-67	GE-69	GE-68	GE-67	GA-69	ZN-68	GA-68	GA-67	ZN-66	ZN-65
	6.10	-2.50	-14.69	9.11	2.48	-1.22	-9.50	13.52	2.49
ZN-68	GE-70	GE-69	GE-68	GA-70	ZN-69	GA-69	GA-68	ZN-67	ZN-66
	7.42	-4.10	-12.71	6.55	-1.22	-1.10	-11.42	10.37	3.32
ZN-70	GE-72	GE-71	GE-70	GA-72	ZN-71	GA-71	GA-70	ZN-69	ZN-68
	9.89	-.86	-8.27	6.68	-1.68	.16	-9.15	11.38	4.88
GA-69	AS-71	AS-70	AS-69	GE-71	GA-70	GE-70	GE-69	GA-68	GA-67
	5.43	-6.22	-15.41	8.22	-.08	.80	-10.73	10.25	1.97
GA-71	AS-73	AS-72	AS-71	GE-73	GA-72	GE-72	GE-71	GA-70	GA-69
	7.65	-3.13	-11.52	8.80	-1.20	2.02	-8.74	11.26	3.62

HE-3 REACTION Q-VALUES

TARGET	N	2N	3N	P	2P	P,N	P,2N	HE4	HE4,N
GE-70	SE-72	SE-71	SE-70	AS-72	GE-71	AS-71	AS-70	GE-69	GE-68
	3.92	-8.28	MU	5.30	-.31	-3.09	-14.74	9.05	.44
GE-72	SE-74	SE-73	SE-72	AS-74	GE-73	AS-73	AS-72	GE-71	GE-70
	6.49	-5.62	-14.24	5.92	-.93	-2.09	-12.86	9.82	2.41
GE-73	SE-75	SE-74	SE-73	AS-75	GE-74	AS-74	AS-73	GE-72	GE-71
	7.73	-.29	-12.40	9.38	2.48	-.87	-8.87	13.79	3.04
GE-74	SE-76	SE-75	SE-74	AS-76	GE-75	AS-75	AS-74	GE-73	GE-72
	8.70	-2.46	-10.49	6.51	-1.23	-.82	-11.06	10.38	3.59
GE-76	SE-78	SE-77	SE-76	AS-78	GE-77	AS-77	AS-76	GE-75	GE-74
	10.67	.18	-7.24	7.18	-1.69	.28	-9.42	11.13	4.64
AS-75	BR-77	BR-76	BR-75	SE-77	AS-76	SE-76	SE-75	AS-74	AS-73
	7.06	-3.61	-13.16	9.21	-.39	1.80	-9.37	10.33	2.32
SE-74	KR-76	KR-75	KR-74	BR-76	SE-75	BR-75	BR-74	SE-73	SE-72
	4.08	-9.36	-19.50	6.06	.31	-3.48	-15.30	8.46	-.16
SE-76	KR-78	KR-77	KR-76	BR-78	SE-77	BR-77	BR-76	SE-75	SE-74
	5.75	-6.12	-15.11	5.83	-.30	-2.45	-13.13	9.41	1.39
SE-77	KR-79	KR-78	KR-77	BR-79	SE-78	BR-78	BR-77	SE-76	SE-75
	6.71	-1.67	-13.53	9.12	2.77	-1.58	-9.87	13.16	2.00
SE-78	KR-80	KR-79	KR-78	BR-80	SE-79	BR-79	BR-78	SE-77	SE-76
	7.73	-3.78	-12.16	6.50	-.75	-1.37	-12.07	10.08	2.67
SE-80	KR-82	KR-81	KR-80	BR-82	SE-81	BR-81	BR-80	SE-79	SE-78
	9.70	-1.29	-9.14	7.39	-1.00	-.21	-10.37	10.67	3.70
SE-82	KR-84	KR-83	KR-82	BR-84	SE-83	BR-83	BR-82	SE-81	SE-80
	11.71	1.19	-6.28	7.79	-1.79	1.00	-8.59	11.31	4.60
BR-79	RB-81	RB-80	RB-79	KR-81	BR-80	KR-80	KR-79	BR-78	BR-77
	6.22	-4.49	MU	9.24	.16	1.39	-10.12	9.87	1.59
BR-81	RB-83	RB-82	RB-80	KR-83	BR-82	KR-82	KR-81	BR-80	BR-79
	8.05	-2.76	-14.45	9.65	-.12	2.19	-8.80	10.41	2.53
KR-78	SR-80	SR-79	NR	RB-80	KR-79	RB-79	RB-78	KR-77	KR-76
	MU	MU	--	6.30	.67	MU	MU	8.71	-.28
KR-80	SR-82	SR-81	SR-80	RB-82	KR-81	RB-81	RB-80	KR-79	KR-78
	4.99	MU	MU	6.17	.13	-2.89	-13.59	9.07	.68
KR-82	SR-84	SR-83	SR-82	RB-84	KR-83	RB-83	RB-82	KR-81	KR-80
	6.91	-4.85	-13.85	6.81	-.25	-1.86	-12.67	9.58	1.73
KR-83	SR-85	SR-84	SR-83	RB-85	KR-84	RB-84	RB-83	KR-82	KR-81
	7.92	-.56	-12.32	9.81	2.80	-.66	-9.33	13.11	2.12
KR-84	SR-86	SR-85	SR-84	RB-86	KR-85	RB-85	RB-84	KR-83	KR-82
	8.93	-2.60	-11.08	7.93	-.60	-.71	-11.18	10.05	2.59

HE-3 REACTION Q-VALUES

TARGET	N	2N	3N	P	2P	P,N	P,2N	HE4	HE4,N
KR-86	SR-88	SR-87	SR-86	RB-88	KR-87	RB-87	RB-86	KR-85	KR-84
	11.49	.39	-9.82	7.03	-2.21	.90	-9.03	10.73	3.60
RB-85	Y-87	Y-86	Y-85	SR-87	RB-86	SR-86	SR-85	RB-84	RB-83
	7.85	-4.14	-13.65	10.35	.92	1.91	-9.61	10.10	1.44
RB-87	Y-89	Y-88	Y-87	SR-89	RB-88	SR-88	SR-87	RB-86	RB-85
	9.95	-1.53	-10.72	9.27	-1.59	2.87	-8.23	10.64	2.00
SR-84	ZR-86	ZR-85	ZR-84	Y-86	SR-85	Y-85	Y-84	SR-83	SR-82
	4.25	MU	MU	6.23	.76	-3.28	-14.80	8.81	-.19
SR-86	ZR-88	ZR-87	ZR-86	Y-88	SR-87	Y-87	Y-86	SR-85	SR-84
	6.13	-6.06	-15.75	7.42	.72	-1.78	-13.77	9.05	.57
SR-87	ZR-89	ZR-88	ZR-87	Y-89	SR-88	Y-88	Y-87	SR-86	SR-85
	6.84	-2.31	-14.50	10.46	3.38	-1.02	-10.22	12.14	.62
SR-88	ZR-90	ZR-89	ZR-88	Y-90	SR-89	Y-89	Y-88	SR-87	SR-86
	7.74	-4.26	-13.41	6.25	-1.33	-.64	-12.12	9.47	1.04
Y-89	NB-91	NB-90	NB-89	ZR-91	Y-90	ZR-90	ZR-89	Y-88	Y-87
	5.93	-6.23	-16.00	7.86	-.82	.66	-11.33	9.10	-.10
ZR-90	MO-92	MO-91	MO-90	NB-92	ZR-91	NB-91	NB-90	ZR-89	ZR-88
	4.89	-7.69	-17.88	5.33	-.52	-2.45	-14.61	8.58	-.57
ZR-91	MO-93	MO-92	MO-91	NB-93	ZR-92	NB-92	NB-91	ZR-90	ZR-89
	5.75	-2.30	-14.89	6.95	.92	-1.87	-9.64	13.38	1.38
ZR-92	MO-94	MO-93	MO-92	NB-94	ZR-93	NB-93	NB-92	ZR-91	ZR-90
	6.80	-2.89	-10.94	5.54	-1.00	-1.69	-10.51	11.93	4.74
ZR-94	MO-96	MO-95	MO-94	NB-96	ZR-95	NB-95	NB-94	ZR-93	ZR-92
	8.39	-.77	-8.14	6.02	-1.25	-.91	-9.40	12.35	5.63
ZR-96	MO-98	MO-97	MO-96	NB-98	ZR-97	NB-97	NB-96	ZR-95	ZR-94
	9.54	.90	-5.92	5.72	-2.14	-.25	-8.29	12.74	6.27
NB-93	TC-95	TC-94	TC-93	MO-95	NB-94	MO-94	MO-93	NB-92	NB-91
	5.71	-4.27	-12.89	8.15	-.49	.77	-8.92	11.75	3.98
MO-92	RU-94	RU-93	RU-92	TC-94	MO-93	TC-93	TC-92	MO-91	MO-90
	MU	MU	MU	4.98	.33	-3.63	-16.55	7.99	-2.20
MO-94	RU-96	RU-95	RU-94	TC-96	MO-95	TC-95	TC-94	MO-93	MO-92
	4.52	-5.60	MU	5.10	-.34	-2.79	-12.76	10.88	2.83
MO-95	RU-97	RU-96	RU-95	TC-97	MO-96	TC-96	TC-95	MO-94	MO-93
	5.19	-2.85	-12.97	7.17	1.44	-2.28	-10.16	13.20	3.51
MO-96	RU-98	RU-97	RU-96	TC-98	MO-97	TC-97	TC-96	MO-95	MO-94
	6.29	-3.97	-12.01	5.37	-.90	-1.98	-11.43	11.42	4.04
MO-97	RU-99	RU-98	RU-97	TC-99	MO-98	TC-98	TC-97	MO-96	MO-95
	6.94	-.53	-10.78	7.43	.92	-1.45	-8.80	13.76	4.60

HE-3 REACTION Q-VALUES

TARGET	N	2N	3N	P	2P	P,N	P,2N	HE4	HE4,N
MO-98	RU-100	RU-99	RU-98	TC-100	MO-99	TC-99	TC-98	MO-97	MO-96
	7.97	-1.70	-9.17	5.38	-1.80	-1.21	-10.09	11.93	5.12
MO-100	RU-102	RU-101	RU-100	TC-102	MO-101	TC-101	TC-100	MO-99	MO-98
	9.77	.56	-6.25	6.06	-2.33	-.29	-8.84	12.27	6.36
RU-96	PD-98	PD-97	NR	RH-98	RU-97	RH-97	RH-96	RU-95	RU-94
	MU	MU	--	5.59	.32	-3.95	MU	10.45	MU
RU-98	PD-100	PD-99	PD-98	RH-100	RU-99	RH-99	RH-98	RU-97	RU-96
	3.62	-7.71	MU	5.00	-.25	-3.13	-12.70	10.32	2.28
RU-99	PD-101	PD-100	PD-99	RH-101	RU-100	RH-100	RH-99	RU-98	RU-97
	4.64	-3.85	-15.18	7.42	1.95	-2.47	-10.60	13.10	2.85
RU-100	PD-102	PD-101	PD-100	RH-102	RU-101	RH-101	RH-100	RU-99	RU-98
	5.56	-5.03	-13.52	5.20	-.91	-2.25	-12.14	10.90	3.43
RU-101	PD-103	PD-102	PD-101	RH-103	RU-102	RH-102	RH-101	RU-100	RU-99
	6.37	-1.24	-11.83	7.70	1.50	-1.61	-9.06	13.77	4.10
RU-102	PD-104	PD-103	PD-102	RH-104	RU-103	RH-103	RH-102	RU-101	RU-100
	7.17	-2.85	-10.46	5.49	-1.47	-1.51	-10.82	11.36	4.55
RU-104	PD-106	PD-105	PD-104	RH-106	RU-105	RH-105	RH-104	RU-103	RU-102
	8.68	-.87	-7.96	5.92	-947.69	-.65	-9.65	11.69	5.44
RH-103	AG-105	AG-104	AG-103	PD-105	RH-104	PD-104	PD-103	RH-102	RH-101
	5.98	-4.08	-12.43	8.06	-.72	.97	-9.05	11.26	3.81
PD-102	CD-104	CD-103	NR	AG-104	PD-103	AG-103	AG-102	PD-101	PD-100
	2.88	MU	--	4.86	-.11	-3.48	-13.80	9.98	1.49
PD-104	CD-106	CD-105	CD-104	AG-106	PD-105	AG-105	AG-104	PD-103	PD-102
	4.58	-6.29	-14.75	5.17	-.63	-2.71	-12.77	10.55	2.94
PD-105	CD-107	CD-106	CD-105	AG-107	PD-106	AG-106	AG-105	PD-104	PD-103
	5.41	-2.51	-13.38	7.61	1.83	-1.92	-9.80	13.48	3.46
PD-106	CD-108	CD-107	CD-106	AG-108	PD-107	AG-107	AG-106	PD-105	PD-104
	6.20	-4.13	-12.06	5.34	-1.19	-1.93	-11.46	11.03	3.94
PD-108	CD-110	CD-109	CD-108	AG-110	PD-109	AG-109	AG-108	PD-107	PD-106
	7.68	-2.19	-9.56	5.59	-1.57	-1.24	-10.42	11.35	4.81
PD-110	CD-112	CD-111	CD-110	AG-112	PD-111	AG-111	AG-110	PD-109	PD-108
	9.10	-.30	-7.28	5.87	-1.97	-.57	-9.37	11.77	5.62
AG-107	IN-109	IN-108	IN-107	CD-109	AG-108	CD-108	CD-107	AG-106	AG-105
	4.99	-4.88	-14.19	7.79	-.44	.42	-9.92	11.04	3.16
AG-109	IN-111	IN-110	IN-109	CD-111	AG-110	CD-110	CD-109	AG-108	AG-107
	6.30	-3.52	-11.47	8.17	-.89	1.20	-8.67	11.39	4.12
CD-106	SN-108	SN-107	SN-106	IN-108	CD-107	IN-107	IN-106	CD-105	CD-104
	MU	MU	MU	5.24	.21	-4.06	-15.04	9.70	1.24

HE-3 REACTION Q-VALUES

TARGET	N	2N	3N	P	2P	P,N	P,2N	HE4	HE4,N
CD-108	SN-110 MU	SN-109 MU	SN-108 MU	IN-110 4.81	CD-109 -.35	IN-109 -3.15	IN-108 -13.02	CD-107 10.24	CD-106 2.31
CD-110	SN-112 5.16	SN-111 -5.91	SN-110 MU	IN-112 5.28	CD-111 -.74	IN-111 -2.61	IN-110 -12.43	CD-109 10.71	CD-108 3.34
CD-111	SN-113 5.93	SN-112 -1.81	SN-111 -12.89	IN-113 7.73	CD-112 1.68	IN-112 -1.69	IN-111 -9.59	CD-110 13.60	CD-109 3.73
CD-112	SN-114 6.85	SN-113 -3.47	SN-112 -11.21	IN-114 5.65	CD-113 -1.18	IN-113 -1.66	IN-112 -11.09	CD-111 11.17	CD-110 4.20
CD-113	SN-115 7.85	SN-114 .31	SN-113 -10.01	IN-115 8.14	CD-114 1.33	IN-114 -.89	IN-113 -8.20	CD-112 14.04	CD-111 4.64
CD-114	SN-116 8.36	SN-115 -1.20	SN-114 -8.74	IN-116 5.82	CD-115 -1.58	IN-115 -.90	IN-114 -9.93	CD-113 11.53	CD-112 4.99
CD-116	SN-118 9.80	SN-117 .47	SN-116 -6.47	IN-118 6.38	CD-117 -1.95	IN-117 -.22	IN-116 -9.02	CD-115 11.88	CD-114 5.74
IN-113	SB-115 4.52	SB-114 -6.26	SB-113 -14.78	SN-115 8.33	IN-114 -.40	SN-114 .80	SN-113 -9.52	IN-112 11.15	IN-111 3.25
IN-115	SB-117 5.89	SB-116 -3.78	SB-115 -11.82	SN-117 8.49	IN-116 -.99	SN-116 1.55	SN-115 -8.01	IN-114 11.55	IN-113 4.23
SN-112	TE-114 MU	TE-113 MU	TE-112 MU	SB-114 3.29	SN-113 .03	SB-113 -5.23	SB-112 MU	SN-111 9.50	SN-110 MU
SN-114	TE-116 1.70	TE-115 -9.28	TE-114 MU	SB-116 4.05	SN-115 -.18	SB-115 -3.99	SB-114 -14.78	SN-113 10.25	SN-112 2.51
SN-115	TE-117 1.90	TE-116 -5.83	TE-115 -16.81	SB-117 6.18	SN-116 1.85	SB-116 -3.49	SB-115 -11.53	SN-114 13.04	SN-113 2.72
SN-116	TE-118 3.00	TE-117 -7.66	TE-116 -15.39	SB-118 4.08	SN-117 -.78	SB-117 -3.38	SB-116 -13.05	SN-115 11.01	SN-114 3.47
SN-117	TE-119 3.66	TE-118 -3.94	TE-117 -14.61	SB-119 6.73	SN-118 1.61	SB-118 -2.87	SB-117 -10.32	SN-116 13.63	SN-115 4.07
SN-118	TE-120 4.61	TE-119 -5.67	TE-118 -13.27	SB-120 4.41	SN-119 -1.24	SB-119 -2.60	SB-118 -12.20	SN-117 11.24	SN-116 4.30
SN-119	TE-121 5.10	TE-120 -1.87	TE-119 -12.16	SB-121 7.17	SN-120 1.39	SB-120 -2.08	SB-119 -9.08	SN-118 14.09	SN-117 4.76
SN-120	TE-122 6.05	TE-121 -4.01	TE-120 -10.98	SB-122 4.86	SN-121 -1.54	SB-121 -1.94	SB-120 -11.19	SN-119 11.46	SN-118 4.98
SN-122	TE-124 7.42	TE-123 -1.99	TE-122 -8.93	SB-124 5.28	SN-123 -1.79	SB-123 -1.15	SB-122 -10.12	SN-121 11.77	SN-120 5.59
SN-124	TE-126 8.68	TE-125 -.42	TE-124 -7.02	SB-126 5.74	SN-125 -1.95	SB-125 -.39	SB-124 -9.15	SN-123 12.07	SN-122 6.14

HE-3 REACTION Q-VALUES

TARGET	N	2N	3N	P	2P	P,N	P,2N	HE4	HE4,N
SB-121	I-123	I-122	I-121	TE-123	SB-122	TE-122	TE-121	SB-120	SB-119
	5.08	-4.65	-12.93	7.21	-.92	.27	-9.79	11.32	4.32
SB-123	I-125	I-124	I-123	TE-125	SB-124	TE-124	TE-123	SB-122	SB-121
	6.52	-3.11	-10.70	7.45	-1.29	.85	-8.56	11.60	4.80
TE-120	XE-122	XE-121	XE-120	I-122	TE-121	I-121	I-120	TE-119	TE-118
	MU	-8.45	MU	4.39	-.74	-3.88	-13.90	10.29	2.69
TE-122	XE-124	XE-123	XE-122	I-124	TE-123	I-123	I-122	TE-121	TE-120
	4.02	-6.49	MU	4.68	-.77	-2.91	-12.64	10.52	3.54
TE-123	XE-125	XE-124	XE-123	I-125	TE-124	I-124	I-123	TE-122	TE-121
	4.68	-2.92	-13.44	7.36	1.69	-2.26	-9.85	13.63	3.57
TE-124	XE-126	XE-125	XE-124	I-126	TE-125	I-125	I-124	TE-123	TE-122
	5.51	-4.73	-12.33	5.05	-1.11	-2.05	-11.67	11.17	4.22
TE-125	XE-127	XE-126	XE-125	I-127	TE-126	I-126	I-125	TE-124	TE-123
	6.27	-1.09	-11.33	7.59	1.37	-1.56	-8.65	13.97	4.56
TE-126	XE-128	XE-127	XE-126	I-128	TE-127	I-127	I-126	TE-125	TE-124
	6.66	-2.82	-10.18	5.30	-1.40	-1.50	-10.65	11.48	4.88
TE-128	XE-130	XE-129	XE-128	I-130	TE-129	I-129	I-128	TE-127	TE-126
	7.76	-1.50	-8.41	5.55	-1.60	-.90	-9.77	11.82	5.51
TE-130	XE-132	XE-131	XE-130	I-132	TE-131	I-131	I-130	TE-129	TE-128
	8.79	-.14	-6.74	6.02	-1.82	-.33	-8.95	12.19	6.07
I-127	CS-129	CS-128	CS-127	XE-129	I-128	XE-128	XE-127	I-126	I-125
	5.47	-4.28	-11.93	7.35	-.92	.44	-9.04	11.42	4.33
XE-124	BA-126	BA-125	BA-124	CS-126	XE-125	CS-125	CS-124	XE-123	XE-122
	MU	MU	MU	4.54	-.12	-3.97	MU	10.06	MU
XE-126	BA-128	BA-127	BA-126	CS-128	XE-127	CS-127	CS-126	XE-125	XE-124
	2.93	-7.79	MU	4.41	-.36	-3.24	-13.30	10.33	2.73
XE-128	BA-130	BA-129	BA-128	CS-130	XE-129	CS-129	CS-128	XE-127	XE-126
	4.34	-5.92	-13.91	4.68	-.80	-2.69	-12.43	11.09	3.74
XE-129	BA-131	BA-130	BA-129	CS-131	XE-130	CS-130	CS-129	XE-128	XE-127
	5.06	-2.57	-12.83	7.01	1.54	-2.23	-9.60	13.66	4.18
XE-130	BA-132	BA-131	BA-130	CS-132	XE-131	CS-131	CS-130	XE-129	XE-128
	5.36	-4.20	-11.83	4.96	-1.12	-2.25	-9.49	11.31	4.40
XE-131	BA-133	BA-132	BA-131	CS-133	XE-132	CS-132	CS-131	XE-130	XE-129
	6.12	-1.24	-10.80	7.39	1.21	-1.65	-8.86	13.97	4.71
XE-132	BA-134	BA-133	BA-132	CS-134	XE-133	CS-133	CS-132	XE-131	XE-130
	6.44	-2.81	-10.17	5.16	-1.19	-1.54	-10.58	11.64	5.04
XE-134	BA-136	BA-135	BA-134	CS-136	XE-135	CS-135	CS-134	XE-133	XE-132
	7.88	-1.35	-8.55	5.83	-1.16	-.78	-9.83	12.11	5.58

HE-3 REACTION Q-VALUES

TARGET	N	2N	3N	P	2P	P,N	P,2N	HE4	HE4,N
XE-136	BA-138 8.93	BA-137 .39	BA-136 -6.56	CS-138 4.88	XE-137 -3.26	CS-137 -.00	CS-136 -8.61	XE-135 12.69	XE-134 6.13
CS-133	LA-135 5.52	LA-134 -4.29	LA-133 -11.97	BA-135 7.46	CS-134 -1.01	BA-134 .26	BA-133 -8.99	CS-132 11.54	CS-131 4.33
BA-130	CE-132 1.89	CE-131 -9.83	CE-130 MU	LA-132 3.87	BA-131 -.09	LA-131 -3.83	LA-130 -14.10	BA-129 10.31	BA-128 2.32
BA-132	CE-134 3.42	CE-133 -6.92	CE-132 -15.30	LA-134 4.34	BA-133 -.35	LA-133 -3.34	LA-132 -13.32	BA-131 11.01	BA-130 3.38
BA-134	CE-136 4.56	CE-135 -5.43	CE-134 -13.19	LA-136 5.06	BA-135 -.52	LA-135 -2.46	LA-134 -12.27	BA-133 11.32	BA-132 3.96
BA-135	CE-137 5.20	CE-136 -2.64	CE-135 -12.63	LA-137 7.18	BA-136 1.51	LA-136 -2.14	LA-135 -9.66	BA-134 13.37	BA-133 4.12
BA-136	CE-138 5.44	CE-137 -4.03	CE-136 -11.87	LA-138 5.21	BA-137 -.77	LA-137 -2.05	LA-136 -11.37	BA-135 11.34	BA-134 4.14
BA-137	CE-139 6.00	CE-138 -1.51	CE-137 -10.98	LA-139 7.05	BA-138 .82	LA-138 -1.74	LA-137 -9.00	BA-136 13.62	BA-135 4.39
BA-138	CE-140 6.49	CE-139 -2.54	CE-138 -10.05	LA-140 3.51	BA-139 -3.01	LA-139 -1.49	LA-138 -10.28	BA-137 12.03	BA-136 5.08
LA-138	PR-140 4.93	PR-139 -2.87	PR-138 -12.73	CE-140 9.06	LA-139 1.07	CE-139 .02	CE-138 -7.49	LA-137 13.31	LA-136 3.99
LA-139	PR-141 5.50	PR-140 -3.85	PR-139 -11.66	CE-141 5.71	LA-140 -2.72	CE-140 .27	CE-139 -8.77	LA-138 11.78	LA-137 4.52
CE-136	ND-138 MU	ND-137 MU	ND-136 MU	PR-138 4.35	CE-137 .12	PR-137 -3.48	PR-136 MU	CE-135 10.58	CE-134 2.82
CE-138	ND-140 3.62	ND-139 -6.57	ND-138 MU	PR-140 4.71	CE-139 -.21	PR-139 -3.10	PR-138 -12.96	CE-137 11.10	CE-136 3.26
CE-140	ND-142 4.74	ND-141 -5.06	ND-140 -12.92	PR-142 3.37	CE-141 -2.28	PR-141 -2.48	PR-140 -11.84	CE-139 11.54	CE-138 4.03
CE-142	ND-144 6.03	ND-143 -1.80	ND-142 -7.90	PR-144 3.82	CE-143 -2.61	PR-143 -1.95	PR-142 -9.28	CE-141 13.36	CE-140 7.93
PR-141	PM-143 3.70	PM-142 -6.07	PM-141 -14.70	ND-143 5.61	PR-142 -1.86	ND-142 -.49	ND-141 -10.30	PR-140 11.22	PR-139 3.41
ND-142	SM-144 2.83	SM-143 -7.63	SM-142 MU	PM-144 2.97	ND-143 -1.62	PM-143 -3.53	PM-142 -13.30	ND-141 10.76	ND-140 2.91
ND-143	SM-145 3.49	SM-144 -3.27	SM-143 -13.73	PM-145 4.93	ND-144 .11	PM-144 -3.13	PM-143 -9.63	ND-142 14.47	ND-141 4.66
ND-144	SM-146 4.11	SM-145 -4.34	SM-144 -11.10	PM-146 3.36	ND-145 -1.97	PM-145 -2.90	PM-144 -10.96	ND-143 12.74	ND-142 6.64

HE-3 REACTION Q-VALUES

TARGET	N	2N	3N	P	2P	P,N	P,2N	HE4	HE4,N
ND-145	SM-147	SM-146	SM-145	PM-147	ND-146	PM-146	PM-145	ND-144	ND-143
	4.69	-1.63	-10.08	5.25	-.16	-2.38	-8.64	14.83	7.00
ND-146	SM-148	SM-147	SM-146	PM-148	ND-147	PM-147	PM-146	ND-145	ND-144
	5.27	-2.87	-9.20	3.60	-2.43	-2.31	-9.94	13.01	7.27
ND-148	SM-150	SM-149	SM-148	PM-150	ND-149	PM-149	PM-148	ND-147	ND-146
	6.48	-1.50	-7.35	3.84	-2.68	-1.79	-9.01	13.25	7.96
ND-150	SM-152	SM-151	SM-150	PM-152	ND-151	PM-151	PM-150	ND-149	ND-148
	7.94	-.28	-5.89	5.23	-2.31	-.69	-8.54	13.24	8.20
SM-144	GD-146	GD-145	GD-144	EU-146	SM-145	EU-145	EU-144	SM-143	SM-142
	.96	MU	MU	2.85	-.95	-4.49	-14.82	10.11	MU
SM-147	GD-149	GD-148	GD-147	EU-149	SM-148	EU-148	EU-147	SM-146	SM-145
	2.73	-4.22	-13.28	4.73	.42	-3.45	-10.30	14.25	5.80
SM-148	GD-150	GD-149	GD-148	EU-150	SM-149	EU-149	EU-148	SM-147	SM-146
	3.31	-5.41	-12.37	3.08	-1.87	-3.41	-11.59	12.43	6.11
SM-149	GD-151	GD-150	GD-149	EU-151	SM-150	EU-150	EU-149	SM-148	SM-147
	3.98	-2.54	-11.26	5.17	.26	-2.77	-9.26	14.73	6.59
SM-150	GD-152	GD-151	GD-150	EU-152	SM-151	EU-151	EU-150	SM-149	SM-148
	4.51	-4.00	-10.52	3.48	-2.11	-2.82	-10.75	12.59	6.75
SM-152	GD-154	GD-153	GD-152	EU-154	SM-153	EU-153	EU-152	SM-151	SM-150
	5.77	-2.84	-9.32	4.57	-1.83	-1.81	-10.36	12.35	6.74
SM-154	GD-156	GD-155	GD-154	EU-156	SM-155	EU-155	EU-154	SM-153	SM-152
	6.96	-1.57	-6.02	5.30	-1.90	-1.03	-9.22	12.67	6.78
EU-151	TB-153	TB-152	TB-151	GD-153	EU-152	GD-152	GD-151	EU-150	EU-149
	3.46	-5.35	-12.37	6.09	-1.43	-.39	-8.90	12.64	6.15
EU-153	TB-155	TB-154	TB-153	GD-155	EU-154	GD-154	GD-153	EU-152	EU-151
	4.64	-4.32	-11.37	6.32	-1.33	-.14	-8.74	12.03	5.74
GD-152	DY-154	DY-153	DY-152	TB-154	GD-153	TB-153	TB-152	GD-151	GD-150
	2.61	-6.75	-13.88	3.18	-1.24	-3.87	-12.68	12.06	5.54
GD-154	DY-156	DY-155	DY-154	TB-156	GD-155	TB-155	TB-154	GD-153	GD-152
	4.07	-5.82	-12.48	4.08	-1.26	-2.94	-11.90	11.97	5.49
GD-155	DY-157	DY-156	DY-155	TB-157	GD-156	TB-156	TB-155	GD-154	GD-153
	4.43	-2.39	-12.28	6.31	.81	-2.38	-9.40	14.12	5.51
GD-156	DY-158	DY-157	DY-156	TB-158	GD-157	TB-157	TB-156	GD-155	GD-154
	4.74	-4.09	-10.92	4.58	-1.37	-2.21	-10.90	12.05	5.59
GD-157	DY-159	DY-158	DY-157	TB-159	GD-158	TB-158	TB-157	GD-156	GD-155
	5.24	-1.61	-10.44	6.41	.21	-1.77	-8.56	14.23	5.70
GD-158	DY-160	DY-159	DY-158	TB-160	GD-159	TB-159	TB-158	GD-157	GD-156
	5.91	-2.68	-9.54	4.86	-1.69	-1.52	-9.70	12.64	6.30

HE-3 REACTION Q-VALUES

TARGET	N	2N	3N	P	2P	P,N	P,2N	HE4	HE4,N
GD-160	DY-162 7.15	DY-161 -1.05	DY-160 -7.50	TB-162 5.13	GD-161 -2.08	TB-161 -.86	TB-160 -8.55	GD-159 13.20	GD-158 7.17
TB-159	HO-161 4.58	HO-160 -4.38	HO-159 -11.47	DY-161 6.16	TB-160 -1.33	DY-160 -.29	DY-159 -8.88	TB-158 12.40	TB-157 5.61
DY-156	ER-158 MU	ER-157 MU	ER-156 MU	HO-158 3.11	DY-157 -.90	HO-157 MU	HO-156 MU	DY-155 10.68	DY-154 4.03
DY-158	ER-160 MU	ER-159 MU	ER-158 MU	HO-160 3.64	DY-159 -.87	HO-159 -3.45	HO-158 -12.54	DY-157 11.74	DY-156 4.92
DY-160	ER-162 3.56	ER-161 -5.63	ER-160 MU	HO-162 3.99	DY-161 -1.27	HO-161 -2.85	HO-160 -11.80	DY-159 11.98	DY-158 5.13
DY-161	ER-163 3.95	ER-162 -2.89	ER-161 -12.08	HO-163 5.95	DY-162 .49	HO-162 -2.46	HO-161 -9.30	DY-160 14.13	DY-159 5.54
DY-162	ER-164 4.54	ER-163 -4.25	ER-162 -11.09	HO-164 4.30	DY-163 -1.47	HO-163 -2.26	HO-162 -10.66	DY-161 12.37	DY-160 5.92
DY-163	ER-165 4.94	ER-164 -1.71	ER-163 -10.50	HO-165 6.09	DY-164 -.06	HO-164 -1.95	HO-163 -8.51	DY-162 14.32	DY-161 6.12
DY-164	ER-166 5.83	ER-165 -2.72	ER-164 -9.36	HO-166 4.76	DY-165 -2.08	HO-165 -1.57	HO-164 -9.61	DY-163 12.92	DY-162 6.66
HO-165	TM-167 4.17	TM-166 -4.15	TM-165 -11.22	ER-167 6.12	HO-166 -1.39	ER-166 -.32	ER-165 -8.87	HO-164 12.53	HO-163 5.97
ER-162	YB-164 MU	YB-163 MU	YB-162 MU	TM-164 3.18	ER-163 -.87	TM-163 -3.93	TM-162 -13.39	ER-161 11.38	ER-160 MU
ER-164	YB-166 2.61	YB-165 -6.94	YB-164 MU	TM-166 3.65	ER-165 -1.07	TM-165 -3.43	TM-164 -12.46	ER-163 11.78	ER-162 4.93
ER-166	YB-168 3.27	YB-167 -5.71	YB-166 -12.58	TM-168 3.99	ER-167 -1.28	TM-167 -3.23	TM-166 -11.54	ER-165 12.02	ER-164 5.38
ER-167	YB-169 3.62	YB-168 -3.17	YB-167 -12.15	TM-169 5.61	ER-168 .05	TM-168 -2.45	TM-167 -9.66	ER-166 14.14	ER-165 5.59
ER-168	YB-170 4.41	YB-169 -4.14	YB-168 -10.94	TM-170 4.22	ER-169 -1.72	TM-169 -2.16	TM-168 -10.22	ER-167 12.80	ER-166 6.37
ER-170	YB-172 6.12	YB-171 -2.01	YB-170 -8.77	TM-172 5.02	ER-171 -2.04	TM-171 -1.33	TM-170 -8.96	ER-169 13.39	ER-168 7.39
TM-169	LU-171 3.23	LU-170 -5.34	LU-169 -12.74	YB-171 5.61	TM-170 -1.34	YB-170 -1.15	YB-169 -9.70	TM-168 12.52	TM-167 5.30
YB-168	HF-170 MU	HF-169 MU	HF-168 MU	LU-170 3.43	YB-169 -.93	LU-169 -3.97	LU-168 -13.10	YB-167 11.59	YB-166 4.72
YB-170	HF-172 MU	HF-171 MU	HF-170 MU	LU-172 3.69	YB-171 -.96	LU-171 -3.34	LU-170 -11.91	YB-169 12.02	YB-168 5.23

HE-3 REACTION Q-VALUES

TARGET	N	2N	3N	P	2P	P,N	P,2N	HE4	HE4,N
YB-171	HF-173	HF-172	HF-171	LU-173	YB-172	LU-172	LU-171	YB-170	YB-169
	MU	MU	MU	5.42	.41	-3.07	-10.10	13.81	5.26
YB-172	HF-174	HF-173	HF-172	LU-174	YB-173	LU-173	LU-172	YB-171	YB-170
	3.13	MU	MU	3.92	-1.24	-2.71	-11.20	12.44	5.68
YB-173	HF-175	HF-174	HF-173	LU-175	YB-174	LU-174	LU-173	YB-172	YB-171
	3.87	-3.35	MU	5.24	-.28	-2.56	-9.19	14.09	5.96
YB-174	HF-176	HF-175	HF-174	LU-176	YB-175	LU-175	LU-174	YB-173	YB-172
	4.23	-3.57	-10.79	3.99	-1.89	-2.20	-10.00	13.13	6.65
YB-176	HF-178	HF-177	HF-176	LU-178	YB-177	LU-177	LU-176	YB-175	YB-174
	5.74	-1.88	-8.24	4.27	-2.19	-1.59	-8.48	13.93	8.10
LU-175	TA-177	TA-176	TA-175	HF-177	LU-176	HF-176	HF-175	LU-174	LU-173
	3.13	MU	MU	5.07	-1.53	-1.29	-9.09	12.77	6.14
LU-176	TA-178	TA-177	TA-176	HF-178	LU-177	HF-177	HF-176	LU-175	LU-174
	3.81	-3.06	MU	6.50	-.83	-1.12	-7.48	14.38	6.58
HF-174	W-176	W-175	W-174	TA-176	HF-175	TA-175	TA-174	HF-173	HF-172
	MU	MU	MU	MU	-.50	MU	MU	MU	MU
HF-176	W-178	W-177	W-176	TA-178	HF-177	TA-177	TA-176	HF-175	HF-174
	MU	MU	MU	3.57	-1.36	-3.30	MU	12.77	5.55
HF-177	W-179	W-178	W-177	TA-179	HF-178	TA-178	TA-177	HF-176	HF-175
	MU	MU	MU	5.07	-.10	-2.79	-9.66	14.21	6.41
HF-178	W-180	W-179	W-178	TA-180	HF-179	TA-179	TA-178	HF-177	HF-176
	3.95	MU	MU	4.23	-1.65	-2.55	-10.41	12.95	6.59
HF-179	W-181	W-180	W-179	TA-181	HF-180	TA-180	TA-179	HF-178	HF-177
	4.83	-2.12	MU	5.80	-.39	-1.84	-8.62	14.50	6.88
HF-180	W-182	W-181	W-180	TA-182	HF-181	TA-181	TA-180	HF-179	HF-178
	5.49	-2.50	-9.45	4.46	-1.77	-1.53	-9.17	13.24	7.17
TA-180	RE-182	RE-181	RE-180	W-182	TA-181	W-181	W-180	TA-179	TA-178
	3.29	MU	MU	6.94	-.08	-1.05	-8.00	13.79	5.93
TA-181	RE-183	RE-182	RE-181	W-183	TA-182	W-182	W-181	TA-180	TA-179
	3.83	-4.35	MU	5.48	-1.73	-.70	-8.69	12.93	6.15
W-180	OS-182	OS-181	OS-180	RE-182	W-181	RE-181	RE-180	W-179	W-178
	MU	MU	MU	3.57	-.77	MU	MU	MU	MU
W-182	OS-184	OS-183	OS-182	RE-184	W-183	RE-183	RE-182	W-181	W-180
	2.71	MU	MU	3.48	-1.53	-3.19	-11.36	12.59	5.64
W-183	OS-185	OS-184	OS-183	RE-185	W-184	RE-184	RE-183	W-182	W-181
	3.33	-3.47	MU	5.12	-.30	-2.71	-9.37	14.39	6.40
W-184	OS-186	OS-185	OS-184	RE-186	W-185	RE-185	RE-184	W-183	W-182
	4.21	-4.09	-10.89	3.92	-1.97	-2.30	-10.13	13.16	6.97

HE-3 REACTION Q-VALUES

TARGET	N	2N	3N	P	2P	P,N	P,2N	HE4	HE4,N
W-186	OS-188 5.33	OS-187 -2.51	OS-186 -8.75	RE-188 4.00	W-187 -2.26	RE-187 -1.73	RE-186 -9.04	W-185 13.36	W-184 7.61
RE-185	IR-187 2.66	IR-186 -5.80	IR-185 MU	OS-187 5.06	RE-186 -1.47	OS-186 -1.18	OS-185 -9.48	RE-184 12.77	RE-183 6.11
RE-187	IR-189 3.99	IR-188 -4.27	IR-187 -10.89	OS-189 5.34	RE-188 -1.99	OS-188 -.66	OS-187 -8.50	RE-186 13.26	RE-185 7.02
OS-184	PT-186 MU	PT-185 MU	PT-184 MU	IR-186 2.77	OS-185 -.91	IR-185 MU	IR-184 MU	OS-183 MU	OS-182 MU
OS-186	PT-188 1.46	PT-187 MU	PT-186 MU	IR-188 2.75	OS-187 -1.48	IR-187 -3.87	IR-186 -12.33	OS-185 12.28	OS-184 5.47
OS-187	PT-189 2.41	PT-188 -4.78	PT-187 MU	IR-189 4.77	OS-188 .12	IR-188 -3.49	IR-187 -10.11	OS-186 14.33	OS-185 6.03
OS-188	PT-190 3.25	PT-189 -5.43	PT-188 -12.62	IR-190 3.22	OS-189 -1.72	IR-189 -3.07	IR-188 -11.33	OS-187 12.73	OS-186 6.49
OS-189	PT-191 3.93	PT-190 -2.75	PT-189 -11.43	IR-191 5.47	OS-190 .05	IR-190 -2.78	IR-189 -9.07	OS-188 14.57	OS-187 6.73
OS-190	PT-192 4.51	PT-191 -3.84	PT-190 -10.52	IR-192 3.84	OS-191 -1.83	IR-191 -2.30	IR-190 -10.55	OS-189 12.80	OS-188 6.80
OS-192	PT-194 5.67	PT-193 -2.71	PT-192 -9.00	IR-194 4.20	OS-193 -2.23	IR-193 -1.89	IR-192 -9.68	OS-191 12.95	OS-190 7.06
IR-191	AU-193 3.50	AU-192 -5.21	AU-191 -11.99	PT-193 5.38	IR-192 -1.58	PT-192 -.91	PT-191 -9.26	IR-190 12.32	IR-189 6.03
IR-193	AU-195 4.95	AU-194 -3.45	AU-193 -10.43	PT-195 5.96	IR-194 -1.63	PT-194 -.16	PT-193 -8.55	IR-192 12.78	IR-191 6.65
PT-190	HG-192 .74	HG-191 MU	HG-190 MU	AU-192 3.02	PT-191 -1.04	AU-191 -3.77	AU-190 -12.93	PT-189 11.89	PT-188 4.70
PT-192	HG-194 2.53	HG-193 -6.43	HG-192 -14.29	AU-194 3.66	PT-193 -1.43	AU-193 -3.31	AU-192 -12.01	PT-191 12.22	PT-190 5.54
PT-194	HG-196 3.98	HG-195 -4.84	HG-194 -12.14	AU-196 4.08	PT-195 -1.59	AU-195 -2.60	AU-194 -11.01	PT-193 12.19	PT-192 5.90
PT-195	HG-197 4.49	HG-196 -2.15	HG-195 -10.97	AU-197 6.03	PT-196 .21	AU-196 -2.05	AU-195 -8.73	PT-194 14.45	PT-193 6.06
PT-196	HG-198 5.19	HG-197 -3.44	HG-196 -10.08	AU-198 4.60	PT-197 -1.86	AU-197 -1.90	AU-196 -9.98	PT-195 12.65	PT-194 6.52
PT-198	HG-200 6.46	HG-199 -1.57	HG-198 -8.22	AU-200 5.03	PT-199 -2.15	AU-199 -1.25	AU-198 -8.81	PT-197 13.01	PT-196 7.16
AU-197	TL-199 4.14	TL-198 -4.87	TL-197 -12.23	HG-199 6.02	AU-198 -1.22	HG-198 -.63	HG-197 -9.26	AU-196 12.49	AU-195 5.81

HE-3 REACTION Q-VALUES

TARGET	N	2N	3N	P	2P	P,N	P,2N	HE4	HE4,N
HG-196	PB-198	PB-197	PB-196	TL-198	HG-197	TL-197	TL-196	HG-195	HG-194
	.72	-8.92	-16.71	3.31	-1.08	-4.07	-13.10	11.75	4.45
HG-198	PB-200	PB-199	PB-198	TL-200	HG-199	TL-199	TL-198	HG-197	HG-196
	2.00	-6.90	-14.55	3.73	-1.07	-2.95	-11.96	11.94	5.30
HG-199	PB-201	PB-200	PB-199	TL-201	HG-200	TL-200	TL-199	HG-198	HG-197
	2.59	-4.65	-13.55	5.35	.31	-2.93	-9.60	13.92	5.29
HG-200	PB-202	PB-201	PB-200	TL-202	HG-201	TL-201	TL-200	HG-199	HG-198
	3.43	-5.43	-12.68	4.27	-1.49	-2.68	-10.95	12.55	5.89
HG-201	PB-203	PB-202	PB-201	TL-203	HG-202	TL-202	TL-201	HG-200	HG-199
	4.14	-2.79	-11.66	5.74	.04	-1.96	-8.91	14.35	6.32
HG-202	PB-204	PB-203	PB-202	TL-204	HG-203	TL-203	TL-202	HG-201	HG-200
	4.62	-3.62	-10.55	4.64	-1.73	-2.02	-9.72	12.81	6.59
HG-204	PB-206	PB-205	PB-204	TL-206	HG-205	TL-205	TL-204	HG-203	HG-202
	5.96	-2.13	-8.86	5.22	-2.18	-1.31	-8.85	13.08	7.09
TL-203	BI-205	BI-204	BI-203	PB-205	TL-204	PB-204	PB-203	TL-202	TL-201
	2.17	-6.29	-13.29	5.66	-1.06	-1.07	-9.32	12.88	5.93
TL-205	BI-207	BI-206	BI-205	PB-207	TL-206	PB-206	PB-205	TL-204	TL-203
	3.10	-4.84	-12.02	6.28	-1.19	-.45	-8.54	13.04	6.38
PB-204	PO-206	PO-205	PO-204	BI-206	PB-205	BI-205	BI-204	PB-203	PB-202
	.08	-8.81	-16.19	2.71	-.98	-4.47	-12.94	12.33	5.40
PB-206	PO-208	PO-207	PO-206	BI-208	PB-207	BI-207	BI-206	PB-205	PB-204
	.55	-7.86	-14.74	2.74	-.98	-4.17	-12.11	12.49	5.75
PB-207	PO-209	PO-208	PO-207	BI-209	PB-208	BI-208	BI-207	PB-206	PB-205
	.78	-6.19	-14.59	3.46	-.34	-3.99	-10.90	13.84	5.76
PB-208	PO-210	PO-209	PO-208	BI-210	PB-209	BI-209	BI-208	PB-207	PB-206
	1.06	-6.59	-13.56	.68	-3.77	-3.92	-11.37	13.20	6.46
BI-209	AT-211	AT-210	AT-209	PO-211	BI-210	PO-210	PO-209	BI-208	BI-207
	.23	-7.35	-14.66	1.81	-3.12	-2.74	-10.39	13.12	6.21
TH-232	U-234	U-233	U-232	PA-234	TH-233	PA-233	PA-232	TH-231	TH-230
	4.17	-2.68	-8.42	2.73	-2.93	-2.47	-8.98	14.14	9.02
PA-231	NP-233	NP-232	NP-231	U-233	PA-232	U-232	U-231	PA-230	PA-229
	2.30	-4.97	-11.54	4.14	-2.15	-1.59	-8.86	13.77	7.99
U-234	PU-236	PU-235	PU-234	NP-236	U-235	NP-235	NP-234	U-233	U-232
	2.12	-5.23	-11.46	2.39	-2.42	-3.32	-10.32	13.72	7.99
U-235	PU-237	PU-236	PU-235	NP-237	U-236	NP-236	NP-235	U-234	U-233
	2.67	-3.18	-10.53	3.68	-1.18	-2.91	-8.62	15.27	8.42
U-238	PU-240	PU-239	PU-238	NP-240	U-239	NP-239	NP-238	U-237	U-236
	4.05	-2.48	-8.13	2.75	-2.92	-2.42	-8.64	14.43	9.30

TECHNICAL INFORMATION DIVISION
LAWRENCE RADIATION LABORATORY
UNIVERSITY OF CALIFORNIA
BERKELEY, CALIFORNIA 94720